Curry, W.B., Shackleton, N.J., Richter, C., et al., 1995
Proceedings of the Ocean Drilling Program, Initial Reports, Vol. 154

5. SITE 926[1]

Shipboard Scientific Party[2]

HOLE 926A

Date occupied: 19 February 1994

Date departed: 21 February 1994

Time on hole: 1 day, 23 hr, 45 min

Position: 3°43.146′N, 42°54.489′W

Bottom felt (drill-pipe measurement from rig floor, m): 3609.5

Distance between rig floor and sea level (m): 11.1

Water depth (drill-pipe measurement from sea level, m): 3598.4

Total depth (from rig floor, m): 3936.50

Penetration (m): 327.00

Number of cores (including cores having no recovery): 35

Total length of cored section (m): 327.00

Total core recovered (m): 334.92

Core recovery (%): 102.4

Oldest sediment cored:
Depth (mbsf): 327.00
Nature: clayey nannofossil chalk and nannofossil chalk with clay and foraminifers
Age: early Miocene
Measured velocity (km/s): 2.0

HOLE 926B

Date occupied: 21 February 1994

Date departed: 25 February 1994

Time on hole: 4 days, 8 hr, 30 min

Position: 3°43.148′N, 42°54.507′W

Bottom felt (drill-pipe measurement from rig floor, m): 3609.5

Distance between rig floor and sea level (m): 11.2

Water depth (drill-pipe measurement from sea level, m): 3598.3

Total depth (from rig floor, m): 4215.30

Penetration (m): 605.80

Number of cores (including cores having no recovery): 64

Total length of cored section (m): 605.80

Total core recovered (m): 593.25

Core recovery (%): 97.9

Oldest sediment cored:
Depth (mbsf): 605.80
Nature: nannofossil chalk with clay and foraminifers and clayey nannofossil chalk
Age: early Oligocene
Measured velocity (km/s): 2.3

HOLE 926C

Date occupied: 25 February 1994

Date departed: 27 February 1994

Time on hole: 1 day, 21 hr

Position: 3°43.130′N, 42°54.508′W

Bottom felt (drill-pipe measurement from rig floor, m): 3609.5

Distance between rig floor and sea level (m): 11.2

Water depth (drill-pipe measurement from sea level, m): 3598.3

Total depth (from rig floor, m): 4007.80

Penetration (m): 398.30

Number of cores (including cores having no recovery): 42

Total length of cored section (m): 397.80

Total core recovered (m): 394.21

Core recovery (%): 99.1

Oldest sediment cored:
Depth (mbsf): 397.80
Nature: clayey nannofossil chalk with foraminifers and claystone with nannofossils and radiolarians
Age: early Miocene
Measured velocity (km/s): N/A

Comments: Drilled from 0.0 to 0.5 mbsf

Principal results: Site 926 is at the midpoint of the depth transect of sites on the Ceara Rise. The site is located beneath warm surface waters having a mean annual temperature around 27°C. The seafloor at a depth of 3598 m is bathed by North Atlantic Deep Water (NADW) above the present-day carbonate lysocline. The site was chosen to provide material for investigating the geological history of surface- and deep-water properties in the region.

Three holes were drilled at Site 926. Hole 926A was cored with the APC to 327 mbsf. Hole 926B was cored with the APC from the mud line to 254 mbsf and deepened with the XCB to 605.7 mbsf. Hole 926B was logged with the Quad combination tool, the magnetometer/magnetic susceptibility tool, and the geochemical combination tool. Hole 926C was cored with the APC from the mud line to 247.5 mbsf and extended with the XCB to 398.3 mbsf. Detailed comparisons between the magnetic susceptibility records generated on the MST and high-resolution color reflectance generated using a handheld Minolta color analyzer demonstrated that the sedimentary sequence to 336 mbsf had been completely recovered.

The recovered sedimentary sequence at Site 926 spans the interval from the late Oligocene to the Holocene without any detectable stratigraphic break. The entire sequence is characterized by rhythmic sedimentary cycles, and a preliminary evaluation suggests that these are chiefly related to the orbital precession cycle. These sedimentary cycles were well recorded by magnetic susceptibility, color, and natural gamma emission.

[1] Curry, W.B., Shackleton, N.J., Richter, C., et al., 1995. *Proc. ODP, Init. Repts.,* 154: College Station, TX (Ocean Drilling Program).

[2] Shipboard Scientific Party is as given in the list of participants preceding the contents.

All three parameters were shown to record variations in the ratio of terrigenous material to biogenic carbonate in the sediments. Because of a pervasive magnetic overprint, it proved impossible to obtain any magnetostratigraphic data for the site.

Biostratigraphic age control was provided by calcareous nannofossils and foraminifers throughout. In both of these fossil groups, rich assemblages are preserved throughout the sequence, providing an outstanding biostratigraphic sequence and excellent opportunities for the investigation of evolutionary processes and ecological studies. Close sampling (generally 1.5 m or better, corresponding to 0.05 to 0.1 m.y.) in both fossil groups gives almost no suggestion of any breaks in the stratigraphic record; the prediction of hiatuses in the Miocene was not substantiated. The latest Oligocene appears to be more complete than that sampled at Site 925. Microfossil preservation is excellent in the Pleistocene and Pliocene part of the section, but is much more strongly affected by carbonate dissolution below that, especially in the middle Miocene.

Sedimentation rates were highest in the Pleistocene (33 m/m.y.), lowest in the middle Miocene (11 m/m.y.), and intermediate in the lower Miocene and late Oligocene (20–25 m/m.y.). Since the Miocene, sedimentation rates have increased because of greater accumulation of terrigenous material, presumably derived from the nearby Amazon Fan. This increase has been most pronounced for the last 5 m.y. Within the Miocene, sedimentation rates were reduced by dissolution and by lower terrigenous input. The most severe episode of dissolution occurred from about 10 to 13 Ma. Throughout the Miocene, sedimentation rates averaged only about 75% of coeval sedimentation rates in Site 925. During the Pliocene–Pleistocene and in the late Oligocene, sedimentation rates were nearly the same at Sites 926 and 925, implying that the lysocline was deeper than 3600 m throughout most of the late Neogene.

BACKGROUND AND OBJECTIVES

Site 926 was planned as the middle of the depth range of a bathymetric transect of sites drilled on the Ceara Rise. It is located on a plateau at 3598 mbsl and is the southernmost site of the transect, and therefore the site most distant from the Amazon River outflow (see "Introduction" chapter, Fig. 2, this volume). The site is in an area of uniform relief; hydrosweep bathymetry coverage shows a range of only 10 m for several kilometers in all directions around the site (Fig. 1). The seismic section here (Fig. 2) is similar to the sections observed elsewhere in the rise, with an upper layered sequence down to about 0.25 to 0.3 s two-way traveltime (TWT) (200–250 m); a middle, more seismically incoherent unit between about 0.3 and 0.85 s TWT (250–780 m); a unit with some parallel reflectors between 0.85 and 1.15 s TWT (780–1150 m); and a fairly prominent reflector at around 1.15 s TWT (1150 m) that appears to represent the base of the pelagic section. Based on the seismic sections, the sedimentary section here is about 12% thinner than at Site 925. The objective of drilling the site was to sample the pelagic section through the Neogene and into the late Paleogene to provide the middle element of a paleoceanographic depth transect.

Oceanographic conditions in this region have probably been directly affected by the closure of the Panama Isthmus and uplift of the Andes during this time, as well as having been affected by the globally pervasive effect of increased glaciation. In many sections drilled in the Atlantic region, hiatuses are reported in the Miocene. One objective of this site, therefore, was to evaluate the relationship between these hiatuses and excursions of the carbonate compensation depth.

OPERATIONS

Site 926

The transit from Site 925 to Site 926 covered about 50 nmi at an average speed of 10 kt. The *JOIDES Resolution* was navigated directly to the site coordinates of proposed Site CR-3 with neither a departure nor an arrival survey. After a transit of 5 hr, the final approach was made from a way point about 1.5 nmi to the southwest so that steerage way could be maintained directly into the prevailing wind and current. An acoustic beacon was launched at 1045 hr (local time) on 19 February.

Hole 926A

The PDC core bit used for APC/XCB coring at Site 925 again was chosen for Site 926. The BHA was shortened by two drill collars so that logs could be recorded to shallower depths in the critical late Neogene section.

Hole 926A was spudded at 2315 hr on 19 February with a "mudline" APC core. Water depth was found to be 3598 m. Coring proceeded with continuous cores and orientation from Core 154-926A-3H (Table 1).

Incomplete stroke indication began with Core 154-926A-27H at about 250 mbsf and continued through Core 154-926A-35H, with the exception of Cores 154-926A-31H and -32H, which indicated full stroke. Incomplete recovery and a catastrophic liner failure on Core 154-926A-35H prompted the declaration of APC refusal. The drill string then was pulled clear of the seafloor for a repeat of the APC section.

Hole 926B

The ship was moved 30 m west by automatic station keeping (ASK) offsets, the top drive and APC system were deployed, and Hole 926B was spudded at 1200 hr on 21 February.

To provide overlapping core intervals, the seafloor core was actuated from 3 m deeper than Core 154-926A-1H. Core orientation began with the initial core and continued for all APC cores (Table 1).

Incomplete stroke began with Core 154-926B-26H. One additional APC core was taken, also with incomplete stroke, to 254 mbsf. Coring then continued in the XCB mode to 605.7 mbsf, where the target depth was reached. Core recovery was 94% in the XCB interval and core quality was quite good, with the exception of considerable "biscuiting" in the clay-rich zones.

Logging at Hole 926B

Preparations for logging included a wiper trip to 70 mbsf, flushing the hole with drilling mud, and deployment of a go-devil to open the lockable float valve (LFV) before the bit was positioned at logging depth.

With the bit positioned at 81 mbsf for logging, the Quad combination tool string was made up, with the exception of the neutron porosity module, and run into the hole. A good log was recorded up from apparent hole fill at 22 m above total depth. The tool encountered resistance at the bit and could not be pulled back inside the drill string until pump circulation was initiated. Apparently, either the LFV had not been locked open by the go-devil, or passage of the logging tool had somehow unlocked it. When the logging tool had been recovered and rigged down, three stands of drill pipe were added to put the bit below the largest diameter washed-out hole and a second go-devil was deployed. The GHMT magnetic log was run after the pipe had been raised back to logging depth. The tool found a solid obstruction at 440 mbsf, and the log was recorded up from that depth. The geochemical combination was the third tool string run. Again, the tool set down at 440 mbsf. After a good log had been recorded up to the drill pipe, that tool also was stopped at the bit. Pump circulation did not solve the problem, but after about an hour of repeated attempts, the tool was pulled inside the pipe and recovered.

Logging time was running out and the risk of losing or damaging the FMS tool was considered unacceptable, so logging operations were halted. The tools were rigged down and the bit was pulled above the seafloor to end operations at Hole 926B.

Table 1. Coring summary, Site 926.

Core no.	Date (Feb. 1994)	Time (UTC)	Depth (mbsf)	Length cored (m)	Length recovered (m)	Recovery (%)
154-926A-						
1H	20	0330	0.0–4.0	4.0	3.93	98.2
2H	20	0430	4.0–13.5	9.5	9.65	101.0
3H	20	0530	13.5–23.0	9.5	9.43	99.2
4H	20	0615	23.0–32.5	9.5	9.83	103.0
5H	20	0715	32.5–42.0	9.5	9.83	103.0
6H	20	0810	42.0–51.5	9.5	10.04	105.7
7H	20	0920	51.5–61.0	9.5	9.80	103.0
8H	20	1005	61.0–70.5	9.5	9.82	103.0
9H	20	1105	70.5–80.0	9.5	10.06	105.9
10H	20	1200	80.0–89.5	9.5	9.99	105.0
11H	20	1300	89.5–99.0	9.5	9.71	102.0
12H	20	1350	99.0–108.5	9.5	9.65	101.0
13H	20	1445	108.5–118.0	9.5	9.34	98.3
14H	20	1530	118.0–127.5	9.5	9.44	99.3
15H	20	1620	127.5–137.0	9.5	9.31	98.0
16H	20	1710	137.0–146.5	9.5	9.99	105.0
17H	20	1800	146.5–156.0	9.5	9.93	104.0
18H	20	1900	156.0–165.5	9.5	9.11	95.9
19H	20	1950	165.5–175.0	9.5	10.04	105.7
20H	20	2050	175.0–184.5	9.5	9.86	104.0
21H	20	2130	184.5–194.0	9.5	9.82	103.0
22H	20	2235	194.0–203.5	9.5	9.99	105.0
23H	20	2335	203.5–213.0	9.5	9.90	104.0
24H	21	0030	213.0–222.5	9.5	10.26	108.0
25H	21	0125	222.5–232.0	9.5	10.20	107.3
26H	21	0230	232.0–241.5	9.5	9.95	105.0
27H	21	0335	241.5–251.0	9.5	10.17	107.0
28H	21	0445	251.0–260.5	9.5	9.98	105.0
29H	21	0540	260.5–270.0	9.5	10.05	105.8
30H	21	0640	270.0–279.5	9.5	9.95	105.0
31H	21	0735	279.5–289.0	9.5	10.03	105.6
32H	21	0830	289.0–298.5	9.5	9.89	104.0
33H	21	0920	298.5–308.0	9.5	8.08	85.0
34H	21	1020	308.0–317.5	9.5	10.08	106.1
35H	21	1130	317.5–327.0	9.5	7.81	82.2
Coring totals				327.0	334.92	102.4
154-926B-						
1H	21	1615	0.0–7.0	7.0	6.88	98.3
2H	21	1705	7.0–16.5	9.5	9.86	104.0
3H	21	1800	16.5–26.0	9.5	9.71	102.0
4H	21	1900	26.0–35.5	9.5	9.89	104.0
5H	21	1950	35.5–45.0	9.5	9.74	102.0
6H	21	2045	45.0–54.5	9.5	9.76	103.0
7H	21	2140	54.5–64.0	9.5	9.70	102.0
8H	21	2225	64.0–73.5	9.5	9.67	102.0
9H	21	2335	73.5–83.0	9.5	10.06	105.9
10H	22	0030	83.0–92.5	9.5	9.97	105.0
11H	22	0250	92.5–102.0	9.5	9.94	104.0
12H	22	0355	102.0–111.5	9.5	10.05	105.8
13H	22	0455	111.5–121.0	9.5	9.93	104.0
14H	22	0540	121.0–130.5	9.5	9.96	105.0
15H	22	0630	130.5–140.0	9.5	9.94	104.0
16H	22	0705	140.0–149.5	9.5	9.70	102.0
17H	22	0750	149.5–159.0	9.5	10.19	107.2
18H	22	0850	159.0–168.5	9.5	9.73	102.0
19H	22	1000	168.5–178.0	9.5	9.47	99.7
20H	22	1055	178.0–187.5	9.5	9.76	103.0
21H	22	1145	187.5–197.0	9.5	8.65	91.0
22H	22	1235	197.0–206.5	9.5	9.49	99.9
23H	22	1330	206.5–216.0	9.5	10.11	106.4
24H	22	1415	216.0–225.5	9.5	10.14	106.7
25H	22	1505	225.5–235.0	9.5	10.19	107.2
26H	22	1545	235.0–244.5	9.5	9.83	103.0
27H	22	1655	244.5–254.0	9.5	10.04	105.7
28X	22	1820	254.0–259.0	5.0	6.51	130.0
29X	22	1935	259.0–268.6	9.6	9.74	101.0
30X	22	2040	268.6–278.3	9.7	8.90	91.7
31X	22	2150	278.3–288.0	9.7	9.70	100.0
32X	22	2310	288.0–297.6	9.6	9.57	99.7
33X	23	0015	297.6–307.3	9.7	9.82	101.0
34X	23	0110	307.3–316.9	9.6	5.38	56.0
35X	23	0350	316.9–326.5	9.6	9.73	101.0
36X	23	0450	326.5–336.2	9.7	6.13	63.2
37X	23	0540	336.2–345.8	9.6	8.10	84.4
38X	23	0625	345.8–355.5	9.7	9.55	98.4
39X	23	0710	355.5–365.1	9.6	9.71	101.0
40X	23	0810	365.1–374.4	9.3	9.02	97.0
41X	23	0900	374.4–384.1	9.7	7.19	74.1
42X	23	1000	384.1–393.7	9.6	9.22	96.0
43X	23	1040	393.7–403.4	9.7	9.18	94.6
44X	23	1135	403.4–413.1	9.7	9.71	100.0
45X	23	1230	413.1–422.8	9.7	9.76	100.0
46X	23	1325	422.8–432.4	9.6	9.34	97.3
47X	23	1415	432.4–442.1	9.7	9.09	93.7
48X	23	1500	442.1–451.7	9.6	9.86	103.0
49X	23	1555	451.7–461.4	9.7	8.92	91.9
50X	23	1650	461.4–471.0	9.6	9.42	98.1
51X	23	1755	471.0–480.5	9.5	9.84	103.0
51X	23	1755	471.0–480.5	9.5	9.84	103.0
52X	23	1850	480.5–490.2	9.7	9.83	101.0
53X	23	1945	490.2–499.9	9.7	9.24	95.2
54X	23	2040	499.9–509.5	9.6	9.80	102.0
55X	23	2124	509.5–519.2	9.7	9.08	93.6
56X	23	2300	519.2–528.9	9.7	9.81	101.0
57X	24	0000	528.9–538.5	9.6	9.63	100.0
58X	24	0110	538.5–548.2	9.7	9.40	96.9
59X	24	0230	548.2–557.9	9.7	9.77	101.0
60X	24	0450	557.9–567.6	9.7	8.29	85.4
61X	24	0630	567.6–577.2	9.6	7.83	81.5
62X	24	0820	577.2–586.9	9.7	5.16	53.2
63X	24	1010	586.9–596.5	9.6	9.83	102.0
64X	24	1135	596.5–605.8	9.3	9.83	105.0
Coring totals				605.8	593.25	97.9
154-926C-						
		*****Drilled from 0.0 to 0.5 mbsf*****				
1H	26	0050	0.5–10.0	9.5	9.87	104.0
2H	26	0145	10.0–19.5	9.5	9.76	103.0
3H	26	0230	19.5–29.0	9.5	9.70	102.0
4H	26	0320	29.0–38.5	9.5	9.68	102.0
5H	26	0405	38.5–48.0	9.5	9.69	102.0
6H	26	0515	48.0–57.5	9.5	9.75	102.0
7H	26	0600	57.5–67.0	9.5	9.73	102.0
8H	26	0650	67.0–76.5	9.5	9.75	102.0
9H	26	0800	76.5–86.0	9.5	10.00	105.2
10H	26	0845	86.0–95.5	9.5	9.15	96.3
11H	26	0945	95.5–105.0	9.5	9.74	102.0
12H	26	1100	105.0–114.5	9.5	9.87	104.0
13H	26	1145	114.5–124.0	9.5	9.58	101.0
14H	26	1240	124.0–133.5	9.5	9.86	104.0
15H	26	1335	133.5–143.0	9.5	9.51	100.0
16H	26	1425	143.0–152.5	9.5	9.69	102.0
17H	26	1520	152.5–162.0	9.5	9.67	102.0
18H	26	1615	162.0–171.5	9.5	10.07	106.0
19H	26	1710	171.5–181.0	9.5	10.23	107.7
20H	26	1805	181.0–190.5	9.5	10.12	106.5
21H	26	1900	190.5–200.0	9.5	10.01	105.3
22H	26	1950	200.0–209.5	9.5	9.63	101.0
23H	26	2040	209.5–219.0	9.5	10.15	106.8
24H	26	2125	219.0–228.5	9.5	8.76	92.2
25H	26	2210	228.5–238.0	9.5	10.18	107.1
26H	26	2305	238.0–247.5	9.5	9.28	97.7
27X	27	0030	247.5–254.0	6.5	9.63	148.0
28X	27	0120	254.0–263.7	9.7	9.53	98.2
29X	27	0220	263.7–273.3	9.6	9.16	95.4
30X	27	0310	273.3–282.9	9.6	9.76	101.0
31X	27	0400	282.9–292.6	9.7	6.66	68.6
32X	27	0455	292.6–302.2	9.6	9.68	100.8
33X	27	0540	302.2–311.9	9.7	5.16	53.2
34X	27	0625	311.9–321.5	9.6	8.56	89.1
35X	27	0710	321.5–331.1	9.6	7.97	83.0
36X	27	0800	331.1–340.8	9.7	6.55	67.5
37X	27	0850	340.8–350.4	9.6	9.60	100.0
38X	27	0940	350.4–360.1	9.7	9.13	94.1
39X	27	1030	360.1–369.7	9.6	9.92	103.0
40X	27	1120	369.7–379.0	9.3	9.75	105.0
41X	27	1210	379.0–388.7	9.7	9.77	101.0
42X	27	1305	388.7–398.3	9.6	9.82	102.0
Coring totals				397.8	394.21	99.1
Drilled				0.5		
Total				398.3		

Note: UTC = Universal Time Coordinated.

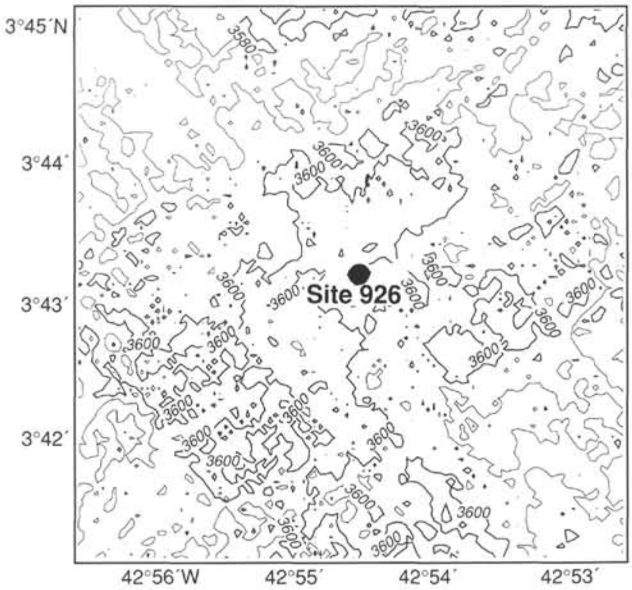

Figure 1. High-resolution swath bathymetry in the region of Site 926. The data were obtained during Cruise Ew9209 using the hydrosweep swath-mapping system. Regional bathymetric variability within several kilometers of Site 926 is less than 10 m of water depth.

Hole 926C

After a 30-m offset to the south, the APC was deployed and Core 154-926C-1H was "shot" from 3 m deeper than Core 154-926B-1H.

All APC cores were oriented. Because of fracturing disturbance noted in earlier holes, the switch to XCB coring was made after Core 154-926C-26H, well before either overpull or penetration refusal (Table 1). Coring with the XCB then continued, with over 93% average recovery, to 398 mbsf. At that point, the allotted time had expired and our scientific objectives had been fulfilled. The drill string was tripped after Core 154-926C-42X had been recovered.

At 1600 hr on 27 February, the drilling assembly was on deck, the beacons had been recovered, and preparations were in progress for departure.

LITHOSTRATIGRAPHY

Introduction

The 605-m sequence of sediment recovered from three holes drilled at Site 926 is predominantly ooze and chalk with varying amounts of nannofossils, foraminifers, and clay (Fig. 3). Minor components throughout the sequence include iron oxides and sulfides. The early Miocene interval contains minor amounts of radiolarians and diatoms. Distinct cyclic changes in color that are related to changes in the proportions of carbonate, clay minerals, and, to a lesser extent, iron oxides and sulfides, occur at decimeter to meter scales throughout the section.

Although Site 926 at a water depth of 3598 m is about 600 m deeper than Site 925, it contains a very similar sequence of lithostratigraphic units, which span the Pleistocene to the late Oligocene time interval. Unit I (0–130 mbsf) consists of Holocene to early Pliocene alternating clayey nannofossil ooze and nannofossil clay. Unit II (130–240 mbsf) consists of early Pliocene to middle Miocene nannofossil ooze with clay and foraminifers. Unit III (240–605 mbsf) consists of middle Miocene to early Oligocene nannofossil chalk with clay.

These units and their subunits, which are based on more subtle changes in lithologic character, were differentiated on the basis of visual core description, smear-slide examination, XRD analysis, and measurements of percent carbonate, reflectance spectrophotometry, and magnetic susceptibility. Each lithostratigraphic unit is described in detail in the following section.

Description of Lithostratigraphic Units

Lithologic Unit I

Intervals: Cores 154-926A-1H through -15H, Cores 154-926B-1H through -14H, Cores 154-926C-1H through -14H
Age: Holocene to early Pliocene
Depth: 0–130 mbsf

Unit I is divided into two subunits defined by variation in carbonate and clay content. Subunit IA (0–30 m) is characterized by alternating beds of light grayish brown (2.5YR 6/2) nannofossil clay with foraminifers, and grayish brown (10YR 5/2) clay with nannofossils. The cyclic color changes occur every 50 to 120 cm throughout the subunit. Subunit IB (30–130 m) is composed primarily of interbedded light gray (2.5Y 6/1) nannofossil ooze with clay and foraminifers, and gray (2.5Y 5/1) nannofossil clay with foraminifers. The transition between the subunits is marked by a distinct change in the carbonate content (see Fig. 3). Subunit IA has an average carbonate content of 30%. In Subunit IB, the carbonate content gradually increases with depth to about 70%. This increase is paralleled by an increase in the average percentage reflectance values (550 nm) and by a decrease in clay content and the magnetic susceptibility values (see Fig. 3).

One characteristic feature of Unit I is the frequent occurrence of dark gray, iron sulfide-rich horizons, including pyrite staining in thin horizontal bands and/or sparsely disseminated pyrite. In general, these horizons are adjacent to distinct thin yellow-brown color bands. This banding suggests a diagenetic origin related to diffusion gradients. Presumably, the pyrite forms as a result of diagenetic, microbial reduction of pore-water sulfate to sulfide, which combines with iron derived from clay-enriched intervals. Thus, it is likely that the yellow-brown color bands indicate diagenetic oxidation fronts.

Lithologic Unit II

Intervals: Cores 154-926A-15H through -26H, Cores 154-926B-15H through -26H, Cores 154-926C-14H through -25H
Age: early Pliocene to middle Miocene
Depth: 130–240 mbsf

Unit II consists of nannofossil ooze with varying amounts of clay and foraminifers and is early Pliocene to middle Miocene in age. The measured carbonate content fluctuates between 50% and 80%. Unit II is divided into two subunits based on variations in foraminifer abundance and is separated from Unit I above and Unit III below by its distinct brown color.

Subunit IIA (130–190 mbsf) contains interbedded light gray (2.5Y 7/2) nannofossil ooze with clay and light brownish gray (10YR 6/2) clayey nannofossil ooze. Foraminifers are rare to absent. Subunit IIB extends from 190 to 240 mbsf and consists of interbedded light gray (5Y 7/2) foraminifer nannofossil ooze with clay and brown (7.5YR 5/4) clayey nannofossil ooze.

Unit II is characterized by high ratios of the red/blue (680/420 nm) percentage reflectance and by high-amplitude variations in this ratio (Fig. 4). Millimeter-scale iron oxide color banding is common within the darker layers. Brown layers, enriched in iron oxides (5%–10%), occur predominantly in Subunit IIB and are associated with pronounced maxima in the red/blue reflectance ratio and maxima in the magnetic susceptibility data (see Fig. 3).

An interval of slumping identified in Unit II at Site 925 was not observed in Unit II at Site 926. However, three small turbidites (<30 cm thick) were identified at Site 926 (180, 186, and 219 mbsf). These turbidites consist of sand-size foraminifer ooze with nannofossils. They show sharp basal contacts, graded bedding (fining upward), and gradational, bioturbated upper contacts.

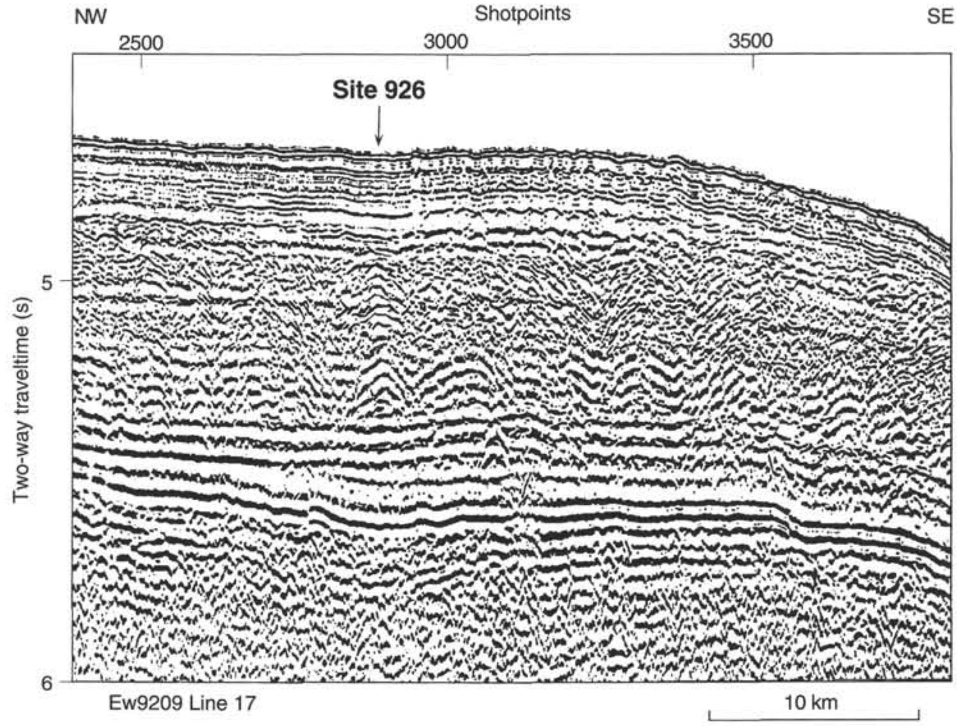

Figure 2. High-resolution, single-channel seismic record (Ew9209 Line 17) for Site 926. The data were obtained using an air-gun array (1350 cm^3, tuned to minimize the bubble pulse) during the Ew9209 site survey cruise (see "Site Survey" chapter, this volume).

Lithologic Unit III

Intervals: Cores 154-926A-26H through -35H, Cores 154-926B-26H through -64X, Cores 154-926C-26H through -42X
Age: middle Miocene to late Oligocene
Depth: 240–605 mbsf

Unit III is the thickest unit defined at Site 926, extending from the middle Miocene to the late Oligocene. It consists of light greenish gray (7.5GY 7/1) nannofossil chalk with foraminifers alternating with greenish gray (7.5GY 6/1) clayey nannofossil chalk. Carbonate content varies from 60% in the darker layers to 80% in the lighter ones. The sequence exhibits a high percentage reflectance and a persistently low magnetic susceptibility. Unit III is distinguished from Unit II by a significant color change from brown hues in the upper unit to green hues in the lower unit. This color change can also be observed by the drop in the red/blue reflectance ratio (680/420 nm) from maximum values to a ratio of about 1.0, indicating reduced sediment below this shift (see Fig. 4). In addition, the top of Unit III is marked by a drop in magnetic susceptibility, by an increase in the percentage reflectance (at 550 nm), and by the transition from ooze to chalk (defined by the increase in shear strength from 2.5 to >4.5 kg/m^2; see "Physical Properties" section, this chapter). Unit III can be divided into three subunits on the basis of the appearance of minor, but significant amounts of biosiliceous fragments, mainly radiolarians, spanning the middle interval of Unit III from 370 to 460 mbsf.

Subunit IIIA (240–370 mbsf) exhibits meter-scale cyclic changes from light gray (7.5GY 7/1) nannofossil chalk with clay to greenish gray (7.5GY 6/1) clayey nannofossil chalk. The carbonate content ranges from 80% in the light layers to 60% in the darker layers. The amount of foraminifers, which are restricted to the carbonate-rich layers, varies from 2% to 10%.

Subunit IIIB (370–460 mbsf) is similar to Subunit IIIA, with the addition of up to 15% biosiliceous fragments, predominantly radiolarians (3%–8%), with minor amounts of diatoms (0%–3%) and silicoflagellates (0%–3%). Compared to the overlying unit, there is a higher percentage of foraminifers in the carbonate-rich layers. The top of this subunit is marked by a distinct decrease in color reflectance (Fig. 3) associated with dark olive gray (5Y 4/1), clay-rich (up to 90%) layers that occur between 225 and 240 mbsf. These layers are also very low in carbonate (<5%) and mark the extreme of progressively darker horizons abruptly alternating with light layers. These sawtooth-shaped color changes are similar to changes in Unit I, which are related to late Pleistocene deglaciation events.

Subunit IIIC (460–605 mbsf) exhibits lithologies that in general vary similarly in components, color, and carbonate content to the lithologies of Subunit IIIA. The only difference is the smaller amount of foraminifers in the carbonate-rich layers found in the uppermost subunit.

In contrast to the overlying units, trace fossils are more common in Unit III. *Chondrites, Planolites, Zoophycos,* and centimeter-scale vertical burrows occur throughout the section in all lithologies. Irregular features like graded bedding, sharp contacts, displaced blocks, and microfaults have been identified in only two distinct intervals within Unit III (at 305 and 307 mbsf). These features occur as decimeter-thick beds, indicating slumps and turbidites.

Interpretation

The Holocene to Oligocene sediment record from Site 926 differs from the neighboring shallower Site 925 due to depth-dependent changes in deep-water circulation and chemistry. Because of the very short distance (50 km) separating these sites, it is appropriate to assume that the supply of both carbonate and terrigenous clay is the same at each site, and that any differences in lithology are caused by depth-related dissolution of carbonate, except for downslope transport and redeposition of sediment.

The Pleistocene to early Pliocene sections of both sites, defined as Unit I, are very similar in both lithology and thickness (135 mbsf

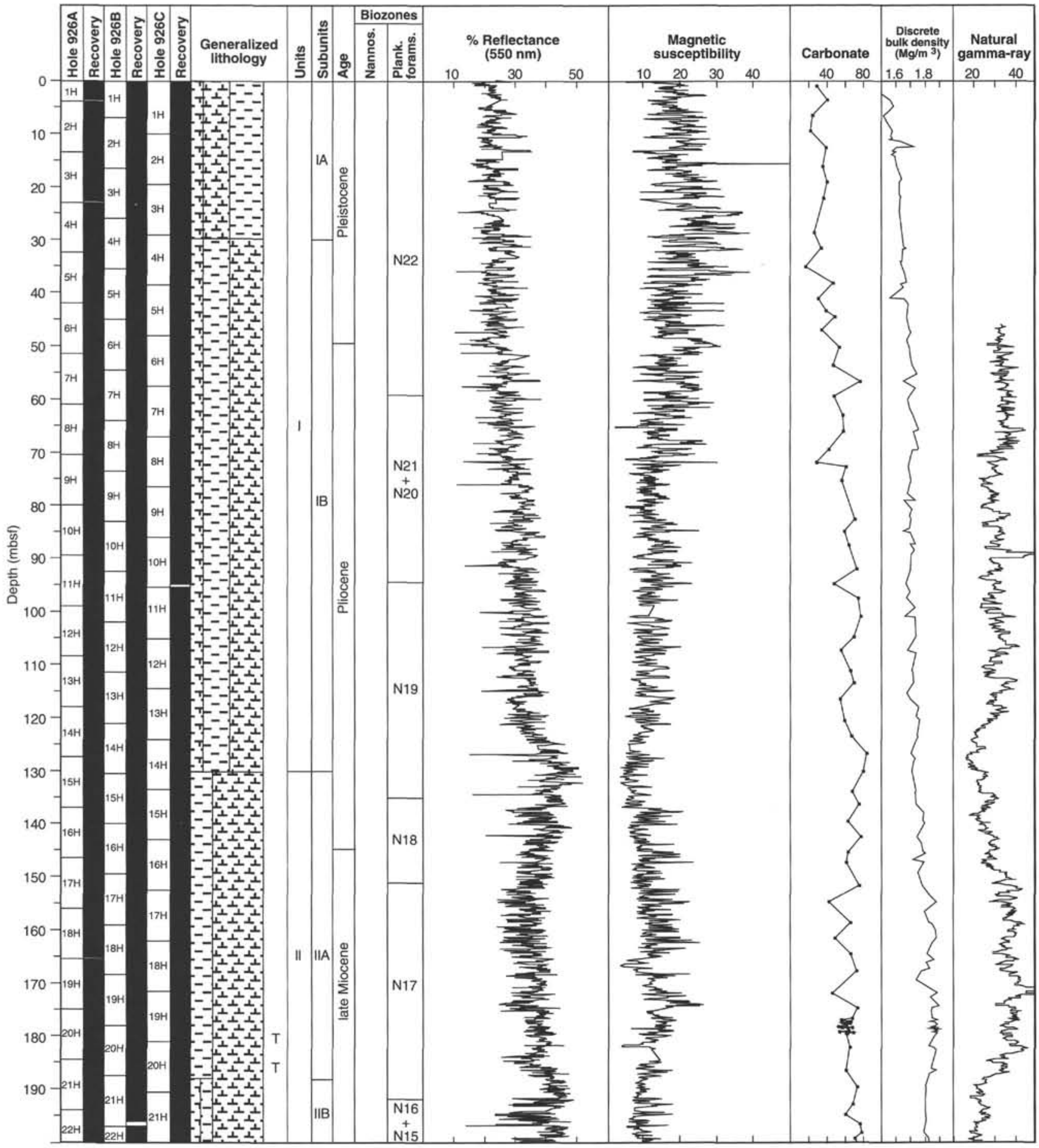

Figure 3. Core recovery, lithostratigraphy, age, biozones, percentage of reflectance (550 nm), magnetic susceptibility, carbonate content, bulk density, and natural gamma of sediments recovered at Holes 926A through 926C. Locations of slumps (S), turbidites (T), and minor, but significant amounts of biosiliceous components (radiolarians + diatoms) are shown in the column adjacent to the generalized lithostratigraphy. Percentage reflectance and magnetic susceptibility are from Hole 926B.

at Site 925 and 130 mbsf at Site 926). This is also apparent in their similar patterns of the downward-increasing percentage of reflectance and decreasing susceptibility data. The average carbonate contents of Subunit IA (33% vs. 32%) and Subunit IB (61% vs. 56%) indicate the deeper site to be only slightly more affected by dissolution. This suggests that the lysocline in the equatorial Atlantic remained well below 3600 m not only during the late Pleistocene to Holocene (Curry and Lohmann, 1990) but also for the early Pleistocene and most of the Pliocene.

Major differences between the two sites occur in the late to early Miocene interval of Unit II, which extends 50 m further down at the shallower site (290 mbsf at Site 925 and 240 mbsf at Site 926). The average carbonate content is about 8% lower at the deeper site (72% vs. 64%). The average values in magnetic susceptibility, and in the ratio of red to blue reflectance (Fig. 4) are about one third higher at deeper Site 926 than at Site 925, revealing less carbonate dilution of the terrigenous components, including iron oxides. In addition, foraminifers are less common in Subunit IIA at Site 926 than in the

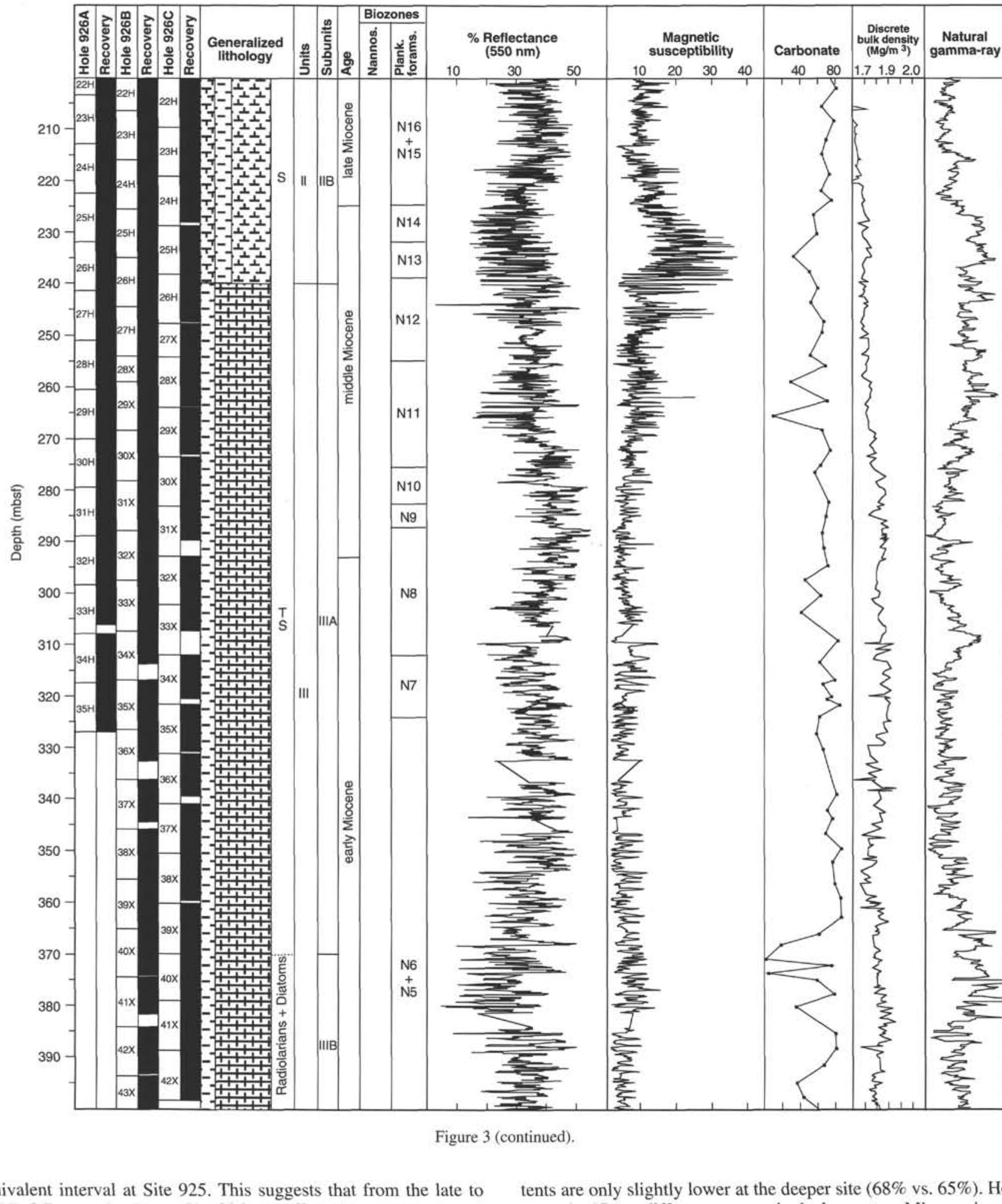

Figure 3 (continued).

equivalent interval at Site 925. This suggests that from the late to middle Miocene the deeper Site 926 was affected to a greater extent by carbonate dissolution. About 10–15 m of the greater thickness of Unit II at Site 925 can be attributed to downslope transport and redeposition of sediment, whereas only two thin turbidites were observed at Site 926. Thus, dissolution may be responsible for 35–40 m of thinning in Unit II at Site 926.

The top of the middle Miocene to late Oligocene interval of Unit III is marked at both sites by the apparent transition from ooze to chalk and occurs in strata with an age of about 11.5 Ma. The overall composition of the sediments is similar, and the average carbonate contents are only slightly lower at the deeper site (68% vs. 65%). However, significant differences occur in the lowermost Miocene interval from 19 to 24 Ma, where small amounts (up to 15%) of biosiliceous components appear at Site 926 (Subunit IIIB). Because almost no difference was observed in the carbonate content at both sites, as well as no difference in the amplitude variations of the magnetic susceptibility, the occurrence of biogenic opal with increasing water depth might be related to changes in deep-water chemistry (silica solubility) rather than to increased carbonate dissolution and therefore lower dilution of biosiliceous components. Evidence for increased opal preservation in the lowermost Miocene (19–24 Ma) exists also in the

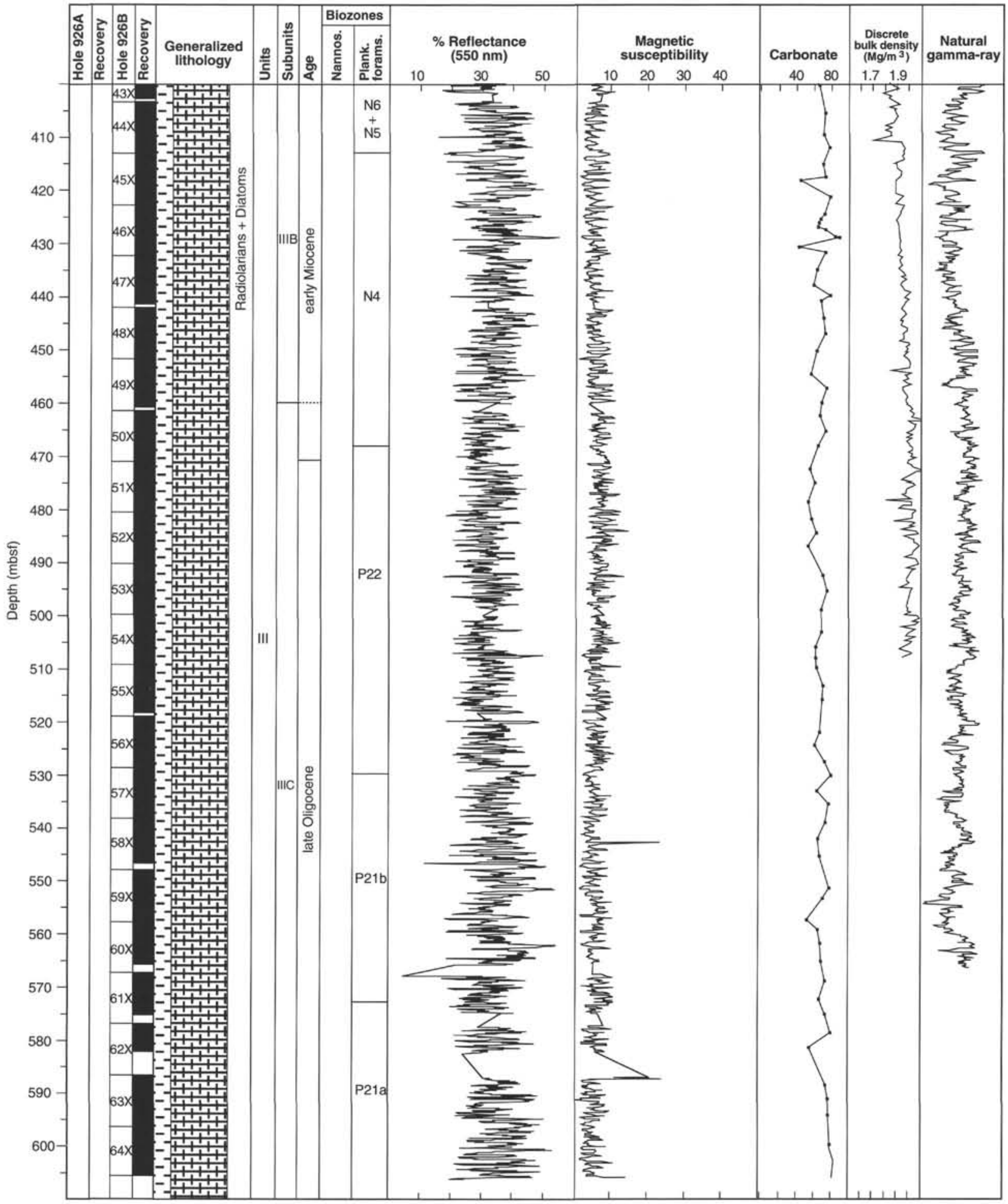

Figure 3 (continued).

eastern equatorial Atlantic (ODP Site 667, Ruddiman et al., 1988) and the northern Atlantic (DSDP Site 610, Baldauf, 1987). Wright et al. (1992) attribute this occurrence of opal in the deep Atlantic to an interval of little to no Northern Component Water production, consistent with deep-water circulation patterns reconstructed using $\delta^{13}C$ of benthic foraminifers.

In summary, the differences in the lithology at Sites 925 and 926 are generally small. However, the sediment records of the late and early Miocene provide preliminary evidence for long-term changes in the deep-water circulation and chemistry at the Ceara Rise.

BIOSTRATIGRAPHY

Introduction

Site 926 is the southernmost site on Leg 154. It is located on the southeastern flank of the Ceara Rise at 3°43.15′N, 42°54.50′W, and

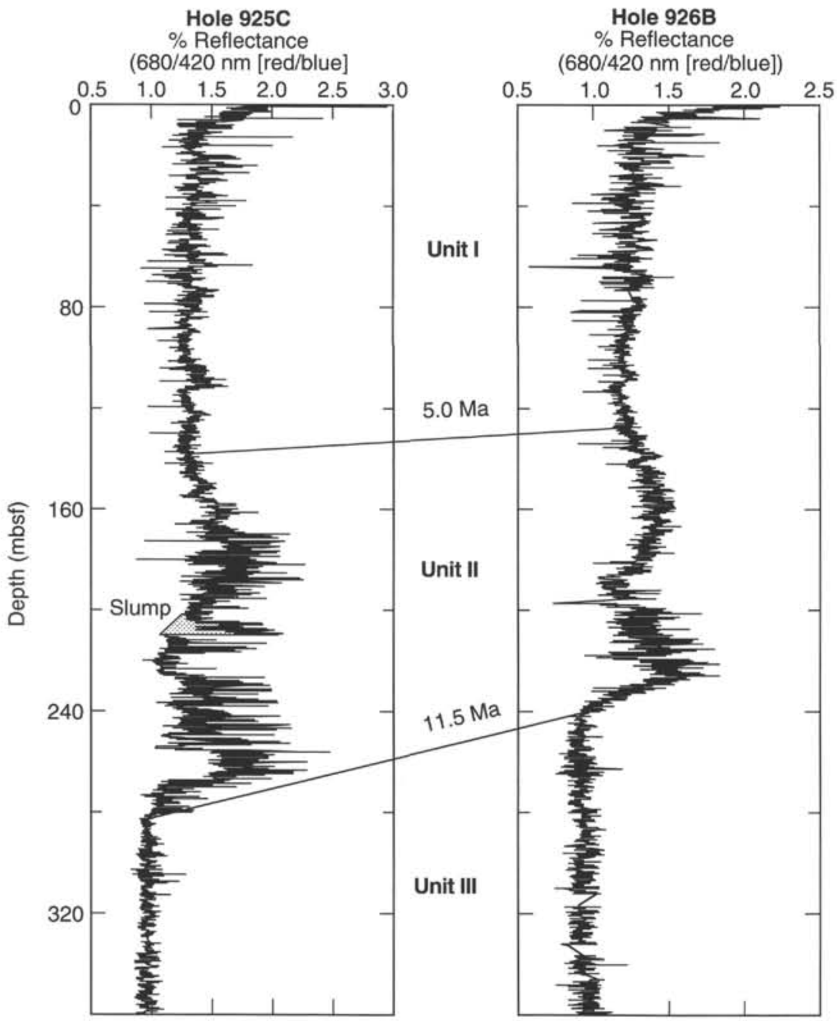

Figure 4. Ratio of percentage of reflectance at 680 nm (red) to 420 nm (blue) vs. depth in Holes 925C and 926B. Iron-oxide and oxyhydroxide layers are emphasized by this ratio, particularly in Unit II.

3598 m water depth. Hole 926B is the deepest of the three holes drilled at this site, penetrating to 605.7 mbsf. Biostratigraphic control was provided by analyses of calcareous nannoplankton and planktonic foraminifers. Faunal assemblage changes in benthic foraminifers were also studied. No hiatuses were detected at Site 926.

The cyclic variations in physical properties that were apparent in the sediments at Site 925 are also evident at Site 926. The pattern of preservation at Site 926 is similar to that of Site 925, but the effect of dissolution on planktonic foraminifers and calcareous nannoplankton is slightly greater, as would be expected with increased water depth. Variations in preservation state correspond to variations in the physical properties: preservation is less good in the darker layers.

Calcareous Nannofossils

Calcareous nannofossils are abundant throughout the sediments cored at Site 926, as indicated by the investigation of over 600 smear slides. Most samples show signs of dissolution. The most enhanced dissolution was observed in middle Miocene and upper lower Miocene assemblages. Oligocene and lower Miocene discoasters are generally overgrown with secondary calcite. The biostratigraphic resolution offered by nannofossils indicates that the continuously cored sections at Site 926 are complete. The core-catcher samples of the mud-line cores in two of the three holes showed upper Pleistocene assemblages belonging to Zone CN15. An exception occurs in Hole 926C, which contained upper Pleistocene assemblages belonging to Subzone CN14b, above the range of *Pseudoemiliania lacunosa* but below the range of *Emiliania huxleyi*. The bottom of Hole 926A can be correlated to the short interval between the top of *Sphenolithus belemnos* and the base of *Sphenolithus heteromorphus;* that is, virtually at the CN2/CN3 zonal boundary. The bottom of the deepest hole (926B) can be correlated to the rather poorly constrained and long Zone CP18 in the lower Oligocene, with the absence of *Sphenolithus distentus, Sphenolithus predistentus,* and *Reticulofenestra umbilicus.* The bottom of Hole 926C can be correlated to the long Zone CN1 of the lower Miocene, below the range of *S. belemnos,* but within the range of *Triquetrorhabdulus carinatus* and above the range of Oligocene sphenoliths.

The results from the detailed biostratigraphic investigations of the calcareous nannofossils are presented in Table 2 and Figure 5. Most nannofossil events in Holes 926A and 926B were determined to within 0.4–0.8 m. Hole 926C was chiefly investigated by means of core-catcher samples.

Pleistocene–Pliocene

Pleistocene assemblages are virtually identical in composition and gross abundance relationships to those observed at Site 925 (approximately 600 m shallower). The whole suite of Pleistocene events based on changes in the size of *Gephyrocapsa* was recovered, as was the suite of late and middle Pliocene discoaster extinctions. However, *Discoaster pentaradiatus, Discoaster surculus,* and *Discoaster tamalis* are rare in the uppermost parts of their ranges, suggesting that better resolved, quantitative studies are needed to improve our understanding of their abundance relationships in the critical final parts of their ranges in the Ceara Rise region. Rare, presumably indigenous, occurrences of

Table 2. Calcareous nannoplankton events in Holes 926A, 926B and 926C.

Events	Age (Ma)	Sample ID (top to bottom)	Depth (mbsf)	Mean depth (mbsf)	Depth (mcd)	Mean depth (mcd)
Hole 926A:						
B *Emiliania huxleyi*	0.26	1H-CC to 2H-CC	3.93–13.65	8.79	3.99–15.95	9.97
T *Pseudoemiliania lacunosa*	0.46	3H-1, 120 to 3H-2, 40	14.70–15.40	15.05	15.79–16.49	16.14
Reentrance medium *Gephyrocapsa* spp.	1.03	4H-6, 115 to 4H-7, 40	31.65–32.40	32.02	34.23–34.98	34.60
T large *Gephyrocapsa* spp.	1.24	4H-CC to 5H-3, 120	32.83–36.70	34.76	35.41–40.11	37.76
B large *Gephyrocapsa* spp.	1.46	5H-6, 120 to 5H-CC	41.20–42.33	41.75	44.61–45.74	45.18
T *Calcidiscus macintyrei*	1.60	6H-3, 80 to 6H-3, 120	45.80–46.20	46.00	49.87–50.27	50.07
B medium *Gephyrocapsa* spp.	1.67	6H-4, 120 to 6H-5, 40	47.70–48.40	48.05	51.77–52.47	52.12
T *Discoaster brouweri*	1.95	7H-2, 80 to 7H-2, 120	53.80–54.20	54.00	60.33–60.73	60.53
B acme *Discoaster triradiatus*	2.15	7H-6, 80 to 7H-7, 10	59.80–60.60	60.20	66.43–67.13	66.73
T *Discoaster pentaradiatus*	2.44	8H-3, 124 to 8H-4, 80	65.24–66.30	65.77	73.29–74.23	73.86
T *Discoaster tamalis*	2.76	9H-4, 80 to 9H-CC	75.80–80.56	77.90	85.30–90.05	87.72
T *Sphenolithus spp.*	3.62	11H-CC to 12H-5, 80	99.21–105.80	102.51	111.26–118.16	114.71
T *Reticulofenestra pseudoumbilicus*	3.77	12H-5, 80 to 12H-5, 120	105.80–106.20	106.00	118.26–118.56	118.36
B *Ceratolithus rugosus*	5.04	15H-7, 40 to 15H-CC	136.40–136.86	136.63	153.20–153.80	153.44
T *Ceratolithus acutus*	5.04	15H-CC to 16H-1, 40	136.86–137.40	137.13	153.67–155.36	154.51
T *Triquetrorhabdulus rugosus*	5.34	16H-4, 80 to 6H-4, 120	142.30–142.70	142.50	160.26–160.66	160.46
B *Ceratolithus acutus*	5.34	16H-5, 80 to 16H-5, 120	143.80–144.20	144.00	161.76–162.16	161.96
T *Discoaster quinqueramus*	5.56	16H-CC to 17-1, 80	147.04–147.30	147.17	165.00–166.28	165.64
T *Amaurolithus amplificus*	5.88	17H-7, 40 to 17H-CC	155.90–156.48	156.17	174.88–175.46	175.17
B *Amaurolithus amplificus*	6.5	19H-3, 83 to 19H to 4, 83	169.33–170.83	170.08	190.47–191.97	191.22
B *Amaurolithus primus*	7.3	20H-1, 80 to 20H-3, 80	175.80–178.80	177.30	197.78–200.78	199.28
B *Discoaster berggrenii*	8.4	22H-1, 80 to 22H-1, 120	194.80–195.20	195.00	217.52–217.92	217.72
T *Catinaster calyculus*	9.36	23H-CC to 24H-1, 40	213.41–213.40	213.41	237.47–238.00	237.74
T *Discoaster hamatus*	9.4	23H-CC to 24H-1, 80	213.41–213.80	213.40	237.47–238.40	237.94
B *Discoaster hamatus*	10.4	25H-1, 80 to 25H-1, 122	223.30–223.72	223.51	249.15–249.57	249.36
B *Catinaster coalitus*	10.7	25H-4, 80 to 25H-4, 120	227.80–228.20	228.00	253.65–254.05	253.85
T *Coccolithus miopelagicus*	10.4	25H-5, 120 to 25H-6, 20	229.70–230.20	229.95	255.55–256.05	255.80
Tc *Discoaster kugleri*	11.3	26H-2, 40 to 26H-2, 120	233.90–234.70	234.30	262.26–263.06	262.66
Bc *Discoaster kugleri*	11.7	26H-4, 120 to 26H-5, 40	237.70–238.40	238.05	266.06–266.76	266.41
Tc *Cyclicargolithus floridanus*	13.2	28H-6, 119 to 28H-CC	259.69–261.01	260.39	288.88–290.20	289.54
T *Sphenolithus heteromorphus*	13.6	29H-4, 40 to 29H-4, 80	265.40–265.80	265.60	294.11–294.51	294.31
T *Helicosphaera ampliaperta*	15.8	32H-2, 40 to 32H-3, 40	290.90–292.40	291.65	319.46–320.96	320.21
T abundant *Discoaster deflandrei*	16.2	33H-2, 120 to 33H-3, 120	301.20–302.70	301.95	330.30–331.80	331.05
B *Sphenolithus heteromorphus*	18.1	34H-CC to 35H-1, 120	318.05–318.70	318.38	347.15–349.01	348.08
Hole 926B:						
B *Emiliania huxleyi*	0.26	1H-CC to 2H-CC	6.88–16.86	11.87	6.88–18.31	12.60
T *Pseudoemiliania lacunosa*	0.46	2H-6, 1 to 2H-6, 80	14.51–15.30	14.90	15.96–16.75	16.35
Reentrance medium *Gephyrocapsa* spp.	1.03	3H-CC to 4H-CC	26.21–35.89	31.05	28.62–39.12	33.87
T large *Gephyrocapsa* spp.	1.24	4H-CC to 5H-CC	35.89–45.24	40.57	39.12–49.70	44.41
B large *Gephyrocapsa* spp.	1.46	4H-CC to 5H-CC	35.89–45.24	40.57	39.12–49.70	44.41
T *Calcidiscus macintyrei*	1.60	4H-CC to 5H-CC	35.89–45.24	40.57	39.12–49.70	44.41
B medium *Gephyrocapsa* spp.	1.67	5H-CC to 6H-CC	45.24–54.76	50.00	49.70–60.71	55.21
T *Discoaster brouweri*	1.95	6H-CC to 7H-CC	54.76–64.20	59.48	60.71–70.82	65.77
B acme *Discoaster triradiatus*	2.15	6H-CC to 7H-CC	54.76–64.20	59.48	60.71–70.82	65.77
T *Discoaster pentaradiatus*	2.44	7H-CC to 8H-CC	64.20–73.67	68.94	70.82–81.95	76.39
T *Discoaster tamalis*	2.76	8H-CC to 9H-CC	73.67–83.56	78.62	81.95–92.55	87.25
T *Sphenolithus* spp.	3.62	10H-CC to 11H-CC	92.97–102.47	97.72	104.77–114.31	109.54
T *Reticulofenestra pseudoumbilicus*	3.77	12H-3, 120 to 12H-4, 40	106.20–106.90	106.55	118.70–119.40	119.05
B *Ceratolithus rugosus*	5.04	15H-6, 40 to 15H-6, 80	138.40–138.80	138.60	155.27–155.67	155.47
T *Triquetrorhabdulus rugosus*	5.34	15H-CC to 16H-4, 120	140.45–145.70	143.08	157.32–164.04	160.68
B *Ceratolithus acutus*	5.34	15H-CC to 16H-4, 120	140.45–145.70	143.08	157.32–164.04	160.68
T *Discoaster quinqueramus*	5.56	16H-5, 120 to 16H-6, 40	147.20–147.90	147.55	165.54–166.24	165.89
T *Amaurolithus amplificus*	5.88	17H-5, 40 to 17H-5, 120	155.90–156.70	155.30	175.37–176.17	175.77
B *Amaurolithus amplificus*	6.5	18H-C to 19H-2, 40	168.78–170.40	169.59	188.82–191.74	190.28
B *Amaurolithus primus*	7.3	19H-CC to 20H-1, 20	177.97–178.20	178.13	199.31–200.89	200.10
Bc *Discoaster surculus*	7.8	20H-4, 40 to 20H-4, 80	182.90–183.30	183.10	205.59–205.99	205.79
B *Discoaster berggrenii*	8.4	21H-CC to 22H-1, 80	196.15–197.80	196.98	218.34–220.16	219.25
T *Catinaster calyculus*	9.36	23H-5, 120 to 23H-6, 40	213.70–214.40	214.05	238.27–239.00	238.65
T *Discoaster hamatus*	9.4	23H-5, 120 to 23H-6, 40	213.70–214.40	214.05	238.30–238.97	238.62
B *Discoaster hamatus*	10.4	24H-6, 40 to 24H-6, 80	223.90–224.30	224.10	249.42–249.82	249.62
B *Catinaster coalitus*	10.7	25H-2, 40 to 25H-2, 80	227.40–227.80	227.60	253.41–253.81	253.61
T *Coccolithus miopelagicus*	10.4	25H-4, 80 to 25H-4, 120	230.80–231.20	231.00	256.81–257.21	257.01
Tc *Discoaster kugleri*	11.3	25H-6, 120 to 25H-7, 40	234.20–234.90	234.55	260.21–260.91	260.56
Bc *Discoaster kugleri*	11.7	26H-2, 120 to 26H-2, 147	237.70–237.97	237.83	265.97–266.24	266.11
Tc *Cyclicargolithus floridanus*	13.2	28X-4, 120 to 28X-5, 20	259.70–260.20	259.95	288.91–289.41	289.16
T *Sphenolithus heteromorphus*	13.6	29X-4, 40 to 29X-4, 120	263.90–264.70	264.30	293.71–294.51	294.11
T *Helicosphaera ampliaperta*	15.8	32X-1, 40 to 32X-1, 80	288.40–288.80	288.60	318.21–318.61	318.41
T abundant *Discoaster deflandrei*	16.2	33X-5, 120 to 33X-CC	304.80–307.45	306.13	334.61–337.26	335.94
B *Sphenolithus heteromorphus*	18.1	34X-CC to 35X-1, 40	312.64–317.30	314.97	342.45–347.11	344.78
T *Sphenolithus belemnos*	18.4	35X-4, 120 to 35X-5, 40	322.60–323.30	322.95	352.41–353.11	352.76
B *Sphenolithus belemnos*	19.7	38X-5, 120 to 38X-6, 80	353.00–354.10	353.55	382.81–383.91	383.36
T *Sphenolithus delphix*	23.7	50X-6, 80 to 50X-6, 110	469.70–470.00	469.85	499.51–499.81	499.66
B *Sphenolithus delphix*	24.4	51X-1, 120 to 51X-2, 40	472.20–472.90	472.55	502.01–502.71	502.36
T *Sphenolithus ciperoensis*	24.7	53X-4, 72 to 53X-CC	495.42–499.43	497.43	525.23–529.24	527.24
T *Cyclicargolithus abisectus* >10μm		54X-6, 40 to 54X-6, 100	507.80–508.40	508.10	537.61–538.21	537.91
T *Sphenolithus distentus*	26.5	60X-CC to 61X-CC	566.15–575.44	570.80	595.96–605.25	600.61
Hole 926C:						
T *Pseudoemiliania lacunosa*	0.46	1H-CC to 2H-CC	10.37–19.76	15.07	12.55–23.17	17.86
Reentrance medium *Gephyrocapsa* spp.	1.03	3H-CC to 4H-CC	29.20–38.68	33.94	32.97–42.42	37.70
T large *Gephyrocapsa* spp.	1.24	3H-CC to 4H-CC	29.20–38.68	33.94	32.97–42.42	37.70
B large *Gephyrocapsa* spp.	1.46	4H-CC to 5H-CC	38.68–48.19	43.44	42.42–52.57	47.50
T *Calcidiscus macintyrei*	1.60	4H-CC to 5H-CC	38.68–48.19	43.44	42.42–52.57	47.50
B medium *Gephyrocapsa* spp.	1.67	4H-CC to 5H-CC	38.68–48.19	43.44	42.42–52.57	47.50
T *Discoaster brouweri*	1.95	5H-CC to 6H-CC	48.19–57.75	52.97	52.57–63.38	57.98
B acme *Discoaster triradiatus*	2.15	6H-CC to 7H-CC	57.75–67.23	62.49	63.38–72.47	67.93

Table 2 (continued).

Events	Age (Ma)	Sample ID (top to bottom)	Depth (mbsf)	Mean depth (mbsf)	Depth (mcd)	Mean depth (mcd)
T *Discoaster pentaradiatus*	2.44	8H-1, 40 to 8H-1, 120	67.40–68.20	67.80	73.92–74.72	74.32
T *Discoaster surculus*	2.61	8H-4, 60 to 8H-4, 110	72.10–72.60	72.35	78.62–79.12	78.87
T *Discoaster tamalis*	2.76	9H-2, 60 to 9H-2, 110	78.60–79.10	78.85	86.57–87.07	86.83
T *Sphenolithus* spp.	3.62	10H-CC to 11H-CC	95.15–105.20	100.18	115.67–103.96	109.82
T *Reticulofenestra pseudoumbilicus*	3.77	11H-CC to 12H-CC	105.20–114.91	110.10	115.67–127.52	121.60
B *Ceratolithus rugosus*	5.04	14H-CC to 15H-CC	133.98–142.99	138.49	160.44–150.17	155.31
T *Triquetrorhabdulus rugosus*	5.34	15H-CC to 16H-CC	142.99–152.70	147.85	160.44–171.36	165.90
B *Ceratolithus acutus*	5.34	15H-CC to 16H-CC	142.99–152.70	147.85	160.44–171.36	165.90
T *Discoaster quinqueramus*	5.56	16H-CC to 17H-CC	152.70–162.17	157.44	171.36–181.90	176.63
T *Amaurolithus amplificus*	5.88	16H-CC to 17H-CC	152.70–162.17	157.44	171.36–181.90	176.63
B *Amaurolithus amplificus*	6.5	18H-CC to 19H-CC	172.12–181.77	176.95	191.61–201.84	196.73
B *Amaurolithus primus*	7.3	18H-CC to 19H-CC	172.12–181.77	176.95	191.61–201.84	196.73
B *Discoaster berggrenii*	8.4	21H-CC to 22H-2, 60	200.54–202.10	201.32	217.85–219.18	218.52
T *Catinaster calyculus*	9.36	23H-CC to 24H-CC	219.64–227.73	223.69	237.61–246.64	242.13
T *Discoaster hamatus*	9.4	23H-CC to 24H-CC	219.64–227.73	223.69	237.61–246.64	242.13
B *Discoaster hamatus*	10.4	25H-1, 40 to 25H-1, 120	228.90–229.70	229.30	249.18–249.98	249.58
B *Catinaster coalitus*	10.7	25H-3, 120 to 25H-4, 40	232.70–233.40	233.05	252.98–253.68	253.33
T *Coccolithus miopelagicus*	10.4	25H-4, 40 to 25H-4, 120	233.40–234.20	233.80	253.68–254.48	254.08
Tc *Discoaster kugleri*	11.3	26H-2, 40 to 26H-2, 120	239.90–240.70	240.30	262.53–263.33	262.93
Bc *Discoaster kugleri*	11.7	26H-4, 40 to 26H-4, 120	242.90–243.70	243.30	265.53–266.33	265.93
Tc *Cyclicargolithus floridanus*	13.2	27X-CC to 28X-CC	257.15–263.55	260.35	279.83–288.89	284.36
T *Sphenolithus heteromorphus*	13.6	28X-CC to 29X-CC	263.55–272.91	268.23	288.89–298.19	293.54
T *Helicosphaera ampliaperta*	15.8	31X-CC to 32X-CC	289.60–302.25	295.93	315.20–328.96	322.08
T abundant *Discoaster deflandrei*	16.2	32X-CC to 33X-CC	302.25–307.36	304.81	328.96–335.11	332.04
B *Sphenolithus heteromorphus*	18.1	34X-CC to 35X-CC	320.44–329.47	324.96	346.04–356.08	351.06
T *Sphenolithus belemnos*	18.4	34X-CC to 35X-CC	320.44–329.47	324.96	346.04–356.08	351.06
B *Sphenolithus belemnos*	19.7	36X-CC to 37X-CC	337.67–350.44	344.06	362.57–376.62	369.60

Notes: T = top, B = base, Bc = base common, and Tc = top common. Medium size defined as 4.0–5.5 µm.

Discoaster asymmetricus were observed above the top of *D. pentaradiatus,* contrary to the relationship that has been reported in other regions.

Small (2–4 µm) placoliths with open and/or closed central areas are generally abundant in the middle Pliocene, and they occupy a very large part of the total assemblage in the lower Pliocene (e.g., Sample 154-926B-15H-3, 80 cm). The *Sphenolithus abies/Sphenolithus neoabies* group is the next most abundant form in the lower Pliocene assemblages. The lower lower Pliocene evolution of *Triquetrorhabdulus rugosus* into *Ceratolithus acutus* (associated with odd-looking morphotypes of the former and the presence of the rather bizarre *Ceratolithus atlanticus* in the transition interval) was observed in Core 154-926A-16H. *Ceratolithus armatus* was observed in Sample 154-926A-15H-CC, which lies immediately below the range of *Ceratolithus rugosus.*

Miocene

Small reticulofenestrids, presumably *Reticulofenestra minuta,* are present in exceptionally high abundances at about the upper Miocene levels near the FO of *Amaurolithus primus.* Again, sphenoliths also show markedly high relative abundances together with the small placoliths. The absence interval, or paracme, of *Reticulofenestra pseudoumbilicus* was observed in the middle–upper Miocene transition, in Cores 154-926A-20H through -22H. This absence interval occurred approximately concurrently in all three tropical and subtropical oceans (Rio et al., 1990; Young, 1990; Takayama, 1993; Raffi et al., in press).

The middle and upper Miocene discoaster assemblages are rich in morphotypes and make up a large part of the total nannofossil assemblages. Many forms intergrade between end-member morphologies. Six-rayed forms with bifurcated ray tips were dominant in the middle Miocene ("*Discoaster variabilis*" group) and showed a very large number of forms. All distinctive five- and six-rayed species showed aberrant three- and four-rayed forms, and occasionally asymmetrically arranged five-rayed forms. This variability in ray arrangement also occurred in the *Discoaster brouweri* lineage in the middle and late Pliocene.

The range of common *Discoaster kugleri* (about 1–2 specimens per field of view at ×1000 at a particle density of approximately 100–300 specimens per field of view, or about 1%–10% of the total discoaster assemblage), provides a distinct biostratigraphic event. The FO and LO of *D. kugleri* could not be consistently determined. At Site 926, the entire range of the common interval occurred within a single core (the interval spans about 0.4 m.y.) (Table 2), with beautifully developed specimens in Sample 154-926A-26H-3, 120 cm.

The LO of *Coronocyclus nitescens* is a poor marker because of low abundances in the final part of its range. The top of *Cyclicargolithus floridanus,* which also occurred between the base of common *D. kugleri* and the top of *Sphenolithus heteromorphus,* is distinct in terms of relative abundance pattern, but not as sharp as the LO of *S. heteromorphus.* This species is represented by relatively smaller specimens with a thinner apical spine in the lowermost part of its range.

The LO of *Helicosphaera ampliaperta* approximates the lower/middle Miocene boundary. Another bloomlike occurrence of small placoliths (*R. minuta*) was observed in Sample 154-926B-31X-6, 121 cm, shortly above the LO of *H. ampliaperta.*

Biogenic silica from radiolarians and diatoms was observed in several cores in the lower part of the range of *S. heteromorphus* (e.g., Cores 154-926B-34X and 154-926A-35H). The upper and lower limits of the range of *Sphenolithus belemnos* provided distinct events. At present, it is difficult to subdivide the lower Miocene and uppermost Oligocene interval between the FO of *S. belemnos* and the LO of *Sphenolithus ciperoensis,* owing partly to a lack of distinct nannofossil events. This interval represents about 5 m.y., equal to the total duration of the Pliocene and Pleistocene epochs.

At Site 926, the LO of *Triquetrorhabdulus carinatus* was observed in Core 154-926C-39X, approximately three cores below the lower limit of *S. belemnos.* Rio et al. (1990) and Fornaciari et al. (1990) showed that *Sphenolithus delphix* has a short distinct range across the Oligocene/Miocene boundary, perhaps encompassing a time interval of about 0.7 m.y. This species was observed in Sections 154-926B-50X-6 through -51X-1. These preliminary results, and the sedimentation rates established in the pertinent interval, suggest a considerably shorter duration of the range of *S. delphix* at the Ceara Rise, on the order of 0.1–0.2 m.y.

Oligocene

Helicosphaera truempyi was common and *Dictyococcites hesslandii* (e.g., in Sample 154-926B-60X-CC) was abundant in some Oligocene samples, in contrast to the marker *S. ciperoensis.* The LO of

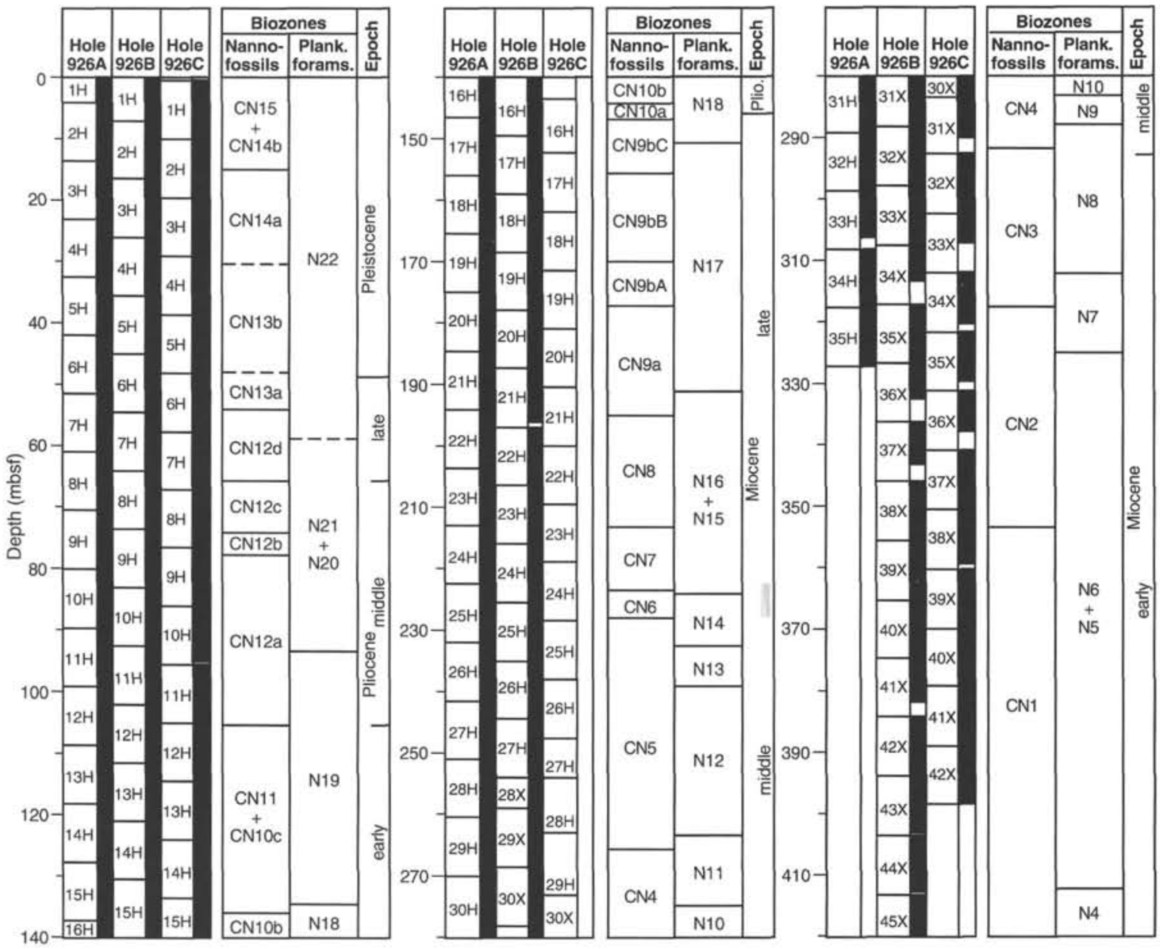

Figure 5. Calcareous nannoplankton and planktonic foraminifer biozonations for Site 926. Note that depths are given in meters below seafloor (mbsf). Stippling indicates uncertainty in placement of epoch boundary.

this species offered a poor event in Site 926 sediments because of its rarity. Its small size also contributed to the problems encountered when trying to follow the final part of its range. Consequently, we are not confident that the LO of *S. ciperoensis* observed between Samples 154-926B-53X-CC and -53X-4, 73 cm, actually represents the extinction event; the extinction may be located slightly higher, but presumably below the lower limit of *S. delphix* in Section 154-926B-51X-1.

The LO of the Oligocene marker *Sphenolithus distentus* was tentatively placed in Core 154-926B-61X. This event is calibrated to magnetostratigraphy in the mid-latitude South Atlantic DSDP Site 522 (Olafsson and Villa, 1992). The preliminary sedimentation rates established at Sites 925 and 926, however, suggest that if the sedimentation rate for the Ceara Rise sites is constant *S. distentus* disappears about 1–2 m.y. earlier in the Ceara Rise region than at Site 522.

Planktonic Foraminifers

Planktonic foraminifers were studied in the Holocene to middle Miocene interval of Hole 926A and in the middle Miocene to Oligocene interval of Hole 926B. Additional samples were also studied from Hole 926C to help in the construction of a composite section. Most planktonic foraminifer datums were constrained to within approximately 1.5 m (one section). Lists of planktonic foraminifer datums from Holes 926A, 926B, and 926C are given in Table 3. Zonal assignments are summarized in Figure 5.

As expected, the biostratigraphy of planktonic foraminifers is similar to that observed at Site 925. Apparent differences in sedimentation rates between the two sites are discussed in the "Sedimentation Rates" section (this chapter). Preservation of planktonic foraminifers is variable, as at Site 925. In general, dissolution is more severe than at Site 925. Dissolution has reduced the number of datums we were able to recognize, particularly for the earliest Miocene.

Pliocene and Pleistocene

At Site 926, a small overlap exists in the ranges of *Pulleniatina finalis* and *Globigerinoides fistulosus*. The FO of *P. finalis* is between Samples 154-926A-7H-4, 70–72 cm, and -7H-5, 70–72 cm. This is considerably lower than the expected level based on the age estimate given by Berggren et al. (1985), which was ultimately derived from the observations of Hays et al. (1969) in the equatorial Pacific Ocean (see also Chaisson and Leckie, 1993; Pearson, in press). It is similar, however, to our determination at Site 925, where an overlap of *P. finalis* and *G. fistulosus* was also recorded. Thus, it seems that the *P. finalis* morphotype appeared earlier in the Ceara Rise region than in the equatorial Pacific (see comments on *Pulleniatina* morphology in the "Biostratigraphy" section, "Site 925" chapter, this volume). Our observations from Sites 925 and 926 suggest a local first appearance of *P. finalis* at about 2.05 Ma, not 1.4 Ma as given in the "Explanatory Notes" chapter following Berggren et al. (1985). Note also that at Sites 925 and 926, the appearance of *P. finalis* occurs directly above an interval in which *Pulleniatina* is absent.

Weaver and Raymo (1989) observed "*Globorotalia triangula*" at ODP Sites 662, 663, and 664 within the Benguela Current, which was an area of divergence and upwelling during the Pliocene and Pleistocene. They did not, however, record it at sites north of this region. This

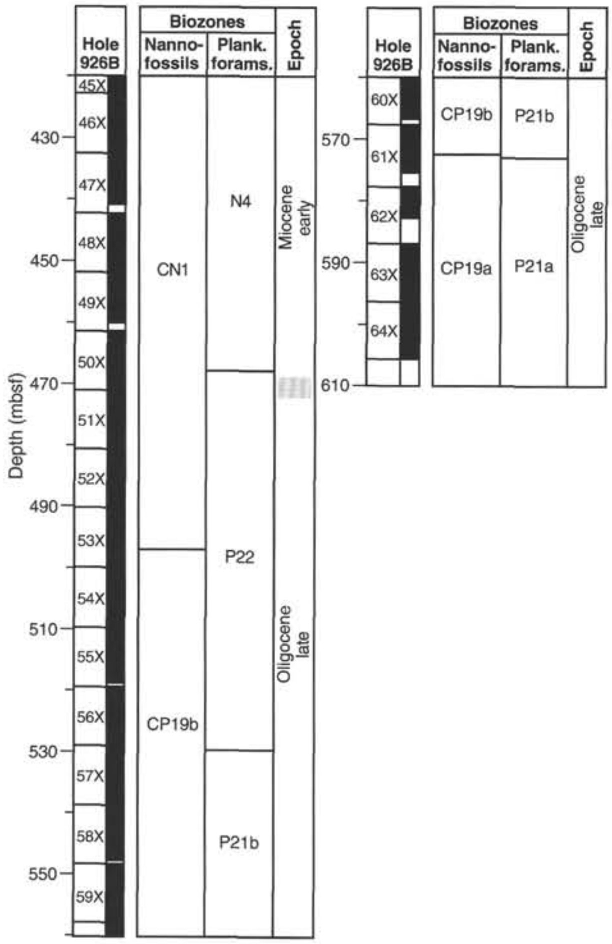

Figure 5 (continued).

morphotype combines the flat spiral and conate umbilical sides that characterize the truncorotaliids with the thick cortex and final whorl composed of three chambers that distinguish *G. inflata.* Weaver and Raymo (1989) regarded "*G. triangula*" as a tropical ecophenotype of *Globorotalia inflata.* The combined stratigraphic range of "*G. triangula*" and *G. inflata* corresponds to the stratigraphic range of *G. inflata* in the South Atlantic (Rio Grande Rise; Berggren et al., 1983). The occurrence of "*G. triangula*" in the Ceara Rise region appears to correspond with its occurrence at the westernmost of the Leg 108 sites (ODP Site 664). At Site 926, it is found in Samples 154-926B-6H-6, 72–74 cm, and -7H-2, 70–72 cm, just above the FO of *Globorotalia truncatulinoides,* but not in older samples, as recorded by Weaver and Raymo (1989) at ODP Sites 662 and 663.

The base of Zone N22 is marked by the first appearance of *Globorotalia truncatulinoides,* which occurs between Samples 154-926A-7H-6, 70–72 cm, and -7H-7, 30–32 cm. As at Site 925, Zones N20 and N21 are not differentiated because of the scarcity of the marker species *Globorotalia tosaensis.* The base of Zone N20/21 is marked by the FO of *Globorotalia miocenica* between Samples 154-926A-8H-3, 74–76 cm, and -8H-4, 68–70 cm. At Site 925, this datum falls a little below the local (Atlantic) reappearance level of *Pulleniatina,* although both events are given the same age estimate in Berggren et al. (1985).

The identification of the FO of *G. miocenica* is complicated by the presence of its homeomorph *Globorotalia pseudomiocenica.* For example, in Hole 926C *G. miocenica* and *G. pseudomiocenica* co-occur from Samples 154-926C-10H-1, 60–62 cm, through -10H-6, 60–62 cm. The most reliable way to distinguish the two forms is to narrowly define *G. miocenica* as having an absolutely flat spiral side. Note that forms of *G. miocenica* found lower in its stratigraphic range are not as highly vaulted on the umbilical side nor as round in equatorial outline as forms higher in its range.

Various intra-Pliocene datums were identified in both Holes 926A and 926C to aid correlation between the holes (see Table 3). Note that although both the *Dentoglobigerina altispira* and *Globorotalia multicamerata* LO datums are given the same age estimate following Berggren et al. (1985) (3.0 Ma on the Leg 154 time scale), it is clear that in the Ceara Rise region *G. multicamerata* survives to a slightly higher level than *D. altispira.* In each of Holes 925B, 926A, and 926C, *G. multicamerata* was observed one section higher than the LO of *D. altispira.*

The FO of *Sphaeroidinella,* which marks the base of Zone N19 and approximates the base of the Pliocene, occurs between Samples 154-926A-15H-6, 70–72 cm, and -15H-7, 30–32 cm.

Miocene

The FO of *Globorotalia tumida,* which marks the base of Zone N18, is between Samples 154-926A-17H-3, 70–72 cm, and -17H-4, 70–72 cm. The FO of *Globorotalia plesiotumida,* which marks the base of Zone N17, occurs between Samples 154-926A-21H-5, 70–72 cm, and -21H-6, 70–72 cm. The rarity of *Neogloboquadrina acostaensis* made it difficult to distinguish Zones N15 and N16 with certainty at Site 926. It was not found in the coarse fraction below Sample 154-926A-22H-4, 70–72 cm. It persists in the fine fraction down to between Samples 154-926A-23H-2, 70–72 cm, and -23H-4, 70–72 cm, where we place the base of Zone N16. The base of Zone N15, which is recognized by the LO of *Paragloborotalia mayeri,* is between Samples 154-926A-25H-1, 70–72 cm, and -25H-2, 70–72 cm. The FO of *Globoturborotalita nepenthes,* which marks the base of Zone N14, is between Samples 154-926A-26H-1, 70–72 cm, and -26H-2, 70–72 cm. Specimens of *G. nepenthes* in the fine fraction are distinguished from *Globigerina druryi,* its immediate ancestor (Kennett and Srinivasan, 1983), by the former's more elongate overall shape, more highly arched aperture, and more delicate apertural lip.

The LO of *Fohsella fohsi* s.l., which is used to recognize the base of Zone N13, is between Samples 154-926A-26H-5, 70–72 cm, and -26H-6, 70–72 cm. All three intergrading forms, *F. fohsi, Fohsella lobata,* and *Fohsella robusta,* are present in Sample 154-926A-26H-6, 70–72 cm. In spite of dissolution that has produced, in some cases, only moderate or poor preservation, the fohsellid evolution was observed in full at Site 926. The FOs of the morphotypes *Fohsella peripheroacuta, Fohsella "praefohsi,"* and *F. fohsi* were used to identify the bases of Zones N10, N11, and N12, respectively.

Although dissolution may have destroyed many fragile orbuline and praeorbuline tests, a similar series of events is observed in the lower middle Miocene of both Hole 926A and Hole 926B. The FO of *Orbulina suturalis,* which marks the base of Zone N8, occurs in Hole 926A between Samples 154-926A-31H-6, 70–72 cm, and -31H-2, 70–72 cm. The FO of *Praeorbulina sicana* is between Samples 154-926A-33H-2, 70–72 cm, and -33H-3, 70–72 cm.

Preservation is poor in many of the samples of the lower Miocene of Hole 926B. Radiolarians were observed in several samples from Cores 154-926B-34X, -35X, and -38X. The base of Zone N7, which is recognized by the LO of the dissolution-resistant *Catapsydrax dissimilis* form, is between Samples 154-926B-33H-3, 70–72 cm, and -33H-4, 70–72 cm, and at a similar level in Hole 926B. Because of taxonomic ambiguities associated with *Globigerinatella insueta,* we did not distinguish Zones N5 and N6.

The base of Zone N5/N6, marked by the LO of *Paragloborotalia kugleri,* is between Samples 154-926B-44X-7, 30–32 cm, and -45X-1, 70–72 cm. *P. kugleri* co-occurs with *Paragloborotalia pseudokugleri* from Sample 154-926B-46X-6, 70–72 cm, down to the base of Zone N4 between Samples 154-926B-50X-3, 68–70 cm, and -50X-4, 70–72 cm. *P. pseudokugleri* has at most six chambers in the final whorl and the sutures on its spiral side are nearly radial. For a

Table 3. Planktonic foraminifer datums recognized at Site 926.

Events	Age (Ma)	Sample range	Depth (mbsf)	Mean depth (mbsf)	Composite depth (m)	Mean composite depth (m)
Hole 926A:						
B *Pulleniatina finalis*	1.4	7H-4, 70–72 cm, to 7H-5, 70–72 cm	56.70–58.20	57.45	63.24–64.74	63.99
T *Globigerinoides fistulosus*	1.7	7H-3, 70–73 cm, to 7H-4, 70–72 cm	55.20–56.70	55.95	61.74–63.24	62.49
T *Globoturborotalita apertura*	1.9	7H-6, 70–72 cm, to 7H-7, 30–32 cm	56.70–60.80	58.75	66.24–67.34	66.79
T *Globigerinoides extremus*	1.9	7H-5, 70–72 cm, to 7H-6, 70–72 cm	58.20–59.70	58.95	64.74–66.24	65.49
B *Globorotalia truncatulinoides*	2.0	7H-6, 70–72 cm, to 7H-7, 30–32 cm	59.70–60.80	60.25	66.24–67.34	66.79
T *Globorotalia exilis*	2.2	7H-7, 30–32 cm, to 8H-1, 68–70 cm	60.80–61.68	61.24	67.34–69.78	68.56
T *Globorotalia miocenica*	2.3	8H-3, 74–76 cm, to 8H-4, 68–70 cm	64.74–66.18	65.46	72.84–74.28	73.56
Reappearance *Pulleniatina*	2.3	8H-1, 68–70 cm, to 8H-2, 68–70 cm	61.68–63.18	62.43	69.78–71.28	70.53
T *Globoturborotalita decoraperta*	2.6	9H-4, 70–72 cm, to 10H-1, 70–72 cm	75.70–80.70	78.20	85.25–91.22	88.24
T *Globorotalia pertenuis*	2.6	9H-3, 70–72 cm, to 9H-4, 70–72 cm	74.20–75.70	74.95	83.75–85.25	84.50
T *Dentoglobigerina altispira*	3.0	10H-2, 70–72 cm, to 10H-3, 70–72 cm	82.20–83.70	82.95	92.72–94.22	93.67
T *Globorotalia multicamerata*	3.0	10H-1, 70–72 cm, to 10H-2, 70–72 cm	80.70–82.20	81.45	91.22–92.72	91.97
T *Sphaeroidinellopsis seminulina*	3.1	10H-7, 70–72 cm, to 11H-1, 70–72 cm	89.70–90.20	89.95	100.22–102.26	101.24
Disappearance, *Pulleniatina*	3.5	11H-3, 70–72 cm, to 11H-4, 70–72 cm	93.20–94.70	93.95	105.26–106.76	106.01
B *Globorotalia pertenuis*	3.5	11H-5, 70–72 cm, to 11H-6, 70–72 cm	96.20–97.70	96.95	108.26–109.76	109.01
B *Globorotalia miocenica*	3.6	11H-3, 70–72 cm, to 11H-4, 70–72 cm	93.20–94.70	93.95	105.26–106.76	106.01
T *Globorotalia margaritae*	3.6	13H-3, 66–68 cm, to 13H-4, 68–70 cm	112.16–113.66	112.91	125.82–127.34	126.58
Pulleniatina S to D	4.0	13H-1, 68–70 cm, to 13H-2, 68–70 cm	109.18–110.68	109.93	122.84–124.34	123.59
T *Globoturborotalita nepenthes*	4.3	14H-4, 70–72 cm, to 14H-5, 70–72 cm	123.20–124.70	123.95	139.02–140.52	139.77
T *Globorotalia plesiotumida*	4.4	15H-1, 70–72 cm, to 15H-2, 70–72 cm	128.20–129.70	128.95	145.02–146.52	145.77
T *Globorotalia cibaoensis*	5.0	15H-1, 70–72 cm, to 15H-2, 70–72 cm	128.20–129.70	128.95	145.02–146.52	145.77
T *Neogloboquadrina acostaensis*	5.1	14H-7, 70–72 cm, to 15H-1, 70–72 cm	126.70–128.20	127.45	142.52–145.02	143.77
T *Globoquadrina baroemoenensis*	5.4	15H-3, 70–72 cm, to 15H-4, 70–72 cm	131.20–132.70	131.95	148.02–149.52	148.77
B *Sphaeroidinella dehiscens*	5.6	15H-6, 70–72 cm, to 15H-7, 30–32 cm	135.70–136.30	136.00	152.52–153.12	152.82
B *Globorotalia tumida*	5.9	17H-3, 70–72 cm, to 17H-4, 70–72 cm	150.20–151.70	150.95	169.19–170.69	169.94
B *Globorotalia margaritae*	5.7	17H-5, 70–72 cm, to 17H-6, 70–72 cm	153.20–154.70	153.95	172.19–173.69	172.94
B *Globorotalia cibaoensis*	7.7	18H-6, 70–72 cm, to 19H-1, 70–72 cm	164.20–166.20	165.20	183.86–187.35	185.60
B *Globigerinoides extremus*	8.0	20H-6, 70–72 cm, to 20H-7, 70–72 cm	183.21–184.71	183.96	205.19–206.69	205.94
B *Globorotalia plesiotumida*	8.2	21H-5, 70–72 cm, to 21H-6, 70–72 cm	191.20–192.70	191.95	213.90–215.40	214.65
B *Neogloboquadrina acostaensis*	10.0	23H-2, 70–72 cm, to 23H-4, 70–72 cm	205.71–208.71	207.21	229.77–232.77	231.27
T *Paragloborotalia mayeri*	10.3	25H-1, 70–72 cm, to 25H-2, 70–72 cm	223.20–224.70	223.95	249.06–250.56	249.81
B *Globoturborotalita apertura*	10.8	25H-6, 70–72 cm, to 25H-7, 30–32 cm	230.70–231.80	231.25	256.56–257.65	257.10
B *Globoturborotalita nepenthes*	10.8	26H-1, 70–72 cm, to 26H-2, 70–72 cm	232.70–234.20	233.45	261.07–262.56	261.81
B *Globoturborotalita decoraperta*	11.2	25H-6, 70–72 cm, to 25H-7, 30–32 cm	230.70–231.80	231.25	256.56–257.66	257.11
T *Fohsella fohsi* s.l.	11.8	26H-5, 70–72 cm, to 26H-6, 70–72 cm	238.70–240.20	239.45	267.07–268.57	267.82
B *Fohsella robusta*	12.7	28H-3, 70–72 cm, to 28H-4, 70–72 cm	254.70–256.20	255.45	283.90–285.40	284.65
B *Fohsella fohsi*	13.5	29H-2, 25–27 cm, to 29H-3, 10–12 cm	262.26–263.61	262.93	290.97–292.32	291.64
B *Fohsella praefohsi*	14.0	30H-2, 81–83 cm, to 30H-3, 70–72 cm	272.31–273.70	273.01	301.42–302.81	302.11
T *Fohsella peripheroronda*	14.6	30H-3, 70–72 cm, to 30H-4, 70–72 cm	273.70–275.20	274.45	302.81–304.31	303.56
B *Fohsella peripheroacuta*	14.7	31H-3, 70–72 cm, to 31H-4, 70–72 cm	283.20–284.70	283.95	312.31–313.81	313.06
B *Globorotalia praemenardii*	14.9	31H-4, 70–72 cm, to 31H-5, 70–72 cm	284.70–286.20	285.45	313.81–315.31	314.56
B *Orbulina*	15.1	31H-6, 70–72 cm, to 32H-2, 70–72 cm	287.71–291.21	289.46	316.81–319.77	318.29
B *Globorotalia archeomenardii*	15.5	32H-6, 70–72 cm, to 33H-1, 70–72 cm	297.20–299.20	298.08	325.77–328.31	327.04
B *Praeorbulina circularis*	16.0	31H-6, 70–72 cm, to 32H-2, 70–72 cm	287.71–291.21	289.46	316.81–319.77	318.29
B *Praeorbulina glomerosa*	16.1	32H-4, 70–72 cm, to 32H-5, 70–72 cm	294.21–295.71	294.95	322.77–324.27	323.52
B *Praeorbulina sicana*	16.4	33H-2, 70–72 cm, to 33H-3, 70–72 cm	300.70–302.20	301.45	329.81–331.31	330.56
T *Catapsydrax dissimilis*	17.3	33H-3, 70–72 cm, to 33H-4, 70–72 cm	302.21–303.71	302.96	331.31–332.81	332.06
Hole 926B:						
T *Praeorbulina sicana*	14.8	31X-3, 73–75 cm, to 31X-4, 73–75 cm	283.23–284.74	283.98	311.85–313.35	312.60
B *Orbulina suturalis*	15.1	31X-6, 73–75 cm, to 32X-1, 70–72 cm	286.53–288.70	287.62	316.35–318.52	317.43
B *Globorotalia archeomenardii*	15.5	32X-2, 70–72 cm, to 32X-3, 70–72 cm	290.20–291.70	290.95	320.02–321.52	320.77
B *Praeorbulina circularis*	16.0	32X-2, 70–72 cm, to 32X-3, 70–72 cm	290.20–291.70	290.95	320.02–321.52	320.77
B *Praeorbulina glomerosa*	16.1	32X-3, 70–72 cm, to 32X-4, 70–72 cm	291.70–293.20	292.45	321.52–323.02	322.27
B *Praeorbulina sicana*	16.4	34X-3, 70–72 cm, to 34X-4, 20–22 cm	311.01–312.01	311.51	340.32–341.82	341.06
T *Catapsydrax dissimilis*	17.3	33X-6, 70–71 cm, to 34X-2, 70–72 cm	305.81–309.51	307.66	335.62–339.32	337.47
T *Globorotalia binaiensis*	19.1	39X-4, 70–72 cm, to 39X-5, 70–72 cm	360.70–362.20	361.45	390.52–392.02	391.27
T *Paragloborotalia kugleri*	21.6	44X-6, 70–72 cm, to 45X-1, 70–72 cm	411.60–413.80	412.70	441.41–443.61	442.51
B *Paragloborotalia kugleri*	23.7	50X-3, 70–72 cm, to 50X-4, 70–72 cm	465.08–466.60	465.84	494.92–496.42	495.67
B *Paragloborotalia pseudokugleri*	26.3	54X-4, 72–74 cm, to 54X-5, 68–70 cm	505.13–506.54	505.86	534.92–536.42	535.67
T *Paragloborotalia opima*	27.1	56X-6, 70–72 cm, to 57X-1, 70–72 cm	527.41–529.61	528.51	557.22–559.42	558.32
Tc *Chiloguembelina cubensis*	28.5	61X-4, 70–73 cm, to 61X-5, 70–73 cm	572.81–574.31	573.56	602.62–604.12	603.37
Hole 926C:						
T *Globorotalia pertenuis*	2.6	9H-1, 70–72 cm, to 9H-2, 70–72 cm	77.21–78.71	77.96	85.18–86.68	85.93
T *Dentoglobigerina altispira*	3.0	9H-6, 70–72 cm, to 9H-7, 50–52 cm	84.71–86.01	85.36	92.68–93.98	93.33
T *Globorotalia multicamerata*	3.0	9H-5, 70–72 cm, to 9H-6, 70–72 cm	83.21–84.71	83.96	91.18–92.68	91.93
T *Sphaeroidinellopsis seminulina*	3.1	9H-7, 50–52 cm, to 10H-1, 60–62 cm	86.01–86.61	85.31	93.98–95.42	94.70

Note: T = top, B = base, and Tc = top common occurrence.

brief interval in upper Zone P22, *P. pseudokugleri* is the only member of the lineage found. However, in several samples in Cores 154-926B-52X, -53X, and -54X, *Paragloborotalia mendacis* co-occurs with *P. pseudokugleri*. We follow Blow (1969) and regard *P. mendacis* as a stratigraphically low member of the *P. kugleri* lineage, possessing curved sutures on the spiral side and up to seven and a half chambers in its final whorl, and therefore resembling its ultimate descendant *P. kugleri*.

Preservation in the uppermost part of Zone P22 (Samples 154-926B-50X-4, 70–72 cm, to -51X-6, 70–72 cm) is poor. Below this interval, to the bottom of the section, preservation is better and the effects of dissolution are moderate. The base of Zone P22 is recognized by the LO of *Paragloborotalia opima* (specimens larger than 0.39 mm) between Samples 154-926B-56X-6, 70–72 cm, and -57X-1, 70–72 cm. *Paragloborotalia nana* occurs regularly throughout the upper Oligocene section at this site. It is 0.35–0.39 mm in some samples in Zone P22, and in Zones P21b and P21a, where it co-occurs with *P. opima*.

The LO of "common" *Chiloguembelina cubensis*, which marks the base of Zone P21b, is between Samples 154-926B-61X-5, 70–73 cm, and -62X-2, 70–72 cm. Rare *C. cubensis* was also found in Sample 154-926B-61X-4, 70–73 cm. "*Globigerina*" *angulisuturalis* co-occurs with *C. cubensis* to the bottom of the hole. Hence, the lowest sample analyzed (Sample 154-926B-64X-6, 70–72 cm) is placed in Subzone P21a.

Benthic Foraminifers

At Site 926, benthic foraminifers are generally well or moderately preserved and rare to common in abundance in the Pleistocene through middle Miocene. For a short interval of the late Miocene (Cores 154-926A-15H through -19H), planktonic foraminifers are strongly dissolved, and consequently the relative abundance of benthic foraminifers is high. The fauna from the early Miocene is poorly preserved, except for scattered samples. The earliest early Miocene to Oligocene benthic foraminifers are moderately preserved and rare to few in abundance and include characteristic Paleogene forms. Benthic foraminifer fauna at Site 926 are divided into three major groups as follows:

1. In Cores 154-926A-1H through -10H, the fauna is characterized by marked abundance fluctuations of *Epistominella exigua, Ioanella pusillus, Nuttallides umbonifera, Chilostomella oolina, Uvigerina proboscidea, Uvigerina hispida,* and *Pyrgo murrhina.* Compared with Site 925, *N. umbonifera* and *E. exigua* are more abundant, and small individuals of *N. umbonifera, E. exigua, Ioanella pusilla,* and *Ioanella tumidula* are also abundant. However, *Uvigerina peregrina,* which is considered to be a glacial deep-water species in the North Atlantic, does not occur in any of the core-catcher samples of Holes 926A and 926B. On the other hand, spinose uvigerinids such as *U. proboscidea, U. hispida,* and *U. hispidocostata* are abundant in Samples 154-926A-4H-CC and -6H-CC.
2. In Cores 154-926A-11H through -35H, the main benthic foraminifer faunal components are *Globocassidulina subglobosa, Oridorsalis umbonatus, Nuttallides umbonifera,* and several species of cibicidoids and gyroidinoids. Another association is similar to that observed at higher levels; it includes *Stilostomella* spp., *Planulina renzi, Anomalinoides globolosus, Laticarinina pauperata,* and *Pullenia* spp. *Epistominella exigua* is observed from Samples 154-926A-1H-CC to -25H-CC, but it is few to rare or absent in this interval. A continuous occurrence of *Pyrgo murrhina,* which is representative of the Holocene NADW fauna, is recognized from Samples 154-926A-1H-CC through -19H-CC. The LO of *Pullenia miocenica* is in Sample 154-926A-12H-CC. In the earliest Pliocene to latest Miocene (Samples 154-926A-15H-CC through -19H-CC), the benthic foraminifers are relatively very abundant because of the dissolution of planktonic foraminifers, and preservation is good in spite of a corrosive condition. Similar conditions also occur in Samples 154-926A-25H-CC and -27H-CC.
3. In the interval representing the early Miocene and Oligocene (Samples 154-926B-36X-CC through -64X-CC), samples were sieved at >150 µm to concentrate the rare benthic foraminifers. In Samples 154-926A-31H-CC through -35H-CC, 154-926B-31X-CC through -35X-CC, and -42X-CC through -45X-CC, the sediment is more lithified and benthic foraminifers are very rare and poorly preserved. The most common species throughout the early Miocene were *Oridorsalis umbonatus* and *Globocassidulina subglobosa.* In earliest early Miocene through late early Oligocene (Samples 154-926B-48X-CC through -54X-CC), the benthic foraminifer fauna included various cibicidoids such as *Cibicidoides praemundulus, C. havanesis, C. barnetti, C. crebbsi, C. perlucidus,* and *C. laurisae.* Another association includes *Globocassidulina subglobosa, Gyroidinoides neosoldanii, Gyroidinoides soldanii, Gyroidinoides orbicularis, Pullenia bulloides, Pullenia osloensis, Pullenia miocenica, Stilostomella* spp., and *Pleurostomella* spp.

A major benthic foraminifer faunal break for the early middle Miocene was reported by Woodruff and Douglas (1981) from the equatorial Pacific. However, at this site Paleogene benthic foraminifer species disappeared during the early Miocene, and no distinct faunal break for the early middle Miocene was observed here.

PALEOMAGNETISM

Measurements of the magnetic remanence at Site 925 indicated a strong drilling-induced overprint. Our efforts at Site 926 concentrated on trying to understand the remagnetization in more detail. We conducted experiments to (1) analyze the geometry of the remagnetization, (2) confirm its persistence at Site 926, and (3) locate its source. In the course of these efforts, we conducted pass-through measurements of Cores 154-926A-6H to -22H and Cores 154-926C-1H to -12H, as well as numerous measurements of discrete samples from Hole 926A.

Our observation of clustered 0° declinations in the vast majority of split archive and working sections measured at the previous site suggested either that the remagnetization occurred after splitting, or that it was not uniform. We discounted the first possibility because we could not measure any large magnetic fields in the laboratory and could not reproduce any remagnetization of discrete samples within the lab. Thus, we hypothesized that the remagnetization might have a radial symmetry and investigated a whole-round sample from Core 154-925E-4H. We cut a 2-cm disk from the bottom of this whole-round sample and then split the sample normally. Pass-through measurements of the working and archive halves revealed that both had large +Z components. The Y component of magnetization was, as expected, of the opposite sign in the opposing halves; however, a strong +X component (out of the split face of the core) could be observed in both halves at several demagnetization levels. Such direct measurements indicated that the sediments were most likely affected by a magnetization that pointed radially inward and downward.

We further investigated the remagnetization by taking subsamples from the disk we had removed from the bottom of the whole-round sample (four discrete samples around the perimeter and one from the axis of the core). We performed progressive alternating-field (AF) demagnetization on each of these and confirmed that the magnetization around the perimeter was indeed radially symmetric (Fig. 6). The intensity of magnetization of the central sample was an order of magnitude smaller and revealed a magnetization with an upward-shallowing inclination. This upward-shallowing inclination (something we had to this point only rarely observed in any of our discrete sample measurements) suggests the presence of a primary remanence. The weak magnetization of the central sample could simply result from the superposition of opposing, radial remagnetizations. Therefore, even the interpretation of shallow directions from discrete samples is problematic.

We performed a second experiment with sediment samples to pursue the possibility that the BHA might be the source of the pervasive remagnetization. We fully demagnetized a number of discrete samples, packaged these in oriented positions within short sections of core liner, and, with the aid of the drillers, lowered the samples through the different portions of the BHA. In each case, the samples acquired a large downward magnetization. The isothermal remanent magnetization (IRM), however, was quite soft and could be readily removed with less than 10-mT AF treatment (Fig. 7). Thus, we concluded that an IRM from the BHA would not explain the remagnetization that remained after an AF demagnetization with more than 30 mT.

Our measurements of sediments from Hole 926A revealed that the radially symmetric remagnetization observed at Site 925 also occurred at this site: the magnetic declinations of pass-through measurements are clustered near 0° both before and after demagnetization; moreover, discrete samples (taken from the opposite side of the core) show declinations that clustered around 180° (Fig. 8). These discrete sample directions are as would be expected of a radial remagnetization: the discrete samples are taken from the working half of the cores and, hence, should tend to show magnetization directed toward the archive half of the core (i.e., toward 180°).

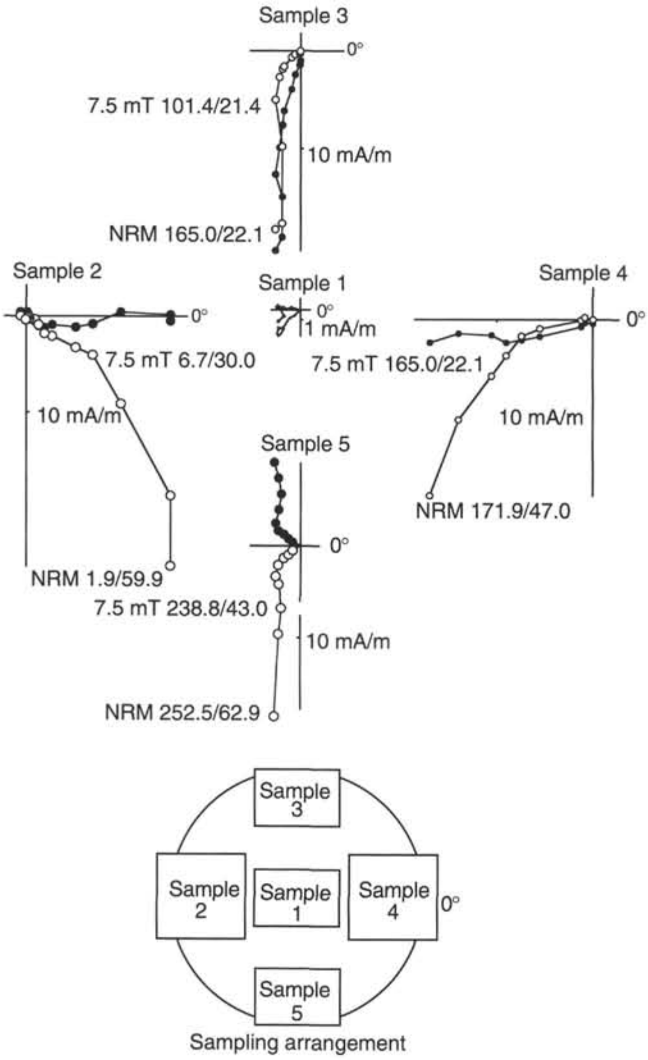

Figure 6. Orthogonal demagnetization diagrams for five subsamples of a whole-round sample from Sample 154-925E-4H-2, 8–10 cm. Samples 2 through 5 were taken from the perimeter; Sample 1 from the axis of the core. Directions (declination/inclination) are shown for natural remanent magnetization (NRM) and 7.5-mT demagnetization steps.

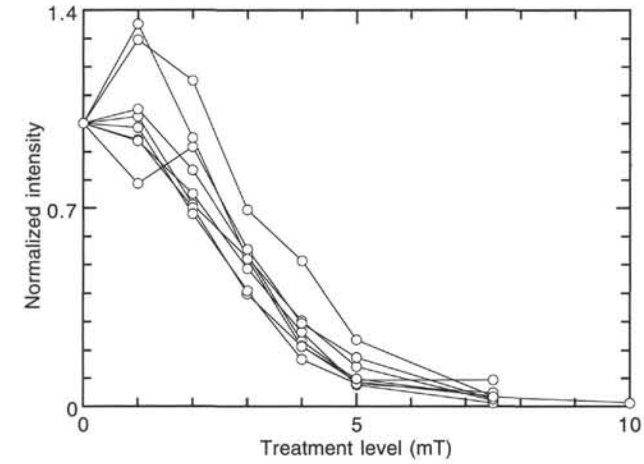

Figure 7. Normalized demagnetization curves for previously demagnetized discrete samples from Hole 925B exposed to the internal fields of the bottom-hole assembly.

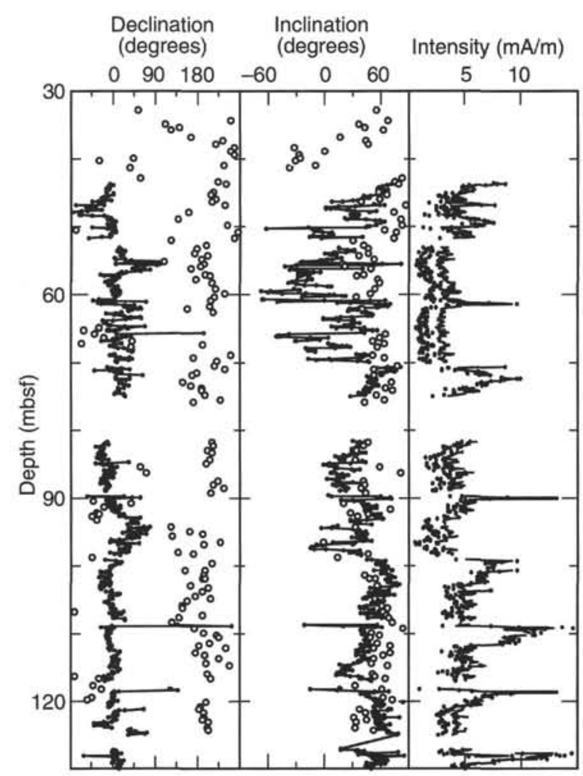

Figure 8. Downcore profiles of remanence after 20-mT demagnetization showing opposing declination in pass-through (solid circles) and discrete sample (open circles) measurements from Hole 926A.

The pass-through measurements of cores from Hole 926A further indicated a tendency for the intensity of the remagnetization to be higher near the core tops. This was particularly evident in the sequence of measurements on Cores 154-926A-11H to -14H (between 89.5 and 127.5 mbsf in Fig. 8), which prompted us to request that a different APC core barrel be used to see whether the inner core barrels might be imparting the remagnetization. With the drillers once again obliging our increasingly desperate requests, we measured the uppermost 12 cores in Hole 926C to investigate whether we could detect any core barrel signature. The results showed no clear alternation that could be associated with the new core barrel. However, we did observe that the remanent inclination for Cores 154-926C-6H, -9H, and -12H were much steeper than typical in Hole 926A or at the previous site (Fig. 9). These three high-inclination examples are notable because the APC inner barrels used to take these cores were fitted with an instrumented cutting shoe for in situ temperature measurements. Thus, we surmise that the cutting shoe may have contributed to the pervasive radial remagnetization (PRR) in some yet unexplained way. A solution to the PRR problem was not evident, however.

COMPOSITE SECTION

Continuity of the sedimentary sequence was documented in at least the upper 200 mbsf of the three holes drilled at Site 926, which extends down to the late Miocene. The composite depth section from Site 926 demonstrates overlap of cores from the three adjacent holes. On the composite depth scale (expressed in mcd [meters composite depth]), sedimentary features present in adjacent holes are aligned so that they occur at approximately the same depth. Working sequentially from the top, for each core in each hole a constant was added to the mbsf (meters below seafloor) depth to arrive at an mcd for that core. The depth offsets that comprise the composite depth section are given in Table 4.

Magnetic susceptibility data collected on the MST and color reflectance from Holes 926A through 926C were the primary parameters used to determine depth offsets of the composite depth section. Because of low-amplitude variations, GRAPE wet bulk density was not a useful lithologic parameter for composite depth section construction at Site 926. Time considerations prevented natural gamma measurements from being taken in every hole at Site 926, so natural gamma variations could not be used for hole-to-hole correlations. Although magnetic susceptibility has a low-amplitude signal, oscillations in magnetic susceptibility were correlatable between offset holes throughout most of the section. Magnetic susceptibility measurements were taken at high sensitivity (but at lower sampling resolution; i.e., at 8 or 10 cm) where the amplitude of variations was particularly low (<10 instrument units). Where the magnetic susceptibility signal was higher in amplitude, measurements were taken at lower sensitivity but at higher sampling resolution (3 cm).

Color reflectance data collected on the split cores (generally at 5-cm sampling resolution) were very useful for hole-to-hole correlations, as the reflectance data often provided a higher relative signal-to-noise ratio than the susceptibility. In general, color reflectance was inversely correlated to susceptibility. Although large-scale lithologic features were recorded similarly by both susceptibility and reflectance, small scale (<1 m) features were often different. Correlations between holes based on both susceptibility and reflectance were integrated to arrive at a composite depth section for Site 926. Both of these records on the Site 926 composite depth scale are shown in Figure 10.

In general, the composite depth section demonstrates excellent agreement between the three holes from Site 926. Relative stretching and compression of sedimentary features in aligned cores indicates distortion of the cored sequence. Because stretching and squeezing occurs on scales of less than 9 m, it is not possible to align every feature in the susceptibility and reflectance records accurately by simply adding a constant to the mbsf core depth. Within-core depth scale changes will be required to align smaller scale sedimentary features.

Verification of the hole-to-hole correlations of the composite depth scale was provided by the biostratigraphic data. Correlations in two intervals in particular were greatly aided by biostratigraphic information. The first interval is from about 80 to 95 mcd (70–85 mbsf). Because of significant coring disturbance in Core 154-926A-9H and the top of Core 154-926B-9H, the core overlap between Holes 926A, 926B, and 926C could not be determined on the basis of susceptibility and reflectance data alone. However, two foraminifer events at the base of Core 154-926C-9H and in the top of Core 154-926A-10H helped to constrain the coring overlap. The LO of *Globorotalia multicamerata* occurs in the interval between 91.2 and 92.6 mcd in both holes, and the LO of *Dentoglobigerina altispira* occurs between 92.70 and 93.90 mcd in both holes.

The second depth interval where biostratigraphic information was used to constrain the composite depth section is at 217 mcd, where the occurrence of *Discoaster bergrennii* in Holes 926A, 926B, and 926C requires that Core 154-926C-21H be moved upcore by approximately 2.5 m. In the composite depth section, this forces the top of Core 154-926C-21H (which has minor core-top disturbance) to overlap the base of Core 154-926C-20H. This overlap in a single hole destroys the between-hole core depth offset. Subsequently, the composite depths of Cores 154-926A-21H, 154-926B-21H, and 154-926C-21H all end within a meter of one another (216.19, 217.19, and 216.81 mcd, respectively). This interval of uncertain between-hole core overlap propagates downhole to the base of Core 154-926B-22H and the top of Cores 154-926A-23H and 154-926C-23H. Overlap between cores from adjacent holes was resumed from Core 154-926A-23H (about 230 mcd) through -28H.

The overlap of cores between holes was lost again at about 290 mcd, where the bases of Cores 154-926A-28H, 154-926B-28X, and 154-926C-28X have almost identical composite depths. Composite depth construction ended at this depth because between-core overlaps could no longer be documented. The successive cores from Hole 926B below Core 154-926B-28X were placed at original (mbsf) depths plus the accumulated mcd offset. The remaining cores from Holes 926A (Cores 154-926A-29H through -35H) and 926C (Cores 154-926C-29X through -42X) were adjusted slightly so that features common to all three holes were aligned with Hole 926B.

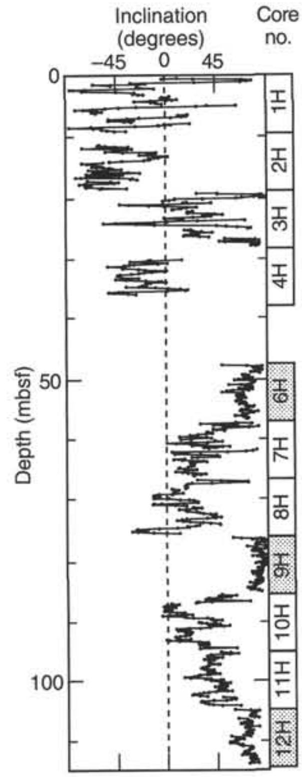

Figure 9. Remanent inclination from pass-through measurements of cores from Hole 926C after 20-mT demagnetization. Shading indicates cores (Cores 154-926C-6H, -9H, and -12H) taken using the cutting shoe outfitted with a temperature sensor.

The depth offsets (Table 4 and CD-ROM, back pocket) required to transform mbsf depth to the mcd depth scale are plotted vs. mbsf depth in Figure 11. With the exception of Hole 926C below Core 154-926C-21H, the three holes maintained excellent overlap throughout the composite depth section. From 0 to 100 mbsf (0 to about 112 mcd), the mcd scale growth relative to the mbsf scale is about 10%. The scatter of offsets for cores in the three holes in the upper part of the composite section is not unusual. From 100 mbsf to approximately 187 mbsf (through Core 154-926C-20H), mcd scale growth is about 11%. In this interval, the points for Holes 926A, 926B, and 926C follow one another perfectly, implying that the nominal 3-m adjustments that were made to the drill pipe between successive holes were maintained well. The anomalous offsets in the lower part of Hole 926C (Fig. 11) are puzzling. The apparent offsets for Hole 926C change by about 3 m at Core 154-926C-20H and by 5 m at Core 154-926C-21H, whereas the offsets in Holes 926A and 926B remain relatively constant. Below this 5-m discrepancy in the coring offset for Hole 926C, the coring offset is again relatively constant down to Core 154-926C-27X. From 200 through 260 mbsf (Cores 154-926C-23H through -28X), the growth of the mcd scale is again about 10%. With the exception of Cores 154-926C-21H, coring gaps over the entire Site 926 composite section average just over 1 m.

The anomalous coring offset in Cores 154-926C-20H and -21H can be explained in two ways: either the drill-string advance was

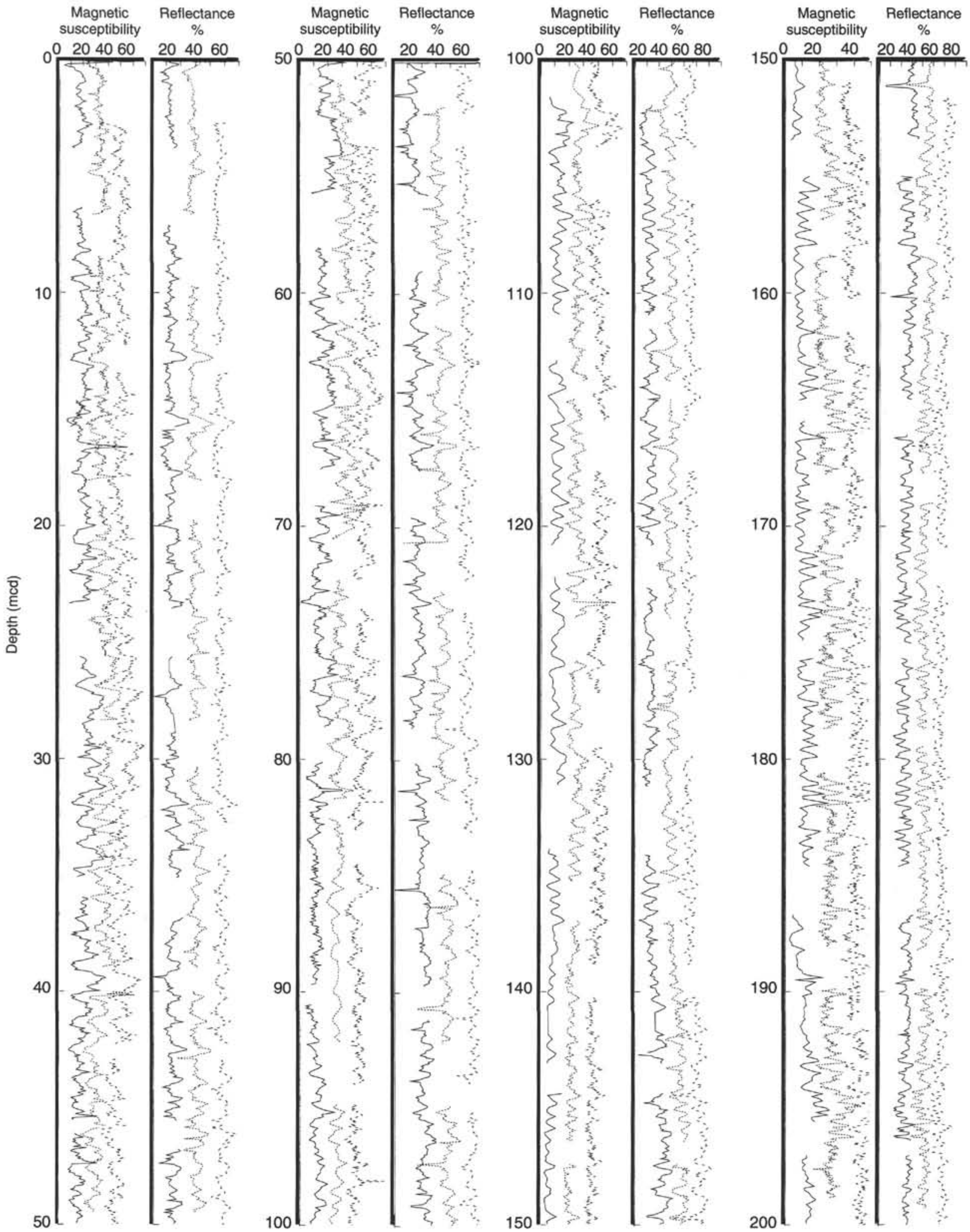

Figure 10. Magnetic susceptibility and percentage of reflectance from Site 926 on the composite depth (mcd) scale. Data are included on CD-ROM (back pocket). Plot lines are horizontally offset from one another. Hole 926A = solid line, Hole 926B = dotted line, and Hole 926C = dashed line. Magnetic susceptibility values are in uncorrected instrument units.

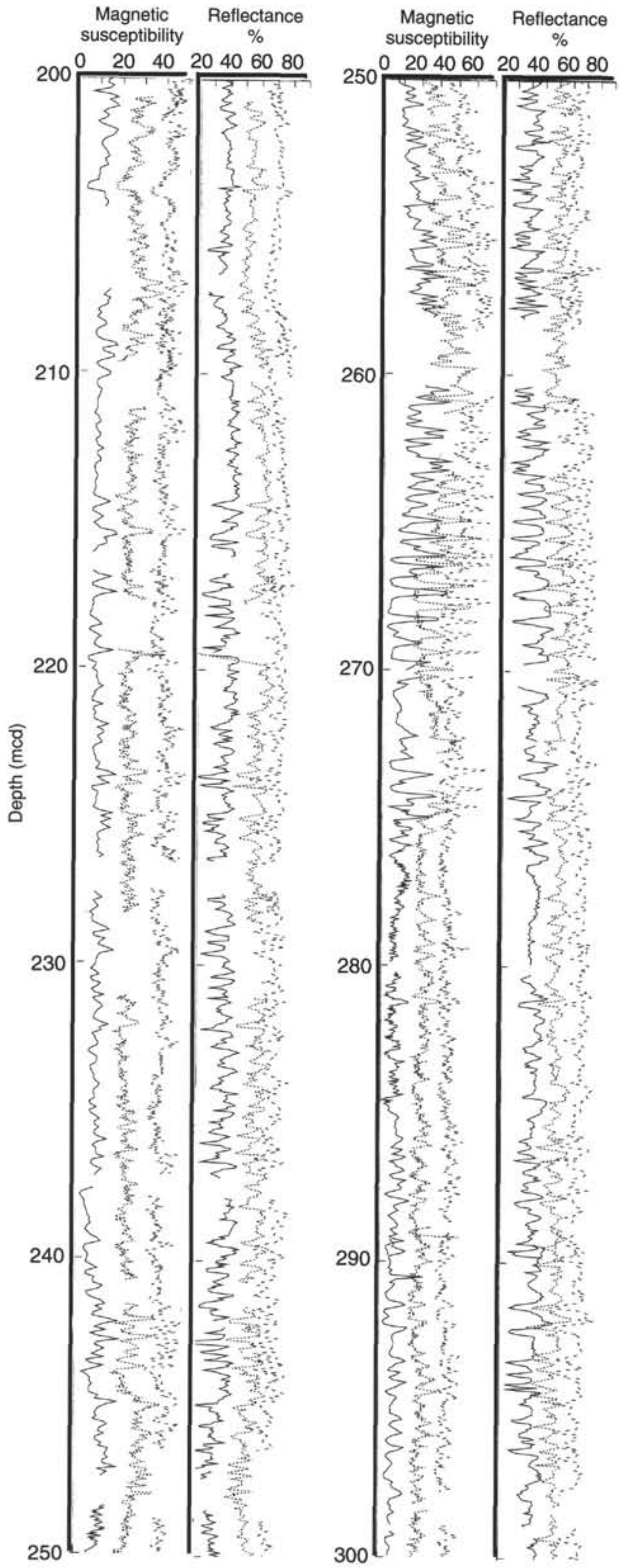

Figure 10 (continued).

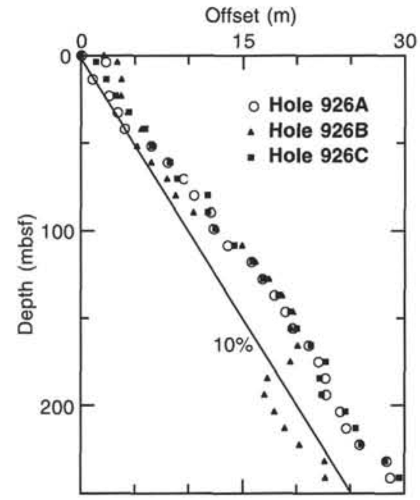

Figure 11. Depth offsets of successive cores on the mcd scale relative to mbsf depth, indicating the "growth" of the composite depth scale with increasing depth.

inadvertently less than the intended amount for these cores, after which the normal advance was resumed, or the strata sloped so that the horizon found at 190 mbsf in Holes 926A and 926B is at 185 mbsf in Hole 926C. However, a slope would require that part of the section recovered in Hole 926C be significantly condensed by comparison with the other two holes, or by the presence of a hiatus in Hole 926C. The composite section over this interval strongly suggests that the section recovered in Hole 926C is very similar to that recovered in the other two holes, and that there is apparent overlap between successive Cores 154-926C-19H, -20H, and -21H. This implies that the drill-string advance at Cores 154-926C-20H and -21H was less than 9.5 m, or that some other factor such as tidal current or ship position affected the position of the drill string in the hole.

Following construction of the composite depth section for Site 926, a single spliced record was assembled from the aligned cores. The Site 926 splice can be used as a sampling guide to recover a single sedimentary sequence from the top 250 mbsf (290 mcd) of Site 926, which spans approximately the past 13 m.y. The composite depths were aligned so that the tie points linking adjacent holes occurred at exactly the same depth in meters composite depth (within the sampling resolution of the magnetic susceptibility). In constructing the splice, we avoided intervals that were reported to have significant disturbance or distortion. Below the point where the between-hole overlap of cores was lost (below Core 154-926B-28X), the cores from Hole 926B were appended to the composite splice. The tie points for the Site 926 splice are given in Table 5, and spliced records of magnetic susceptibility and reflectance are shown in Figure 12.

SEDIMENTATION RATES

A 606-m-thick sedimentary section covering the interval from the Holocene through the upper Oligocene was recovered at Site 926. Magnetostratigraphy was not obtained at Site 926 because of severe overprint problems. The sedimentation rates for Site 926 were established from the biostratigraphy of calcareous nannofossils and planktonic foraminifers.

Hole 926A was cored with the APC to terminal depth at 325.36 mbsf, whereas Holes 926B and 926C were cored with the APC and the XCB to 606.29 and 398.55 mbsf, respectively. Detailed biostratigraphies were obtained from Holes 926A and 926B, resulting in well over 100 age-depth indications. About 90 of these were used to

Table 4. Composite depth section, Site 926.

Core and section	Section length (cm)	Depth (mbsf)	Offset (m)	Composite depth (mcd)
154-926A-				
1H-1	150	0	0.06	0.06
1H-2	150	1.5	0.06	1.56
1H-3	78	3	0.06	3.06
1H-CC	15	3.78	0.06	3.84
2H-1	150	4	2.3	6.3
2H-2	150	5.5	2.3	7.8
2H-3	150	7	2.3	9.3
2H-4	150	8.5	2.3	10.8
2H-5	150	10	2.3	12.3
2H-6	150	11.5	2.3	13.8
2H-7	47	13	2.3	15.3
2H-CC	18	13.47	2.3	15.77
3H-1	150	13.5	1.09	14.59
3H-2	150	15	1.09	16.09
3H-3	150	16.5	1.09	17.59
3H-4	150	18	1.09	19.09
3H-5	150	19.5	1.09	20.59
3H-6	130	21	1.09	22.09
3H-7	55	22.3	1.09	23.39
3H-CC	8	22.85	1.09	23.94
4H-1	150	23	2.58	25.58
4H-2	150	24.5	2.58	27.08
4H-3	150	26	2.58	28.58
4H-4	150	27.5	2.58	30.08
4H-5	150	29	2.58	31.58
4H-6	150	30.5	2.58	33.08
4H-7	54	32	2.58	34.58
4H-CC	29	32.54	2.58	35.12
5H-1	150	32.5	3.41	35.91
5H-2	150	34	3.41	37.41
5H-3	150	35.5	3.41	38.91
5H-4	150	37	3.41	40.41
5H-5	150	38.5	3.41	41.91
5H-6	150	40	3.41	43.41
5H-7	63	41.5	3.41	44.91
5H-CC	20	42.13	3.41	45.54
6H-1	150	42	4.07	46.07
6H-2	150	43.5	4.07	47.57
6H-3	150	45	4.07	49.07
6H-4	150	46.5	4.07	50.57
6H-5	150	48	4.07	52.07
6H-6	150	49.5	4.07	53.57
6H-7	72	51	4.07	55.07
6H-CC	32	51.72	4.07	55.79
7H-1	150	51.5	6.53	58.03
7H-2	150	53	6.53	59.53
7H-3	150	54.5	6.53	61.03
7H-4	150	56	6.53	62.53
7H-5	150	57.5	6.53	64.03
7H-6	150	59	6.53	65.53
7H-7	60	60.5	6.53	67.03
7H-CC	20	61.1	6.53	67.63
8H-1	150	61	8.09	69.09
8H-2	150	62.5	8.09	70.59
8H-3	150	64	8.09	72.09
8H-4	150	65.5	8.09	73.59
8H-5	150	67	8.09	75.09
8H-6	150	68.5	8.09	76.59
8H-7	59	70	8.09	78.09
8H-CC	23	70.59	8.09	78.68
9H-1	150	70.5	9.54	80.04
9H-2	150	72	9.54	81.54
9H-3	150	73.5	9.54	83.04
9H-4	150	75	9.54	84.54
9H-5	150	76.5	9.54	86.04
9H-6	150	78	9.54	87.54
9H-7	71	79.5	9.54	89.04
9H-CC	35	80.21	9.54	89.75
10H-1	150	80	10.51	90.51
10H-2	150	81.5	10.51	92.01
10H-3	150	83	10.51	93.51
10H-4	150	84.5	10.51	95.01
10H-5	150	86	10.51	96.51
10H-6	150	87.5	10.51	98.01
10H-7	61	89	10.51	99.51
10H-CC	38	89.61	10.51	100.12
11H-1	150	89.5	12.05	101.55
11H-2	150	91	12.05	103.05
11H-3	150	92.5	12.05	104.55
11H-4	150	94	12.05	106.05
11H-5	150	95.5	12.05	107.55
11H-6	150	97	12.05	109.05
11H-7	40	98.5	12.05	110.55
11H-CC	31	98.9	12.05	110.95
12H-1	150	99	12.36	111.36
12H-2	150	100.5	12.36	112.86
12H-3	150	102	12.36	114.36
12H-4	150	103.5	12.36	115.86
12H-5	150	105	12.36	117.36
12H-6	150	106.5	12.36	118.86
12H-7	47	108	12.36	120.36
12H-CC	18	108.5	12.36	120.86
13H-1	150	108.5	13.65	122.15
13H-2	150	110	13.65	123.65
13H-3	150	111.5	13.65	125.15
13H-4	150	113	13.65	126.65
13H-5	150	114.5	13.65	128.15
13H-6	100	116	13.65	129.65
13H-7	53	117	13.65	130.65
13H-CC	31	117.5	13.65	131.15
14H-1	150	118	15.81	133.81
14H-2	150	119.5	15.81	135.31
14H-3	150	121	15.81	136.81
14H-4	150	122.5	15.81	138.31
14H-5	98	124	15.81	139.81
14H-6	100	125	15.81	140.81
14H-7	128	126	15.81	141.81
14H-CC	18	127.3	15.81	143.11
15H-1	150	127.5	16.81	144.31
15H-2	150	129	16.81	145.81
15H-3	150	130.5	16.81	147.31
15H-4	150	132	16.81	148.81
15H-5	150	133.5	16.81	150.31
15H-6	100	135	16.81	151.81
15H-7	65	136	16.81	152.81
15H-CC	16	136.7	16.81	153.51
16H-1	150	137	17.96	154.96
16H-2	150	138.5	17.96	156.46
16H-3	150	140	17.96	157.96
16H-4	150	141.5	17.96	159.46
16H-5	150	143	17.96	160.96
16H-6	150	144.5	17.96	162.46
16H-7	65	146	17.96	163.96
16H-CC	34	146.7	17.96	164.66
17H-1	150	146.5	18.98	165.48
17H-2	150	148	18.98	166.98
17H-3	150	149.5	18.98	168.48
17H-4	150	151	18.98	169.98
17H-5	150	152.5	18.98	171.48
17H-6	150	154	18.98	172.98
17H-7	55	155.5	18.98	174.48
17H-CC	38	156.1	18.98	175.08
18H-1	150	156	19.65	175.65
18H-2	150	157.5	19.65	177.15
18H-3	150	159	19.65	178.65
18H-4	150	160.5	19.65	180.15
18H-5	150	162	19.65	181.65
18H-6	149	163.5	19.65	183.15
18H-CC	12	165	19.65	184.65
19H-1	150	165.5	21.14	186.64
19H-2	150	167	21.14	188.14
19H-3	150	168.5	21.14	189.64
19H-4	150	170	21.14	191.14
19H-5	150	171.5	21.14	192.64
19H-6	150	173	21.14	194.14
19H-7	77	174.5	21.14	195.64
19H-CC	27	175.3	21.14	196.44
20H-1	150	175	21.98	196.98
20H-2	150	176.5	21.98	198.48
20H-3	150	178	21.98	199.98
20H-4	150	179.5	21.98	201.48
20H-5	150	181	21.98	202.98
20H-6	150	182.5	21.98	204.48
20H-7	65	184	21.98	205.98
20H-CC	21	184.7	21.98	206.68
21H-1	150	184.5	22.69	207.19
21H-2	150	186	22.69	208.69
21H-3	150	187.5	22.69	210.19
21H-4	150	189	22.69	211.69
21H-5	150	190.5	22.69	213.19
21H-6	150	192	22.69	214.69
21H-7	62	193.5	22.69	216.19
21H-CC	20	194.1	22.69	216.79
22H-1	150	194	22.72	216.72
22H-2	150	195.5	22.72	218.22
22H-3	150	197	22.72	219.72
22H-4	150	198.5	22.72	221.22
22H-5	150	200	22.72	222.72
22H-6	150	201.5	22.72	224.22
22H-7	76	203	22.72	225.72
22H-CC	23	203.8	22.72	226.52
23H-1	150	203.5	24.06	227.56
23H-2	150	205	24.06	229.06
23H-3	150	206.5	24.06	230.56
23H-4	150	208	24.06	232.06

Table 4 (continued).

Core and section	Section length (cm)	Depth (mbsf)	Offset (m)	Composite depth (mcd)
23H-5	150	209.5	24.06	233.56
23H-6	150	211	24.06	235.06
23H-7	69	212.5	24.06	236.56
23H-CC	21	213.2	24.06	237.26
24H-1	150	213	24.6	237.6
24H-2	150	214.5	24.6	239.1
24H-3	150	216	24.6	240.6
24H-4	150	217.5	24.6	242.1
24H-5	150	219	24.6	243.6
24H-6	150	220.5	24.6	245.1
24H-7	77	222	24.6	246.6
24H-CC	49	222.8	24.6	247.4
25H-1	150	222.5	25.85	248.35
25H-2	150	224	25.85	249.85
25H-3	150	225.5	25.85	251.35
25H-4	150	227	25.85	252.85
25H-5	150	228.5	25.85	254.35
25H-6	150	230	25.85	255.85
25H-7	79	231.5	25.85	257.35
25H-CC	41	232.3	25.85	258.15
26H-1	150	232	28.36	260.36
26H-2	150	233.5	28.36	261.86
26H-3	150	235	28.36	263.36
26H-4	150	236.5	28.36	264.86
26H-5	150	238	28.36	266.36
26H-6	150	239.5	28.36	267.86
26H-7	69	241	28.36	269.36
26H-CC	26	241.7	28.36	270.06
27H-1	150	241.5	28.71	270.21
27H-2	150	243	28.71	271.71
27H-3	150	244.5	28.71	273.21
27H-4	150	246	28.71	274.71
27H-5	150	247.5	28.71	276.21
27H-6	150	249	28.71	277.71
27H-7	70	250.5	28.71	279.21
27H-CC	47	251.2	28.71	279.91
28H-1	150	251	29.19	280.19
28H-2	150	252.5	29.19	281.69
28H-3	150	254	29.19	283.19
28H-4	150	255.5	29.19	284.69
28H-5	150	257	29.19	286.19
28H-6	150	258.5	29.19	287.69
28H-7	67	260	29.19	289.19
28H-CC	31	260.7	29.19	289.89
29H-1	150	260.5	28.71	289.21
29H-2	150	262	28.71	290.71
29H-3	150	263.5	28.71	292.21
29H-4	150	265	28.71	293.71
29H-5	150	266.5	28.71	295.21
29H-6	150	268	28.71	296.71
29H-7	69	269.5	28.71	298.21
29H-CC	36	270.2	28.71	298.91
30H-1	150	270	29.1	299.1
30H-2	150	271.5	29.1	300.6
30H-3	150	273	29.1	302.1
30H-4	150	274.5	29.1	303.6
30H-5	150	276	29.1	305.1
30H-6	150	277.5	29.1	306.6
30H-7	66	279	29.1	308.1
30H-CC	29	279.7	29.1	308.8
31H-1	150	279.5	29.1	308.6
31H-2	150	281	29.1	310.1
31H-3	150	282.5	29.1	311.6
31H-4	150	284	29.1	313.1
31H-5	150	285.5	29.1	314.6
31H-6	150	287	29.1	316.1
31H-7	66	288.5	29.1	317.6
31H-CC	37	289.2	29.1	318.3
32H-1	150	289	28.56	317.56
32H-2	150	290.5	28.56	319.06
32H-3	150	292	28.56	320.56
32H-4	150	293.5	28.56	322.06
32H-5	150	295	28.56	323.56
32H-6	150	296.5	28.56	325.06
32H-7	33	298	28.56	326.56
32H-CC	56	298.3	28.56	326.86
33H-1	150	298.5	29.1	327.6
33H-2	150	300	29.1	329.1
33H-3	150	301.5	29.1	330.6
33H-4	150	303	29.1	332.1
33H-5	150	304.5	29.1	333.6
33H-6	30	306	29.1	335.1
33H-CC	28	306.3	29.1	335.4
34H-1	150	308	29.1	337.1
34H-2	150	309.5	29.1	338.6
34H-3	150	311	29.1	340.1
34H-4	150	312.5	29.1	341.6
34H-5	150	314	29.1	343.1
34H-6	150	315.5	29.1	344.6
34H-7	73	317	29.1	346.1
34H-CC	35	317.7	29.1	346.8
35H-1	150	317.5	30.31	347.81
35H-2	150	319	30.31	349.31
35H-3	150	320.5	30.31	350.81
35H-4	115	322	30.31	352.31
35H-5	150	323.2	30.31	353.51
35H-CC	66	324.7	30.31	355.01
154-926B-				
1H-1	150	0	0	0
1H-2	150	1.5	0	1.5
1H-3	150	3	0	3
1H-4	150	4.5	0	4.5
1H-5	66	6	0	6
1H-CC	22	6.66	0	6.66
2H-1	150	7	1.45	8.45
2H-2	150	8.5	1.45	9.95
2H-3	150	10	1.45	11.45
2H-4	150	11.5	1.45	12.95
2H-5	150	13	1.45	14.45
2H-6	150	14.5	1.45	15.95
2H-7	63	16	1.45	17.45
2H-CC	23	16.63	1.45	18.08
3H-1	150	16.5	2.41	18.91
3H-2	150	18	2.41	20.41
3H-3	150	19.5	2.41	21.91
3H-4	150	21	2.41	23.41
3H-5	150	22.5	2.41	24.91
3H-6	150	24	2.41	26.41
3H-7	46	25.5	2.41	27.91
3H-CC	25	25.96	2.41	28.37
4H-1	150	26	3.23	29.23
4H-2	150	27.5	3.23	30.73
4H-3	150	29	3.23	32.23
4H-4	150	30.5	3.23	33.73
4H-5	150	32	3.23	35.23
4H-6	150	33.5	3.23	36.73
4H-7	73	35	3.23	38.23
4H-CC	16	35.73	3.23	38.96
5H-1	150	35.5	4.46	39.96
5H-2	150	37	4.46	41.46
5H-3	150	38.5	4.46	42.96
5H-4	150	40	4.46	44.46
5H-5	150	41.5	4.46	45.96
5H-6	150	43	4.46	47.46
5H-7	54	44.5	4.46	48.96
5H-CC	20	45.04	4.46	49.5
6H-1	150	45	5.95	50.95
6H-2	150	46.5	5.95	52.45
6H-3	150	48	5.95	53.95
6H-4	150	49.5	5.95	55.45
6H-5	150	51	5.95	56.95
6H-6	150	52.5	5.95	58.45
6H-7	54	54	5.95	59.95
6H-CC	22	54.54	5.95	60.49
7H-1	150	54.5	6.62	61.12
7H-2	150	56	6.62	62.62
7H-3	150	57.5	6.62	64.12
7H-4	150	59	6.62	65.62
7H-5	150	60.5	6.62	67.12
7H-6	150	62	6.62	68.62
7H-7	53	63.5	6.62	70.12
7H-CC	17	64.03	6.62	70.65
8H-1	150	64	8.28	72.28
8H-2	150	65.5	8.28	73.78
8H-3	150	67	8.28	75.28
8H-4	150	68.5	8.28	76.78
8H-5	150	70	8.28	78.28
8H-6	150	71.5	8.28	79.78
8H-7	49	73	8.28	81.28
8H-CC	18	73.49	8.28	81.77
9H-1	150	73.5	8.99	82.49
9H-2	150	75	8.99	83.99
9H-3	150	76.5	8.99	85.49
9H-4	150	78	8.99	86.99
9H-5	150	79.5	8.99	88.49
9H-6	150	81	8.99	89.99
9H-7	67	82.5	8.99	91.49
9H-CC	39	83.17	8.99	92.16
10H-1	150	83	11.8	94.8
10H-2	150	84.5	11.8	96.3
10H-3	150	86	11.8	97.8
10H-4	150	87.5	11.8	99.3
10H-5	150	89	11.8	100.8
10H-6	150	90.5	11.8	102.3
10H-7	57	92	11.8	103.8

Table 4 (continued).

Core and section	Section length (cm)	Depth (mbsf)	Offset (m)	Composite depth (mcd)
10H-CC	40	92.57	11.8	104.37
11H-1	150	92.5	11.84	104.34
11H-2	150	94	11.84	105.84
11H-3	150	95.5	11.84	107.34
11H-4	150	97	11.84	108.84
11H-5	150	98.5	11.84	110.34
11H-6	133	100	11.84	111.84
11H-7	64	101.3	11.84	113.14
11H-CC	47	102	11.84	113.84
12H-1	150	102	12.5	114.5
12H-2	150	103.5	12.5	116
12H-3	150	105	12.5	117.5
12H-4	150	106.5	12.5	119
12H-5	150	108	12.5	120.5
12H-6	150	109.5	12.5	122
12H-7	51	111	12.5	123.5
12H-CC	54	111.5	12.5	124
13H-1	150	111.5	14.25	125.75
13H-2	150	113	14.25	127.25
13H-3	150	114.5	14.25	128.75
13H-4	150	116	14.25	130.25
13H-5	150	117.5	14.25	131.75
13H-6	150	119	14.25	133.25
13H-7	56	120.5	14.25	134.75
13H-CC	37	121.1	14.25	135.35
14H-1	150	121	15.91	136.91
14H-2	150	122.5	15.91	138.41
14H-3	150	124	15.91	139.91
14H-4	150	125.5	15.91	141.41
14H-5	150	127	15.91	142.91
14H-6	150	128.5	15.91	144.41
14H-7	71	130	15.91	145.91
14H-CC	25	130.7	15.91	146.61
15H-1	150	130.5	16.87	147.37
15H-2	150	132	16.87	148.87
15H-3	150	133.5	16.87	150.37
15H-4	150	135	16.87	151.87
15H-5	150	136.5	16.87	153.37
15H-6	150	138	16.87	154.87
15H-7	59	139.5	16.87	156.37
15H-CC	35	140.1	16.87	156.97
16H-1	150	140	18.34	158.34
16H-2	150	141.5	18.34	159.84
16H-3	150	143	18.34	161.34
16H-4	150	144.5	18.34	162.84
16H-5	150	146	18.34	164.34
16H-6	150	147.5	18.34	165.84
16H-7	45	149	18.34	167.34
16H-CC	25	149.5	18.34	167.84
17H-1	150	149.5	19.47	168.97
17H-2	150	151	19.47	170.47
17H-3	150	152.5	19.47	171.97
17H-4	150	154	19.47	173.47
17H-5	150	155.5	19.47	174.97
17H-6	150	157	19.47	176.47
17H-7	76	158.5	19.47	177.97
17H-CC	43	159.3	19.47	178.77
18H-1	150	159	20.04	179.04
18H-2	150	160.5	20.04	180.54
18H-3	150	162	20.04	182.04
18H-4	150	163.5	20.04	183.54
18H-5	150	165	20.04	185.04
18H-6	150	166.5	20.04	186.54
18H-7	15	168	20.04	188.04
18H-CC	58	168.2	20.04	188.24
19H-1	150	168.5	21.34	189.84
19H-2	150	170	21.34	191.34
19H-3	150	171.5	21.34	192.84
19H-4	150	173	21.34	194.34
19H-5	150	174.5	21.34	195.84
19H-6	150	176	21.34	197.34
19H-7	47	177.5	21.34	198.84
20H-1	150	178	22.69	200.69
20H-2	150	179.5	22.69	202.19
20H-3	150	181	22.69	203.69
20H-4	150	182.5	22.69	205.19
20H-5	150	184	22.69	206.69
20H-6	150	185.5	22.69	208.19
20H-7	18	187	22.69	209.69
20H-CC	58	187.2	22.69	209.89
21H-1	150	187.5	22.19	209.69
21H-2	150	189	22.19	211.19
21H-3	150	190.5	22.19	212.69
21H-4	150	192	22.19	214.19
21H-5	150	193.5	22.19	215.69
21H-6	60	195	22.19	217.19
21H-CC	55	195.6	22.19	217.79
22H-1	150	197	22.36	219.36
22H-2	150	198.5	22.36	220.86
22H-3	150	200	22.36	222.36
22H-4	150	201.5	22.36	223.86
22H-5	150	203	22.36	225.36
22H-6	150	204.5	22.36	226.86
22H-7	30	206	22.36	228.36
22H-CC	19	206.3	22.36	228.66
23H-1	150	206.5	24.57	231.07
23H-2	150	208	24.57	232.57
23H-3	150	209.5	24.57	234.07
23H-4	150	211	24.57	235.57
23H-5	150	212.5	24.57	237.07
23H-6	150	214	24.57	238.57
23H-7	68	215.5	24.57	240.07
23H-CC	43	216.2	24.57	240.77
24H-1	150	216	25.52	241.52
24H-2	150	217.5	25.52	243.02
24H-3	150	219	25.52	244.52
24H-4	150	220.5	25.52	246.02
24H-5	150	222	25.52	247.52
24H-6	150	223.5	25.52	249.02
24H-7	76	225	25.52	250.52
24H-CC	38	225.8	25.52	251.32
25H-1	150	225.5	26.01	251.51
25H-2	150	227	26.01	253.01
25H-3	150	228.5	26.01	254.51
25H-4	150	230	26.01	256.01
25H-5	150	231.5	26.01	257.51
25H-6	150	233	26.01	259.01
25H-7	82	234.5	26.01	260.51
25H-CC	37	235.3	26.01	261.31
26H-1	150	235	28.27	263.27
26H-2	150	236.5	28.27	264.77
26H-3	150	238	28.27	266.27
26H-4	150	239.5	28.27	267.77
26H-5	150	241	28.27	269.27
26H-6	150	242.5	28.27	270.77
26H-7	57	244	28.27	272.27
26H-CC	26	244.6	28.27	272.87
27H-1	150	244.5	29.56	274.06
27H-2	150	246	29.56	275.56
27H-3	150	247.5	29.56	277.06
27H-4	150	249	29.56	278.56
27H-5	150	250.5	29.56	280.06
27H-6	150	252	29.56	281.56
27H-7	68	253.5	29.56	283.06
27H-CC	36	254.2	29.56	283.76
28X-1	150	254	29.21	283.21
28X-2	150	255.5	29.21	284.71
28X-3	150	257	29.21	286.21
28X-4	150	258.5	29.21	287.71
28X-5	34	260	29.21	289.21
28X-CC	17	260.3	29.21	289.51
29X-1	150	259	29.81	288.81
29X-2	150	260.5	29.81	290.31
29X-3	150	262	29.81	291.81
29X-4	150	263.5	29.81	293.31
29X-5	150	265	29.81	294.81
29X-6	150	266.5	29.81	296.31
29X-7	42	268	29.81	297.81
29X-CC	32	268.4	29.81	298.21
30X-1	150	268.6	29.81	298.41
30X-2	150	270.1	29.81	299.91
30X-3	150	271.6	29.81	301.41
30X-4	150	273.1	29.81	302.91
30X-5	150	274.6	29.81	304.41
30X-6	108	276.1	29.81	305.91
30X-CC	32	277.2	29.81	307.01
31X-1	150	278.3	29.81	308.11
31X-2	150	279.8	29.81	309.61
31X-3	150	281.3	29.81	311.11
31X-4	150	282.8	29.81	312.61
31X-5	150	284.3	29.81	314.11
31X-6	150	285.8	29.81	315.61
31X-7	49	287.3	29.81	317.11
31X-CC	21	287.8	29.81	317.61
32X-1	150	288	29.81	317.81
32X-2	150	289.5	29.81	319.31
32X-3	150	291	29.81	320.81
32X-4	150	292.5	29.81	322.31
32X-5	150	294	29.81	323.81
32X-6	150	295.5	29.81	325.31
32X-7	41	297	29.81	326.81
32X-CC	16	297.4	29.81	327.21
33X-1	150	297.6	29.81	327.41
33X-2	150	299.1	29.81	328.91
33X-3	150	300.6	29.81	330.41
33X-4	150	302.1	29.81	331.91

Table 4 (continued).

Core and section	Section length (cm)	Depth (mbsf)	Offset (m)	Composite depth (mcd)
33X-5	150	303.6	29.81	333.41
33X-6	150	305.1	29.81	334.91
33X-7	47	306.6	29.81	336.41
33X-CC	35	307.1	29.81	336.91
34X-1	150	307.3	29.81	337.11
34X-2	150	308.8	29.81	338.61
34X-3	150	310.3	29.81	340.11
34X-4	34	311.8	29.81	341.61
34X-CC	54	312.1	29.81	341.91
35X-1	150	316.9	29.81	346.71
35X-2	150	318.4	29.81	348.21
35X-3	150	319.9	29.81	349.71
35X-4	150	321.4	29.81	351.21
35X-5	150	322.9	29.81	352.71
35X-6	150	324.4	29.81	354.21
35X-7	46	325.9	29.81	355.71
35X-CC	27	326.4	29.81	356.21
36X-1	150	326.5	29.81	356.31
36X-2	150	328	29.81	357.81
36X-3	150	329.5	29.81	359.31
36X-4	137	331	29.81	360.81
36X-CC	26	332.4	29.81	362.21
37X-1	150	336.2	29.81	366.01
37X-2	150	337.7	29.81	367.51
37X-3	150	339.2	29.81	369.01
37X-4	150	340.7	29.81	370.51
37X-5	150	342.2	29.81	372.01
37X-6	16	343.7	29.81	373.51
37X-CC	44	343.9	29.81	373.71
38X-1	150	345.8	29.81	375.61
38X-2	150	347.3	29.81	377.11
38X-3	150	348.8	29.81	378.61
38X-4	150	350.3	29.81	380.11
38X-5	150	351.8	29.81	381.61
38X-6	150	353.3	29.81	383.11
38X-7	50	354.8	29.81	384.61
38X-CC	5	355.3	29.81	385.11
39X-1	150	355.5	29.81	385.31
39X-2	150	357	29.81	386.81
39X-3	150	358.5	29.81	388.31
39X-4	150	360	29.81	389.81
39X-5	150	361.5	29.81	391.31
39X-6	150	363	29.81	392.81
39X-7	20	364.5	29.81	394.31
39X-CC	51	364.7	29.81	394.51
40X-1	150	365.1	29.81	394.91
40X-2	150	366.6	29.81	396.41
40X-3	150	368.1	29.81	397.91
40X-4	150	369.6	29.81	399.41
40X-5	150	371.1	29.81	400.91
40X-6	138	372.6	29.81	402.41
40X-CC	14	374	29.81	403.81
41X-1	96	374.4	29.81	404.21
41X-2	150	375.4	29.81	405.21
41X-3	150	376.9	29.81	406.71
41X-4	150	378.4	29.81	408.21
41X-5	144	379.9	29.81	409.71
41X-CC	29	381.3	29.81	411.11
42X-1	150	384.1	29.81	413.91
42X-2	150	385.6	29.81	415.41
42X-3	150	387.1	29.81	416.91
42X-4	150	388.6	29.81	418.41
42X-5	150	390.1	29.81	419.91
42X-6	150	391.6	29.81	421.41
42X-7	20	393.1	29.81	422.91
42X-CC	2	393.3	29.81	423.11
43X-1	150	393.7	29.81	423.51
43X-2	150	395.2	29.81	425.01
43X-3	150	396.7	29.81	426.51
43X-4	150	398.2	29.81	428.01
43X-5	150	399.7	29.81	429.51
43X-6	104	401.2	29.81	431.01
43X-CC	64	402.2	29.81	432.01
44X-1	150	403.4	29.81	433.21
44X-2	150	404.9	29.81	434.71
44X-3	150	406.4	29.81	436.21
44X-4	150	407.9	29.81	437.71
44X-5	150	409.4	29.81	439.21
44X-6	150	410.9	29.81	440.71
44X-7	39	412.4	29.81	442.21
44X-CC	32	412.8	29.81	442.61
45X-1	150	413.1	29.81	442.91
45X-2	150	414.6	29.81	444.41
45X-3	150	416.1	29.81	445.91
45X-4	150	417.6	29.81	447.41
45X-5	150	419.1	29.81	448.91
45X-6	150	420.6	29.81	450.41
45X-7	11	422.1	29.81	451.91
45X-CC	65	422.2	29.81	452.01
46X-1	150	422.8	29.81	452.61
46X-2	150	424.3	29.81	454.11
46X-3	150	425.8	29.81	455.61
46X-4	150	427.3	29.81	457.11
46X-5	150	428.8	29.81	458.61
46X-6	120	430.3	29.81	460.11
46X-7	33	431.5	29.81	461.31
46X-CC	31	431.8	29.81	461.61
47X-1	150	432.4	29.81	462.21
47X-2	150	433.9	29.81	463.71
47X-3	150	435.4	29.81	465.21
47X-4	150	436.9	29.81	466.71
47X-5	150	438.4	29.81	468.21
47X-6	125	439.9	29.81	469.71
47X-CC	34	441.2	29.81	471.01
48X-1	150	442.1	29.81	471.91
48X-2	150	443.6	29.81	473.41
48X-3	150	445.1	29.81	474.91
48X-4	150	446.6	29.81	476.41
48X-5	150	448.1	29.81	477.91
48X-6	150	449.6	29.81	479.41
48X-7	43	451.1	29.81	480.91
48X-CC	43	451.5	29.81	481.31
49X-1	150	451.7	29.81	481.51
49X-2	150	453.2	29.81	483.01
49X-3	150	454.7	29.81	484.51
49X-4	150	456.2	29.81	486.01
49X-5	150	457.7	29.81	487.51
49X-6	89	459.2	29.81	489.01
49X-CC	53	460.1	29.81	489.91
50X-1	150	461.4	29.81	491.21
50X-2	150	462.9	29.81	492.71
50X-3	150	464.4	29.81	494.21
50X-4	150	465.9	29.81	495.71
50X-5	150	467.4	29.81	497.21
50X-6	138	468.9	29.81	498.71
50X-CC	54	470.3	29.81	500.11
51X-1	150	471	29.81	500.81
51X-2	150	472.5	29.81	502.31
51X-3	150	474	29.81	503.81
51X-4	150	475.5	29.81	505.31
51X-5	150	477	29.81	506.81
51X-6	150	478.5	29.81	508.31
51X-7	42	480	29.81	509.81
51X-CC	42	480.4	29.81	510.21
52X-1	150	480.5	29.81	510.31
52X-2	150	482	29.81	511.81
52X-3	150	483.5	29.81	513.31
52X-4	150	485	29.81	514.81
52X-5	150	486.5	29.81	516.31
52X-6	150	488	29.81	517.81
52X-7	50	489.5	29.81	519.31
52X-CC	33	490	29.81	519.81
53X-1	150	490.2	29.81	520.01
53X-2	150	491.7	29.81	521.51
53X-3	150	493.2	29.81	523.01
53X-4	150	494.7	29.81	524.51
53X-5	150	496.2	29.81	526.01
53X-6	111	497.7	29.81	527.51
53X-CC	63	498.8	29.81	528.61
54X-1	150	499.9	29.81	529.71
54X-2	150	501.4	29.81	531.21
54X-3	150	502.9	29.81	532.71
54X-4	150	504.4	29.81	534.21
54X-5	150	505.9	29.81	535.71
54X-6	150	507.4	29.81	537.21
54X-7	40	508.9	29.81	538.71
54X-CC	40	509.3	29.81	539.11
55X-1	150	509.5	29.81	539.31
55X-2	150	511	29.81	540.81
55X-3	150	512.5	29.81	542.31
55X-4	150	514	29.81	543.81
55X-5	150	515.5	29.81	545.31
55X-6	129	517	29.81	546.81
55X-CC	29	518.3	29.81	548.11
56X-1	150	519.2	29.81	549.01
56X-2	150	520.7	29.81	550.51
56X-3	150	522.2	29.81	552.01
56X-4	150	523.7	29.81	553.51
56X-5	150	525.2	29.81	555.01
56X-6	150	526.7	29.81	556.51
56X-7	40	528.2	29.81	558.01
56X-CC	41	528.6	29.81	558.41
57X-1	150	528.9	29.81	558.71
57X-2	150	530.4	29.81	560.21
57X-3	150	531.9	29.81	561.71
57X-4	150	533.4	29.81	563.21

Table 4 (continued).

Core and section	Section length (cm)	Depth (mbsf)	Offset (m)	Composite depth (mcd)
57X-5	150	534.9	29.81	564.71
57X-6	100	536.4	29.81	566.21
57X-7	57	537.4	29.81	567.21
57X-CC	56	538	29.81	567.81
58X-1	150	538.5	29.81	568.31
58X-2	150	540	29.81	569.81
58X-3	150	541.5	29.81	571.31
58X-4	150	543	29.81	572.81
58X-5	150	544.5	29.81	574.31
58X-6	150	546	29.81	575.81
58X-7	22	547.5	29.81	577.31
58X-CC	18	547.7	29.81	577.51
59X-1	150	548.2	29.81	578.01
59X-2	150	549.7	29.81	579.51
59X-3	150	551.2	29.81	581.01
59X-4	150	552.7	29.81	582.51
59X-5	150	554.2	29.81	584.01
59X-6	150	555.7	29.81	585.51
59X-7	30	557.2	29.81	587.01
59X-CC	47	557.5	29.81	587.31
60X-1	150	557.9	29.81	587.71
60X-2	150	559.4	29.81	589.21
60X-3	150	560.9	29.81	590.71
60X-4	150	562.4	29.81	592.21
60X-5	150	563.9	29.81	593.71
60X-6	24	565.4	29.81	595.21
60X-CC	55	565.6	29.81	595.41
61X-1	150	567.6	29.81	597.41
61X-2	150	569.1	29.81	598.91
61X-3	150	570.6	29.81	600.41
61X-4	150	572.1	29.81	601.91
61X-5	139	573.6	29.81	603.41
61X-CC	44	575	29.81	604.81
62X-1	150	577.2	29.81	607.01
62X-2	150	578.7	29.81	608.51
62X-3	150	580.2	29.81	610.01
62X-4	58	581.7	29.81	611.51
62X-CC	8	582.3	29.81	612.11
63X-1	150	586.9	29.81	616.71
63X-2	150	588.4	29.81	618.21
63X-3	150	589.9	29.81	619.71
63X-4	150	591.4	29.81	621.21
63X-5	150	592.9	29.81	622.71
63X-6	150	594.4	29.81	624.21
63X-7	35	595.9	29.81	625.71
63X-CC	48	596.3	29.81	626.11
64X-1	150	596.5	29.81	626.31
64X-2	150	598	29.81	627.81
64X-3	150	599.5	29.81	629.31
64X-4	150	601	29.81	630.81
64X-5	150	602.5	29.81	632.31
64X-6	150	604	29.81	633.81
64X-7	44	605.5	29.81	635.31
64X-CC	39	605.9	29.81	635.71
154-926C-				
1H-1	150	0.5	2.18	2.68
1H-2	150	2	2.18	4.18
1H-3	150	3.5	2.18	5.68
1H-4	150	5	2.18	7.18
1H-5	150	6.5	2.18	8.68
1H-6	150	8	2.18	10.18
1H-7	55	9.5	2.18	11.68
1H-CC	32	10.05	2.18	12.23
2H-1	150	10	3.41	13.41
2H-2	150	11.5	3.41	14.91
2H-3	150	13	3.41	16.41
2H-4	150	14.5	3.41	17.91
2H-5	150	16	3.41	19.41
2H-6	150	17.5	3.41	20.91
2H-7	62	19	3.41	22.41
2H-CC	14	19.62	3.41	23.03
3H-1	150	19.5	3.77	23.27
3H-2	150	21	3.77	24.77
3H-3	150	22.5	3.77	26.27
3H-4	150	24	3.77	27.77
3H-5	150	25.5	3.77	29.27
3H-6	150	27	3.77	30.77
3H-7	50	28.5	3.77	32.27
3H-CC	20	29	3.77	32.77
4H-1	150	29	3.74	32.74
4H-2	150	30.5	3.74	34.24
4H-3	150	32	3.74	35.74
4H-4	150	33.5	3.74	37.24
4H-5	150	35	3.74	38.74
4H-6	150	36.5	3.74	40.24
4H-7	53	38	3.74	41.74
4H-CC	15	38.53	3.74	42.27
5H-1	150	38.5	4.38	42.88
5H-2	150	40	4.38	44.38
5H-3	150	41.5	4.38	45.88
5H-4	150	43	4.38	47.38
5H-5	150	44.5	4.38	48.88
5H-6	150	46	4.38	50.38
5H-7	51	47.5	4.38	51.88
5H-CC	18	48.01	4.38	52.39
6H-1	150	48	5.63	53.63
6H-2	150	49.5	5.63	55.13
6H-3	150	51	5.63	56.63
6H-4	150	52.5	5.63	58.13
6H-5	150	54	5.63	59.63
6H-6	150	55.5	5.63	61.13
6H-7	55	57	5.63	62.63
6H-CC	20	57.55	5.63	63.18
7H-1	150	57.5	5.24	62.74
7H-2	150	59	5.24	64.24
7H-3	150	60.5	5.24	65.74
7H-4	150	62	5.24	67.24
7H-5	150	63.5	5.24	68.74
7H-6	150	65	5.24	70.24
7H-7	57	66.5	5.24	71.74
7H-CC	16	67.07	5.24	72.31
8H-1	150	67	6.52	73.52
8H-2	150	68.5	6.52	75.02
8H-3	150	70	6.52	76.52
8H-4	150	71.5	6.52	78.02
8H-5	150	73	6.52	79.52
8H-6	150	74.5	6.52	81.02
8H-7	57	76	6.52	82.52
8H-CC	18	76.57	6.52	83.09
9H-1	150	76.5	7.97	84.47
9H-2	150	78	7.97	85.97
9H-3	150	79.5	7.97	87.47
9H-4	150	81	7.97	88.97
9H-5	150	82.5	7.97	90.47
9H-6	150	84	7.97	91.97
9H-7	53	85.5	7.97	93.47
9H-CC	47	86.03	7.97	94
10H-1	150	86	8.81	94.81
10H-2	150	87.5	8.81	96.31
10H-3	150	89	8.81	97.81
10H-4	150	90.5	8.81	99.31
10H-5	150	92	8.81	100.81
10H-6	148	93.5	8.81	102.31
10H-CC	17	94.98	8.81	103.79
11H-1	150	95.5	10.47	105.97
11H-2	150	97	10.47	107.47
11H-3	150	98.5	10.47	108.97
11H-4	150	100	10.47	110.47
11H-5	150	101.5	10.47	111.97
11H-6	150	103	10.47	113.47
11H-7	54	104.5	10.47	114.97
11H-CC	20	105	10.47	115.47
12H-1	150	105	12.61	117.61
12H-2	150	106.5	12.61	119.11
12H-3	150	108	12.61	120.61
12H-4	150	109.5	12.61	122.11
12H-5	150	111	12.61	123.61
12H-6	150	112.5	12.61	125.11
12H-7	56	114	12.61	126.61
12H-CC	31	114.6	12.61	127.21
13H-1	150	114.5	14.96	129.46
13H-2	150	116	14.96	130.96
13H-3	150	117.5	14.96	132.46
13H-4	150	119	14.96	133.96
13H-5	150	120.5	14.96	135.46
13H-6	150	122	14.96	136.96
13H-7	38	123.5	14.96	138.46
13H-CC	20	123.9	14.96	138.86
14H-1	150	124	16.19	140.19
14H-2	150	125.5	16.19	141.69
14H-3	150	127	16.19	143.19
14H-4	150	128.5	16.19	144.69
14H-5	150	130	16.19	146.19
14H-6	150	131.5	16.19	147.69
14H-7	81	133	16.19	149.19
14H-CC	18	133.8	16.19	149.99
15H-1	150	133.5	17.45	150.95
15H-2	150	135	17.45	152.45
15H-3	150	136.5	17.45	153.95
15H-4	150	138	17.45	155.45
15H-5	150	139.5	17.45	156.95
15H-6	150	141	17.45	158.45
15H-7	32	142.5	17.45	159.95
15H-CC	19	142.8	17.45	160.25
16H-1	150	143	18.66	161.66

Table 4 (continued).

Core and section	Section length (cm)	Depth (mbsf)	Offset (m)	Composite depth (mcd)
16H-2	150	144.5	18.66	163.16
16H-3	150	146	18.66	164.66
16H-4	150	147.5	18.66	166.16
16H-5	150	149	18.66	167.66
16H-6	150	150.5	18.66	169.16
16H-7	29	152	18.66	170.66
16H-CC	40	152.3	18.66	170.96
17H-1	150	152.5	19.73	172.23
17H-2	150	154	19.73	173.73
17H-3	150	155.5	19.73	175.23
17H-4	150	157	19.73	176.73
17H-5	150	158.5	19.73	178.23
17H-6	150	160	19.73	179.73
17H-7	30	161.5	19.73	181.23
17H-CC	37	161.8	19.73	181.53
18H-1	150	162	19.49	181.49
18H-2	150	163.5	19.49	182.99
18H-3	150	165	19.49	184.49
18H-4	150	166.5	19.49	185.99
18H-5	150	168	19.49	187.49
18H-6	150	169.5	19.49	188.99
18H-7	75	171	19.49	190.49
18H-CC	32	171.8	19.49	191.29
19H-1	150	171.5	20.07	191.57
19H-2	150	173	20.07	193.07
19H-3	150	174.5	20.07	194.57
19H-4	150	176	20.07	196.07
19H-5	150	177.5	20.07	197.57
19H-6	150	179	20.07	199.07
19H-7	76	180.5	20.07	200.57
19H-CC	47	181.3	20.07	201.37
20H-1	150	181	19.42	200.42
20H-2	150	182.5	19.42	201.92
20H-3	150	184	19.42	203.42
20H-4	150	185.5	19.42	204.92
20H-5	150	187	19.42	206.42
20H-6	150	188.5	19.42	207.92
20H-7	77	190	19.42	209.42
20H-CC	35	190.8	19.42	210.22
21H-1	150	190.5	17.31	207.81
21H-2	150	192	17.31	209.31
21H-3	150	193.5	17.31	210.81
21H-4	150	195	17.31	212.31
21H-5	150	196.5	17.31	213.81
21H-6	150	198	17.31	215.31
21H-7	57	199.5	17.31	216.81
21H-CC	44	200.1	17.31	217.41
22H-1	150	200	17.08	217.08
22H-2	150	201.5	17.08	218.58
22H-3	150	203	17.08	220.08
22H-4	150	204.5	17.08	221.58
22H-5	150	206	17.08	223.08
22H-6	150	207.5	17.08	224.58
22H-7	55	209	17.08	226.08
22H-CC	8	209.6	17.08	226.68
23H-1	150	209.5	17.97	227.47
23H-2	150	211	17.97	228.97
23H-3	150	212.5	17.97	230.47
23H-4	150	214	17.97	231.97
23H-5	150	215.5	17.97	233.47
23H-6	150	217	17.97	234.97
23H-7	71	218.5	17.97	236.47
23H-CC	44	219.2	17.97	237.17
24H-1	150	219	18.91	237.91
24H-2	150	220.5	18.91	239.41
24H-3	150	222	18.91	240.91
24H-4	150	223.5	18.91	242.41
24H-5	150	225	18.91	243.91
24H-6	103	226.5	18.91	245.41
24H-CC	23	227.5	18.91	246.41
25H-1	150	228.5	20.28	248.78
25H-2	150	230	20.28	250.28
25H-3	150	231.5	20.28	251.78
25H-4	150	233	20.28	253.28
25H-5	150	234.5	20.28	254.78
25H-6	150	236	20.28	256.28
25H-7	76	237.5	20.28	257.78
25H-CC	42	238.3	20.28	258.58
26H-1	150	238	22.63	260.63
26H-2	150	239.5	22.63	262.13
26H-3	150	241	22.63	263.63
26H-4	150	242.5	22.63	265.13
26H-5	150	244	22.63	266.63
26H-6	150	245.5	22.63	268.13
26H-7	28	247	22.63	269.63
27X-1	150	247.5	22.68	270.18
27X-2	150	249	22.68	271.68
27X-3	150	250.5	22.68	273.18
27X-4	150	252	22.68	274.68
27X-5	150	253.5	22.68	276.18
27X-6	150	255	22.68	277.68
27X-7	28	256.5	22.68	279.18
27X-CC	35	256.8	22.68	279.48
28X-1	150	254	25.34	279.34
28X-2	150	255.5	25.34	280.84
28X-3	150	257	25.34	282.34
28X-4	150	258.5	25.34	283.84
28X-5	150	260	25.34	285.34
28X-6	150	261.5	25.34	286.84
28X-7	38	263	25.34	288.34
28X-CC	15	263.4	25.34	288.74
29X-1	150	263.7	25.28	288.98
29X-2	150	265.2	25.28	290.48
29X-3	150	266.7	25.28	291.98
29X-4	150	268.2	25.28	293.48
29X-5	150	269.7	25.28	294.98
29X-6	135	271.2	25.28	296.48
29X-CC	31	272.6	25.28	297.88
30X-1	150	273.3	25.6	298.9
30X-2	150	274.8	25.6	300.4
30X-3	150	276.3	25.6	301.9
30X-4	150	277.8	25.6	303.4
30X-5	150	279.3	25.6	304.9
30X-6	150	280.8	25.6	306.4
30X-7	43	282.3	25.6	307.9
30X-CC	33	282.7	25.6	308.3
31X-1	150	282.9	25.6	308.5
31X-2	150	284.4	25.6	310
31X-3	150	285.9	25.6	311.5
31X-4	150	287.4	25.6	313
31X-5	56	288.9	25.6	314.5
31X-CC	10	289.5	25.6	315.1
32X-1	150	292.6	26.71	319.31
32X-2	150	294.1	26.71	320.81
32X-3	150	295.6	26.71	322.31
32X-4	150	297.1	26.71	323.81
32X-5	150	298.6	26.71	325.31
32X-6	150	300.1	26.71	326.81
32X-7	23	301.6	26.71	328.31
32X-CC	45	301.8	26.71	328.51
33X-1	150	302.2	27.75	329.95
33X-2	150	303.7	27.75	331.45
33X-3	150	305.2	27.75	332.95
33X-4	30	306.7	27.75	334.45
33X-CC	36	307	27.75	334.75
34X-1	150	311.9	25.6	337.5
34X-2	150	313.4	25.6	339
34X-3	150	314.9	25.6	340.5
34X-4	150	316.4	25.6	342
34X-5	150	317.9	25.6	343.5
34X-6	52	319.4	25.6	345
34X-CC	54	319.9	25.6	345.5
35X-1	150	321.5	26.61	348.11
35X-2	150	323	26.61	349.61
35X-3	150	324.5	26.61	351.11
35X-4	150	326	26.61	352.61
35X-5	150	327.5	26.61	354.11
35X-CC	47	329	26.61	355.61
36X-1	150	331.1	24.9	356
36X-2	150	332.6	24.9	357.5
36X-3	150	334.1	24.9	359
36X-4	150	335.6	24.9	360.5
36X-5	18	337.1	24.9	362
36X-CC	37	337.3	24.9	362.2
37X-1	150	340.8	26.18	366.98
37X-2	150	342.3	26.18	368.48
37X-3	150	343.8	26.18	369.98
37X-4	150	345.3	26.18	371.48
37X-5	150	346.8	26.18	372.98
37X-6	100	348.3	26.18	374.48
37X-7	56	349.3	26.18	375.48
37X-CC	54	349.9	26.18	376.08
38X-1	150	350.4	26.27	376.67
38X-2	150	351.9	26.27	378.17
38X-3	150	353.4	26.27	379.67
38X-4	150	354.9	26.27	381.17
38X-5	150	356.4	26.27	382.67
38X-6	123	357.9	26.27	384.17
38X-CC	40	359.1	26.27	385.37
39X-1	150	360.1	26.61	386.71
39X-2	150	361.6	26.61	388.21
39X-3	150	363.1	26.61	389.71
39X-4	150	364.6	26.61	391.21
39X-5	150	366.1	26.61	392.71
39X-6	150	367.6	26.61	394.21
39X-7	43	369.1	26.61	395.71

Table 4 (continued).

Core and section	Section length (cm)	Depth (mbsf)	Offset (m)	Composite depth (mcd)
39X-CC	49	369.5	26.61	396.11
40X-1	150	369.7	26.7	396.4
40X-2	150	371.2	26.7	397.9
40X-3	150	372.7	26.7	399.4
40X-4	150	374.2	26.7	400.9
40X-5	150	375.7	26.7	402.4
40X-6	150	377.2	26.7	403.9
40X-7	43	378.7	26.7	405.4
40X-CC	32	379.1	26.7	405.8
41X-1	150	379	25.87	404.87
41X-2	150	380.5	25.87	406.37
41X-3	150	382	25.87	407.87
41X-4	150	383.5	25.87	409.37
41X-5	150	385	25.87	410.87
41X-6	150	386.5	25.87	412.37
41X-7	48	388	25.87	413.87
41X-CC	29	388.5	25.87	414.37
42X-1	150	388.7	27.51	416.21
42X-2	150	390.2	27.51	417.71
42X-3	150	391.7	27.51	419.21
42X-4	150	393.2	27.51	420.71
42X-5	150	394.7	27.51	422.21
42X-6	150	396.2	27.51	423.71
42X-7	47	397.7	27.51	425.21
42X-CC	35	398.2	27.51	425.71

constrain the sedimentation rates (Figs. 13–14 and Table 6). These 90 events have an average depth uncertainty of ±0.7 m, corresponding to a resolution of one half core section. A handful of these 90 events were subsequently chosen as control points in the age-depth plots (Table 7). These control points were derived from Hole 926A in the interval between 0 and 348.44 mcd (318.13 mbsf), and from Hole 926B below that level.

The sedimentation rate history shows high values in the latest Miocene through Pleistocene interval, ranging between 27 and 35 m/m.y., using the mcd scale. Planktonic foraminifers account for most of the scatter of age-depth points in this interval, owing to problems related to time-scale calibration. For example, the base of *Pulleniatina finalis* has been assigned an age of 1.4 Ma from studies in central equatorial Pacific cores (Hays et al., 1969). Results from Leg 154 show that this event occurred approximately 0.6 m.y. earlier in the western equatorial Atlantic. Such calibration problems account for much of the scatter observed among the planktonic foraminifers (Fig. 13). (Precise recalibration of this event for the equatorial Atlantic will require shore-based work.)

The sedimentation rates in the late early Miocene through late Miocene interval (5.9–18.1 Ma) range from 12 to 20 m/m.y., which is 24%–64% lower than the rates observed in the Pliocene–Pleistocene interval. Two nannofossil events occur below the chosen rate line in the Miocene, namely, the FO of *Amaurolithus amplificus* and the top of the high abundance interval of *Discoaster deflandrei.* Results from Sites 925 and 926 indicate that these events occurred earlier in the western equatorial Atlantic, in comparison with the sites in which their age estimates were derived. The difference seems to amount to a few hundred thousand years in both cases.

The depth offsets between the mbsf and mcd scales show little change from below the top of Core 154-926A-26H at 260.36 mcd (232.00 mbsf) to the terminal depth of this hole at 355.67 mcd (325.36 mbsf), varying only between 28.36 and 30.31 m (see "Composite Section" section, this chapter). This explains why the mcd and mbsf sedimentation rates are virtually identical below the control point provided by the base of common *Discoaster kugleri* at 266.41 mcd (238.05 mbsf).

Sedimentation rates in the two holes were linked between the base of *Sphenolithus heteromorphus* and the base of *Sphenolithus belemnos* (383.36 mcd, 353.55 mbsf). Biostratigraphic control points below the base of *Sphenolithus belemnos* are few, resulting in poor resolution. A linear rate is assumed over a 4-m.y.-long interval between 19.7 and 23.7 Ma, with a single intermediate point supporting the rate line (Fig. 13).

The few points provided by nannofossils and foraminifers diverge in the Oligocene. The discrepancy is greatest at the bottom of the section, where the LO of *Sphenolithus distentus* (26.5 Ma) occurred at 600.61 mcd, and where the top of common *Chiloguembelina cubensis* (28.5 Ma) occurred at 603.38 mcd. Obviously, either one or both is not correctly calibrated, or the LO of one or both species has not been correctly recognized in Hole 926B. We note that the LO of *Sphenolithus distentus* relative to the *Chiloguembelina cubensis* and *Paragloborotalia opima* datums is different at Sites 925 and 926.

Because the top of common *Chiloguembelina cubensis* was used at Site 925 as a control point for estimating sedimentation rates, this point was also chosen at Site 926. This facilitated the comparison of the late Oligocene sedimentation rates at the two sites, and resulted in only a minor rate change at the Oligocene/Miocene transition. Judging from the nearly constant wavelength of the sediment color cycles, and assuming that the force causing these cycles occurred at a constant periodicity (i.e., obliquity-induced cycles; see "Lithostratigraphy" section, this chapter), the sedimentation rate for the late Oligocene should not differ much from that for the early Miocene. Indeed, estimating the wavelength of obliquity cycles may provide the most accurate tool for establishing late Oligocene sedimentation rates at Site 926.

The sedimentation rates at Site 926, which are uncorrected for compaction, are summarized in Figure 14. Three longer time intervals with characteristic sedimentation rates can be discerned at Site 926: a high rate interval encompassing the Pliocene and Pleistocene, a low rate interval encompassing the late and middle Miocene, and an intermediate high rate interval encompassing the early Miocene and late Oligocene (Fig. 14). Sites 925 and 926 were both drilled on the southern Ceara Rise approximately 30 nmi apart under similar conditions of deposition, the main difference being the approximately 600-m greater water depth at Site 926. Sedimentation rates in the three time intervals from Site 926 have been compared with corresponding intervals from Site 925 (Fig. 14). The difference in sedimentation rate between the two sites is negligible in the Pliocene–Pleistocene interval (1.8% lower at Site 926). There is a large difference in the middle to late Miocene interval, where the sedimentation rate for Site 926 is 25.2% lower than for Site 925. This large difference is caused partly by carbonate dissolution, but it is also caused by material added to the Site 925 section through slumping (see "Lithostratigraphy" section, "Site 925" chapter, this volume). The relationship between sedimentation rates at the two sites is inverted in the early Miocene–late Oligocene interval, where the rate is 8.5% higher at Site 926. Considering the short distance between Sites 925 and 926, and therefore assuming identical pelagic input at any given time slice, and also considering the fact that carbonate dissolution increases as a function of increasing water depth, this implies that the higher sedimentation rates at the deeper site must result from downslope transport processes or that some material has been lost at Site 925.

GEOCHEMISTRY

Hydrocarbon Geochemistry

We routinely measured the volatile hydrocarbon content in all sediment cores from Hole 926A and from the deep section of Hole 926B, for a total of 64 analyses. Concentrations of methane remained at or near background levels at all depths, as at Site 925, with no heavier hydrocarbons identified. These results suggest that biogenic methanogenesis was minimal at Site 926, probably because of the low organic carbon input. This interpretation is consistent with sediment total carbon measurements and interstitial-water sulfate determinations at this site, which indicate relatively low organic carbon input to the site and incomplete sulfate reduction throughout the section (see "Interstitial-water Geochemistry" and "Solid-phase Geochemistry" sections, below).

Table 5. Splice tie points, Site 926.

Core, section, interval (cm)	Depth (mbsf)	Depth (mcd)		Core, section, interval (cm)	Depth (mbsf)	Depth (mcd)
				154-926B-1H-1, 0.0	0.00	0.00
154-926B-1H-4, 34.5	4.84	4.84	tie to	154-926C-1H-2, 66.5	2.66	4.84
154-926C-1H-6, 96.5	8.97	11.15	tie to	154-926B-2H-2, 112.7	9.63	11.15
154-926B-2H-5, 82.5	13.82	15.34	tie to	154-926C-2H-2, 42.5	11.93	15.34
154-926C-2H-6, 102.5	18.52	21.93	tie to	154-926B-3H-3, 1.7	19.52	21.93
154-926B-3H-6, 44.5	24.44	26.85	tie to	154-926C-3H-3, 57.5	23.08	26.85
154-926C-3H-6, 39.5	27.40	31.17	tie to	154-926B-4H-2, 44.5	27.94	31.17
154-926B-4H-4, 109.5	31.59	34.82	tie to	154-926C-4H-2, 57.5	31.08	34.82
154-926C-4H-6, 111.5	37.62	41.36	tie to	154-926B-5H-1, 139.5	36.90	41.31
154-926B-5H-4, 119.5	41.19	45.60	tie to	154-926C-5H-2, 126.7	41.27	45.59
154-926C-5H-6, 147.5	47.47	51.79	tie to	154-926B-6H-1, 89.5	45.90	51.79
154-926B-6H-3, 84.6	48.85	54.74	tie to	154-926C-6H-1, 111.5	49.12	54.74
154-926C-6H-7, 3.6	57.04	62.66	tie to	154-926B-7H-2, 4.6	56.05	62.66
154-926B-7H-3, 9.5	57.60	64.21	tie to	154-926C-7H-1, 147.6	58.98	64.21
154-926C-7H-6, 114.5	66.14	71.37	tie to	154-926A-8H-2, 79.0	63.29	71.37
154-926A-8H-5, 129.1	68.29	76.37	tie to	154-926C-8H-2, 135.5	69.86	76.37
154-926C-8H-6, 21.5	74.71	81.22	tie to	154-926A-9H-1, 119.1	71.69	81.22
154-926A-9H-4, 99.0	75.99	85.52	tie to	154-926C-9H-1, 105.5	77.56	85.52
154-926C-9H-6, 117.5	85.18	93.14	tie to	154-926A-10H-2, 114.0	82.64	93.14
154-926A-10H-4, 134.0	85.84	96.34	tie to	154-926C-10H-2, 3.5	87.54	96.34
154-926C-10H-6, 87.5	94.38	103.18	tie to	154-926A-11H-2, 14.0	91.14	103.18
154-926A-11H-4, 64.0	94.64	106.68	tie to	154-926C-11H-1, 72.5	96.22	106.68
154-926C-11H-6, 93.5	103.93	114.39	tie to	154-926A-12H-3, 4.1	102.04	114.39
154-926A-12H-6, 14.4	106.64	118.99	tie to	154-926C-12H-1, 138.5	106.39	118.99
154-926C-12H-6, 123.5	113.74	126.34	tie to	154-926B-13H-1, 59.5	112.10	126.34
154-926B-13H-5, 134.5	118.85	133.09	tie to	154-926C-13H-3, 63.5	118.14	133.09
154-926C-13H-5, 147.5	121.97	136.92	tie to	154-926A-14H-3, 14.5	121.14	136.92
154-926A-14H-5, 54.5	124.54	140.32	tie to	154-926C-14H-1, 15.5	124.15	140.32
154-926C-14H-7, 51.5	133.51	149.68	tie to	154-926B-15H-2, 84.5	132.85	149.68
154-926B-15H-6, 69.6	138.70	155.53	tie to	154-926C-15H-4, 9.5	138.10	155.53
154-926C-15H-5, 96.5	140.46	157.89	tie to	154-926A-16H-2, 144.5	139.95	157.89
154-926A-16H-6, 74.5	145.24	163.18	tie to	154-926C-16H-2, 3.5	144.54	163.18
154-926C-16H-6, 27.5	150.77	169.41	tie to	154-926B-17H-1, 45.5	149.96	169.41
154-926B-17H-4, 99.5	154.99	174.44	tie to	154-926C-17H-2, 72.5	154.73	174.44
154-926C-17H-6, 132.5	161.32	181.03	tie to	154-926B-18H-2, 48.5	160.99	181.03
154-926B-18H-6, 24.5	166.74	186.78	tie to	154-926C-18H-4, 78.5	167.29	186.78
154-926C-18H-6, 117.5	170.68	190.17	tie to	154-926B-19H-1, 33.5	168.84	190.17
154-926B-19H-6, 99.5	176.99	198.32	tie to	154-926A-20H-1, 134.8	176.35	198.32
154-926A-20H-5, 84.4	181.84	203.81	tie to	154-926B-20H-3, 12.5	181.13	203.81
154-926B-20H-6, 117.5	186.68	209.36	tie to	154-926A-21H-2, 84.4	186.84	209.36
154-926A-21H-5, 144.4	191.94	214.46	tie to	154-926B-21H-4, 33.5	192.34	214.46
154-926B-21H-6, 42.5	195.43	217.55	tie to	154-926C-22H-1, 51.5	200.51	217.55
154-926C-22H-5, 87.5	206.88	223.92	tie to	154-926B-22H-4, 6.5	201.57	223.92
154-926B-22H-6, 105.5	205.55	227.90	tie to	154-926A-23H-1, 34.7	203.85	227.90
154-926A-23H-5, 54.6	210.05	234.10	tie to	154-926B-23H-3, 3.5	209.54	234.10
154-926B-23H-6, 87.5	214.88	239.44	tie to	154-926A-24H-2, 34.7	214.85	239.44
154-926A-24H-5, 4.7	219.05	243.64	tie to	154-926B-24H-2, 63.5	218.13	243.64
154-926B-24H-7, 36.5	225.37	250.88	tie to	154-926A-25H-2, 103.7	225.04	250.88
154-926A-25H-5, 144.6	229.95	255.79	tie to	154-926B-25H-3, 129.5	229.79	255.79
154-926B-25H-7, 30.5	234.80	260.80	tie to	154-926A-26H-1, 44.6	232.45	260.80
154-926A-26H-4, 144.6	237.95	266.30	tie to	154-926B-26H-3, 3.5	238.04	266.30
154-926B-26H-5, 111.5	242.12	270.38	tie to	154-926C-27X-1, 24.5	247.74	270.38
154-926C-27X-4, 78.5	252.79	275.43	tie to	154-926B-27H-1, 138.5	245.88	275.43
154-926B-27H-5, 117.6	251.68	281.23	tie to	154-926A-28H-1, 105.5	252.05	281.23
154-926A-28H-6, 76.5	259.27	288.45	tie to	154-926B-29X-1, 24.5	259.24	288.45
154-926B-64X-7, 34.5	605.84	635.65				

Interstitial-water Geochemistry

We collected interstitial water from 25 samples at Site 926: 15 from Hole 926A at depths ranging from 2.95 to 302.95 mbsf, and 10 from Hole 926B at depths ranging from 329.4 to 591.25 mbsf (Table 8). The samples from Holes 926A and 926B are considered to constitute a single depth profile. As at Site 925, chemical gradients in the interstitial water at Site 926 are controlled primarily by biogenic sediment diagenesis in a low organic carbon environment, and by alteration reactions in the underlying basalt. We found similar silica and alkalinity highs around 300–450 mbsf as at Site 925, which indicates that organic carbon and biogenic silica inputs to the site may have been greater than is reflected in the present sediment composition.

Chlorinity, as measured by titration, steeply increases from a low of 550 mM at 2.45 mbsf to 560 mM at 36.95 mbsf (Fig. 15). Deeper in the section, chlorinity fluctuates between values of 560 and 575 mM. The most prominent feature in the chloride profile is a pronounced low in the sample taken at 534.75 mbsf. Sodium concentrations, as calculated by charge balance, gradually decrease downsection from concentrations of about 474 mM near the top of Hole 926A to a low value of 447 mM in the deepest sample from Hole 926B (Fig. 15). There is considerable fluctuation within this trend. Because alkalinity was not measured on Sample 154-926B-57X-4, 135–150 cm, the sodium concentration was not calculated for this sample. Salinity, as measured by a handheld refractometer, varies little, with values ranging from 34 to 35.5 g/kg throughout most of the section (Fig. 15). As with chloride, a distinct low is prominent in the sample from 534.75 mbsf.

The alkalinity profile is similar to that measured at Site 925, with fairly constant low values between 3.1 and 3.5 mM to a depth of 131.95 mbsf, and then an increase to a maximum of 10.3 mM at 417.50 mbsf (Fig. 15). Alkalinity decreases again deeper in the hole (to 6.7 mM), but the peak of high alkalinity is very broad, extending from about 300 to 500 mbsf. This is much higher alkalinity than is typically found at low-latitude, pelagic carbonate sites (i.e., Leg 115, Swart and Burns, 1990; ODP Site 758 of Leg 121, Shipboard Scientific Party, 1989; Leg 130, Kroenke, Berger, Janecek, et al., 1991; Leg 138, Mayer, Pisias, Janecek, et al., 1992). The pH varies erratically with depth, between 6.4 and 7.6 (Fig. 15). The pH generally decreases from the top of the section to about 360 mbsf, dropping from 7.5 to 6.4 over that interval; deeper in the section, pH is higher on average, with values fluctuating between 7.2 and 7.6. In the top 200 mbsf of the section, dissolved silica concentrations are low (near 100 µM; Fig. 15). Values increase

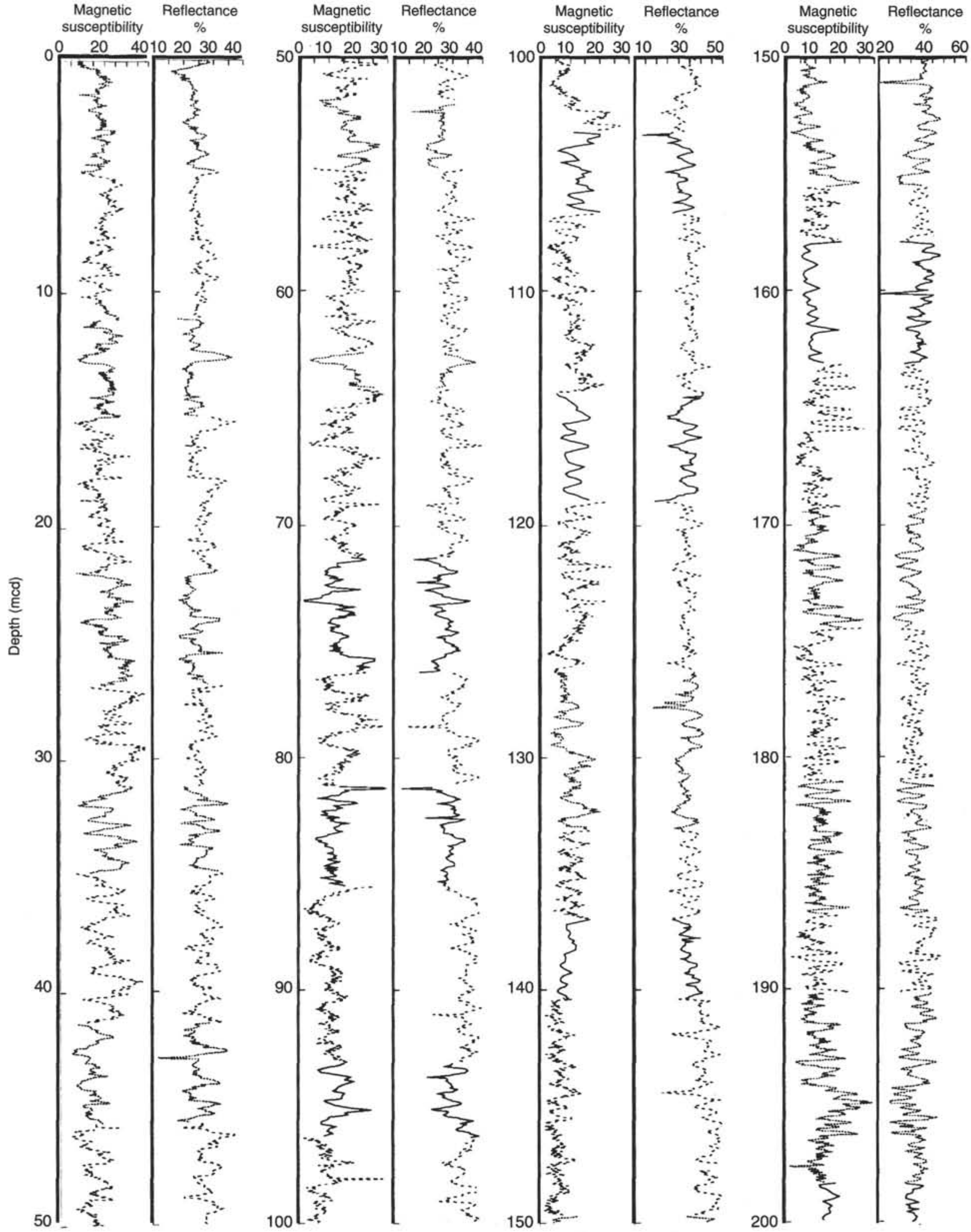

Figure 12. Spliced records of magnetic susceptibility and percentage of reflectance from the upper 300 mcd of Site 926. Tie points for forming the splice are given in Table 5. Hole 926A = solid line, Hole 926B = dotted line, and Hole 926C = dashed line.

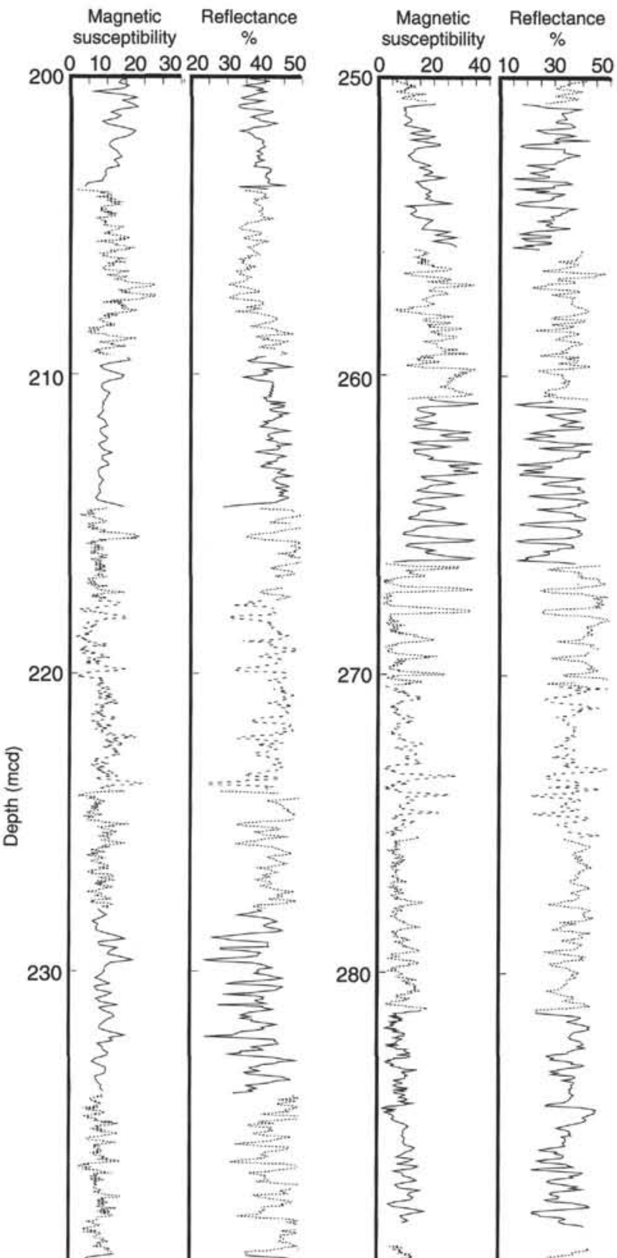

Figure 12 (continued).

abruptly to near-saturation values of about 1000–1300 µM between 200 and 300 mbsf, with a broad peak centered around 400 mbsf. Values gradually decrease to around 700 µM in our deepest sample at 591.25 mbsf. The maximum silica concentrations at Site 926 are significantly greater than at Site 925 (where they were less than 1000 µM), and at Site 926 siliceous microfossils are common in lithologic Subunit IIIB from 370 to 460 mbsf. This indicates that the original biogenic silica deposits are still a significant source of dissolved silica to the pore waters at Site 926, whereas at Site 925 they have been more completely dissolved. In combination with higher sedimentation rates determined for this interval at Site 926 (see "Sedimentation Rates" section, this chapter), the higher dissolved silica peak at this site suggests a higher silica burial rate at Site 926 relative to Site 925.

Sulfate decreases and ammonium increases with depth within the drilled interval (Fig. 15), with the two profiles highly negatively correlated ($r = -0.93$) because ammonium is a byproduct of organic matter degradation, whereas sulfate is consumed in the same process (Gieskes, 1981). Sulfate concentrations decrease by nearly 70% over the sampled sequence, but sulfate is never fully reduced. This is consistent with the observation that methane concentrations were near background levels throughout the cored sequence (see "Hydrocarbon Geochemistry" section, above), as methane production occurs below the zone of sulfate reduction (Gieskes, 1981). The sulfate gradient is the steepest in the top 60 mbsf, decreases from about 75 to 160 mbsf, and then slightly increases again. This suggests that active organic matter degradation and sulfate reduction are still occurring deeper in the section and that initial organic carbon inputs may have been greater in the deeper sediments. Ammonium concentrations increase from <100 µM near the sediment-water interface to >1000 µM in the deepest samples. The concave down-gradient of ammonium in the top 50 mbsf indicates that ammonium is presently being produced in this interval. A similar trend exists deeper in the section, from about 240 to 360 mbsf. The irregular pattern deeper than 360 mbsf is harder to interpret.

Strontium concentrations increase from a near-seawater value of 94 µM close to the sediment-water interface to a maximum of 2008 µM at 591.25 mbsf (Fig. 15). The strontium maximum here is unusually high, but it is comparable with that at Site 925. The high strontium values indicate calcite recrystallization within the section, although sparry calcite is not evident by visual inspection within the cored interval.

Lithium pore-water values increase steadily from near-seawater values of 25 µM at the top of the section to 1168 µM at 591.25 mbsf (Fig. 15). Such high concentrations of lithium are unusual in pelagic carbonates, with measured concentrations at this site an order of magnitude greater than those at equatorial Pacific sites (Leg 130, Kroenke, Berger, Janecek, et al., 1991; Leg 138, Mayer, Pisias, Janecek, et al., 1992). Similarly high lithium concentrations were measured in pore water from the Guaymas Basin and from the Peru continental slope and are attributed to the effects of crustal alteration (Gieskes et al., 1982; Martin et al, 1991).

Calcium concentrations increase with depth (4.91 mM/100 m), whereas magnesium concentrations decrease (–4.09 mM/100 m) (Fig. 15). The calcium and magnesium profiles reflect alteration of basement, with magnesium replacing calcium in altered basement rocks. Potassium concentrations decrease with depth from 11.6 mM at 1.45 mbsf to 5.6 mM at 591.25 mbsf (Fig. 15), presumably also because of an uptake of potassium during basement alteration.

In summary, the interstitial-water profiles at Site 926 are quite similar to those at Site 925. The redox state is the same as at Site 925 and reflects reduction of a relatively low organic carbon input to the site. Higher pore-water silica concentrations at Site 926, prevalent siliceous microfossils within lithologic Subunit IIIB, and higher sedimentation rates in that interval may indicate higher silica burial at Site 926, the deeper site. As at Site 925, the high strontium values indicate that recrystallization has affected the biogenic carbonate component of the sediments. High lithium concentrations at both sites are unusual for pelagic carbonate sediments. Calcium, magnesium, and potas-

Table 6. Biostratigraphic events and sedimentation rate data from Holes 926A and 926B.

Marker species	Age (Ma)	Depth (mbsf)	(±)	Nannofossils (mbsf)	Foraminifers (mbsf)	Nannofossils (mcd)	Foraminifers (mcd)
Hole 926A:							
T *Pseudoemiliania lacunosa*	0.46	14.70–15.40	0.35	15.05		16.14	
Reentrance medium *Gephyrocapsa*	1.03	31.65–32.40	0.38	32.03		34.61	
Tlarge *Gephyrocapsa*	1.24	32.83–36.70	1.94	34.77		37.76	
B *Pulleniatina finalis*	1.4	56.71–58.21	0.75		57.46		63.99
B large *Gephyrocapsa*	1.46	41.20–42.33	0.56	41.77		45.18	
T *Calcidiscus macintyrei*	1.60	45.80–46.20	0.20	46.00		50.07	
B *Gephyrocapsa* medium	1.67	47.70–48.40	0.35	48.05		52.12	
T *Globigerinoides fistulosus*	1.7	55.22–56.72	0.75		55.97		62.50
T *Globoturborotalita apertura*	1.9	59.71–60.81	0.55		60.26		66.79
T *Globigerinoides extremus*	1.9	58.21–59.71	0.75		58.96		65.49
T *Discoaster brouweri*	1.95	53.80–54.20	0.20	54.00		60.53	
B *Globorotalia truncatulinoides*	2.0	59.71–60.81	0.55		60.26		66.79
B acme *Discoaster triradiatus*	2.15	59.80–60.60	0.40	60.20		66.73	
T *Globorotalia exilis*	2.2	60.81–61.69	0.44		61.25		68.56
T *Globorotalia miocenica*	2.3	64.75–66.19	0.72		65.47		73.56
Reappearance *Pulleniatina*	2.3	61.69–63.19	0.75		62.44		70.53
T *Discoaster pentaradiatus*	2.44	65.24–66.30	0.53	65.77		73.86	
T *Globoturborotalita decoraperta*	2.6	75.71–80.71	2.50		78.21		88.24
T *Globorotalia pertenuis*	2.6	74.21–75.71	0.75		74.96		84.50
T *Discoaster tamalis*	2.76	75.80–80.56	2.38	78.18		87.72	
T *Dentoglobigerina altispira*	3.0	82.21–83.71	0.75		82.96		93.47
T *Globorotalia multicamerata*	3.0	80.71–82.21	0.75		81.46		91.97
T *Sphaeroidinellopsis seminulina*	3.1	89.71–90.21	0.25		89.96		101.24
B *Globorotalia pertenuis*	3.5	96.21–97.71	0.75		96.96		109.01
Disappearance *Pulleniatina*	3.5	93.21–94.71	0.75		93.96		106.01
B *Globorotalia miocenica*	3.6	93.21–94.71	0.75		93.96		106.01
T *Reticulofenestra pseudoumbilicus*	3.77	105.80–106.20	0.20	106.00		118.36	
S to D *Pulleniatina*	4.0	109.19–110.69	0.75		109.94		123.59
T *Globoturborotalita nepenthes*	4.3	123.21–124.71	0.75		123.96		139.77
T *Globorotalia plesiotumida*	4.4	128.21–129.71	0.75		128.96		145.77
T *Globorotalia ciaboensis*	5.0	128.21–129.71	0.75		128.96		145.77
B *Ceratolithus rugosus*	5.04	136.40–136.86	0.23	136.63		153.44	
T *Nenogloboquadrina acostaensis*	5.1	126.70–128.21	0.75		127.45		143.77
T *Ceratolithus acutus*	5.04	136.86–137.40	0.27	137.13		154.52	
B *Ceratolithus acutus*	5.34	143.80–144.20	0.20	144.00		161.96	
T *Triquetrorhabdulus rugosus*	5.34	142.30–142.70	0.35	142.50		160.46	
T *Globoquadrina baroemoenensis*	5.4	131.21–132.71	0.75		131.96		148.77
T *Discoaster quinqueramus*	5.56	147.04–147.30	0.13	147.17		165.64	
B *Sphaeroidinella dehiscens*	5.6	135.71–136.30	0.29		136.00		152.82
T *Amaurolithus amplificus*	5.88	155.90–156.48	0.29	156.19		175.17	
B *Globorotalia tumida*	5.9	150.21–151.71	0.75		150.96		169.94
B *Globorotalia margaritae*	6.2	153.21–154.71	0.75		153.96		172.94
B *Amaurolithus amplificus*	6.5	169.33–170.83	0.75	170.08		191.22	
B *Amaurolithus primus*	7.3	175.80–178.80	1.50	177.30		199.28	
B *Globorotalia cibaoensis*	7.7	164.21–166.21	1.00		165.21		185.60
B *Globigerinoides extremus*	8.0	183.21–184.71	0.75		183.96		205.94
B *Globorotalia plesiotumida*	8.2	191.21–192.71	0.75		191.96		214.65
B *Discoaster berggrenii*	8.4	194.80–195.20	0.20	195.00		217.72	
T *Discoaster hamatus*	9.4	213.41–213.80	0.20	213.61		237.94	
T *Catinaster calyculus*	9.4	213.41–213.40	0.00	213.41		237.74	
T *Paragloborotalia mayeri*	10.3	223.21–224.71	0.75		223.96		249.81
B *Discoaster hamatus*	10.4	223.30–223.72	0.21	223.51		249.36	
B *Coccolithus miopelagicus*	10.8	229.70–230.20	0.25	229.95		255.80	
B *Catinaster coalitus*	10.7	227.80–228.20	0.20	228.00		253.85	
B *Globoturborotalita nepenthes*	10.8	232.71–234.21	0.75		233.46		261.82
B *Globoturborotalita decoraperta*	11.2	230.71–232.71	1.00		231.71		258.82
Tc *Discoaster kugleri*	11.3	233.90–234.70	0.40	234.30		262.66	
Bc *Discoaster kugleri*	11.7	237.70–238.40	0.35	238.05		266.41	
T *Fohsella fohsi* s.l.	11.8	238.71–240.21	0.75		239.46		267.82
B *Fohsella robusta*	12.7	254.71–256.21	0.75		255.46		284.65
T *Cyclicargolithus floridanus*	13.2	259.69–261.01	0.66	260.35		289.54	
T *Sphenolithus heteromorphus*	13.6	265.40–265.80	0.20	265.60		294.31	
B *Fohsella fohsi*	13.5	262.26–263.61	0.68		262.94		291.65
B *Fohsella "praefoshi"*	14.0	272.32–273.71	0.69		273.02		302.12
B *Fohsella peripheroronda*	14.6	273.71–275.21	0.75		274.46		303.56
B *Fohsella peripheroacuta*	14.7	283.21–284.71	0.75		283.96		313.06
B *Globorotalia praemenardii*	14.9	284.71–286.21	0.75		285.46		314.56
B *Praeorbulina circularis*	16.0	287.71–291.21	1.75		289.46		318.29
B *Praeorbulina glomerosa*	16.1	294.21–295.71	0.75		294.96		323.52
T *Catapsydrax dissimilis*	17.3	302.21–303.71	0.75		302.96		332.06
T *Discoaster deflandrei* abund	16.2	301.20–302.70	0.75	301.95		331.05	
B *Sphenolithus heteromorphus*	18.1	318.05–318.70	0.32	318.38		348.08	
Hole 926B:							
T *Praeorbulina sicana*	14.8	282.04–283.54	0.75		282.79		312.60
B *Orbulina suturalis*	15.1	286.54–288.71	1.08		287.63		317.44
B *Globorotalia archeomenardii*	15.5	290.21–291.71	0.75		290.96		320.77
T *Helicosphaera ampliaperta*	15.8	288.40–288.80	0.20	288.60		318.41	
B *Praeorbulina circularis*	16.0	290.21–291.71	0.75		290.96		320.77
B *Praeorbulina glomerosa*	16.1	291.71–293.21	0.75		292.46		322.27
B *Praeorbulina sicana*	16.4	311.01–312.01	0.50		311.51		341.32
T *Sphenolithus belemnos*	18.4	322.60–323.30	0.35	322.95		352.76	
T *Globorotalia binaiensis*	19.1	360.71–362.21	0.75		361.46		391.27
B *Sphenolithus belemnos*	19.7	353.00–354.10	0.55	353.55		383.36	
T *Paragloborotalia kugleri*	21.6	411.61–413.81	1.10		412.71		442.52
B *Paragloborotalia kugleri*	23.7	465.11–466.61	0.75		465.86		495.67
T *Sphenolithus delphix*	23.7	469.70–470.00	0.15	469.85		499.66	
B *Sphenolithus delphix*	24.4	472.20–472.90	0.35	472.55		502.36	
T *Sphenolithus ciperoensis*	24.7	495.42–499.43	2.01	497.43		527.24	
B *Paragloborotalia pseudokugleri*	26.3	505.13–506.59	0.73		505.86		535.67
T *Sphenolithus distentus*	26.5	566.15–575.44	4.65	570.80		600.61	
T *Paragloborotalia opima*	27.1	527.41–529.61	1.10		528.51		558.32
Tc *Chiloguembelina cubensis*	28.5	572.82–574.32	0.75		573.57		603.38

Notes: T = top, Tl = top large (>5.5 µm), B = base, Bl = base large (>5.5 µm), Ba = base acme, S to D = sinistral to dextral coiling, Bc = base common, and Tc = top common. Medium size defined as 4.0–5.5 µm.

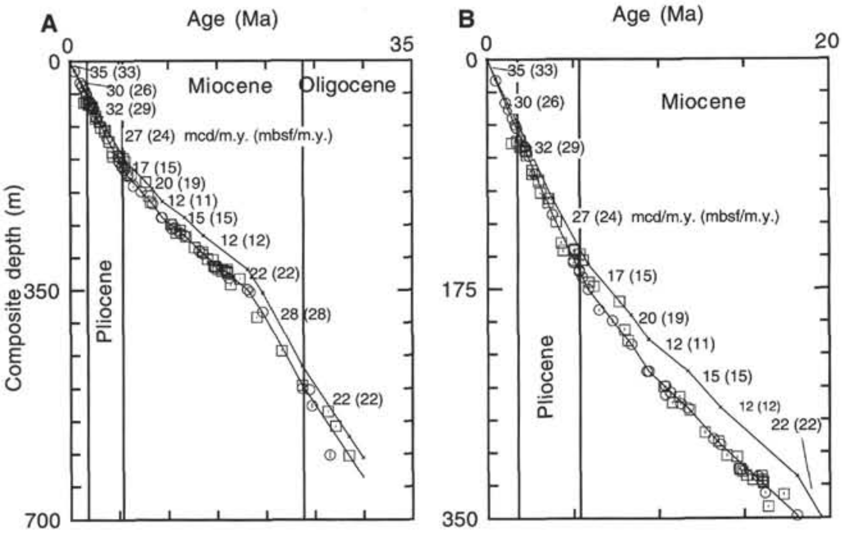

Figure 13. Age-depth plots of calcareous nannofossil (open circles) and planktonic foraminifer (open squares) events at Site 926, using data from Holes 926A and 926B. **A.** Late Oligocene to Holocene. **B.** Early Miocene to Holocene. The vertical bar within symbols represents depth uncertainty. The events are plotted on the mcd depth scale. The solid upper line represents the corresponding sedimentation rate line on the mbsf depth scale. Sedimentation rates are given for both scales; that is, "35 (33)" represents rates expressed in meters per million years on the mcd and mbsf (in parentheses) scales, respectively.

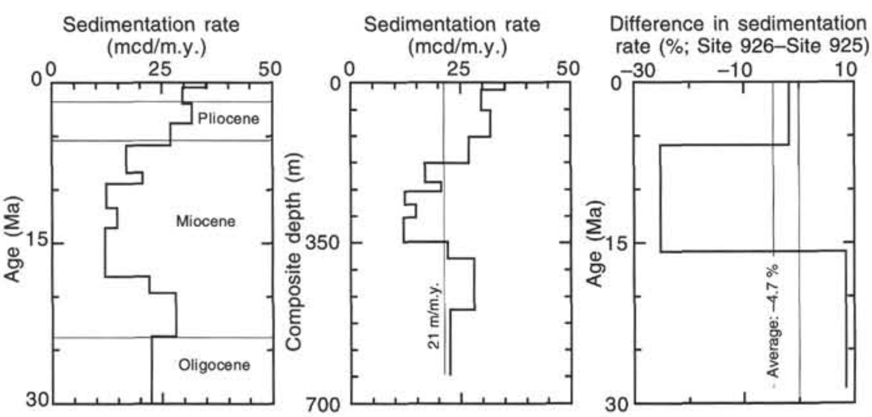

Figure 14. Plots of sedimentation rates at Site 926 on the mcd depth scale vs. age and mcd depth scale vs. mcd depth. In addition, a comparison of sedimentation rates for Sites 925 and 926 is shown in three time segments on the right. The middle figure shows the average sedimentation rate at Site 926 using the mcd scale.

Table 7. Biostratigraphic control points for Site 926 sedimentation rates.

Hole	Biostratigraphic control point	Age (Ma)	Depth (mbsf)	Sedimentation rate (mbsf/m.y.)	Depth (mcd)	Sedimentation rate (mcd/m.y.)
926A	Top section	0.0	0.00		0.00	
926A	T *Pseudoemiliania lacunosa*	0.46	15.05	33	16.14	35
926A	T *Discoaster brouweri*	1.95	54.00	26	60.53	30
926A	T *Reticulofenestra pseudoumbilicus*	3.77	106.00	29	118.36	32
926A	T *Amaurolithus amplificus*	5.88	156.19	24	175.17	27
926A	B *Discoaster berggrenii*	8.4	195.00	15	217.72	17
926A	T *Discoaster hamatus*	9.4	213.61	19	237.94	20
926A	Bc *Discoaster kugleri*	11.7	238.05	11	266.41	12
926A	T *Sphenolithus heteromorphus*	13.6	265.60	15	294.31	15
926A	B *Sphenolithus heteromorphus*	18.1	318.38	12	348.08	12
926B	B *Sphenolithus belemnos*	19.7	353.55	22	383.66	22
926B	B *Paragloborotalia kugleri*	23.7	465.86	28	495.67	28
926B	Tc *Chiloguembelina cubensis*	28.5	573.57	22	603.38	22
926B	Bottom of section, Site 926	30.0	606.29	22	636.10	22

Note: T = top, B = base, Bc = base common, and Tc = top common.

sium profiles are similar to those at Site 925 and are controlled by the alteration of basalt and subsequent diffusion of the constituents to the sediment-water interface.

Solid-phase Geochemistry

A total of 217 samples were measured for calcium carbonate content, comprising approximately a 3-m sampling interval from one complete stratigraphic section from Site 926 (Table 9). One set of closely spaced samples was analyzed from Core 154-926A-20H to compare with high-resolution physical properties, magnetic susceptibility, and color reflectance data. A subset of 85 samples was measured for total carbon, nitrogen, and sulfur content (Table 9).

Calcium carbonate is the dominant sedimentary component at Site 926, ranging from 50% to 80% throughout most of the sedimentary section (Fig. 16). Terrigenous material, most of which is derived from the Amazon River outflow, constitutes the bulk of the noncarbonate portion of the sediments. Several broad-scale features seen at nearby

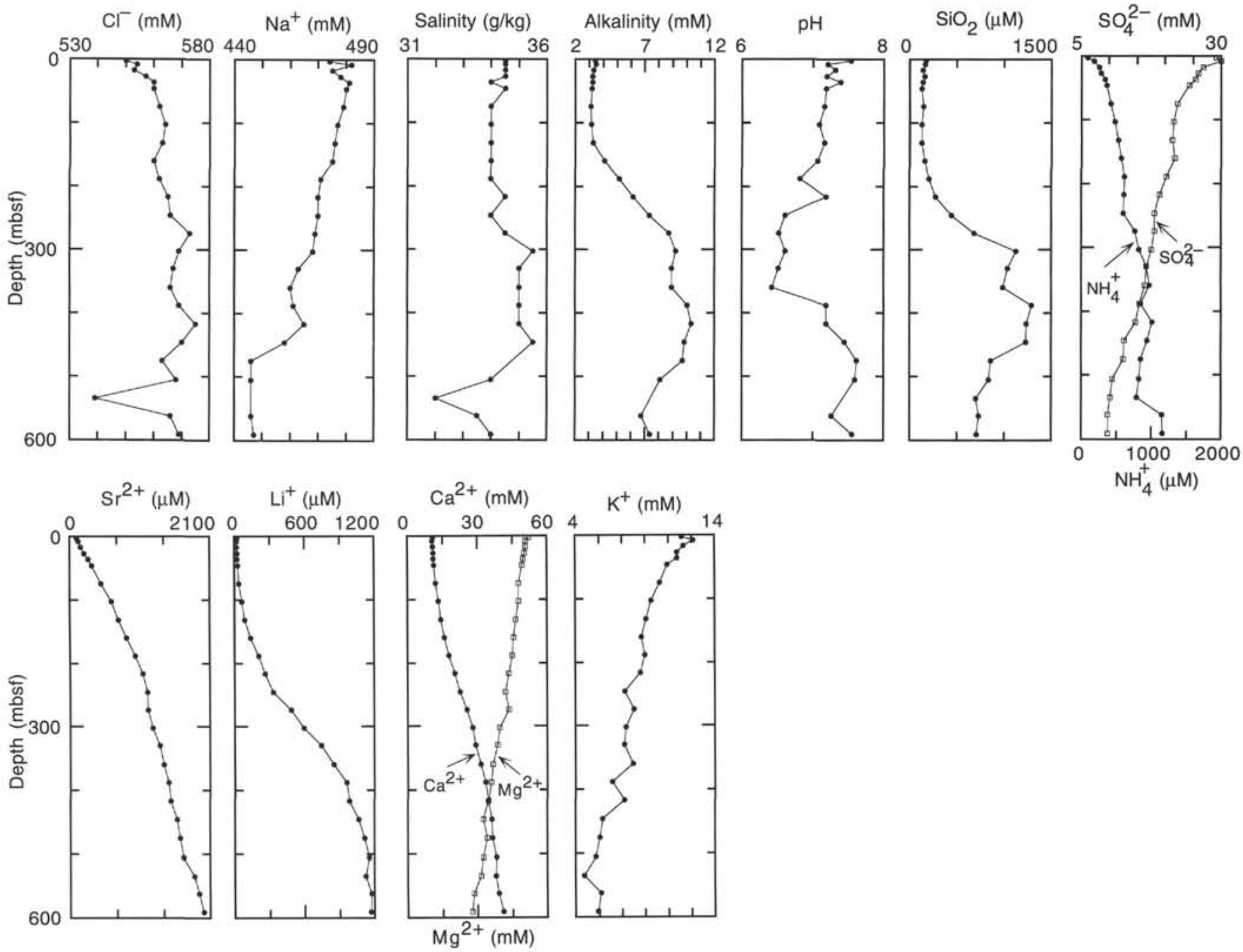

Figure 15. Interstitial-water geochemistry vs. depth.

Table 8. Summary of interstitial-water geochemistry for samples from Holes 926A and 926B.

Core, section, interval (cm)	Depth (mbsf)	Salinity (ppt)	Alkalinity (mM)	pH	Cl^- (mM)	Na^+ (mM)	SiO_2 (µM)	SO_4^{2-} (mM)	NH_4^+ (µM)	Sr^{2+} (µM)	Li^+ (µM)	Ca^{2+} (mM)	Mg^{2+} (mM)	K^+ (mM)
154-926A-														
1H-2, 145–150	2.95	34.5	3.441	7.54	550	474	172.61	29.17	88.66	105	25	10.82	52.34	11.63
2H-3, 145–150	8.45	34.5	3.497	7.21	554	482	164.91	29.98	182.78	132	22	10.65	51.00	12.46
3H-3, 145–150	17.95	34.5	3.316	7.32	553	475	137.43	26.83	253.70	166	22	10.81	50.82	11.77
4H-3, 145–150	27.45	34.5	3.231	7.20	557	478	158.31	25.94	281.67	215	24	11.08	50.53	11.30
5H-3, 145–150	36.95	34.0	3.230	7.39	560	481	142.92	25.44	338.27	275	26	11.04	49.95	11.31
6H-3, 145–150	46.45	34.5	3.209	7.19	560	480	127.53	24.35	362.82	328	30	11.20	49.42	10.61
9H-3, 145–150	74.95	34.0	3.109	7.16	562	479	147.32	22.25	420.79	473	40	11.95	48.09	10.05
12H-3, 145–150	103.45	34.0	3.156	7.09	564	477	130.83	21.56	475.35	626	63	12.95	47.99	9.46
15H-3, 145–150	131.95	34.0	3.275	7.16	563	476	131.93	21.29	525.14	730	89	13.88	46.91	9.06
18H-3, 145–150	160.45	34.0	4.111	7.06	560	475	158.31	21.77	572.20	848	139	15.15	45.91	8.76
21H-3, 145–150	188.95	34.0	5.195	6.82	562	471	206.69	20.28	620.62	977	209	17.21	45.35	8.98
24H-3, 145–150	217.45	34.5	6.158	7.19	565	470	271.55	19.01	614.48	1094	264	19.45	44.04	8.67
27H-3, 145–150	245.95	34.0	7.311	6.61	566	470	443.06	18.16	606.30	1161	332	21.59	42.52	7.56
30H-3, 145–150	274.45	34.5	8.721	6.52	573	469	686.03	18.05	765.89	1170	488	24.56	43.93	8.20
33H-3, 145–150	302.95	35.5	9.244	6.61	569	468	1126.09	17.64	822.49	1241	595	27.00	39.88	7.62
154-926B-														
36X-2, 140–150	329.40	35.0	8.946	6.51	567	463	1037.83	16.62	936.39	1344	742	28.23	39.00	7.51
39X-3, 140–150	359.90	35.0	8.930	6.42	566	460	990.91	16.30	972.53	1404	853	30.28	37.00	8.11
42X-3, 140–150	388.50	35.0	10.065	7.19	569	461	1292.54	15.42	851.82	1475	959	32.40	36.22	6.64
45X-3, 140–150	417.50	35.0	10.343	7.19	575	465	1237.80	14.74	1016.18	1512	986	33.55	35.05	7.49
48X-3, 140–150	446.50	35.5	9.851	7.45	570	458	1228.87	12.67	941.16	1605	1064	34.87	32.86	5.92
51X-3, 135–150	475.35		9.715	7.62	563	446	859.09	12.55	852.50	1652	1117	35.25	34.58	5.72
54X-4, 135–150	505.75	34.0	8.094	7.59	568	446	833.39	10.56	823.17	1704	1154	36.97	32.92	5.45
57X-4, 135–150	534.75	32.0			539		699.34	10.17	792.48	1864	1127	36.56	31.83	4.63
60X-3, 135–150	562.25	33.5	6.748	7.26	566	446	730.62	9.78	1155.99	1936	1177	37.71	29.00	5.81
63X-3, 135–150	591.25	34.0	7.351	7.55	569	447	709.39	9.78	1164.17	2008	1168	39.70	28.28	5.60

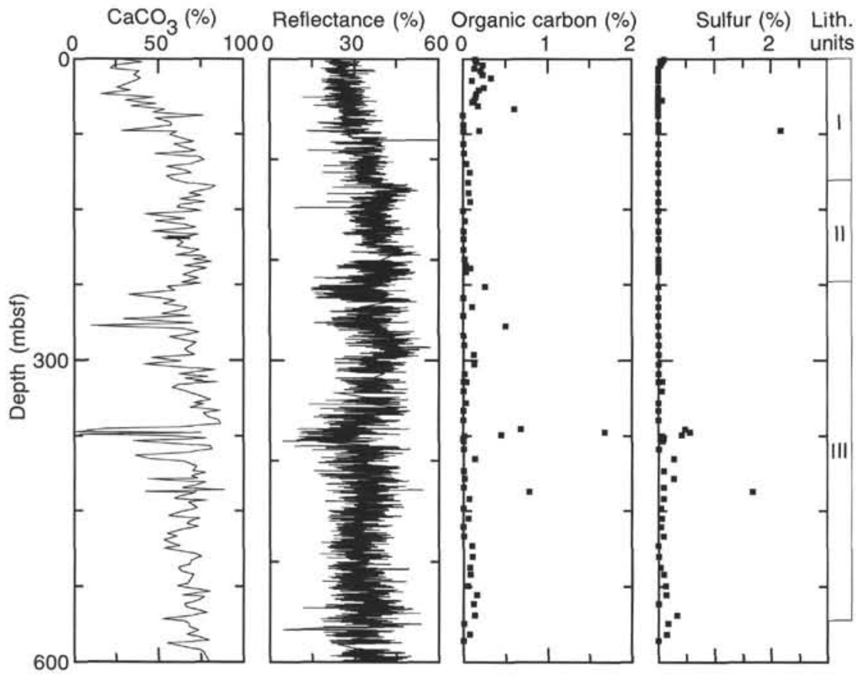

Figure 16. Calcium carbonate, color reflectance in the green (550 nm) wavelength, organic carbon, and sulfur vs. depth, Site 926. Lithologic unit boundaries are shown on the right side of the diagram.

Site 925 are also apparent in the Site 926 carbonate concentration data. A significant decrease in the mean content is observed over the top 100 m of both sites (0–2.5 Ma), between 10 and 12 Ma, and near 20 Ma (Fig. 17). These same features are evident in the 5-cm-spaced measurements of color reflectance (Fig. 16). The interval of lower mean carbonate content between 10 and 12 Ma corresponds to an interval of more dissolved calcareous microfossils, as compared with Site 925 (see "Biostratigraphy" section, this chapter). The low carbonate values near 375 mbsf (~20 Ma) are characterized by consistently low color reflectance and high concentrations of sulfur and organic carbon (Fig. 16).

Except for a few samples in the intervals of lower calcium carbonate content, organic carbon, as measured for the difference of total carbon and carbonate carbon, is below 0.4%. In fact, many of the samples have concentrations below the detection limits of the technique, and the difference between total carbon and carbonate carbon yields negative values.

Siliceous microfossils are absent throughout much of the section cored. However, diatoms and radiolarians were noted in cores from lithologic Subunit IIIB (375–460 mbsf), corresponding to the interval where pore-water silica values are near 1000 μM. As noted previously, the greater amount of solid phase silica and silica in the pore waters near 400 mbsf at Site 926 may be related to increased sedimentation rates within the early Miocene at this site compared with Site 925. The silica increase at Site 926 may also be related to silica concentration differences in the bottom waters at the two sites. The deeper Site 926 may have had a greater proportion of Antarctic Bottom Water compared to Northern Component Water, which is relatively depleted in silica. Lower bottom-water silica concentrations at the shallower site would enhance dissolution and therefore be responsible for the pattern observed.

One suite of closely spaced samples was taken from a 4-m interval in Core 154-926A-20H to evaluate the correlations of $CaCO_3$ concentration, magnetic susceptibility, reflectance, and sediment density in lithologic Unit II (Fig. 18). The figure shows the high correlation among $CaCO_3$ (%), magnetic susceptibility, and reflectance. To a first order, the density changes exhibit the same variations. Scatter plots of reflectance, magnetic susceptibility, and density vs. calcium carbonate concentration show that reflectance is more closely linked to carbonate variation than either magnetic susceptibility or bulk density within the interval studied (Fig. 19).

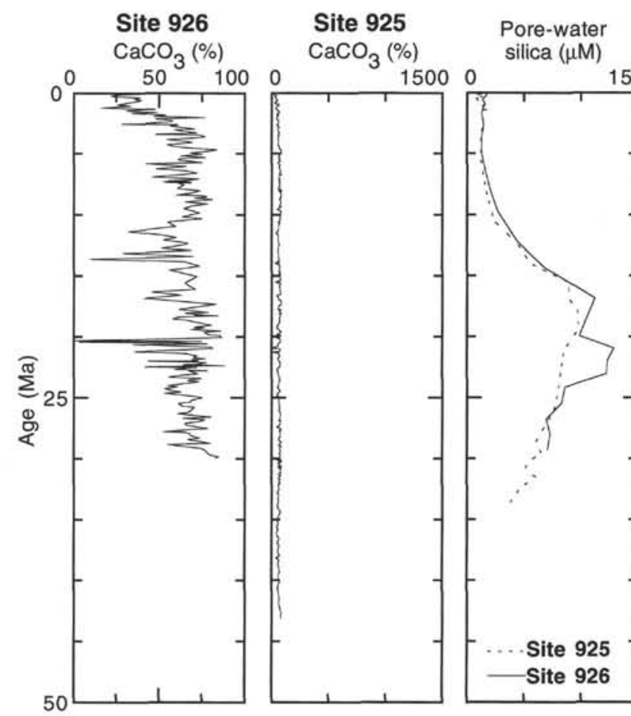

Figure 17. Calcium carbonate for Sites 926 and 925, and pore-water silica profiles for both sites vs. age.

Accumulation Rates

The age model for Site 926, based on recognized biostratigraphic datums (see "Sedimentation Rates" section, this chapter), was used to determine the mass accumulation rate (MAR) of the carbonate and noncarbonate sediment components (Fig. 20). Because the biostratigraphic age model provides the long-term (10^5 to 10^6 yr) changes in sedimentation rate, only the large-scale features in the accumulation rates are interpreted. The MARs were determined on a subset of 200 of the 217 samples analyzed for calcium carbonate content, corresponding to those with dry-bulk-density measurements

Table 9. Concentrations of inorganic (carbonate) carbon, calcium carbonate, total carbon, organic carbon (total – inorganic), nitrogen, and sulfur in samples from Holes 926A and 926B.

Core, section, interval (cm)	Depth (mbsf)	Inorganic carbon (%)	$CaCO_3$ (%)	Total carbon (%)	Organic carbon (%)	Nitrogen (%)	Sulfur (%)
154-926A-							
1H-1, 96–98	0.96	3.46	28.83	3.60	0.14	0.09	0.10
1H-3, 57–59	3.57	4.81	40.08	4.97	0.16	0.08	0.07
2H-2, 98–100	6.48	2.89	24.08	3.12	0.23	0.08	0.04
2H-4, 93–95	9.43	2.62	21.83	2.76	0.14	0.07	0.00
2H-6, 91–93	12.41	4.63	38.58	4.84	0.21	0.08	0.00
3H-2, 103–104	16.03	4.27	35.58	4.50	0.23	0.07	0.00
3H-4, 103–104	19.03	4.75	39.58	5.08	0.33	0.00	0.00
3H-6, 98–99	21.98	4.37	36.42	4.47	0.10	0.08	0.00
4H-4, 102–103	28.52	3.06	25.50	3.31	0.25	0.07	0.00
4H-6, 102–103	31.52	4.01	33.42	4.20	0.19	0.00	0.00
5H-2, 97–99	34.97	1.93	16.08	2.09	0.16	0.06	0.00
5H-4, 103–105	38.03	5.65	47.08	5.80	0.15	0.07	0.00
5H-6, 103–105	41.03	3.68	30.67	3.82	0.14	0.08	0.06
6H-1, 129–130	43.29	4.73	39.42	4.84	0.11	0.00	0.00
6H-2, 98–99	44.48	5.80	48.33	5.80	0.00	0.00	0.00
6H-4, 30–31	46.80	4.11	34.25	4.29	0.18	0.00	0.00
6H-6, 65–66	50.15	6.42	53.50	7.03	0.61	0.05	0.00
7H-2, 44–45	53.44	5.63	46.91				
7H-4, 50–51	56.50	9.20	76.66	9.16	0.00	0.00	0.00
7H-6, 36–37	59.36	5.76	48.00				
8H-2, 35–36	62.85	6.85	57.08				
8H-4, 51–52	66.01	6.92	57.66	6.81	0.00	0.07	0.00
8H-6, 91–92	69.41	5.06	42.16				
9H-1, 126–127	71.76	3.39	28.25	3.58	0.19	0.07	2.17
9H-2, 56–57	72.56	7.30	60.83	7.15	0.00	0.00	0.00
9H-4, 25–26	75.25	6.78	56.50				
10H-2, 92–93	82.42	8.49	70.75				
10H-4, 25–26	84.75	7.09	59.08	7.08	0.00	0.00	0.00
10H-5, 131–132	87.31	7.63	63.58				
11H-2, 96–97	91.96	8.64	72.00				
11H-4, 60–61	94.60	5.76	48.00	5.77	0.01	0.00	0.00
11H-6, 41–42	97.41	8.88	74.00				
12H-2, 32–33	100.82	9.21	76.75				
12H-4, 112–113	104.62	8.31	69.25	8.35	0.04	0.00	0.00
12H-6, 69–70	107.19	6.59	54.91				
13H-2, 106–107	111.06	7.86	65.50				
13H-4, 31–32	113.31	8.34	69.50	8.42	0.08	0.00	0.00
13H-6, 37–38	116.37	6.55	54.58				
14H-2, 90–91	120.40	7.07	58.91				
14H-4, 90–91	123.40	7.98	66.50	8.04	0.06	0.00	0.00
14H-7, 60–61	126.58	10.01	83.41				
15H-2, 92–93	129.92	9.58	79.83				
15H-5, 14–15	133.64	8.16	68.00	8.23	0.07	0.00	0.00
15H-7, 17–18	136.17	9.05	75.41				
16H-2, 84–86	139.34	7.53	62.75				
16H-4, 87–89	142.37	9.28	77.33	9.36	0.08	0.00	0.00
16H-6, 75–77	145.25	7.57	63.08				
17H-1, 70–71	147.20	7.35	61.25				
17H-4, 59–61	151.59	9.06	75.50	9.04	0.00	0.00	0.00
17H-6, 66–68	154.66	5.04	42.00				
18H-2, 106–107	158.56	.85	65.41				
18H-4, 88–89	161.38	5.81	48.41	5.84	0.03	0.00	0.00
18H-6, 81–82	164.31	7.89	65.75				
19H-2, 57–58	167.57	8.65	72.08				
19H-5, 27–28	171.77	5.52	46.00	5.52	0.00	0.00	0.00
19H-7, 7–8	174.57	8.79	73.25				
20H-2, 4–6	176.54	8.07	67.25				
20H-2, 37–38	176.87	6.75	56.25				
20H-2, 38–40	176.88	6.64	55.33				
20H-2, 68–70	177.18	7.86	65.50				
20H-2, 88–90	177.38	6.78	56.50				
20H-2, 100–102	177.50	7.74	64.50				
20H-2, 112–114	177.62	7.06	58.83				
20H-2, 126–128	177.76	7.33	61.08				
20H-3, 7–9	178.07	6.27	52.25				
20H-3, 22–24	178.22	8.17	68.08				
20H-3, 36–38	178.36	6.80	56.66				
20H-3, 51–53	178.51	7.60	63.33				
20H-3, 87–89	178.87	7.63	63.58				
20H-3, 103–105	179.03	6.42	53.50				
20H-3, 121–123	179.21	8.24	68.66				
20H-3, 136–137	179.36	7.47	62.25	7.47	0.00	0.00	0.00
20H-3, 137–139	179.37	7.31	60.91				
20H-5, 104–105	182.04	7.75	64.58				
21H-2, 39–40	186.39	7.30	60.83				
21H-4, 54–55	189.54	8.85	73.75	8.84	0.00	0.00	0.00
21H-6, 73–74	192.73	8.22	68.50				
22H-1, 73–74	194.73	7.19	59.91				
22H-2, 93–94	196.43	9.10	75.83				
22H-3, 107–108	198.07	9.37	78.08				
22H-4, 73–74	199.23	8.47	70.58	8.49	0.02	0.00	0.00
22H-6, 50–51	202.00	9.73	81.08				
23H-2, 55–56	205.55	7.80	65.00	7.83	0.03	0.00	0.00
23H-4, 28–29	208.28	9.38	78.16	9.46	0.08	0.00	0.00
23H-6, 98–99	211.98	8.32	69.33	8.35	0.03	0.00	0.00

Table 9 (continued).

Core, section, interval (cm)	Depth (mbsf)	Inorganic carbon (%)	$CaCO_3$ (%)	Total carbon (%)	Organic carbon (%)	Nitrogen (%)	Sulfur (%)
24H-2, 32–34	214.82	7.76	64.66				
24H-4, 113–115	218.63	8.82	73.50	8.80	0.00	0.00	0.00
24H-6, 130–132	221.80	7.65	63.75	7.72	0.00	0.00	0.00
25H-1, 118–117	223.68	8.98	74.83				
25H-3, 89–90	226.39	6.60	55.00	6.85	0.25	0.00	0.00
25H-6, 8–9	230.08	7.13	59.41				
26H-2, 107–108	234.57	3.89	32.42				
26H-4, 102–103	237.52	6.09	50.75	6.04	0.00	0.00	0.00
26H-6, 110–111	240.60	7.21	60.08				
27H-2, 47–48	243.47	6.33	52.75				
27H-4, 110–111	247.10	8.00	66.66	8.11	0.11	0.00	0.00
27H-6, 30–31	249.30	7.82	65.16				
28H-2, 110–111	253.60	6.22	51.83				
28H-4, 19–20	255.69	8.26	68.83	8.24	0.00	0.00	0.00
28H-6, 34–35	258.84	3.52	29.33				
29H-2, 54–55	262.54	8.43	70.25				
29H-4, 43–44	265.43	1.17	9.75	1.67	0.50	0.09	0.00
29H-6, 28–29	268.28	7.79	64.91				
30H-2, 70–71	272.20	8.86	73.83				
30H-4, 47–48	274.97	7.54	62.83	7.50	0.00	0.00	0.00
30H-5, 33–34	276.33	6.74	56.16				
31H-2, 112–113	282.12	8.63	71.91				
31H-4, 90–91	284.90	8.30	69.16	8.31	0.01	0.00	0.00
31H-6, 118–119	288.18	7.80	65.00				
32H-2, 53–54	291.03	8.05	67.08				
32H-4, 95–96	294.45	8.55	71.25	8.67	0.12	0.00	0.00
32H-6, 73–74	297.23	5.51	45.91				
33H-2, 40–41	300.40	7.55	62.91				
33H-4, 50–51	303.50	4.95	41.25	5.08	0.13	0.00	0.00
34H-1, 106–108	309.06	9.99	83.25				
34H-4, 87–89	313.37	7.41	61.75	7.43	0.02	0.00	0.00
34H-6, 114–116	316.64	9.44	78.66				
35H-2, 92–93	319.92	9.07	75.58				
35H-3, 109–111	321.59	10.12	84.33	10.16	0.04	0.00	0.00
154-926B-							
35X-1, 55–56	317.45	7.85	65.41				
35X-3, 55–56	320.45	8.50	70.83	8.48	0.00	0.00	0.07
35X-5, 96–97	323.86	7.38	61.50				
36X-1, 56–57	327.06	6.96	58.00				
36X-3, 57–58	330.07	7.87	65.58	7.85	0.00	0.00	0.06
37X-2, 126–127	338.96	9.67	80.58				
37X-4, 134–135	342.04	8.49	70.75	8.52	0.03	0.00	0.00
37X-5, 141–142	343.61	9.19	76.58				
38X-1, 65–67	346.45	8.25	68.75				
38X-3, 60–61	349.40	10.35	86.25	10.20	0.00	0.00	0.00
38X-5, 22–24	352.02	9.17	76.41				
39X-1, 69–71	356.19	9.47	78.91				
39X-3, 56–57	359.06	10.28	85.66	10.25	0.00	0.00	0.00
39X-5, 126–128	362.76	10.40	86.66				
40X-1, 85–87	365.95	7.37	61.41				
40X-3, 4–6	368.14	2.15	17.92	2.83	0.68	0.09	0.48
40X-4, 125–127	370.85	0.13	1.08	1.81	1.68	0.11	0.56
40X-5, 100–102	372.10	8.98	74.83				
40X-6, 105–107	373.65	0.43	3.58	0.88	0.45	0.08	0.42
41X-1, 50–52	374.90	7.07	58.91	7.09	0.02	0.00	0.07
41X-3, 75–77	377.61	9.36	78.00	9.24	0.00	0.00	0.09
41X-5, 27–29	380.13	4.18	34.83	4.20	0.02	0.05	0.07
42X-1, 111–112	385.21	9.63	80.25				
42X-3, 105–106	388.15	9.74	81.16	9.69	0.00	0.00	0.00
42X-5, 138–139	391.48	8.01	66.75				
43X-1, 104–105	394.74	4.34	36.17				
43X-3, 93–95	397.63	5.30	44.16	5.44	0.14	0.06	0.27
43X-5, 66–68	400.36	7.84	65.33				
44X-2, 61–63	405.51	8.69	72.41				
44X-5, 13–15	409.53	8.42	70.16	8.37	0.00	0.00	0.09
44X-6, 106–108	411.96	9.26	77.16				
45X-2, 46–48	415.06	8.33	69.41				
45X-3, 140–150	417.50	8.71	72.58	8.73	0.02	0.00	0.28
45X-4, 49–50	418.09	5.21	43.41				
45X-6, 64–66	421.24	9.32	77.66				
46X-2, 17–19	424.47	8.62	71.83				
46X-2, 107–109	425.37	7.96	66.33				
46X-3, 34–35	426.14	7.74	64.50	7.65	0.00	0.00	0.09
46X-3, 108–109	426.88	7.68	64.00				
46X-4, 10–11	427.40	8.69	72.41				
46X-4, 140–141	428.70	10.09	84.08				
46X-5, 6–7	428.86	10.61	88.41				
46X-6, 39–40	430.69	5.02	41.83	5.80	0.78	0.00	1.67
46X-7, 6–7	431.56	8.64	72.00				
47X-2, 98–100	434.88	7.51	62.58				
47X-4, 79–80	437.69	7.12	59.33	7.19	0.07	0.00	0.09
47X-5, 128–130	439.68	9.42	78.50				
47X-6, 81–82	440.71	8.10	67.50				
48X-2, 30–32	443.90	8.46	70.50				
48X-4, 31–33	446.91	8.73	72.75	8.64	0.00	0.04	0.05
48X-6, 53–55	450.13	7.58	63.16				
49X-2, 123–125	454.43	6.71	55.91				

Table 9 (continued).

Core, section, interval (cm)	Depth (mbsf)	Inorganic carbon (%)	$CaCO_3$ (%)	Total carbon (%)	Organic carbon (%)	Nitrogen (%)	Sulfur (%)
49X-4, 77–78	456.97	8.90	74.16	8.96	0.06	0.00	0.06
49X-6, 67–68	459.87	8.21	68.41				
50X-1, 83–84	462.23	8.00	66.66				
50X-3, 78–79	465.18	8.79	73.25	8.75	0.00	0.00	0.05
50X-5, 57–58	467.97	7.72	64.33				
51X-1, 123–124	472.23	6.64	55.33				
51X-3, 83–84	474.83	7.30	60.83	7.31	0.01	0.00	0.10
51X-5, 140–141	478.40	6.37	53.08				
52X-1, 124–125	481.74	6.91	57.58				
52X-3, 80–81	484.30	7.52	62.66	7.62	0.10	0.00	0.00
52X-5, 24–25	486.74	6.37	53.08				
53X-2, 45–46	492.15	8.49	70.75				
53X-4, 38–39	495.08	8.98	74.83	9.09	0.11	0.00	0.00
53X-6, 105–106	498.75	8.26	68.83				
54X-2, 144–145	502.84	8.18	68.16				
54X-4, 128–129	505.68	7.38	61.50	7.46	0.08	0.05	0.04
54X-6, 40–41	507.80	7.47	62.25				
55X-1, 10–11	509.60	7.60	63.33				
55X-3, 54–55	513.04	8.46	70.50	8.54	0.08	0.00	0.09
55X-5, 14–15	515.64	8.33	69.41				
56X-2, 104–105	521.74	8.05	67.08				
56X-4, 37–38	524.07	7.32	61.00	7.37	0.05	0.00	0.13
56X-6, 53–54	527.23	8.64	72.00				
57X-1, 94–96	529.84	9.61	80.08				
57X-3, 86–88	532.76	7.68	64.00	7.84	0.16	0.05	0.13
57X-5, 22–23	535.12	9.24	77.00				
58X-1, 20–21	538.70	8.80	73.33				
58X-3, 31–33	541.81	7.81	65.08	7.93	0.12	0.07	0.00
58X-5, 61–63	545.11	7.98	66.50				
59X-2, 134–136	551.04	9.41	78.41				
59X-4, 29–31	552.99	8.49	70.75	8.63	0.14	0.00	0.33
59X-6, 137–139	557.07	6.32	52.66				
60X-1, 86–87	558.76	7.80	65.00				
60X-3, 54–55	561.44	8.13	67.75	8.14	0.01	0.07	0.17
60X-5, 96–97	564.86	8.19	68.25				
61X-1, 99–100	568.59	8.82	73.50				
61X-3, 139–140	571.99	8.01	66.75	8.09	0.08	0.05	0.15
61X-5, 108–109	574.68	8.76	73.00				
62X-1, 112–113	578.32	9.58	79.83	9.56	0.00	0.00	0.00
62X-3, 78–79	580.98	6.61	55.08				
63X-1, 119–121	588.09	8.93	74.41				
63X-3, 84–86	590.74	9.23	76.91	9.15	0.00	0.00	0.00
63X-5, 94–96	593.84	9.31	77.58				
64X-2, 143–144	599.43	9.53	79.41				
64X-4, 141–142	602.41	10.18	84.83	9.88	0.00	0.00	0.00
64X-6, 145–146	605.45	9.93	82.75				

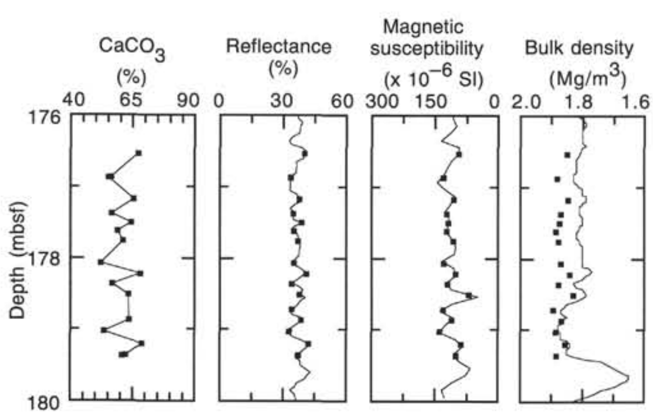

Figure 18. Calcium carbonate, percentage of reflectance, magnetic susceptibility, and bulk density–GRAPE and discrete samples vs. depth for a 4-m section in Core 154-926A-20H. Solid squares on each plot represent the discrete values used in the scatter plots in Figure 19. For $CaCO_3$ and density, these values are the actual measurements on discrete samples. For reflectance and magnetic susceptibility, the values are linearly interpolated from the closest measurements. The GRAPE data have been smoothed with a 9-point Gaussian filter and duplicate measurements were averaged. The apparent offset between GRAPE and the discrete samples is related to the GRAPE calibration over this interval (see "Physical Properties" section, "Site 925" chapter, this volume).

either from the same sample or from adjacent samples (see "Physical Properties" section, this chapter).

The mean accumulation rate of calcium carbonate ranges from a low near 8 g/m^2/yr in the latest Pleistocene to a high near 26 g/m^2/yr in the early Miocene (350–460 mbsf) (Fig. 21). These rates are higher than typical pelagic carbonate sites in oligotrophic settings (i.e., western equatorial Pacific; Kroenke, Berger, Janecek, et al., 1991) and are typical of the rates observed in the Neogene sections cored during ODP Leg 138 in the eastern equatorial Pacific (Mayer, Pisias, Janecek, et al., 1992). In general, the high rates of carbonate accumulation observed throughout the cored sequence are consistent with the observation that, except for a brief interval in the late Miocene, calcareous microfossils are relatively well preserved from the late Oligocene to the Pleistocene. The lows in mean calcium carbonate concentration are also evident as accumulation lows. Within the interval representing 6–18 Ma, carbonate accumulation at Site 926 is 40% lower than at nearby Site 925. This is consistent with the fact that Site 926 is 557 m deeper and more dissolution occurs at the deeper site. However, within the interval representing 20–24 Ma, in which siliceous microfossils were observed, carbonate accumulated at a higher rate at deeper Site 926 (25.9 vs. 16.5 g/m^2/yr). Overall, calcium carbonate MAR is 6% lower at Site 926 compared with Site 925 for the past 30 m.y. (18.4 vs. 19.7 g/m^2/yr).

Noncarbonate MAR reflects the input of terrigenous material largely derived from South America. The current source is Amazon River outflow. The increase in accumulation rate beginning near 8 Ma indicates that this source has been enhanced since that time, possibly associated with Andean uplift and erosion within the late Miocene and

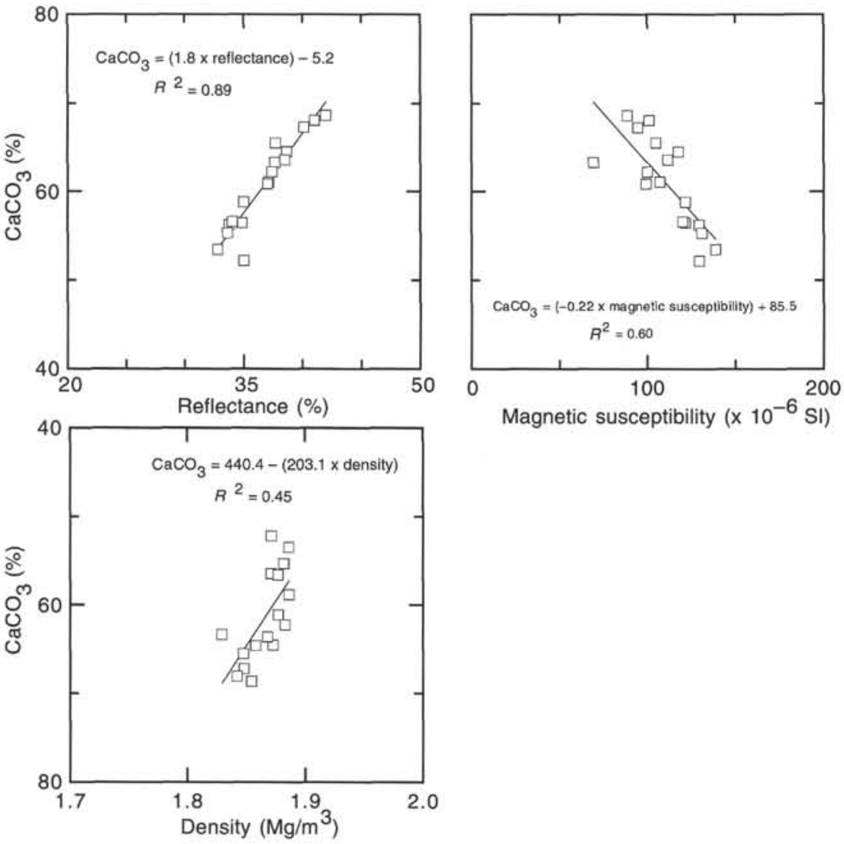

Figure 19. Calcium carbonate vs. percentage of reflectance, magnetic susceptibility, and bulk density. The linear regression lines and associated equations are shown.

early Pliocene (Fig. 21) (Benjamin et al., 1987). This increase is more apparent at Site 926 than at Site 925, although the mean rate is the same over the past 30 m.y. (10 g/m^2/yr).

PHYSICAL PROPERTIES

Physical properties measurements at Site 926 were conducted on both whole-round core sections and on discrete samples from split cores. The whole-round measurements include GRAPE density, compressional-wave velocity (using the *P*-wave logger on the MST), and thermal conductivity. Index properties, compressional-wave velocity (using the DSV and HF), shear strength, and resistivity were measured on split cores from Holes 926A and 926B. The frequency of measurements was three per core over intervals that were recovered from multiple holes. Within the deeper interval from 300 to 600 mbsf, two measurements per section were made in Hole 926B. In Hole 926C, index properties were usually measured once per core except for those cores identified as gaps from the composite depth of Holes 926A and 926B (see "Composite Section" section, this chapter). In these intervals, three measurements per core were made. All measurement methods are described in the "Physical Properties" section of the "Explanatory Notes" chapter (this volume).

Index Properties

Bulk density, porosity, water content (percentage of dry mass), grain density, and dry density determined by measuring the wet mass, wet volume, and dry mass of discrete samples are listed in Table 10. The following description of downhole variations in the bulk-density, porosity, and water-content values refers to the combined results from Holes 926A, 926B, and 926C (Fig. 22).

In the upper 180 m of the sediment column, bulk density increases from 1.5 to 1.85 Mg/m^3, whereas porosity and water content decrease from 70% to 52% and from 100% to 42%, respectively. In this interval, two changes in the slope of the density and water content vs. depth functions occur at 30 and 120 mbsf. These variations are probably related to the lithologic Subunit IA/IB and IB/IIA boundaries that mark the transition from clay to ooze at 30 mbsf and an increase in carbonate content at 130 mbsf (see "Lithostratigraphy" section, this chapter).

Below 180 mbsf, a short interval (20 m) with an inverse depth–index properties relationship is visible in which bulk-density values drop from 1.85 to 1.8 Mg/m^3 and porosity (water content) increases from 52% to 57% (41%–48%). At 200 mbsf, a positive offset in bulk density (+0.1 Mg/m^3), and negative offsets in porosity (–8%) and water content (–10%) occur. The offsets persist between 200 and 240 mbsf. The values correlate with a local maximum in the magnetic susceptibility record at the base of lithologic Unit II.

The Unit II/III boundary (240 mbsf) is marked by a negative offset in bulk density (–0.1 Mg/m^3), and positive offsets in porosity (+8%) and water content (+10%), followed by an interval with an inverse depth–index properties relationship down to 300 mbsf. Another less pronounced reversal occurs at 400 mbsf. Above (300–400 mbsf) and below (400–520 mbsf), bulk density increases with depth at a constant gradient (0.001 Mg/m^4) from 1.75 to 2.0 Mg/m^3, whereas porosity and water content decrease from 58% to 40% and from 50% to 28%, respectively.

Below 520 mbsf to the base of Site 926 at 600 mbsf, the index properties show no significant change with depth and remain at relatively constant values of 2.00 Mg/m^3 bulk density, 40% porosity, and 28% water content.

The overall trend in index properties variations displays features that are very similar to those observed at Site 925. Because of the lower sedimentation rates at this site (see "Biostratigraphy" section, this chapter), offsets and changes in the slope of the index properties occur at slightly shallower depths in the upper part of the section and at significant shallower depths in the lower part.

Table 10. Index properties measured on discrete samples for all holes at Site 926.

Core, section, interval (cm)	Depth (mbsf)	Water content (bulk wt%)	Water content (dry wt%)	Bulk density (Mg/m^3)	Grain density (Mg/m^3)	Dry density (Mg/m^3)	Porosity (%)
154-926A-							
1H-1, 99–101	0.99	52.48	110.45	1.495	3.036	0.710	76.60
1H-3, 59–61	3.59	46.97	88.56	1.561	2.910	0.828	71.55
2H-2, 100–102	6.50	51.66	106.86	1.513	3.083	0.731	76.28
2H-4, 93–95	9.43	45.96	85.05	1.578	2.922	0.853	70.81
2H-6, 94–96	12.44	44.84	81.30	1.603	2.965	0.884	70.18
3H-2, 99–11	15.99	45.59	83.81	1.602	3.037	0.872	71.30
3H-4, 100–102	19.00	44.30	79.52	1.620	3.015	0.903	70.07
3H-6, 95–97	21.95	43.78	77.87	1.626	2.993	0.914	69.47
4H-4, 100–102	28.50	42.79	74.79	1.641	2.985	0.939	68.54
4H-6, 100–102	31.50	41.21	70.11	1.669	2.984	0.981	67.12
5H-2, 100–102	35.00	41.72	71.59	1.639	2.871	0.955	66.73
5H-4, 100–102	38.00	40.45	67.94	1.676	2.950	0.998	66.17
5H-6, 100–102	41.00	40.80	68.92	1.657	2.885	0.981	65.99
6H-2, 100–102	44.50	40.37	67.71	1.676	2.944	0.999	66.05
6H-4, 32–34	46.82	39.26	64.65	1.690	2.915	1.027	64.78
6H-6, 70–72	50.20	38.89	63.63	1.693	2.893	1.034	64.24
7H-2, 41–43	53.41	37.33	59.56	1.709	2.838	1.071	62.26
7H-4, 47–49	56.47	41.75	71.69	1.650	2.932	0.961	67.23
7H-6, 33–35	59.33	38.25	61.94	1.691	2.832	1.044	63.13
8H-2, 36–38	62.86	36.99	58.70	1.718	2.852	1.083	62.04
8H-4, 49–51	65.99	37.19	59.21	1.720	2.876	1.080	62.44
8H-6, 93–95	69.43	36.38	57.18	1.716	2.796	1.092	60.95
9H-2, 53–55	72.53	36.70	57.98	1.685	2.690	1.066	60.35
9H-4, 22–24	75.22	38.15	61.68	1.704	2.883	1.054	63.44
9H-6, 92–94	78.92	36.99	58.72	1.730	2.902	1.090	62.45
10H-2, 88–90	82.38	37.46	59.91	1.702	2.819	1.064	62.24
10H-4, 26–28	84.76	37.70	60.51	1.654	2.633	1.030	60.87
10H-5, 127–129	87.27	37.32	59.54	1.698	2.792	1.065	61.87
11H-2, 120–122	92.20	38.52	62.65	1.698	2.889	1.044	63.86
11H-4, 58–60	94.58	35.38	54.74	1.670	2.551	1.079	57.68
11H-6, 36–38	97.36	39.97	66.59	1.677	2.911	1.007	65.43
12H-2, 30–32	100.80	39.99	66.63	1.663	2.842	0.998	64.89
12H-4, 109–111	104.59	35.96	56.15	1.736	2.846	1.112	60.93
12H-6, 66–68	107.16	34.38	52.38	1.678	2.520	1.101	56.30
13H-2, 106–108	111.06	37.77	60.70	1.712	2.888	1.065	63.12
13H-4, 32–34	113.32	36.46	57.39	1.720	2.820	1.093	61.24
13H-6, 39–41	116.39	34.96	53.75	1.695	2.614	1.102	57.83
14H-2, 93–95	120.43	34.87	53.53	1.759	2.856	1.146	59.88
14H-4, 92–94	123.42	35.38	54.75	1.751	2.863	1.132	60.48
14H-7, 63–65	126.61	37.39	59.72	1.703	2.816	1.066	62.15
15H-2, 92–94	129.92	37.35	59.62	1.711	2.850	1.072	62.38
15H-5, 12–14	133.62	34.40	52.44	1.737	2.734	1.139	58.33
15H-7, 19–21	136.19	36.16	56.64	1.737	2.866	1.109	61.31
16H-2, 81–83	139.31	33.95	51.40	1.782	2.874	1.177	59.04
16H-4, 84–86	142.34	35.36	54.71	1.742	2.823	1.126	60.12
16H-6, 73–75	145.23	33.52	50.41	1.787	2.858	1.188	58.45
17H-1, 67–69	147.17	33.86	51.19	1.790	2.899	1.184	59.16
17H-4, 55–57	151.55	34.13	51.81	1.779	2.879	1.172	59.28
17H-6, 64–66	154.64	30.90	44.72	1.879	2.995	1.298	56.66
18H-2, 103–105	158.53	31.48	45.95	1.824	2.845	1.250	56.06
18H-4, 90–92	161.40	28.69	40.23	1.879	2.826	1.340	52.60
18H-6, 82–84	164.32	31.71	46.44	1.815	2.828	1.239	56.18
19H-2, 59–61	167.59	33.17	49.62	1.776	2.792	1.187	57.49
19H-5, 29–31	171.79	28.62	40.09	1.883	2.836	1.344	52.60
19H-7, 9–11	174.59	27.33	37.61	1.847	2.645	1.342	49.26
20H-2, 4–6	176.54	29.66	42.17	1.848	2.795	1.300	53.50
20H-2, 38–40	176.88	28.70	40.25	1.882	2.838	1.342	52.72
20H-2, 68–70	177.18	30.24	43.35	1.847	2.832	1.288	54.51
20H-2, 88–90	177.38	29.45	41.74	1.871	2.858	1.320	53.80
20H-2, 100–102	177.50	29.37	41.57	1.873	2.855	1.323	53.68
20H-2, 112–114	177.62	28.26	39.38	1.886	2.819	1.353	52.01
20H-2, 126–128	177.76	29.36	41.56	1.877	2.870	1.326	53.80
20H-3, 7–9	178.07	29.71	42.27	1.871	2.877	1.315	54.27
20H-3, 22–24	178.22	30.85	44.61	1.842	2.860	1.274	55.47
20H-3, 36–38	178.36	29.16	41.17	1.877	2.856	1.330	53.44
20H-3, 51–53	178.51	30.80	44.51	1.829	2.812	1.266	54.99
20H-3, 72–74	178.72	28.31	39.49	1.895	2.852	1.359	52.36
20H-3, 87–89	178.87	29.03	40.91	1.868	2.817	1.326	52.94
20H-3, 103–105	179.03	28.13	39.13	1.886	2.810	1.355	51.77
20H-3, 121–123	179.21	30.19	43.25	1.854	2.852	1.294	54.63
20H-3, 137–139	179.37	28.88	40.60	1.883	2.855	1.339	53.08
20H-5, 105–107	182.05	29.72	42.29	1.858	2.834	1.306	53.91
21H-2, 43–45	186.43	28.75	40.35	1.877	2.827	1.338	52.69
21H-4, 56–58	189.56	30.93	44.77	1.804	2.737	1.246	54.46
22H-3, 108–110	198.08	32.38	47.88	1.789	2.783	1.210	56.54
22H-4, 75–77	199.25	31.26	45.48	1.825	2.833	1.255	55.70
22H-6, 52–54	202.02	34.36	52.34	1.757	2.808	1.153	58.92
23H-2, 52–54	205.52	30.35	43.58	1.856	2.872	1.293	54.99
23H-4, 26–28	208.26	32.86	48.94	1.815	2.916	1.219	58.21
23H-6, 95–97	211.95	30.40	43.68	1.849	2.852	1.287	54.87
24H-2, 29–31	214.79	28.64	40.14	1.877	2.819	1.340	52.48
24H-4, 115–117	218.65	30.19	43.25	1.825	2.758	1.274	53.80
24H-5, 21–23	219.21	36.91	58.50	1.706	2.794	1.077	61.47
24H-5, 28–30	219.28	31.05	45.04	1.838	2.862	1.267	55.72
24H-6, 132–134	221.82	26.18	35.46	1.919	2.779	1.416	49.02
25H-1, 119–121	223.69	32.32	47.75	1.794	2.798	1.214	56.60
25H-3, 90–92	226.40	29.07	40.98	1.882	2.863	1.335	53.39
25H-6, 13–15	230.13	30.45	43.78	1.862	2.900	1.295	55.35
26H-2, 108–110	234.58	28.36	39.59	INF	-2.587	INF	INF
26H-4, 100–102	237.50	27.51	37.94	1.914	2.854	1.387	51.39
26H-6, 18–20	239.68	35.62	55.33	1.739	2.833	1.120	60.48
26H-6, 45–47	239.95	30.93	44.78	1.861	2.933	1.285	56.18
26H-6, 112–114	240.62	29.50	41.85	1.868	2.850	1.317	53.80
27H-2, 48–50	243.48	27.21	37.39	1.895	2.777	1.379	50.34
27H-4, 107–109	247.07	28.39	39.64	1.884	2.823	1.349	52.21
27H-6, 27–29	249.27	27.18	37.32	1.920	2.849	1.398	50.93
28H-2, 107–109	253.57	28.16	39.20	1.890	2.825	1.358	51.95
28H-4, 16–18	255.66	32.10	47.28	1.802	2.812	1.224	56.48
28H-6, 22–24	258.72	30.45	43.78	1.845	2.842	1.283	54.85
29H-2, 50–52	262.50	34.26	52.12	1.748	2.765	1.149	58.45
29H-4, 84–86	265.84	33.00	49.25	1.713	2.560	1.148	55.17
29H-6, 29–31	268.29	30.94	44.80	1.838	2.851	1.269	55.49
30H-2, 72–74	272.22	32.56	48.28	1.787	2.788	1.205	56.78
30H-4, 49–51	274.99	30.34	43.55	1.841	2.819	1.282	54.51
30H-5, 35–37	276.35	27.15	37.26	1.922	2.854	1.400	50.93
31H-2, 114–116	282.14	33.05	49.36	1.771	2.767	1.186	57.14
31H-4, 92–94	284.92	29.02	40.89	1.844	2.741	1.309	52.25
31H-6, 120–122	288.20	29.70	42.25	1.851	2.810	1.302	53.68
32H-2, 55–57	291.05	29.59	42.02	1.834	2.745	1.291	52.96
32H-4, 97–99	294.47	28.31	39.49	1.869	2.771	1.340	51.65
32H-6, 74–76	297.24	32.93	49.10	1.770	2.754	1.187	56.90
33H-2, 41–43	300.41	33.44	50.23	1.732	2.653	1.153	56.54
33H-4, 47–49	303.47	31.44	45.86	1.800	2.756	1.234	55.23
34H-1, 104–106	309.04	34.61	52.93	1.717	2.674	1.123	58.01
34H-6, 112–114	316.62	33.48	50.33	1.710	2.579	1.138	55.89
35H-2, 95–97	319.95	32.09	47.26	1.743	2.606	1.183	54.59
35H-3, 111–113	321.61	34.77	53.30	1.667	2.503	1.087	56.56
154-926B-							
1H-2, 29–31	1.79	50.55	102.23	1.473	2.666	0.728	72.68
1H-4, 30–32	4.80	45.47	83.38	1.579	2.878	0.861	70.08
2H-3, 30–32	10.30	46.27	86.11	1.565	2.867	0.841	70.67
2H-3, 78–80	10.78	44.87	81.40	1.578	2.816	0.870	69.11
2H-3, 101–103	11.01	47.10	89.05	1.557	2.896	0.823	71.57
2H-3, 132–134	11.32	41.40	70.64	1.625	2.773	0.952	65.66
2H-5, 16–18	13.16	45.92	84.91	1.575	2.900	0.852	70.61
2H-5, 37–39	13.37	44.62	80.57	1.597	2.903	0.884	69.54
2H-5, 75–77	13.75	46.25	86.04	1.570	2.895	0.844	70.85
2H-5, 116–118	14.16	43.86	78.12	1.594	2.819	0.895	68.25
3H-2, 46–48	18.46	41.50	70.93	1.640	2.860	0.960	66.44
3H-4, 31–33	21.31	43.68	77.56	1.623	2.965	0.914	69.18
3H-6, 42–44	24.42	42.85	74.98	1.623	2.886	0.927	67.87
4H-2, 111–113	28.61	41.20	70.08	1.639	2.825	0.963	65.90
4H-4, 62–64	31.12	41.30	70.37	1.651	2.898	0.969	66.56
4H-6, 51–53	34.01	41.28	70.31	1.639	2.833	0.962	66.03
5H-1, 116–118	36.66	40.80	68.93	1.661	2.906	0.983	66.17
5H-3, 44–46	38.94	41.77	71.74	1.652	2.945	0.962	67.35
5H-5, 53–55	42.03	39.97	66.58	1.687	2.965	1.013	65.83
6H-2, 84–86	47.34	38.97	63.85	1.705	2.959	1.040	64.84
6H-3, 80–82	48.80	40.25	67.36	1.677	2.940	1.002	65.90
6H-5, 74–76	51.74	38.99	63.91	1.698	2.927	1.036	64.61
7H-1, 74–76	55.24	40.16	67.12	1.742	3.286	1.042	68.28
7H-3, 37–39	57.87	37.01	58.77	1.730	2.906	1.090	62.50
7H-5, 115–117	61.65	38.30	62.08	1.692	2.842	1.044	63.27
8H-2, 24–26	65.74	36.01	56.27	1.757	2.938	1.124	61.74
8H-4, 59–61	69.09	35.79	55.75	1.756	2.915	1.127	61.33
8H-5, 115–117	71.15	37.75	60.65	1.699	2.830	1.058	62.62
9H-2, 123–125	76.23	38.06	61.44	1.692	2.822	1.048	62.86
9H-3, 115–117	77.65	38.31	62.09	1.679	2.784	1.036	62.79
9H-5, 107–109	80.57	37.40	59.75	1.711	2.854	1.071	62.47
10H-1, 118–120	84.18	38.28	62.03	1.693	2.846	1.045	63.28
10H-3, 114–116	87.14	36.22	56.78	1.732	2.851	1.105	61.24
10H-5, 19–21	89.19	37.34	59.59	1.706	2.828	1.069	62.19
11H-3, 76–78	96.26	37.55	60.13	1.696	2.798	1.059	62.16
11H-5, 75–77	99.25	35.15	54.20	1.733	2.774	1.124	59.47
12H-3, 95–97	105.95	36.86	58.38	1.710	2.806	1.080	61.53
12H-5, 103–105	109.03	35.41	54.83	1.729	2.775	1.117	59.76
12H-7, 34–36	111.34	35.77	55.70	1.716	2.749	1.102	59.91
13H-3, 70–72	115.20	38.07	61.46	1.676	2.750	1.038	62.26
13H-5, 38–40	117.88	34.47	52.61	1.758	2.821	1.152	59.16
13H–7, 42–44	120.92	37.89	60.99	1.535	2.207	0.954	56.78
14H-2, 88–90	123.38	35.20	54.32	1.744	2.820	1.130	59.93
14H-5, 124–126	128.24	35.91	56.04	1.722	2.783	1.103	60.36
15H-3, 38–40	133.88	35.20	54.32	1.732	2.773	1.123	59.52
15H-5, 49–51	136.99	35.10	54.09	1.601	2.303	1.039	54.87
15H-7, 27–29	139.77	32.69	48.56	1.798	2.840	1.211	57.37
16H-3, 52–54	143.52	33.53	50.45	1.775	2.815	1.180	58.09
16H-5, 60–62	146.60			1.718			
16H-7, 12–14	149.12	33.77	51.00	1.748	2.731	1.157	57.61
17H-3, 48–50	152.98	31.52	46.02	1.818	2.826	1.245	55.94
17H-5, 98–100	156.48	32.66	48.50	1.796	2.829	1.209	57.25
17H-7, 35–37	158.85	30.04	42.94	1.847	2.818	1.292	54.15
18H-3, 42–44	162.42	29.66	42.18	1.846	2.788	1.298	53.44
18H-5, 97–99	165.97	30.80	44.52	1.809	2.745	1.252	54.39
19H-3, 110–112	172.60	30.42	43.71	1.836	2.809	1.278	54.51

Table 10 (continued).

Core, section, interval (cm)	Depth (mbsf)	Water content (bulk wt%)	Water content (dry wt%)	Bulk density (Mg/m^3)	Grain density (Mg/m^3)	Dry density (Mg/m^3)	Porosity (%)
19H-5, 58–60	175.08	29.01	40.87	1.841	2.730	1.307	52.13
19H-7, 15–17	177.65	28.29	39.45	1.883	2.814	1.350	52.01
20H-3, 77–79	181.77	30.04	42.93	1.827	2.752	1.278	53.56
20H-5, 70–72	184.70	29.48	41.80	1.857	2.813	1.310	53.44
20H-7, 8–10	187.08	30.16	43.19	1.831	2.775	1.279	53.92
21H-3, 93–95	191.43	31.58	46.16	1.803	2.777	1.234	55.58
21H-5, 86–88	194.36	31.72	46.45	1.803	2.787	1.231	55.82
22H-3, 121–123	201.21	31.18	45.30	1.815	2.790	1.249	55.23
22H-5, 68–70	203.68	32.99	49.23	1.785	2.815	1.196	57.49
23H-3, 39–41	209.89	32.90	49.04	1.813	2.910	1.216	58.21
23H-5, 45–47	212.95	28.69	40.24	1.874	2.812	1.336	52.48
23H-7, 19–21	215.69	30.98	44.89	1.850	2.900	1.277	55.95
24H-3, 42–44	219.42	25.45	34.14	1.940	2.791	1.446	48.19
24H-5, 121–123	223.21	31.11	45.16	1.827	2.826	1.258	55.47
24H-7, 52–54	225.52	32.87	48.96	1.774	2.762	1.191	56.90
25H-3, 61–63	229.11	26.76	36.53	1.919	2.817	1.405	50.11
25H-5, 125–127	232.75	26.23	35.56	1.910	2.759	1.409	48.92
25H-7, 29–31	234.79	29.28	41.41	1.828	2.707	1.293	52.25
26H-3, 91–93	238.91	28.71	40.28	1.862	2.776	1.327	52.19
26H-5, 137–139	242.37	25.94	35.03	1.907	2.731	1.412	48.28
27H-3, 121–123	248.71	27.51	37.95	1.888	2.776	1.369	50.69
27H-5, 117–119	251.67	29.42	41.69	1.864	2.832	1.316	53.55
27H-7, 42–44	253.92	29.60	42.04	1.846	2.783	1.299	53.32
28X-1, 83–85	254.83	32.26	47.62	1.791	2.781	1.213	56.38
28X-3, 57–59	257.57	28.78	40.42	1.871	2.809	1.332	52.57
29X-1, 40–42	259.40	31.70	46.41				
29X-3, 81–83	262.81	29.92	42.69				
29X-4, 74–76	264.24	34.28	52.17				
29X-5, 148–150	266.48	32.29	47.69				
29X-6, 84–86	267.34	31.94	46.94	1.769	2.684	1.204	55.16
30X-1, 76–78	269.36	35.30	54.55	1.730	2.771	1.119	59.60
30X-2, 100–102	271.10	33.11	49.50	1.803	2.891	1.206	58.28
30X-3, 42–44	272.02	35.55	55.16	1.612	2.359	1.039	55.95
30X-3, 96–98	272.56	34.90	53.62	1.766	2.886	1.150	60.17
30X-5, 86-88	275.46	29.87	42.58	1.960	3.208	1.375	57.15
30X-6, 37–39	276.47	32.11	47.31	1.817	2.866	1.234	56.96
31X-1, 107–109	279.37	30.26	43.39	1.837	2.802	1.281	54.27
31X–3, 5–7	281.35	32.55	48.27	1.790	2.798	1.207	56.86
31X-5, 86–88	285.16	29.76	42.36	1.819	2.709	1.278	52.83
32X-1, 114–116	289.14	32.61	48.39	1.762	2.703	1.187	56.07
32X-3, 107–109	292.07	32.16	47.41	1.777	2.727	1.206	55.78
32X-5, 90–92	294.90	34.79	53.36	1.732	2.743	1.129	58.83
32X-7, 10–12	297.10	34.70	53.13	1.746	2.789	1.140	59.13
33X-1, 83–85	298.43	32.85	48.92	1.733	2.620	1.164	55.58
33X-3, 79–81	301.39	34.19	51.96	1.726	2.679	1.136	57.61
33X-4, 10–12	302.20	31.53	46.06	1.803	2.773	1.234	55.49
33X-5, 28–30	303.88	30.84	44.60	1.801	2.721	1.246	54.23
33X-6, 50–52	305.60			1.768			
34X-1, 27–29	307.57	32.45	48.05	1.669	2.391	1.127	52.86
34X-1, 102–104	308.32	32.07	47.21	1.693	2.448	1.150	53.01
34X-2, 29–31	309.09			1.722			
34X-2, 29–31	309.09	31.17	45.28	1.722	2.488	1.185	52.38
34X-2, 137–139	310.17	30.39	43.65	1.743	2.512	1.213	51.70
34X-3, 30–32	310.60	32.45	48.03	1.694	2.467	1.144	53.63
34X-3, 141–143	311.71	31.40	45.78	1.734	2.538	1.189	53.15
34X-4, 23–25	312.03	28.82	40.49	1.754	2.466	1.249	49.36
35X-1, 52–54	317.42	31.62	46.25	1.802	2.776	1.232	55.62
35X-1, 117–119	318.07	30.85	44.62	1.742	2.534	1.205	52.46
35X-2, 58–60	318.98	33.58	50.55	1.711	2.587	1.136	56.07
35X-2, 145–147	319.85	28.73	40.31	1.837	2.699	1.309	51.50
35X-3, 52–54	320.42	28.91	40.67	1.822	2.667	1.295	51.43
35X-3, 139–141	321.29	30.51	43.90	1.779	2.628	1.236	52.97
35X-4, 64–66	322.04	27.05	37.07	1.860	2.665	1.357	49.09
35X-4, 138–140	322.78	30.19	43.24	1.805	2.693	1.260	53.20
35X-5, 25–27	323.15	29.17	41.19	1.830	2.705	1.296	52.10
35X-5, 94–96	323.84	29.57	41.99	1.858	2.822	1.308	53.63
35X-6, 40–42	324.80	31.73	46.48	1.817	2.837	1.241	56.28
35X-6, 144–146	325.84	29.95	42.76	1.827	2.747	1.280	53.41
36X-1, 58–60	327.08	26.58	36.20	1.898	2.747	1.394	49.25
36X-1, 137–139	327.87	29.59	42.02	1.833	2.741	1.290	52.92
36X-2, 72–74	328.72	30.69	44.28	1.785	2.658	1.237	53.46
36X-2, 132–134	329.32	29.81	42.48	1.793	2.633	1.259	52.19
36X-3, 62–64	330.12	30.22	43.30	1.817	2.731	1.268	53.58
36X-3, 140–142	330.90	29.67	42.19	1.786	2.601	1.256	51.71
36X-4, 25–27	331.25	29.82	42.50	1.822	2.722	1.278	53.03
36X-4, 120–122	332.20	30.64	44.17	1.805	2.719	1.252	53.97
37X-1, 57–59	336.77	30.17	43.19	1.776	2.601	1.240	52.30
37X-1, 144–146	337.64	29.83	42.51	1.811	2.688	1.271	52.73
37X-2, 65–67	338.35	26.96	36.92	1.825	2.566	1.333	48.05
37X-2, 123–125	338.93	30.46	43.81	1.790	2.660	1.245	53.22
37X-3, 76–78	339.96	30.67	44.25	1.777	2.632	1.232	53.20
37X-3, 141–143	340.61	31.79	46.61	1.785	2.730	1.218	55.40
37X-4, 43–45	341.13	30.49	43.87	1.774	2.611	1.233	52.79
37X-4, 131–133	342.01	28.96	40.77	1.839	2.722	1.307	52.00
37X-5, 38–40	342.58	30.14	43.14	1.817	2.727	1.269	53.45
37X-5, 138–140	343.58	29.11	41.06	1.815	2.656	1.287	51.56
38X-1, 65–67	346.45	28.87	40.60	1.834	2.699	1.304	51.68
38X-1, 136–138	347.16	29.66	42.16	1.803	2.652	1.268	52.19
38X-2, 31–33	347.61	30.08	43.02	1.815	2.716	1.269	53.28
38X-2, 135–137	348.65	31.56	46.12	1.797	2.754	1.230	55.36
38X-3, 57–59	349.37	30.42	43.72	1.808	2.717	1.258	53.69
38X-4, 40–42	350.70	29.34	41.53	1.809	2.652	1.278	51.81
38X-4, 129–131	351.59	29.45	41.74	1.806	2.651	1.274	51.93
38X-5, 22–24	352.02	28.46	39.77	1.826	2.652	1.307	50.72
38X-5, 114–116	352.94	27.00	36.98	1.866	2.681	1.362	49.18
38X-6, 34–36	353.64	28.68	40.20	1.822	2.652	1.299	50.99
38X-7, 20–22	355.00	29.54	41.93	1.778	2.570	1.253	51.27
39X-1, 14–16	355.64	27.75	38.42	1.873	2.748	1.353	50.75
39X-1, 135–137	356.85	28.14	39.17	1.834	2.656	1.318	50.38
39X-2, 68–70	357.68	28.03	38.94	1.832	2.642	1.318	50.11
39X-2, 125–127	358.25	27.79	38.49	1.877	2.761	1.355	50.92
39X-3, 56–58	359.06	28.92	40.69	1.798	2.597	1.278	50.77
39X-3, 131–133	359.81	29.74	42.33	1.803	2.657	1.267	52.33
39X-4, 73–75	360.73	24.59	32.60	1.929	2.709	1.455	46.30
39X-5, 12–14	361.62	27.76	38.42	1.825	2.607	1.318	49.44
39X-5, 126–128	362.76	26.94	36.87	1.914	2.816	1.399	50.33
39X-6, 140–142	364.40	28.70	40.26	1.824	2.659	1.300	51.10
39X-7, 11–13	364.61	27.38	37.70	1.880	2.745	1.366	50.25
40X-1, 85–87	365.95	28.27	39.40	1.952	3.036	1.400	53.87
40X-2, 5–7	366.65	27.51	37.95	1.855	2.679	1.345	49.81
40X-2, 94–96	367.54	26.33	35.74	1.883	2.687	1.387	48.39
40X-3, 5–7	368.15	30.14	43.15	1.816	2.725	1.269	53.44
40X-3, 140–142	369.50	26.47	36.00	1.875	2.673	1.378	48.43
40X-4, 43–45	370.03	28.78	40.42	1.847	2.733	1.315	51.88
40X-5, 5–7	371.15	28.61	40.08	1.818	2.638	1.298	50.78
40X-5, 99–101	372.09	27.48	37.89	1.861	2.694	1.350	49.91
40X-6, 32–34	372.92	25.35	33.96	1.915	2.716	1.429	47.38
40X-6, 131–133	373.91	28.76	40.38	1.821	2.655	1.297	51.13
41X-1, 53–55	374.93	28.89	40.62	1.808	2.624	1.286	50.99
41X–2, 7–9	375.43	29.57	41.98	1.850	2.794	1.303	53.38
41X–2, 31–33	375.67	38.17	61.74	1.671	2.737	1.033	62.26
41X-3, 70–72	377.56	28.10	39.09	1.852	2.708	1.332	50.81
41X-4, 26–28	378.62	30.89	44.70	1.797	2.711	1.242	54.19
41X-4, 124–126	379.60	29.45	41.75	1.808	2.657	1.276	51.98
41X-5, 4–6	379.90	28.62	40.10	1.822	2.650	1.301	50.92
42X-1, 112–114	385.22	29.83	42.51	1.865	2.862	1.308	54.29
42X-2, 6–8	385.66	30.30	43.46	1.814	2.726	1.264	53.63
42X-2, 66–68	386.26	31.07	45.07	1.773	2.642	1.222	53.75
42X-2, 124–126	386.84	28.50	39.86	1.757	2.458	1.257	48.89
42X-3, 5–7	387.15	29.67	42.18	1.789	2.611	1.258	51.81
42X-3, 107–109	388.17	31.25	45.46	1.765	2.630	1.214	53.86
42X-4, 8–10	388.68	31.34	45.65	1.760	2.619	1.209	53.85
42X-4, 84–86	389.44	28.46	39.78	1.841	2.697	1.317	51.15
42X-5, 12–14	390.22	29.91	42.67	1.809	2.685	1.268	52.79
42X-5, 139–141	391.49	30.11	43.08	1.790	2.640	1.251	52.61
42X-6, 55–57	392.15	32.45	48.05	1.740	2.620	1.176	55.14
42X-6, 100–102	392.60	33.54	50.47	1.758	2.751	1.168	57.54
42X-6, 112–114	392.72	31.88	46.79	1.778	2.712	1.212	55.33
43X-1, 19–21	393.89	29.79	42.44	1.794	2.633	1.259	52.16
43X-1, 105–107	394.75	30.80	44.51	1.766	2.606	1.222	53.10
43X-2, 86–88	396.06	29.82	42.50	1.800	2.655	1.263	52.41
43X-2, 120–122	396.40	32.00	47.05	1.762	2.664	1.198	55.02
43X-3, 52–54	397.22	27.85	38.60	1.805	2.557	1.302	49.06
43X-3, 91–93	397.61			1.788			
43X-4, 4–6	398.24	28.45	39.77	1.821	2.636	1.303	50.58
43X-4, 105–107	399.25	29.56	41.97	1.821	2.702	1.282	52.53
43X–5, 64–66	400.34	27.87	38.64	1.840	2.656	1.327	50.04
43X–6, 84–86	402.04	25.46	34.15	1.910	2.710	1.424	47.46
44X–1, 14–16	403.54	30.50	43.89	1.780	2.632	1.237	53.00
44X-1, 113–115	404.53	27.59	38.11	1.850	2.669	1.339	49.82
44X-2, 58–60	405.48	28.31	39.49	1.826	2.644	1.309	50.47
44X-3, 26–28	406.66	26.34	35.76	1.881	2.682	1.385	48.35
44X-3, 138–140	407.78	24.18	31.89	1.919	2.659	1.455	45.28
44X-4, 73–75	408.63	27.36	37.66	1.837	2.620	1.335	49.06
44X-4, 132–134	409.22	24.77	32.92	1.894	2.628	1.425	45.78
44X-5, 15–17	409.55	26.18	35.47	1.877	2.663	1.386	47.97
44X-6, 11–13	411.01	26.22	35.54	1.890	2.701	1.394	48.37
44X-6, 104–106	411.94	24.85	33.06	1.903	2.655	1.430	46.15
45X-1, 123–125	414.33	25.85	34.85	1.874	2.635	1.389	47.27
45X-2, 44–46	415.04	27.93	38.76	1.801	2.550	1.298	49.10
45X-2, 122–124	415.82	28.20	39.27	1.857	2.728	1.333	51.12
45X-3, 67–69	416.77	28.66	40.18	1.798	2.582	1.283	50.31
45X-3, 132–134	417.42	27.61	38.13	1.848	2.666	1.338	49.80
45X-4, 47–49	418.07	27.94	38.77	1.844	2.673	1.329	50.29
45X-4, 138–140	418.98	27.72	38.34	1.848	2.671	1.336	49.99
45X-5, 81–83	419.91	23.79	31.22	2.421	4.214	1.845	56.22
45X-5, 136–138	420.46	24.84	33.05	1.700	2.174	1.278	41.22
45X-6, 62–64	421.22	23.77	31.18	1.934	2.674	1.474	44.87
45X-6, 94–96	421.54	23.95	31.49	1.931	2.677	1.469	45.14
46X-1, 57–59	423.37	23.75	31.14	1.964	2.749	1.498	45.52
46X-2, 18–20	424.48	23.13	30.09	1.946	2.668	1.496	43.93
46X-2, 102–104	425.32	23.89	31.39	1.955	2.736	1.488	45.60
46X-3, 35–37	426.15	23.06	29.97	1.944	2.660	1.496	43.76
46X-4, 11–13	427.41	24.26	32.03	1.957	2.763	1.482	46.35
46X-4, 136–138	428.66	25.65	34.51	1.875	2.627	1.394	46.95
46X-5, 5–7	428.85	26.44	35.94	1.894	2.726	1.394	48.88

Table 10 (continued).

Core, section, interval (cm)	Depth (mbsf)	Water content (bulk wt%)	Water content (dry wt%)	Bulk density (Mg/m^3)	Grain density (Mg/m^3)	Dry density (Mg/m^3)	Porosity (%)
46X-6, 37–39	430.67	26.50	36.05	1.899	2.742	1.396	49.10
46X-7, 7–9	431.57	24.40	32.27	1.936	2.715	1.464	46.10
47X-1, 102–104	433.42	25.04	33.41	1.925	2.724	1.443	47.05
47X-2, 98–100	434.88	26.16	35.43	1.888	2.693	1.394	48.23
47X-3, 144–146	436.84	26.23	35.55	1.882	2.678	1.388	48.17
47X-4, 76–78	437.66	25.52	34.27	1.888	2.656	1.406	47.04
47X-5, 126–128	439.66	25.28	33.84	1.883	2.629	1.407	46.48
47X-6, 78–80	440.68	24.45	32.36	1.947	2.748	1.471	46.47
48X-1, 107–109	443.17	26.26	35.62	1.886	2.692	1.391	48.35
48X-2, 32–34	443.92	23.38	30.52	1.956	2.706	1.498	44.63
48X-3, 96–98	446.06	24.06	31.69	1.925	2.668	1.462	45.21
48X-4, 33–35	446.93	24.20	31.93	1.927	2.681	1.461	45.53
48X-5, 86–88	448.96	24.80	32.97	1.890	2.619	1.421	45.73
48X-6, 50–52	450.10	25.43	34.10	1.903	2.690	1.419	47.24
48X-7, 36–38	451.46	25.50	34.23	1.915	2.726	1.427	47.67
49X-1, 47–49	452.17	25.20	33.68	1.915	2.708	1.433	47.10
49X-2, 119–121	454.39	24.99	33.32				
49X-3, 101–103	455.71	25.41	34.07	1.918	2.728	1.430	47.57
49X-4, 40–42	456.60	24.99	33.31	1.926	2.725	1.445	46.97
49X-4, 81–83	457.01	25.25	33.78	1.920	2.725	1.435	47.33
49X–5, 132–134	459.02	26.40	35.87	1.919	2.794	1.412	49.45
49X-6, 65–67	459.85	25.03	33.39	1.935	2.751	1.450	47.27
50X-1, 18–20	461.58	25.21	33.70	1.906	2.684	1.425	46.90
50X-1, 81–83	462.21	24.41	32.29	1.943	2.734	1.469	46.29
50X-2, 46–48	463.36	23.85	31.32	1.923	2.651	1.464	44.76
50X-2, 142–144	464.32	24.44	32.34	1.928	2.698	1.457	46.00
50X-3, 75–77	465.15	23.43	30.60	1.943	2.677	1.488	44.43
50X–4, 29–31	466.19	23.74	31.12	1.912	2.618	1.458	44.30
50X-4, 114–116	467.04	23.30	30.37	1.930	2.638	1.480	43.89
50X-5, 54–56	467.94	22.92	29.74	1.955	2.679	1.507	43.75
50X-5, 132–134	468.72	22.46	28.97	1.966	2.679	1.524	43.10
50X–6, 25–27	469.15	23.79	31.21	1.931	2.669	1.472	44.84
50X-6, 117–119	470.07	21.74	27.79	1.977	2.665	1.547	41.96
51X-1, 5–7	471.05	22.86	29.64	1.939	2.636	1.496	43.26
51X-1, 120–122	472.20	22.24	28.60	1.928	2.578	1.499	41.84
51X-2, 56–58	473.06	22.80	29.53	1.946	2.651	1.503	43.31
51X-2, 116–118	473.66	21.12	26.78	1.952	2.578	1.540	40.26
51X-3, 6–8	474.06	22.60	29.20	1.960	2.673	1.517	43.24
51X-3, 84–86	474.84	19.95	24.92	2.007	2.638	1.607	39.09
51X-4, 46–48	475.96	22.40	28.87	1.978	2.706	1.535	43.26
51X-4, 133–135	476.83	22.79	29.52	1.965	2.697	1.517	43.73
51X-5, 57–59	477.57	21.35	27.15	1.997	2.690	1.571	41.62
51X-5, 140–142	478.40	21.18	26.87	1.970	2.620	1.553	40.73
51X-6, 43–45	478.93	22.26	28.63	1.965	2.665	1.527	42.68
51X-7, 28–30	480.28	22.54	29.10	1.939	2.621	1.502	42.67
52X-1, 6–8	480.56	23.30	30.39	1.937	2.656	1.486	44.06
52X-1, 122–124	481.72	21.29	27.05	1.959	2.601	1.542	40.72
52X-2, 20–22	482.20	21.85	27.96	1.972	2.660	1.541	42.07
52X-2, 71–73	482.71	22.54	29.10	1.973	2.700	1.528	43.41
52X-3, 77–79	484.27	24.02	31.62	1.936	2.693	1.471	45.39
52X-3, 135–137	484.85	25.02	33.37	1.927	2.729	1.445	47.05
52X-4, 9–11	485.09	23.75	31.14	1.946	2.703	1.484	45.11
52X-4, 116–118	486.16	23.33	30.42	1.937	2.657	1.485	44.11
52X-5, 22–24	486.72	23.59	30.87	1.937	2.672	1.480	44.60
52X-5, 124–126	487.74	22.75	29.45	1.986	2.743	1.534	44.09
52X-6, 53–55	488.53	21.83	27.93	1.981	2.679	1.548	42.21
52X-6, 145–147	489.45	23.26	30.31	1.945	2.673	1.493	44.16
53X-1, 15–17	490.35	22.68	29.33	1.955	2.665	1.512	43.27
53X-1, 142–144	491.62	22.94	29.77	1.958	2.687	1.509	43.84
53X-2, 46–48	492.16	24.04	31.64	1.923	2.663	1.461	45.13
53X-2, 110–112	492.80	22.10	28.37	2.000	2.740	1.558	43.15
53X-3, 39–41	493.59	22.06	28.30	2.001	2.740	1.560	43.08
53X-3, 97–99	494.17	22.51	29.04	1.977	2.709	1.532	43.44
53X-4, 39–41	495.09	21.71	27.72	1.990	2.693	1.558	42.16
53X-4, 140–142	496.10	22.16	28.47	1.969	2.669	1.533	42.58
53X-5, 7–9	496.27	21.69	27.69	1.988	2.687	1.557	42.07
53X-5, 146–148	497.66	22.30	28.70	1.953	2.639	1.517	42.51
53X-6, 107–109	498.77	21.22	26.93	1.997	2.682	1.573	41.35
54X-1, 11–13	500.01	21.32	27.09	2.007	2.711	1.579	41.75
54X-1, 145–147	501.35	22.28	28.67	2.220	3.335	1.725	48.27
54X-2, 39–41	501.79	20.76	26.20	2.005	2.677	1.589	40.63
54X-2, 145–147	502.85	20.40	25.62	1.860	2.352	1.481	37.04
54X-3, 71–73	503.61	20.51	25.80	2.017	2.689	1.603	40.38
54X-3, 144–146	504.34	22.94	29.77	1.980	2.740	1.525	44.33
54X-4, 11–13	504.51	22.90	29.70	1.966	2.704	1.516	43.95
54X-4, 130–132	505.70	22.66	29.30	1.998	2.768	1.545	44.19
54X-5, 38–40	506.28	23.65	30.97	1.955	2.720	1.493	45.13
54X-5, 137–139	507.27	22.03	28.25	1.989	2.709	1.551	42.75
54X-6, 42–44	507.82	20.74	26.16	2.018	2.703	1.599	40.84
54X-6, 145–147	508.85	23.88	31.37	1.949	2.719	1.484	45.44
55X-1, 12–14	509.62	22.49	29.01	1.946	2.632	1.508	42.70
55X-1, 139–141	510.89	22.53	29.07	1.968	2.688	1.525	43.2
55X-2, 55–57	511.55	22.11	28.39	1.983	2.699	1.544	42.79
55X-2, 147–149	512.47	21.08	26.72	1.990	2.659	1.570	40.95
55X-3, 54–56	513.04	22.63	29.25	1.977	2.716	1.530	43.67
55X-3, 145–147	513.95	22.66	29.30	1.978	2.719	1.529	43.74
55X-4, 47–49	514.47	21.84	27.94	1.989	2.699	1.555	42.40
55X-4, 105–107	515.05	21.31	27.08	1.983	2.655	1.560	41.24
55X-5, 11–13	515.61	21.15	26.82	2.011	2.711	1.586	41.51
55X-5, 98–100	516.48	20.51	25.80	2.030	2.719	1.614	40.64
55X-6, 13–15	517.13	21.18	26.87	2.010	2.710	1.584	41.55
55X-6, 131–133	518.31	20.11	25.17	2.045	2.728	1.634	40.13
56X-1, 25–27	519.45	21.20	26.90	2.024	2.744	1.595	41.87
56X-1, 145–147	520.65	20.13	25.20	2.101	2.858	1.678	41.28
56X-2, 18–20	520.88	20.59	25.92	1.998	2.651	1.587	40.15
56X-2, 105–107	521.75	19.88	24.82	2.030	2.684	1.626	39.39
56X-3, 11–13	522.31	19.94	24.91	2.057	2.747	1.647	40.04
56X-3, 115–117	523.35	20.08	25.13	2.043	2.723	1.633	40.04
56X-4, 38–40	524.08	20.82	26.30	2.031	2.739	1.608	41.28
56X-4, 137–139	525.07	21.64	27.61	1.981	2.668	1.552	41.83
56X-5, 70–72	525.90	20.74	26.16	2.031	2.734	1.610	41.11
56X-5, 145–147	526.65	21.43	27.28	1.986	2.669	1.560	41.54
56X-6, 55–57	527.25	21.22	26.94	2.021	2.738	1.592	41.86
56X-6, 143–145	528.13	21.49	27.37	1.986	2.672	1.559	41.66
57X-1, 7–9	528.97	20.50	25.78	2.006	2.665	1.595	40.14
57X-1, 84–86	529.74	21.93	28.09	2.013	2.761	1.572	43.09
57X-2, 6–8	530.46	20.72	26.13	2.028	2.725	1.608	41.01
57X-2, 98–100	531.38	19.87	24.80	2.032	2.688	1.629	39.42
57X-3, 16–18	532.06	20.86	26.35	1.996	2.662	1.580	40.64
57X-3, 84–86	532.74	20.50	25.79	2.034	2.727	1.617	40.70
57X-4, 17–19	533.57	20.89	26.41	2.020	2.717	1.598	41.20
57X-4, 78–80	534.18	21.00	26.58	2.060	2.817	1.627	42.23
57X-5, 23–25	535.13	21.02	26.61	1.999	2.677	1.579	41.01
57X-5, 112–114	536.02	21.06	26.68	1.991	2.660	1.571	40.92
57X-6, 28–30	536.68	20.40	25.63	2.027	2.706	1.613	40.37
57X-6, 94–96	537.34	20.73	26.16	2.031	2.733	1.610	41.10
58X-1, 15–17	538.65	18.54	22.76	2.103	2.765	1.713	38.05
58X-1, 58–60	539.08	18.91	23.32	2.063	2.702	1.673	38.09
58X-2, 4–6	540.04	20.26	25.41	2.021	2.685	1.612	39.98
58X-2, 128–130	541.28	20.89	26.41	1.972	2.610	1.560	40.22
58X-3, 33–35	541.83			1.941			
58X-3, 117–119	542.67	19.70	24.53	2.014	2.639	1.617	38.72
58X-3, 148–150	542.98	21.94	28.11	1.993	2.714	1.556	42.68
58X-4, 36–38	543.36			2.035			
58X-4, 82–84	543.82	18.94	23.36	2.051	2.678	1.663	37.91
58X-4, 143–145	544.43	19.36	24.01	2.017	2.629	1.627	38.12
58X-5, 58–60	545.08	17.97	21.90	1.985	2.498	1.629	34.81
58X-6, 84–86	546.84	21.22	26.94	1.978	2.639	1.558	40.97
58X-6, 113–115	547.13	22.46	28.97	1.948	2.636	1.510	42.71
59X-1, 76–78	548.96	19.98	24.96	2.017	2.660	1.614	39.33
59X-1, 105–107	549.25	22.71	29.38	1.810	2.336	1.399	40.12
59X-2, 3–5	549.73	20.25	25.39	2.025	2.693	1.615	40.03
59X-2, 135–137	551.05	20.27	25.42	2.025	2.693	1.614	40.06
59X-3, 6–8	551.26	22.20	28.53	1.953	2.634	1.520	42.32
59X-3, 89–91	552.09			1.922			
59X-4, 26–28	552.96	19.12	23.64	2.052	2.689	1.659	38.29
59X-4, 57–59	553.27	19.54	24.28	2.061	2.732	1.658	39.30
59X-5, 7–9	554.27			2.031			
59X-5, 143–145	555.63	20.05	25.08	2.031	2.695	1.624	39.75
59X-6, 92–94	556.62	25.70	34.60	1.875	2.630	1.393	47.04
59X-6, 133–135	557.03	20.36	25.56	2.024	2.696	1.612	40.22
59X-7, 12–14	557.32	19.75	24.61	2.051	2.723	1.646	39.55
60X-1, 46–48	558.36	21.50	27.38	2.009	2.727	1.578	42.16
60X-1, 84–86	558.74	19.81	24.70	2.042	2.706	1.638	39.48
60X-2, 21–23	559.61	24.75	32.89	1.942	2.753	1.461	46.91
60X-2, 87–89	560.27	18.88	23.28	2.058	2.690	1.669	37.93
60X-3, 52–54	561.42			2.079			
60X-3, 124–126	562.14	22.55	29.11	1.961	2.673	1.519	43.17
60X-4, 91–93	563.31	19.25	23.84	2.048	2.689	1.654	38.48
60X-5, 48–50	564.38	19.03	23.50	2.044	2.669	1.655	37.97
60X-5, 94–96	564.84	18.38	22.51	2.074	2.696	1.693	37.20
60X-6, 21–23	565.61	18.27	22.35	2.088	2.720	1.707	37.24
61X-1, 14–16	567.74	19.92	24.87	2.039	2.705	1.633	39.64
61X-1, 96–98	568.56	19.68	24.50	2.030	2.673	1.630	39.00
61X-2, 65–67	569.75	20.97	26.53	1.972	2.614	1.559	40.37
61X-2, 119–121	570.29	18.99	23.44	2.056	2.690	1.665	38.10
61X-3, 140–142	572.00	19.45	24.14	2.082	2.774	1.677	39.53
61X-4, 19–21	572.29	19.86	24.78	2.082	2.798	1.669	40.35
61X-4, 143–145	573.53	20.88	26.39	1.981	2.630	1.568	40.39
61X-5, 26–28	573.86	18.99	23.44	2.055	2.689	1.665	38.10
61X-5, 105–107	574.65	20.52	25.82	2.026	2.711	1.611	40.59
62X-1, 26–28	577.46	22.04	28.28	1.981	2.692	1.545	42.63
62X-1, 107–109	578.27	22.18	28.50	1.984	2.707	1.544	42.96
62X-2, 12–14	578.82	21.21	26.91	2.003	2.696	1.578	41.46
62X-2, 85–87	579.55	21.45	27.30	1.983	2.664	1.558	41.52
62X-3, 21–23	580.41	24.07	31.70	1.926	2.671	1.462	45.26
62X-3, 75–77	580.95	19.44	24.13	2.034	2.668	1.639	38.59
62X-4, 6–8	581.76	20.57	25.90	2.020	2.700	1.605	40.57
63X-1, 62–64	587.52	21.52	27.43	1.983	2.668	1.556	41.66
63X-1, 116–118	588.06	21.39	27.21	2.000	2.699	1.572	41.75
63X-2, 48–50	588.88	20.39	25.61	1.993	2.629	1.586	39.66
63X-2, 106–108	589.46	19.98	24.96	2.014	2.653	1.611	39.27
63X-3, 29–31	590.19	22.29	28.68	1.971	2.681	1.531	42.87
63X-3, 81–83	590.71	18.55	22.77	2.075	2.708	1.690	37.58
63X-4, 32–34	591.72	17.97	21.91	2.087	2.700	1.712	36.60
63X-4, 133–135	592.73	19.30	23.92	2.030	2.654	1.639	38.25

Table 10 (continued).

Core, section, interval (cm)	Depth (mbsf)	Water content (bulk wt%)	Water content (dry wt%)	Bulk density (Mg/m³)	Grain density (Mg/m³)	Dry density (Mg/m³)	Porosity (%)
63X-5, 22–24	593.12	19.56	24.32	2.081	2.777	1.674	39.73
63X-5, 92–94	593.82	18.08	22.07	2.052	2.636	1.681	36.22
63X-6, 21–23	594.61	21.45	27.31	1.939	2.564	1.523	40.60
63X-6, 107–109	595.47	18.53	22.75	2.054	2.663	1.674	37.16
64X-1, 37–39	596.87	19.05	23.54	1.999	2.575	1.618	37.18
64X-1, 140–142	597.90	19.71	24.55	1.978	2.564	1.588	38.06
64X-2, 12–14	598.12	18.01	21.97	2.051	2.629	1.681	36.05
64X-2, 144–146	599.44	20.44	25.70	1.971	2.585	1.568	39.33
64X-3, 46–48	599.96	18.77	23.11	2.027	2.619	1.646	37.14
64X-3, 112–114	600.62	18.78	23.13	2.007	2.580	1.630	36.80
64X-4, 142–144	602.42	22.14	28.44	1.920	2.555	1.495	41.49
64X-5, 56–58	603.06	20.96	26.52	1.967	2.603	1.555	40.25
64X-5, 141–143	603.91	18.71	23.01	2.018	2.598	1.641	36.85
64X-6, 13–15	604.13	19.05	23.53	2.023	2.626	1.638	37.62
64X-6, 143–145	605.43	21.51	27.40	1.951	2.593	1.531	40.95
154-926C-							
1H-4, 84–86	5.84	47.90	91.95	1.538	2.851	0.801	71.90
2H-2, 78–80	12.28	42.72	74.57	1.719	3.479	0.985	71.69
3H-2, 81–83	21.81	42.53	74.00	1.632	2.909	0.938	67.75
4H-2, 114–116	31.64	40.59	68.32	1.646	2.812	0.978	65.22
4H-4, 53–55	34.03			1.630			
4H-7, 27–29	38.27	41.59	71.19	1.632	2.825	0.953	66.25
5H-2, 86–88	40.86	42.03	72.50	1.561	2.518	0.905	64.05
6H-2, 81–83	50.31	37.77	60.69	1.692	2.800	1.053	62.38
7H-2, 86–88	59.86	37.57	60.19	1.680	2.734	1.049	61.63
8H-2, 92–94	69.42	34.96	53.76	1.748	2.816	1.137	59.64
9H-6, 100–102	79.00	39.14	64.30	1.658	2.753	1.009	63.34
9H-4, 100–102	82.00	36.70	57.98	1.692	2.720	1.071	60.62
9H-6, 100–102	85.00	37.03	58.81	1.700	2.779	1.071	61.47
10H-2, 78–80	88.28	36.19	56.72	1.729	2.834	1.103	61.07
11H-4, 96–98	100.96	36.02	56.31	1.730	2.825	1.107	60.82
12H-2, 121–123	107.71	34.73	53.21	1.738	2.762	1.135	58.92
13H-4, 69–71	119.69	35.41	54.82	1.739	2.817	1.123	60.12
14H-3, 63–65	127.63	35.74	55.62	1.733	2.818	1.114	60.48
15H-3, 132–134	137.82	32.93	49.10	1.792	2.836	1.202	57.61
16H-2, 95–97	145.45	32.49	48.13	1.800	2.833	1.215	57.10
17H-5, 139–141	159.89	29.41	41.66	1.871	2.855	1.321	53.72
18H-3, 46–48	165.46	29.52	41.88	1.861	2.828	1.312	53.62
18H-4, 70–72	167.20	30.71	44.32	1.834	2.821	1.271	54.96
18H-5, 123–125	169.23	34.59	52.89	1.739	2.757	1.138	58.73
19H-2, 130–132	174.30	28.58	40.03	1.894	2.868	1.353	52.84
19H-4, 117–119	177.17	30.38	43.63	1.838	2.814	1.280	54.51
19H-6, 83–85	179.83	29.50	41.85	1.868	2.850	1.317	53.80
20H-2, 13–15	182.63	28.53	39.92	1.876	2.808	1.341	52.25
20H-4, 56–58	186.06	30.54	43.96	1.841	2.833	1.279	54.87
20H-6, 117–119	189.67	31.53	46.04	1.810	2.798	1.239	55.70
21H-4, 69–71	195.69	32.00	47.06	1.810	2.832	1.231	56.54
22H-4, 56–58	205.06	30.86	44.64	1.837	2.845	1.270	55.35
24H-2, 80–82	221.30	31.20	45.36	1.794	2.720	1.234	54.63
25H-2, 81–83	230.81	29.32	41.49	1.850	2.780	1.308	52.96
26H-2, 105–107	240.55	26.34	35.76	1.912	2.769	1.408	49.14
27X-2, 87–89	249.87	27.73	38.38	1.855	2.693	1.340	50.22
28X-2, 53–55	256.03	30.28	43.43	1.824	2.760	1.272	53.91
28X-4, 27–29	258.77	32.94	49.11	1.725	2.598	1.157	55.47
28X-6, 14–16	261.64	28.97	40.78	1.746	2.451	1.241	49.38
29X-2, 14–16	265.34	28.45	39.76	1.809	2.601	1.294	50.23
30X-2, 124–126	276.04	30.62	44.13	1.724	2.468	1.196	51.53
31X-2, 14–16	284.54	27.77	38.44	1.870	2.740	1.351	50.69
32X-1, 87–89	293.47	32.35	47.81	1.675	2.405	1.133	52.88
33X-1, 72–74	302.92	31.65	46.30	1.683	2.395	1.150	51.98
34X-1, 49–51	312.39	33.28	49.87	1.662	2.409	1.109	53.97
35X-1, 26–28	321.76	31.34	45.65	1.714	2.475	1.177	52.45
36X-1, 119–121	332.29	30.71	44.31	1.765	2.597	1.223	52.90
37X-3, 118–120	344.98	30.48	43.85	1.765	2.585	1.227	52.53
38X-2, 60–62	352.50	31.50	45.99	1.781	2.698	1.220	54.78
40X-1, 80–82	370.50	27.19	37.34	1.871	2.707	1.363	49.66
41X-4, 85–87	384.35	28.81	40.47	1.831	2.687	1.304	51.49
42X-2, 18–20	390.38	31.29	45.54	1.781	2.684	1.224	54.40

GRAPE Density

Figure 23 shows bulk densities determined by index properties methods on discrete samples compared to the GRAPE record in the upper 260 mbsf of Hole 926B. This interval is covered by continuous APC coring. From the excellent match of the two data sets shown in Figure 23, it appears that the gamma-ray attenuation method at Site 926 provides reliable bulk-density values for the interval cored by APC.

Acoustic Velocity

At Site 926, acoustic velocities were recorded on whole cores using the *P*-wave logger (PWL) from the MST and on half split sections using two discrete methods: the DSV and the HF (see "Physical Properties" section, "Explanatory Notes" chapter, this volume). The nearly continuous acoustic profiles (2-cm sampling interval) obtained with the PWL have not been processed on board.

For Hole 926A and through 308 mbsf for Hole 926B, compressional-wave velocities were measured at a sampling rate of about three per core. Below 308 mbsf, acoustic velocities were measured at a sampling rate of two per section for Hole 926B. Only 18 measurements have been performed for Hole 926C.

In the soft ooze, longitudinal (perpendicular to bedding) and transverse velocities (parallel to bedding) were measured using the DSV. Beginning at about 175 mbsf in Hole 926A and at 178 mbsf in Hole 926B, the sediment became so stiff that insertion of the DSV probes

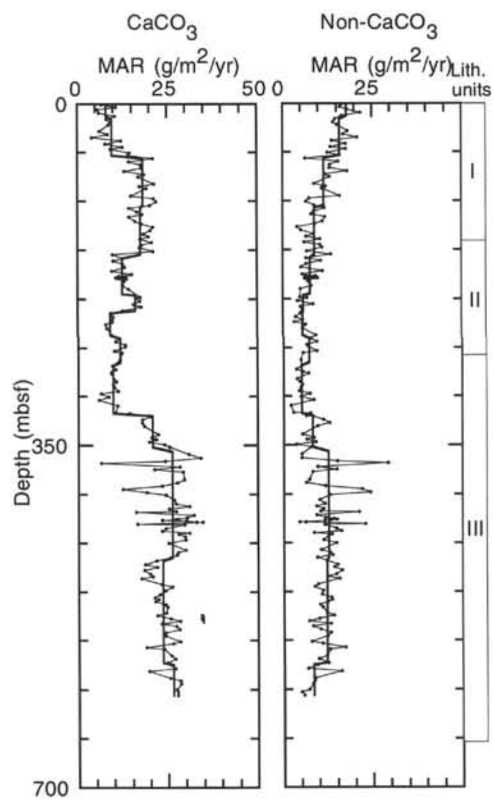

Figure 20. Calcium carbonate and noncarbonate accumulation rates vs. depth, Site 926. Solid dots represent values calculated from discrete carbonate and associated dry-bulk-density measurements. The age and sedimentation rates for each sample were based on linear interpolation between selected age datums (see "Sedimentation Rates" section, this chapter). The thick solid line in the plots is the mean value of the MARs between each of the selected age datums. The lithologic unit boundaries are shown on the right side of the diagram.

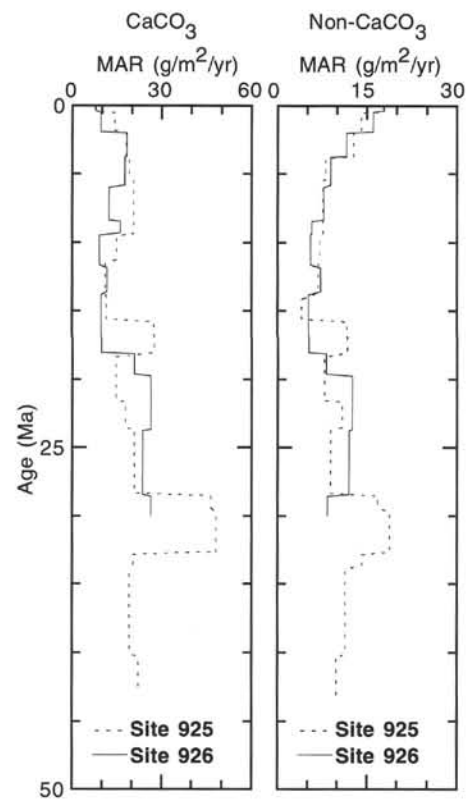

Figure 21. Mean calcium carbonate and noncarbonate accumulations vs. age for Sites 925 and 926. Note that the scale for the carbonate is twice the range of the noncarbonate MAR in the separate plots.

created fractures in the sediment (mostly along the bedding planes), which made it difficult to transmit and receive the acoustic signal. Therefore, at these depths, the DSV apparatus was replaced by the HF. From 175 to about 308 mbsf from Hole 926A and from 178 to 278 mbsf from Hole 926B, the *P*-wave velocities were measured through the core liner on split sections (transverse *P*-wave velocities only). For core recovered below 308 mbsf from Hole 926A and below 278 mbsf from Hole 926B, longitudinal and transverse acoustic velocity measurements were performed on coherent and undisturbed blocks of chalk that were cut using the parallel-blade diamond saw.

Results of velocity analyses are presented in Table 11. All data have been corrected for the speed of sound of the pore fluid at the temperature in situ (gradient of 0.05°C/mbsf; see below). Figure 24 shows the changes of acoustic velocity and velocity anisotropy with depth in Holes 926A and 926B.

At Site 926, acoustic velocities generally increase with depth below seafloor as consolidation takes place (from 1460 m/s at the top of the sediment column, to about 2400 m/s at the bottom of Hole 926B; Fig. 24). This increase is not linear, however, but overlain by steps and changes in gradients that generally correspond to changes in sediment composition or changes in the consolidation state. The slightly higher compressional velocities that were observed in Subunit IB (30–130 mbsf) compared with adjacent Subunits IA (0–30 mbsf) and IIA (130–190 mbsf) may indicate a higher coarse-fraction content (foraminifers) in Subunit IB. Positive changes in the velocity profile at about 460 mbsf correspond to the lithologic Subunit IIIB/IIIC boundary. In the ooze interval, compressional velocity changes likely reflect changes in the coarse-fraction content of the sediments (Mienert et al., 1988; Bassinot, in press).

Compressional velocities corrected for in situ temperature conditions are compared to log sonic velocities in the "Downhole Measurements" section (this chapter; see Fig. 38) Although laboratory velocities are generally lower than log velocities (which results from a decrease of the sediment rigidity modulus during removal of overburden pressure as cores are brought to laboratory conditions), most of the trends in the laboratory data are echoed in the log data, lending credibility to both data sets. However, the marked step observed in the velocity profile from Hole 926B at about 285 mbsf (with velocities increasing abruptly from about 1800 to 1950 m/s; Fig. 24) is not clearly seen in the log profile (which shows a rather continuous increase of velocities over this interval) and may correspond to an artifact of laboratory measurement procedures. This step in the laboratory profile roughly corresponds to the point where we switched from velocity measurements performed through the core liner with the HF to measurements performed on cubes (see above). It is likely that the high compressional velocities measured on selected samples are of good quality, whereas the velocities measured through the core liner are lower because the measurements are influenced by the presence of drilling paste, which fills the interval between the liner and the inner undisturbed part of the sediment core.

There appears to be an unexpected slight negative velocity anisotropy (average –0.5%) in lithologic Unit I (longitudinal velocities higher than transverse velocities). Observations made at Site 925, as well as earlier studies of velocity anisotropy performed on pelagic sediments (i.e., Hamilton, 1970; Johnson et al., 1977), showed that the upper part of calcareous deep-sea sedimentary series exhibits isotropic behavior. Shore-based fabric studies will be necessary to explain the unusual behavior of Site 926 ooze. In the deeper part of the sedimentary section (chalk interval, Unit III), the sediment exhibits a positive anisotropy that increases from 0% to 1% at about 300 mbsf to about 5% at 600 mbsf. This anisotropy suggests the development of a fabric oriented in the horizontal plane with increasing depth,

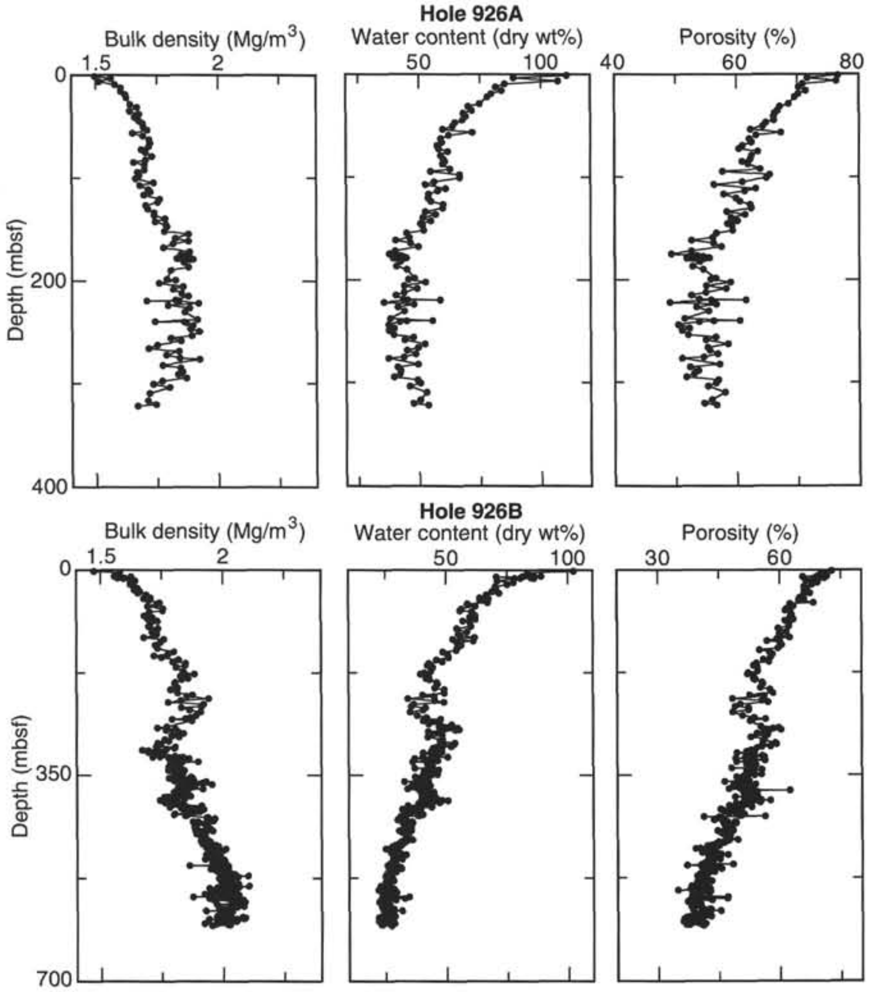

Figure 22. Bulk density, water content, and porosity vs. depth, Site 926. Note differences in scales.

as is usually observed in chalk and limestone (e.g., Carlson and Christensen, 1979; Kim et al., 1985).

Undrained Shear Strength

As at Site 925, much of the upper sediment column at Site 926 is underconsolidated, exhibiting ratios of undrained shear strength to overburden stress that are consistently less than 0.2 (Table 12 and Fig. 25). An incipient zone of increasing normalized shear strength is evident from about 150 to 180 mbsf. Below 230 mbsf, clay-rich beds are consistently normally consolidated (the ratio of S_u/P_o' is underestimated, as the strength exceeds the maximum measured by the pocket penetrometer). This horizon is about 50 m shallower than the equivalent boundary at Site 925 and appears to follow time and lithologic, rather than depth, lines. The marked stiffening of the sediment column occurs at both sites near the base of Subunit IIB, where a sharp increase in the natural gamma log indicates an increased clay content. The shear strength excursion from 150 to 180 mbsf likewise coincides with a natural gamma maximum.

Resistivity

Resistivity at Site 926 was measured using the small ODP probe. Electrical resistivity remains relatively constant in the upper 240 mbsf (Fig. 26 and Table 13). Below 240 mbsf, resistivity increases with depth, as expected for sediment undergoing gravitational consolidation. Resistivity is dependent upon sediment porosity and tortuosity. The general trend of increasing resistivity with depth below seafloor in the lower part of the sediment section is consistent with the index properties results of decreasing porosity with depth below seafloor. In the upper part of the section, porosity decreases with depth. Therefore, the tortuosity may be controlling the electrical resistivity properties. The decrease in tortuosity with depth is possibly associated with dissolution. An identical resistivity pattern with depth below seafloor can be observed in the downhole measurement resistivity log (see "Downhole Measurements" section, this chapter).

The correlation of porosity with resistivity is good in the upper 150 mbsf and below 240 mbsf. The correlation follows the relationship:

$$F = a\, n^{-m},$$

(Archie, 1942), where a represents the cementation coefficient, n is porosity, and m is the tortuosity coefficient. The formation factor (F) is the ratio of the resistivity of the sediment to the resistivity of the pore fluid. Pore fluid is assumed to be seawater at the temperature of the discrete core measurement. For the entire site, the relationship of porosity to formation results in Archie coefficients of 0.3 and –3.2 for a and m, respectively (Fig. 27A). However, when the low correlation interval between 150 and 240 mbsf is removed, the correlation is better and results in coefficients of 1.1 and –1.8, respectively (Fig. 27B). The coefficients for the interval from 150 to 240 mbsf are 0.4 and –2.0 (Fig. 27C). This interval is coincident with lithologic Unit II, which is characterized by a high ratio of red to blue color reflectance (see "Lithostratigraphy" section, this chapter).

Heat Flow

Thermal conductivity of the sediment at Site 926 was measured on whole-core samples from Hole 926C, and, combined with in situ

Table 11. Uncorrected and corrected acoustic velocity measured on discrete samples for all holes at Site 926.

Core, section, interval (cm)	Depth (mbsf)	Longitudinal acoustic velocity (m/s)	Transverse acoustic velocity (m/s)	Temperature (°C)	Corrected longitudinal velocity (m/s)	Corrected transverse velocity (ms)
154-926A-						
1H-1, 100	1.00	1510	1514	22	1426	1429
1H-3, 60	3.60	1542	1582	22	1460	1496
2H-2, 100	6.50	1507	1533	22	1424	1447
2H-4, 95	9.45	1520	1541	22	1442	1461
2H-6, 94	12.44	1529	1545	22	1451	1466
3H-2, 100	16.00	1517	1537	22	1440	1458
3H-4, 100	19.00	1529	1522	22	1453	1446
3H-6, 95	21.95	1548	1529	22	1471	1454
4H-4, 100	28.50	1569	1549	22	1492	1474
4H-6, 100	31.50	1552	1521	22	1479	1450
5H-2, 100	35.00	1564	1561	22	1490	1488
5H-4, 100	38.00	1633	1656	22	1554	1575
5H-6, 100	41.00	1596	1594	22	1521	1520
6H-2, 100	44.50	1602		22	1527	
6H-4, 32	46.82	1614	1582	22	1540	1511
6H-6, 70	50.20	1571	1510	22	1502	1446
7H-2, 41	53.41	1624	1642	22	1553	1570
7H-4, 48	56.48	1596	1633	22	1523	1556
7H-6, 37	59.37	1659	1633	22	1585	1561
8H-2, 37	62.87	1660	1590	22	1588	1524
8H-4, 50	66.00	1657	1647	22	1585	1576
8H-6, 93	69.43	1680	1651	22	1609	1582
9H-2, 53	72.53	1653	1607	23	1581	1539
9H-4, 23	75.23	1602	1629	23	1531	1556
9H-6, 95	78.95	1653	1674	23	1579	1599
10H-2, 91	82.41	1609	1651	23.5	1538	1576
10H-4, 28	84.78	1664	1679	23.5	1590	1604
10H-5, 129	87.29	1655	1647	23.5	1581	1574
11H-2, 121	92.21	1648	1645	23	1576	1573
11H-4, 60	94.60		1635	23		1571
11H-6, 37	97.37	1662	1619	23	1588	1549
12H-2, 31	100.81	1612	1599	23	1543	1531
12H-4, 110	104.60	1662	1645	23	1594	1578
12H-6, 67	107.17	1716	1669	23	1649	1606
13H-2, 107	111.07	1623	1599	23	1557	1535
13H-4, 34	113.34	1628	1628	23	1564	1564
13H-6, 40	116.40	1739	1659	23	1671	1597
14H-2, 100	120.50	1662	1649	23	1598	1586
14H-4, 100	123.50	1647	1638	23	1584	1576
14H-7, 70	126.68	1617	1632	23	1555	1569
15H-2, 100	130.00	1547	1574	23	1491	1516
15H-5, 13	133.63	1626	1602	23	1569	1546
15H-7, 20	136.20	1584	1577	23	1527	1521
16H-2, 75	139.25	1577	1602	23	1523	1547
16H-4, 85	142.35	1637	1609	23	1579	1553
16H-6, 73	145.23	1673	1655	23	1614	1598
17H-1, 75	147.25		1574	23		1522
17H-4, 7	151.07	1621		23		
17H-6, 65	154.65	1696	1705	23	1639	1648
18H-2, 110	158.60	1635	1622	23	1584	1571
18H-4, 90	161.40	1775	1698	23	1719	1646
18H-6, 90	164.40	1700	1642	23	1645	1591
19H-2, 60	167.60	1593	1593	23	1544	1544
19H-5, 30	171.80	1772	1655	23	1718	1608
19H-7, 10	174.60	1678		23	1633	
20H-2, 5	176.55		1672	23		1624
20H-2, 40	176.90		1711	23		1661
20H-2, 69	177.19		1698	23		1647
20H-2, 88	177.38		1706	23		1656
20H-2, 100	177.50		1696	23		1646
20H-2, 112	177.62		1714	23		1665
20H-2, 141	177.91		1711	23		1661
20H-2, 127	177.77		1726	23		1675
20H-3, 8	178.08		1685	23		1636
20H-3, 22	178.22		1666	23		1617
20H-3, 37	178.37		1674	23		1626
20H-3, 52	178.52		1643	23		1595
20H-3, 74	178.74		1721	23		1671
20H-3, 88	178.88		1698	23		1649
20H-3, 104	179.04		1709	23		1661
20H-3, 122	179.22		1683	23		1634
20H-3, 138	179.38		1713	23		1663
20H-5, 106	182.06		1732	23		1681
21H-2, 40	186.40		1693	23		1646
21H-4, 57	189.57		1764	23		1712
22H-3, 109	198.09		1730	23		1680
22H-4, 76	199.26		1739	23		1689
22H-6, 53	202.03		1758	23		1705
23H-2, 53	205.53		1774	23		1724
23H-4, 27	208.27		1795	23		1742
23H-6, 96	211.96		1762	23		1714
24H-2, 30	214.80		1773	23		1727
24H-4, 116	218.66		1756	23		1711
24H-6, 133	221.83		1798	23		1755
25H-1, 114	223.64		1797	23		1749

Table 11 (continued).

Core, section, interval (cm)	Depth (mbsf)	Longitudinal acoustic velocity (m/s)	Transverse acoustic velocity (m/s)	Temperature (°C)	Corrected longitudinal velocity (m/s)	Corrected transverse velocity (ms)
25H-3, 93	226.43		1717	23		1676
25H-6, 11	230.11		1712	23		1670
26H-2, 109	234.59		1771	23		1729
26H-4, 40	236.90		1789	23		1747
26H-4, 68	237.18		1796	23		1754
26H-4, 101	237.51		1827	23		1784
26H-6, 19	239.69		1829	23		1779
26H-6, 46	239.96		1767	23		1724
26H-6, 113	240.63		1843	23		1798
27H-2, 88	243.88		1791	23		1752
27H-4, 113	247.13		1808	23		1768
27H-6, 28	249.28		1812	23		1773
28H-2, 108	253.58		1822	23		1783
28H-4, 17	255.67		1830	23		1787
28H-6, 33	258.83		1782	23		1743
29H-2, 52	262.52		1806	23		1765
29H-2, 81	262.81		1789	23		1749
29H-2, 105	263.05		1760	23		1720
29H-2, 120	263.20		1748	23		1708
29H-2, 69	262.69		1782	23		1742
29H-2, 41	262.41		1798	23		1758
29H-4, 46	265.46		1802	23		1762
29H-4, 130	266.30		1835	23		1795
29H-6, 31	268.31		1821	23		1782
30H-2, 73	272.23		1863	23		1823
30H-2, 126	272.76		1897	23		1857
30H-4, 50	275.00		1863	23		1825
30H-5, 36	276.36		1842	23		1808
31H-4, 95	284.95		1859	24		1820
31H-6, 120	288.20		1761	24		1726
32H-2, 20	290.70		1768	24		1733
32H-4, 98	294.48		1762	24		1729
32H-6, 75	297.25		1792	24		1755
33H-2, 40	300.40		1734	24		1701
33H-4, 49	303.49		1791	24		1757
34H-1, 105	309.05	1978	1949	24	1936	1908
34H-6, 113	316.63	2004	2027	24	1965	1987
35H-2, 96	319.96	1951	1899	24	1916	1865
35H-3, 112	321.62	2027	2005	24	1988	1967
154-926B-						
1H-2, 30	1.80	1517	1486	23	1433	1406
1H-4, 30	4.80	1555	1550	23	1471	1466
2H-3, 32	10.32	1510	1512	23	1431	1432
2H-3, 78	10.78	1526	1526	23	1447	1447
2H-3, 101	11.01	1518	1514	23	1437	1434
2H-3, 133	11.33	1565	1562	23	1486	1483
2H-5, 17	13.17	1526	1517	23	1446	1438
2H-5, 38	13.38	1539	1526	23	1458	1447
2H-5, 76	13.76	1531	1517	23	1450	1438
2H-5, 116	14.16	1564	1562	23	1482	1480
3H-2, 47	18.47	1562	1497	23	1483	1425
3H-4, 32	21.32	1533	1520	23	1454	1443
3H-6, 43	24.43	1545	1559	23	1468	1480
4H-2, 111	28.61	1579	1568	23	1501	1491
4H-4, 63	31.13	1579	1532	23	1501	1458
4H-6, 51	34.01	1614	1495	23	1533	1425
5H-1, 117	36.67	1586	1565	24	1506	1487
5H-3, 46	38.96	1569	1550	24	1490	1472
5H-5, 55	42.05	1593	1593	24	1514	1514
6H-2, 88	47.38	1641	1615	24	1557	1534
6H-3, 89	48.89	1601	1590	24	1520	1510
6H-5, 75	51.75	1632		24	1550	
7H-1, 75	55.25	1641	1606	24	1554	1522
7H-3, 38	57.88	1636	1602	24	1557	1527
7H-5, 116	61.66	1626	1593	24	1548	1518
8H-2, 25	65.75	1653	1605	24	1575	1531
8H-4, 60	69.10	1699	1634	24	1618	1559
8H-5, 114	71.14	1633	1615	24	1558	1541
9H-2, 124	76.24	1662	1631	24	1585	1557
9H-3, 116	77.66	1646	1618	24	1571	1545
9H-5, 108	80.58	1655	1602	24	1578	1529
10H-1, 119	84.19	1600	1605	24	1528	1532
10H-3, 115	87.15	1682	1641	24	1605	1568
10H-5, 19	89.19	1646	1615	23	1577	1548
11H-3, 85	96.35	1615	1618	23	1549	1552
11H-5, 70	99.20	1662	1641	23	1597	1577
12H-3, 95	105.95	1624	1628	23	1560	1564
12H-5, 110	109.10	1701	1679	23	1634	1614
12H-7, 35	111.35	1735	1704	23	1666	1637
13H-3, 80	115.30	1620	1595	23	1558	1535
13H-5, 47	117.97	1729	1662	23	1662	1600
13H-7, 37	120.87	1607	1602	23	1552	1547
14H-2, 98	123.48	1664	1628	23	1603	1569
14H-5, 116	128.16	1620	1618	23	1562	1560
15H-3, 45	133.95	1629	1611	23	1572	1556
15H-5, 43	136.93	1625	1615	23	1573	1563

Table 11 (continued).

Core, section, interval (cm)	Depth (mbsf)	Longitudinal acoustic velocity (m/s)	Transverse acoustic velocity (m/s)	Temperature (°C)	Corrected longitudinal velocity (m/s)	Corrected transverse velocity (ms)
15H-7, 33	139.83	1666	1611	23	1610	1559
16H-3, 53	143.53	1668	1658	23	1612	1602
16H-5, 54	146.54	1644	1598	23	1589	1543
16H-7, 23	149.23		1624	23		1572
17H-3, 44	152.94	1705	1644	23	1650	1593
17H-5, 89	156.39	1634	1618	23	1583	1568
17H-7, 30	158.80	1750	1638	23	1695	1589
18H-3, 44	162.44	1703	1651	23	1652	1603
18H-5, 105	166.05	1744	1668	23	1690	1619
19H-3, 105	172.55	1689	1624	23	1640	1579
19H-5, 153	176.03	1802	1700	23	1755	1653
19H-7, 20	177.70		1740	23		1691
20H-3, 78	181.78		1721	23		1673
20H-5, 70	184.70		1736	23		1688
20H-7, 8	187.08		1745	23		1696
21H-3, 95	191.45		1699	23		1652
21H-5, 87	194.37		1729	23		1681
22H-3, 122	201.22		1762	23		1714
22H-5, 70	203.70		1788	23		1737
23H-3, 35	209.85		1796	23		1745
23H-5, 46	212.96		1795	23		1750
23H-7, 55	216.05		1825	23		1783
24H-3, 43	219.43		1764	23		1725
24H-5, 122	223.22		1796	23		1751
24H-7, 53	225.53		1779	23		1734
25H-3, 62	229.12		1758	23		1720
25H-5, 126	232.76		1805	23		1766
25H-7, 30	234.80		1762	23		1723
26H-3, 92	238.92		1786	23		1747
26H-5, 138	242.38		1851	23		1813
27H-3, 132	248.82		1801	23		1765
27H-5, 118	251.68		1751	23		1715
27H-7, 43	253.93		1775	23		1739
28X-1, 19	254.19		1776	23		1741
28X-3, 52	257.52		1787	23		1752
29X-3, 110	263.10		1880	23		1846
29X-5, 27	265.27		1844	23		1810
30X-3, 47	272.07		1794	23		1760
30X-5, 104	275.64		1883	24		1849
31X-1, 108	279.38	1768	1750	24	1732	1715
31X-3, 6	281.36	1816	1837	24	1777	1797
31X-5, 86	285.16	1697	1749	24	1666	1716
32X-1, 115	289.15	1903	1877	24	1863	1838
32X-3, 108	292.08	1894	1909	24	1855	1869
32X-5, 91	294.91	1964	1903	24	1921	1862
32X-5, 91	294.91	1937		24	1894	
32X-7, 11	297.11	1863	1888	24	1825	1849
33X-1, 83	298.43	1766	1771	24	1734	1739
33X-3, 79	301.39	2034	2028	24	1991	1985
33X-4, 10	302.20	1834	1869	24	1800	1834
33X-5, 28	303.88	1905	1905	24	1869	1870
33X-6, 50	305.60	2072	2073	24	2036	2038
34X-1, 28	307.58	2167	2151	24	2124	2108
34X-1, 103	308.33	1910	1954	24	1877	1919
34X-2, 30	309.10	1938	2045	24	1904	2008
34X-2, 138	310.18	1744	1798	24	1718	1770
34X-3, 31	310.61	1948	2002	24	1913	1965
34X-3, 142	311.72	2072	2168	24	2033	2126
34X-4, 24	312.04	2013	2031	24	1979	1997
35X-1, 118	318.08	2028	1999	24	1994	1965
35X-1, 53	317.43	1920	1962	24	1887	1927
35X-2, 59	318.99	2103	2178	24	2064	2136
35X-2, 146	319.86	1769	1830	24	1744	1803
35X-3, 53	320.43	2020	2040	24	1987	2007
35X-3, 140	321.30	2110	2098	24	2074	2061
35X-4, 65	322.05	1878	1920	24	1851	1892
35X-4, 139	322.79	1912	1977	24	1882	1945
35X-5, 26	323.16	1822	1882	24	1796	1853
35X-5, 95	323.85	1866	1918	24	1837	1888
35X-6, 41	324.81	2010	2015	24	1976	1981
35X-6, 145	325.85	1975	1899	24	1944	1870
36X-1, 59	327.09	1842	1895	24	1817	1869
36X-1, 138	327.88	1921	1903	24	1893	1875
36X-2, 73	328.73	1932	1962	24	1903	1932
36X-2, 133	329.33	2024	2090	24	1993	2057
36X-3, 63	330.13	1917	1973	24	1889	1943
36X-3, 141	330.91	2099	2125	24	2067	2092
36X-4, 26	331.26	1850	1912	24	1825	1884
36X-4, 121	332.21	1846	1907	24	1820	1880
37X-1, 58	336.78	2045	2038	24	2016	2009
37X-1, 145	337.65	1916	1982	24	1890	1955
37X-2, 76	338.46	1660	1629	24	1642	1612
37X-2, 124	338.94	2045	2079	24	2016	2048
37X-3, 77	339.97	2029	2020	24	2001	1992
37X-3, 142	340.62	1826	1867	24	1802	1842
37X-4, 44	341.14	2108	2100	24	2078	2070
37X-4, 132	342.02	1900	1925	24	1876	1900

Table 11 (continued).

Core, section, interval (cm)	Depth (mbsf)	Longitudinal acoustic velocity (m/s)	Transverse acoustic velocity (m/s)	Temperature (°C)	Corrected longitudinal velocity (m/s)	Corrected transverse velocity (ms)
37X-5, 39	342.59	1930	1973	24	1905	1947
37X-5, 139	343.59	2025	2024	24	1998	1997
38X-1, 66	346.46	1941	2001	24	1917	1976
38X-1, 137	347.17	2044	2059	24	2018	2032
38X-2, 32	347.62	1934	1993	24	1910	1967
38X-2, 136	348.66	1795	1826	24	1774	1804
38X-3, 58	349.38	2012	2029	24	1987	2004
38X-4, 41	350.71	2050	2089	24	2025	2063
38X-4, 130	351.60	2090	2069	24	2064	2043
38X-5, 23	352.03	2038	2024	24	2014	2000
38X-5, 115	352.95	1904	1992	24	1884	1970
38X-6, 35	353.65	2059	2094	24	2035	2069
38X-7, 21	355.01	1727	1781	24	1710	1763
38X-7, 21	355.01	1913	1989	24	1896	1971
39X-1, 136	356.86	1939	1934	24	1919	1914
39X-2, 69	357.69	1991	2020	24	1970	1998
39X-2, 126	358.26	1854	1899	24	1836	1880
39X-3, 57	359.07	2107	2079	24	2084	2056
39X-3, 132	359.82	2040	2039	24	2018	2017
39X-4, 74	360.74	2020	2130	24	2001	2109
39X-4, 74	360.74	1947	2029	24	1938	2008
39X-5, 13	361.63	2013	2009	24	1993	1990
39X-5, 127	362.77	1879	1908	24	1862	1890
39X-6, 141	364.41	2045	2120	24	2025	2098
39X-7, 12	364.62	1863	1887	24	1847	1870
40X-1, 85	365.95	1766	1885	24	1750	1867
40X-2, 6	366.66	1922	1988	24	1905	1970
40X-2, 95	367.55	2071	2109	24	2052	2090
40X-3, 6	368.16	1669	1747	24	1656	1732
40X-3, 141	369.51	1759	1795	24	1745	1781
40X-4, 44	370.04	1838	1878	24	1823	1862
40X-5, 6	371.16	2048	2069	24	2030	2050
40X-5, 100	372.10	2021	2085	24	2004	2067
40X-6, 33	372.93	1984	1982	24	1968	1967
40X-6, 132	373.92	1834	1870	24	1819	1855
41X-1, 54	374.94	1891	1938	24	1876	1922
41X-2, 8	375.44	1909	1948	24	1893	1932
41X-3, 71	377.57	2183	2163	24	2164	2144
41X-4, 27	378.63	1878	1937	24	1864	1922
41X-4, 125	379.61	2000	2046	24	1985	2030
41X-5, 5	379.91	2184	2199	24	2166	2181
42X-1, 113	385.23	2116	2138	24	2100	2122
42X-2, 7	385.67	1964	1997	24	1951	1983
42X-2, 125	386.85	2128	2178	24	2114	2163
42X-3, 6	387.16	2088	2099	24	2074	2085
42X-3, 108	388.18	2141	2152	24	2126	2136
42X-4, 9	388.69	1717	1765	24	1707	1755
42X-4, 85	389.45	1854	1920	24	1843	1909
42X-5, 13	390.23	1827	1903	24	1817	1892
42X-5, 140	391.50	1982	2059	24	1971	2046
42X-6, 56	392.16	2212	2207	24	2197	2192
42X-6, 113	392.73	1713	1807	24	1704	1797
43X-1, 20	393.90	2136	2130	24	2123	2118
43X-1, 106	394.76	1713	1788	24	1705	1779
43X-2, 87	396.07	1955	1972	24	1945	1961
43X-2, 121	396.41	1711	1774	24	1703	1765
43X-3, 53	397.23	2040	2017	24	2030	2007
43X-3, 92	397.62	1723	1810	24	1713	1800
43X-4, 5	398.25	1886	1929	24	1878	1920
43X-4, 106	399.26	1751	1803	24	1744	1796
43X-5, 65	400.35	1920	1955	24	1912	1947
43X-6, 85	402.05	1955	2020	24	1947	2012
44X-1, 15	403.55	1846	1970	24	1839	1962
44X-1, 15	403.55	1850		24	1843	
44X-1, 114	404.54	2079	2109	24	2070	2101
44X-2, 59	405.49	2059	2077	24	2051	2069
44X-3, 27	406.67	2040	2079	24	2033	2071
44X-3, 139	407.79	1998	2012	24	1992	2006
44X-4, 74	408.64	1791	1854	24	1786	1848
44X-4, 133	409.23	1963	2029	24	1957	2024
44X-5, 16	409.56	1960	2033	24	1954	2027
44X-5, 99	410.39	2076	2113	24	2070	2107
44X-6, 12	411.02	1886	1941	24	1881	1936
44X-6, 105	411.95	2071	2099	24	2065	2094
45X-1, 124	414.34	2038	2059	24	2034	2054
45X-2, 45	415.05	1962	1998	24	1958	1994
45X-2, 122	415.82	1886	1946	24	1882	1942
45X-3, 68	416.78	1751	1799	24	1748	1796
45X-3, 133	417.43	2254	2253	24	2249	2248
45X-4, 48	418.08	1762	1855	24	1759	1851
45X-4, 139	418.99	2185	2196	24	2181	2192
45X-5, 82	419.92	2044	2044	24	2040	2040
45X-5, 137	420.47	1946	2010	24	1944	2008
45X-6, 63	421.23	2136	2151	24	2133	2148
45X-6, 95	421.55	2018	2093	24	2015	2090
46X-1, 58	423.38	1960	2049	24	1959	2047
46X-2, 19	424.49	2038	2116	24	2037	2114

Table 11 (continued).

Core, section, interval (cm)	Depth (mbsf)	Longitudinal acoustic velocity (m/s)	Transverse acoustic velocity (m/s)	Temperature (°C)	Corrected longitudinal velocity (m/s)	Corrected transverse velocity (ms)
46X-2, 103	425.33	1955	2009	24	1954	2008
46X-3, 36	426.16	2063	2059	24	2061	2058
46X-3, 110	426.90	1894	1986	24	1892	1985
46X-4, 12	427.42	2075	2119	24	2074	2118
46X-4, 137	428.67	2157	2219	24	2156	2218
46X-5, 6	428.86	2106		24	2106	
46X-5, 6	428.86	2104		24	2104	
46X-6, 38	430.68	1822	1911	24	1822	1911
46X-7, 8	431.58	1972	2010	24	1973	2011
47X-1, 102	433.42	2078	2151	24	2079	2152
47X-2, 99	434.89	1877	1982	24	1878	1983
47X-3, 145	436.85	2107	2166	24	2109	2168
47X-4, 77	437.67	1862	1955	24	1864	1957
47X-5, 127	439.67	2173	2222	24	2176	2225
47X-6, 79	440.69	2023	2034	24	2026	2037
48X-1, 108	443.18	2150	2180	24	2154	2184
48X-2, 33	443.93	2014	2099	24	2018	2103
48X-3, 97	446.07	2053	2141	24	2057	2146
48X-4, 34	446.94	2009	2048	24	2013	2053
48X-5, 87	448.97	2108	2185	24	2114	2191
48X-6, 51	450.11	1951	2029	24	1957	2035
48X-7, 37	451.47	2186	2190	24	2193	2197
49X-1, 48	452.18	2122	2115	24	2129	2122
49X-2, 120	454.40	1718	1799	24	1725	1806
49X-3, 101	455.71	2051	2036	24	2059	2044
49X-4, 82	457.02	2075	2109	24	2084	2118
49X-5, 133	459.03	2032	2035	24	2041	2045
49X-7, 66	459.86	2032	2078	24	2041	2087
50X-1, 19	461.59	1908	2001	24	1916	2010
50X-1, 82	462.22	1908	1930	24	1916	1939
50X-2, 47	463.37	1960	2046	24	1968	2055
50X-2, 143	464.33	1926	1966	24	1935	1975
50X-3, 76	465.16	2006	2069	24	2015	2079
50X-4, 115	467.05	2008	2064	24	2018	2074
50X-5, 133	468.73	1929	1996	24	1939	2007
50X-4, 30	466.20	2006	2141	24	2016	2151
50X-5, 55	467.95	1946	2018	24	1956	2028
50X-6, 118	470.08	1909	1981	24	1919	1991
50X-6, 26	469.16	1866	1997	24	1876	2008
51X-1, 6	471.06	1892	1953	24	1902	1963
51X-1, 121	472.21	1898	1977	24	1908	1988
51X-2, 57	473.07	1929	2038	24	1939	2050
51X-2, 117	473.67	1938	1991	24	1948	2002
51X-3, 7	474.07	1938	2025	24	1949	2037
51X-3, 85	474.85	1778	1830	24	1787	1839
51X-4, 47	475.97	1996	2055	24	2009	2068
51X-4, 134	476.84	1895	1960	24	1906	1972
51X-5, 58	477.58	1938	1980	24	1949	1992
51X-5, 141	478.41	1853	1921	24	1863	1932
51X-6, 44	478.94	1938	2034	24	1950	2047
51X-7, 29	480.29	1882	1898	24	1894	1910
52X-1, 7	480.57	1972	2069	24	1986	2083
52X-1, 123	481.73	1861	1933	24	1872	1945
52X-2, 2	482.02	1762	1877	24	1773	1889
52X-2, 70	482.70	2003	2089	24	2017	2104
52X-3, 78	484.28	1982	2059	24	1997	2075
52X-3, 10	483.60	1939	2025	24	1954	2040
52X-3, 136	484.86	1920	2015	24	1935	2031
52X-4, 10	485.10	1904		24	1919	
52X-4, 117	486.17	2009	2077	24	2024	2094
52X-5, 23	486.73	1964	1878	24	1979	1892
52X-5, 125	487.75	1979	2125	24	1994	2143
52X-6, 53	488.53	2064	1957	24	2080	1972
52X-6, 146	489.46	1909	2006	24	1924	2022
53X-1, 16	490.36	1911	2007	24	1926	2023
53X-1, 143	491.63	1921	2084	24	1937	2102
53X-2, 47	492.17	2064	2131	24	2082	2151
53X-2, 111	492.81	2007	2060	24	2024	2078
53X-3, 40	493.60	1857	2014	24	1872	2031
53X-3, 98	494.18	1982	2053	24	1999	2071
53X-4, 40	495.10	2075	2101	24	2094	2120
53X-4, 141	496.11	2059	2138	24	2077	2158
53X-5, 8	496.28	1908	1944	24	1923	1961
53X-5, 147	497.67	1998	1999	24	2016	2017
53X-6, 108	498.78	2059	2152	24	2078	2172
54X-1, 12	500.02	1960	2009	24	1977	2027
54X-1, 146	501.36	1899	2005	24	1919	2027
54X-2, 40	501.80	1951	2076	24	1969	2096
54X-2, 72	502.12	1913	1954	24	1931	1974
54X-2, 146	502.86	1892	1948	24	1907	1964
54X-3, 145	504.35	1960	2036	24	1980	2058
54X-4, 12	504.52	1950	2041	24	1969	2063
54X-4, 131	505.71	2021	2086	24	2042	2109
54X-5, 39	506.29	1913	1988	24	1932	2009
54X-5, 138	507.28	1904	1982	24	1923	2003
54X-6, 43	507.83	1934	2024	24	1952	2044
54X-6, 146	508.86	2070	2178	24	2094	2204

Table 11 (continued).

Core, section, interval (cm)	Depth (mbsf)	Longitudinal acoustic velocity (m/s)	Transverse acoustic velocity (m/s)	Temperature (°C)	Corrected longitudinal velocity (m/s)	Corrected transverse velocity (ms)
55X-1, 13	509.63	2098	2178	24	2122	2203
55X-1, 140	510.90	2009	2066	24	2032	2089
55X-2, 56	511.56	2090	2164	24	2114	2189
55X-2, 148	512.48	2031	2117	24	2053	2141
55X-3, 55	513.05	2065	2173	24	2089	2200
55X-3, 146	513.96	2023	2106	24	2047	2132
55X-4, 48	514.48	2059	2135	24	2083	2161
55X-4, 106	515.06	2130	2204	24	2155	2231
55X-5, 12	515.62	2039	2064	24	2062	2088
55X-5, 99	516.49	1989	2057	24	2011	2081
55X-6, 14	517.14	1960		24	1982	
55X-6, 132	518.32	2026	2123	24	2049	2148
56X-1, 26	519.46	2065	2143	24	2090	2170
56X-1, 146	520.66	2104	2203	24	2130	2232
56X-2, 19	520.89	2025	2095	24	2048	2120
56X-2, 106	521.76	2022	2130	24	2045	2156
56X-3, 12	522.32	2045	2150	24	2070	2176
56X-3, 116	523.36	2092	2158	24	2117	2185
56X-4, 39	524.09	2036	2125	24	2062	2153
56X-4, 138	525.08	2134	2141	24	2162	2170
56X-5, 71	525.91	1985	2095	24	2010	2122
56X-5, 146	526.66	2125	2196	24	2154	2227
56X-6, 56	527.26	2155	2152	24	2185	2182
56X-6, 144	528.14	2167	2230	24	2197	2262
57X-1, 8	528.98	1879	2001	24	1902	2026
57X-1, 8	528.98		2010	24		2035
57X-1, 85	529.75	2146	2155	24	2178	2186
57X-2, 7	530.47	2177	2260	24	2208	2294
57X-2, 99	531.39	2204	2254	24	2235	2286
57X-3, 17	532.07	2196	2242	24	2228	2275
57X-3, 85	532.75	1995	2084	24	2022	2113
57X-4, 18	533.58	2171	2174	24	2203	2206
57X-4, 79	534.19	2032	2063	24	2060	2093
57X-5, 24	535.14	2266	2294	24	2301	2330
57X-5, 113	536.03	2169	2200	24	2201	2233
57X-6, 29	536.69	2074	2167	24	2103	2199
57X-6, 95	537.35	2138	2214	24	2170	2248
58X-1, 16	538.66	2004	2065	24	2030	2093
58X-1, 59	539.09	2115	2207	24	2144	2239
58X-2, 5	540.05	2285	2185	24	2321	2218
58X-2, 129	541.29	2258	2320	24	2294	2358
58X-3, 34	541.84	1961	2020	24	1999	2058
58X-3, 118	542.68	2242	2274	24	2277	2310
58X-4, 37	543.37	2145	2214	24	2180	2249
58X-4, 83	543.83	2092	2167	24	2122	2199
58X-4, 144	544.44	2286	2293	24	2322	2330
58X-5, 59	545.09	2017	2110	24	2043	2139
58X-6, 85	546.85	2308	2333	24	2349	2374
58X-6, 114	547.14	2340	2366	24	2384	2411
59X-1, 77	548.97	1973	2102	24	2002	2135
59X-1, 106	549.26	2298	2332	24	2339	2373
59X-2, 4	549.74	2098	2189	24	2132	2226
59X-2, 136	551.06	2204	2207	24	2242	2245
59X-3, 7	551.27	2227	2218	24	2268	2258
59X-3, 90	552.10	1978	2098	24	2019	2139
59X-4, 27	552.97	2174	2274	24	2209	2313
59X-4, 58	553.28	2076	2190	24	2110	2227
59X-5, 8	554.28	2207	2281	24	2244	2318
59X-5, 144	555.64	2136	2247	24	2173	2288
59X-6, 93	556.63	2261	2262	24	2311	2311
59X-6, 134	557.04	1938	2089	24	1968	2125
59X-7, 13	557.33	2112	2210	24	2148	2250
60X-1, 47	558.37	2127	2180	24	2166	2221
60X-1, 85	558.75	2016	2107	24	2049	2143
60X-2, 22	559.62	2070	2116	24	2112	2160
60X-2, 88	560.28	2090	2200	24	2125	2238
60X-3, 53	561.43	2059	2160	24	2094	2198
60X-3, 125	562.15	2179	2178	24	2222	2221
60X-4, 92	563.32	2159	2234	24	2198	2276
60X-5, 49	564.39	2175	2185	24	2214	2224
60X-5, 95	564.85	2073	2150	24	2108	2187
60X-6, 22	565.62	2138	2191	24	2175	2230
61X-1, 15	567.75	2014	2151	24	2050	2192
61X-1, 97	568.57	2104	2193	24	2142	2235
61X-2, 66	569.76	2343	2315	24	2393	2364
61X-2, 120	570.30	2157	2227	24	2197	2270
61X-3, 141	572.01	2157	2188	24	2199	2231
61X-4, 20	572.30	1881	2020	24	1914	2058
61X-4, 143	573.53	2346	2362	24	2398	2414
61X-5, 27	573.87	2083	2192	24	2121	2234
61X-5, 106	574.66	2289	2352	24	2339	2404
62X-1, 27	577.47	2291	2310	24	2345	2364
62X-1, 108	578.28	2283	2222	24	2338	2273
62X-2, 13	578.83	1973	2108	24	2012	2153
62X-2, 86	579.56	2279	2309	24	2332	2363
62X-3, 22	580.42	2259	2199	24	2316	2253
62X-3, 76	580.96	1921	2046	24	1956	2085

Table 11 (continued).

Core, section, interval (cm)	Depth (mbsf)	Longitudinal acoustic velocity (m/s)	Transverse acoustic velocity (m/s)	Temperature (°C)	Corrected longitudinal velocity (m/s)	Corrected transverse velocity (ms)
62X-4, 7	581.77	2153	2188	24	2199	2236
63X-1, 63	587.53	2283	2319	24	2339	2377
63X-1, 117	588.07	2239	2238	24	2293	2292
63X-2, 49	588.89	2261	2298	24	2314	2353
63X-2, 107	589.47	2088	2222	24	2132	2272
63X-3, 30	590.20	2238	2214	24	2294	2270
63X-3, 82	590.72	2190	2271	24	2237	2322
63X-4, 33	591.73	2025	2144	24	2064	2188
63X-4, 134	592.74	2298	2360	24	2352	2417
63X-5, 23	593.13	2007	2155	24	2049	2204
63X-5, 93	593.83	2135	2188	24	2179	2234
63X-6, 22	594.62	2162	2125	24	2213	2174
63X-6, 108	595.48	2199	2226	24	2248	2276
64X-1, 38	596.88	2269	2307	24	2321	2361
64X-1, 141	597.91	2247	2278	24	2300	2333
64X-2, 13	598.13	2222	2248	24	2271	2298
64X-2, 145	599.45	2262	2248	24	2318	2303
64X-3, 47	599.97	2063	2116	24	2107	2162
64X-3, 113	600.63	2193	2128	24	2242	2174
64X-4, 143	602.43	2258	2290	24	2318	2352
64X-5, 57	603.07	1783	1825	24	1819	1863
64X-5, 142	603.92	2082	1907	24	2127	1945
64X-6, 14	604.14	2106	1976	24	2154	2018
64X-6, 144	605.44	2117	2150	24	2170	2205
154-926C						
4H-2, 115	31.65	1583	1583	22	1511	1511
4H-4, 48	33.98	1610	1605	22	1536	1531
4H-6, 29	36.79	1593	1576	22	1514	1497
9H-2, 100	79.00	1625	1608	22	1550	1533
9H-4, 99	81.99	1662	1605	22	1587	1530
9H-6, 100	85.00	1674	1631	22	1599	1556
18H-3, 48	165.48		1702	22		1647
18H-4, 125	167.75		1668	22		1613
18H-5, 72	168.72		1706	22		1651
19H-2, 32	173.32		1719	22		1664
19H-4, 118	177.18		1681	22		1628
19H-6, 85	179.85		1714	22		1661
20H-2, 14	182.64		1710	22		1657
20H-4, 58	186.08		1713	22		1661
20H-6, 119	189.69		1701	22		1649

temperature measurements, was used to calculate heat flow for the Ceara Rise. Thermal conductivity was measured using the needle-probe method in the full-space mode and corrected to true values of conductivity (see "Physical Properties" section, "Explanatory Notes" chapter, this volume). In situ temperature was measured using the ADARA temperature shoe on four of the APC cores in Hole 926C (154-926C-6H, -9H, -12H, and -17H).

The thermal conductivity at Site 926 increases with depth (Fig. 28 and Table 14), as expected for a sediment column of generally decreasing porosity. A linear least-squares approximation to the decrease in conductivity with depth results in $k = 1.1 + 0.0007z$, where k is thermal conductivity (W/[m·K]) and z is depth in mbsf. The results from the four in situ temperature measurements are excellent, showing good temperature decay curves at each depth measurement (Fig. 29). The predicted in situ temperature from each of these measurements results in a linear temperature gradient of 0.047°C/m (Fig. 30). Combining thermal conductivity with the temperature gradient results in a heat flow of 81 mW/m^2. Estimated heat flow for the crustal age of the Ceara Rise (80 Ma) is 50 to 60 mW/m^2 (from Parsons and Sclater, 1977). This suggests that crustal temperature has been elevated in this region or that the age of the crust in this region is considerably younger.

Summary

The physical properties of the sediments drilled at Site 926 show downhole changes that are similar to Site 925 and reflect the effects of gravitational compaction and diagenesis.

Major changes in the gradients or offsets in the index properties and velocities occur at 30, 180, 300, and 400 mbsf. This is equivalent to possible reflection events at 0.02, 0.165, 0.32, and 0.52 s TWT below the seafloor, as shown in the acoustic impedance profile calculated from discrete-velocity and bulk-density measurements (Fig. 31).

Shear strength data indicate underconsolidation of the sediment column in the upper 240 mbsf. Electrical resistivity remains constant in this interval. Below 240 mbsf, we observe a normal consolidated sediment with increasing resistivity.

Heat flow calculated from in situ temperature and thermal conductivity measurements at Site 926 is 81 mW/m^2, which is 11–21 mW/m^2 higher than the expected heat flow for the assumed age (80 Ma) of the Ceara Rise.

DOWNHOLE MEASUREMENTS

Logging Operations and Log Quality

The Quad, GHMT, and geochemical tool strings were successfully deployed at Hole 926B. The Quad tool string was run without the compensated neutron porosity sonde (CNT-G) because of the generally poor performance of this tool in these high-porosity sediments. Sea-state conditions were mild (about 0.3 m heave), and the wireline heave compensator (WHC) was employed. Main (583.5–55.5 mbsf) and repeat (490.5–120.5 mbsf) Quad logs were run at 900 ft/hr and both standard mode (15 cm sampling) and high-resolution (2.5 cm sampling) data were recorded. The GHMT magnetometer and susceptibility tool string were deployed next and run at 1800 ft/hr from 444.5 to 80.5 mbsf; the total field component of this tool failed downhole, and only the magnetic susceptibility data were recorded. Borehole blockage prevented this and future tool strings from reaching total depth (605 mbsf). The geochemical tool string was run next at 500 ft/hr from 459.5 to 65.5 mbsf. A summary of logging operations is presented in Table 15. Both the Quad and geochemical tool strings encountered difficulties reentering pipe because of problems associated with the

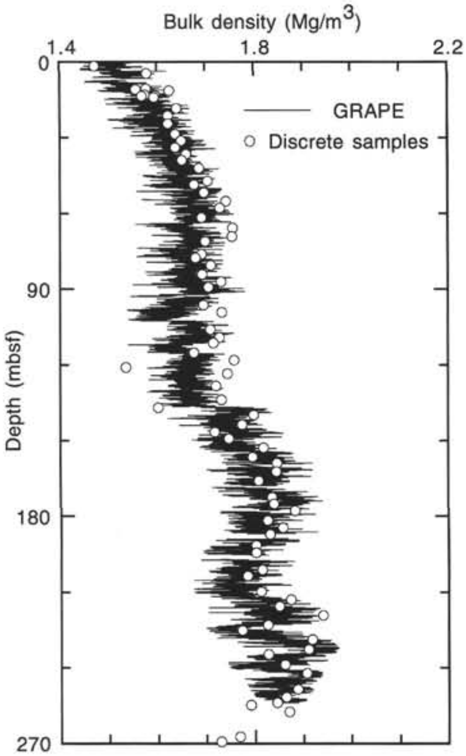

Figure 23. Comparison of bulk densities obtained from GRAPE and index properties methods for the upper 260 mbsf of Hole 926B.

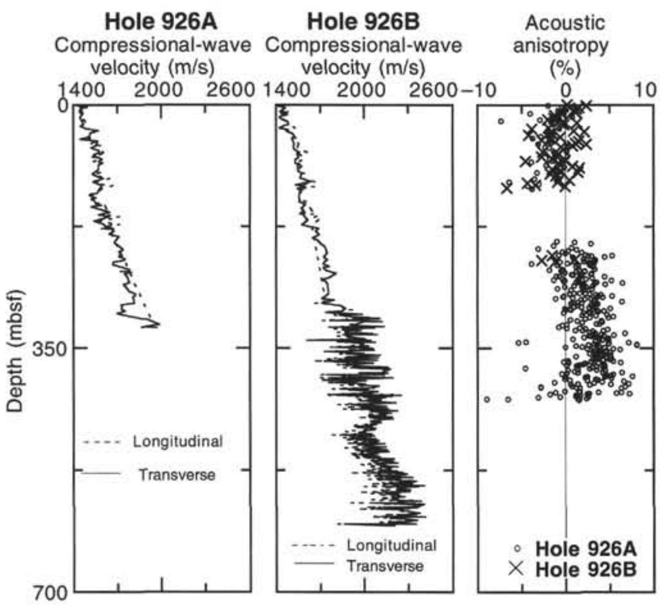

Figure 24. Transverse and longitudinal P-wave velocity and acoustic anisotropy vs. depth, Holes 926A and 926B.

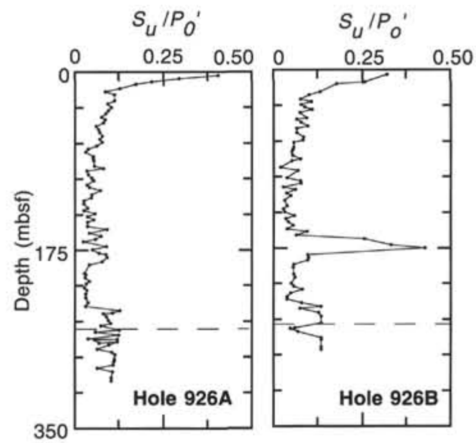

Figure 25. S_u/P_o' ratios calculated from undrained shear strength and bulk density for cores from Holes 926A and 926B.

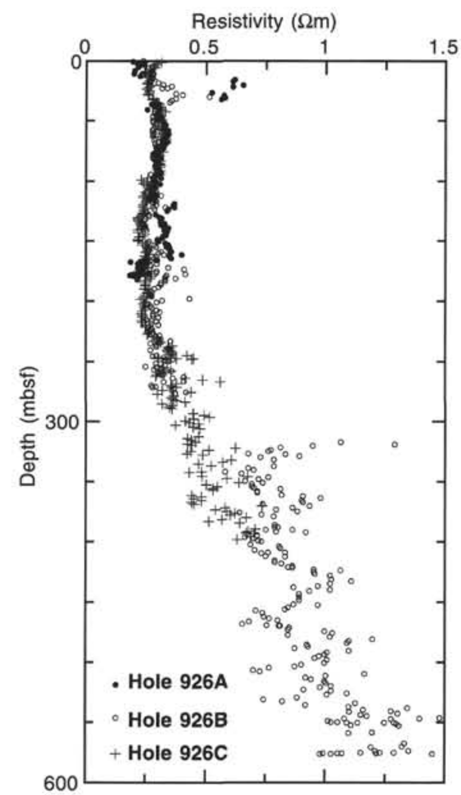

Figure 26. Electrical resistivity vs. depth for Holes 926A, 926B, and 926C.

lockable flapper mechanism at the base of pipe; these operational delays prevented deployment of the FMS tool string.

Data from all three tool strings appear to be of generally excellent quality. Exceptions to this are the density and velocity data from the Quad tool string, which were adversely affected by intermittent borehole washout intervals throughout the logged sequence. Borehole dimensions above 170 mbsf exceed the maximum caliper measurement, so the density and photoelectric effect data above this level must be interpreted with caution. The washout intervals adversely affected velocity data as well, but these data can be restored after analysis of the full sonic waveform data. The borehole diameter appears to be roughly correlated to relative changes in clay content: borehole washouts are most common in higher clay-content intervals (Fig. 32).

Selected Quad logs for Hole 926B are shown in Figure 32. A comparison of the density, photoelectric effect, and velocity logs with the caliper log illustrates the effects of borehole diameter variability (washout) on these log measurements: As observed at Site 925 as well (see "Downhole Measurements" section, "Site 925" chapter, this volume), these measurements shift to lower and more variable values where borehole washouts occur. However, the resistivity, gamma-ray, susceptibility, and geochemical logs are relatively unaffected by borehole washout.

Table 12. Undrained shear strength from miniature vane shear measurements and unconfined compression test results from the pocket penetrometer for all holes at Site 926.

Core, section, interval (cm)	Depth (mbsf)	Overburden stress (kPa)	Undrained shear strength (kPa)	Residual shear strength (kPa)	Pocket penetrometer (kg/cm^2)	S_u/P_o'
154-926A-						
1H-1, 100	1	4.465	6.0	4.1		1.344
1H-3, 60	3.6	17.494	7.1	2.8		0.406
2H-2, 100	6.5	32.070	9.5	2.8		0.296
2H-4, 95	9.45	47.246	10.2	6.1		0.216
2H-6, 94	12.44	59.372	10.2	5.4		0.172
3H-2, 100	16	83.905	10.7	6.0		0.128
3H-4, 100	19	101.157	8.7	4.6		0.086
3H-6, 95	21.95	118.515	13.2	7.4		0.111
4H-4, 100	28.5	157.203	17.5	8.8		0.111
4H-6, 100	31.5	175.850	16.4	8.0		0.093
5H-2, 100	35	197.386	20.6	11.2		0.104
5H-4, 100	38	215.989	20.5	9.6		0.095
5H-6, 100	41	234.976	20.6	8.5		0.088
6H-2, 100	44.5	256.845	19.7	8.5		0.077
6H-4, 32	46.82	271.870	23.5	12.5		0.086
6H-6, 70	50.2	293.926	23.9	11.2		0.081
7H-2, 52	53.52	316.109	19.1	9.5		0.060
7H-4, 35	56.35	334.223	22.8	12.0		0.068
7H-6, 24	59.24	352.336	25.0	15.4		0.071
8H-2, 28	62.78	376.089	29.3	13.7		0.078
8H-4, 61	66.11	398.704	28.4	12.0		0.071
8H-6, 82	69.32	420.704	32.9			0.078
9H-2, 46	72.46	441.501	27.6	15.1		0.063
9H-4, 34	75.34	460.345	17.8	8.3		0.039
9H-6, 84	78.84	484.201	15.6	10.5		0.032
10H-2, 102	82.52	509.385	26.9	14.0		0.053
10H-4, 40	84.9	524.478	27.6	13.5		0.053
10H-5, 119	87.19	539.012	28.8	13.5		0.053
11H-2, 136	92.36	573.866	32.1	17.0		0.056
11H-4, 74	94.74	589.185	48.4			0.082
11H-6, 48	97.48	609.015	21.3	10.0		0.035
12H-2, 41	100.91	628.168	23.5	9.8		0.037
12H-4, 120	104.7	653.545	31.3			0.048
12H-6, 57	107.07	669.455	35.9	15.1		0.054
13H-2, 120	111.2	696.297	23.8	11.3		0.034
13H-4, 45	113.45	711.606	29.6	14.0		0.042
13H-6, 53	116.53	732.142	53.9			0.074
14H-2, 108	120.58	760.043	36.2	11.5		0.048
14H-4, 90	123.4	780.417	36.5	9.0		0.047
14H-7, 61	126.59	802.357	21.6	4.7		0.027
15H-2, 90	129.9	824.349	21.6	4.7		0.026
15H-5, 20	133.7	850.541	31.0	8.8		0.036
15H-7, 28	136.28	868.508	23.3			0.027
16H-2, 85	139.35	890.760	50.2			0.056
16H-4, 93	142.43	912.997	33.1			0.036
16H-6, 85	145.35	934.127	50.2			0.054
17H-1, 83	147.33	949.028	34.3			0.036
17H-4, 65	151.65	980.700	36.5			0.037
17H-6, 73	154.73	1029.700	93.6			0.091
18H-2, 100	158.5	1035.845	43.9			0.042
18H-4, 81	161.31	1058.597	79.7			0.075
18H-6, 97	164.47	1084.291	63.6			0.059
19H-1, 133	166.83	1101.924	26.3			0.024
19H-5, 36	171.86	1141.133	102.1			0.089
19H-7, 4	174.54	1163.728	59.7			0.051
20H-2, 133	177.83	1189.859	82.5			0.069
20H-3, 144	179.44	1203.182	106.8			0.089
20H-5, 133	182.33	1229.356	112.6			0.092
21H-2, 40	186.4	1261.327	97.2			0.077
21H-4, 65	189.65	1287.728	53.5			0.042
22H-3, 123	198.23	1348.198	37.5			0.028
22H-4, 66	199.16	1355.376	42.2			0.031
22H-6, 61	202.11	1377.648	41.7			0.030
23H-2, 58	205.58	1404.215	58.6			0.042
23H-4, 44	208.44	1426.938	48.3			0.034
23H-6, 142	212.42	1459.095	42.2			0.029
24H-2, 24	214.74	1476.434	52.5			0.036
24H-4, 97	218.47	1521.889	47.8			0.031
24H-6, 126	221.76	1560.843	49.9			0.032
25H-3, 96	226.46	1597.324	63.3			0.040
25H-6, 10	230.1	1632.915	51.9			0.032
26H-2, 111	234.61	1616.177			2.1	0.127
26H-4, 45	236.95	1611.783			1.7	0.106
26H-4, 102	237.52	1616.311			1.3	0.082
26H-6, 111	240.61	1639.907			1.5	0.090
27H-2, 90	243.9	1666.474			1.6	0.096
27H-4, 109	247.09	1693.944			1.7	0.101
27H-6, 31	249.31	1712.979			1.3	0.074
28H-2 , 114	253.64	1751.295			2.2	0.126
28H-4, 17	255.67	1767.525			1.0	0.058
28H-6, 30	258.8	1791.889			2.2	0.123
29H-2, 46	262.46	1820.111			0.7	0.038
29H-2, 85	262.85	1822.857			2.2	0.121
29H-2, 111	263.11	1824.651			1.0	0.056

Table 12 (continued).

Core, section, interval (cm)	Depth (mbsf)	Overburden stress (kPa)	Undrained shear strength (kPa)	Residual shear strength (kPa)	Pocket penetrometer (kg/cm²)	S_u/P_o'
29H-4, 129	266.29	1845.913			1.3	0.069
29H-4, 47	265.47	1840.352			2.2	0.120
29H-6, 30	268.3	1860.976			1.8	0.097
30H-2, 125	272.75	1895.767			1.2	0.065
30H-4, 51	275.01	1912.963			2.1	0.105
30H-6, 27	277.77	1936.941			2.2	0.114
31H-2, 115	282.15	1972.207			2.2	0.112
31H-3, 85	283.35	1981.083			2.2	0.111
31H-4, 85	284.85	1988.781			2.2	0.111
31H-6, 124	288.24	2020.458			2.2	0.109
32H-2, 60	291.1	2043.259			1.3	0.065
32H-4, 100	294.5	2071.068			2.2	0.107
33H-2, 40	300.4	2114.664			2.2	0.104
33H-4, 45	303.45	2136.837			2.2	0.103
154-926B-						
1H-2, 19	1.69	7.171	5.0	3.2		0.697
1H-4, 38	4.88	22.998	7.4	5.0		0.322
2H-4, 40	11.9	59.345	15.3	10.2		0.258
2H-5, 83	13.83	70.184	12.4	6.6		0.177
3H-4, 40	21.4	116.198	15.3	10.2		0.132
3H-6, 49	24.49	134.331	13.5	6.6		0.100
4H-2, 117	28.67	159.116	12.1	6.3		0.076
4H-4, 69	31.19	174.503	18.6	10.6		0.107
4H-6, 58	34.08	192.046	15.0	8.2		0.078
5H-1, 127	36.77	208.575	18.3	8.3		0.088
5H-3, 57	39.07	222.829	24.3	14.6		0.109
5H-5, 43	41.93	240.799	18.0	10.0		0.075
6H-2, 77	47.27	276.742	26.0	14.0		0.094
6H-3, 78	48.78	286.894	18.9	8.5		0.066
6H-5, 90	51.9	306.714	23.9	11.2		0.078
7H-1, 85	55.35	330.427	32.0	19.8		0.097
7H-3, 46	57.96	348.717	22.8	15.1		0.065
7H-5, 125	61.75	375.314	25.0	15.8		0.067
8H-2, 37	65.87	402.204	33.9	15.6		0.084
8H-4, 80	69.3	427.171	35.3			0.083
8H-5, 129	71.29	440.790	25.4	11.3		0.058
9H-2, 133	76.33	473.678	27.4	13.5		0.058
9H-3, 130	77.8	483.182	26.6	12.8		0.055
9H-5, 118	80.68	502.118	26.5	12.5		0.053
10H-1, 132	84.32	526.263	28.0	13.0		0.053
10H-3, 123	87.23	545.985	41.6			0.076
10H-5, 29	89.29	560.048	29.0	16.0		0.052
11H-3, 71	96.21	604.749	12.0			0.020
11H-5, 79	99.29	625.638	43.5			0.070
12H-3, 88	105.88	670.838	25.5			0.038
12H-5, 100	109	692.080	52.9			0.076
12H-7, 57	111.57	709.762	54.8			0.077
13H-3, 68	115.18	709.762	20.0			0.028
13H-5, 36	117.86	751.446	46.8			0.062
13H-7, 46	120.96	769.993	28.2			0.037
14H-2, 91	123.41	784.462	38.4			0.049
14H-5, 107	128.07	818.786	26.1			0.032
15H-3, 30	133.8	858.652	32.3			0.038
15H-5, 36	136.86	877.900	25.0			0.028
15H-7, 15	139.65	896.232	28.8			0.032
16H-3, 60	143.6	926.369	54.7			0.059
16H-5, 46	146.46	946.547	33.7			0.036
16H-7, 31	149.31	966.373	40.3			0.042
17H-3, 51	153.01	994.186	55.6			0.056
17H-5, 97	156.47	1020.648	40.0			0.039
17H-7, 22	158.72	1038.160	99.0			0.095
18H-3, 51	162.51	1069.026	68.4			0.064
18H-5, 111	166.11	1097.258	282.0		2.1	0.257
19H-3, 95	172.45	1146.730	381.0		2.9	0.332
19H-5, 50	175	1167.015	500.0		2.75	0.428
19H-7, 20	177.7	1189.236			3.25	
20H-3, 80	181.8	1222.668			2.4	0.096
20H-5, 75	184.75	1246.313			2.5	0.098
20H-7, 10	187.1	1265.260			2.5	0.097
21H-3, 85	191.35	1298.108			1.5	0.057
21H-5, 96	194.46	1321.821			1.5	0.056
22H-3, 122	201.22	1374.281			1.6	0.057
22H-5, 75	203.75	1393.523			1.75	0.062
23H-3, 45	209.95	1439.511			1.5	0.051
23H-5, 50	213	1464.229			1.7	0.057
23H-7, 56	216.06	1489.275			2.5	0.082
24H-3, 41	219.41	1518.055			1.5	0.048
24H-5, 124	223.24	1550.850			1.25	0.040
24H-7, 55	225.55	1568.195			1.25	0.039
25H-3, 60	229.1	1596.540			2.6	0.080
25H-5, 125	232.75	1629.195			>4.5	0.135
25H-7, 28	234.78	1645.977			2.5	0.074
26H-3, 90	238.9	1678.468			4.4	0.129
26H-5, 143	242.43	1708.379			>4.5	0.135
27H-3, 140	248.9	1764.544			>4.5	0.135
27H-7, 50	254	1806.832			2.25	0.061

Table 12 (continued).

Core, section, interval (cm)	Depth (mbsf)	Overburden stress (kPa)	Undrained shear strength (kPa)	Residual shear strength (kPa)	Pocket penetrometer (kg/cm²)	S_u/P_o'
28X-1, 20	254.2	1808.411			1.7	0.046
28X-3, 60	257.6	1839.543			2.6	0.069
29X-3, 120	263.2	1789.723			>4.5	0.135
29X-5, 30	265.3	1766.571			>4.5	0.135
30X-3, 50	272.1	1787.390			>4.5	0.135
30X-5, 30	274.9	1812.315			>4.5	0.135

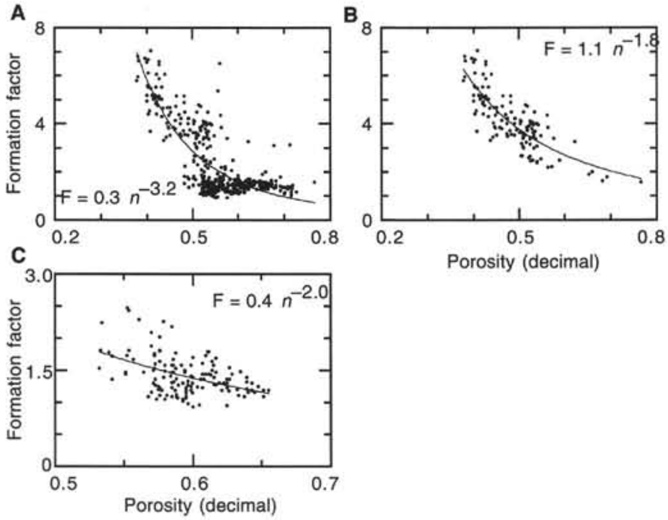

Figure 27. Formation factor vs. porosity for Site 926. **A.** Archie form of relationship for all data from Site 926. **B.** Archie form of relationship for all data from 0 to 150 mbsf and from 240 mbsf to the bottom. **C.** Archie form of relationship for data from 150 to 240 mbsf.

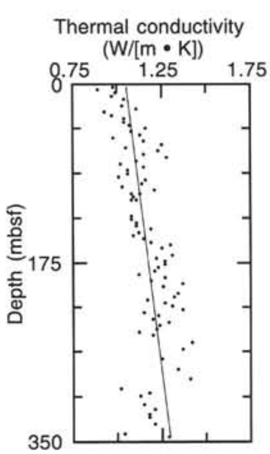

Figure 28. Thermal conductivity vs. depth measured in full-space mode on whole cores from Hole 926C. Linear least-squares approximation is shown as a solid line.

Core-log Data Comparisons

The core and log gamma-ray and magnetic susceptibility data at Hole 926B are shown in Figure 33. The gamma-ray and susceptibility data sets exhibit strong correlations extending to meter-scale variability in high sedimentation-rate cores having expanded bedding cycles.

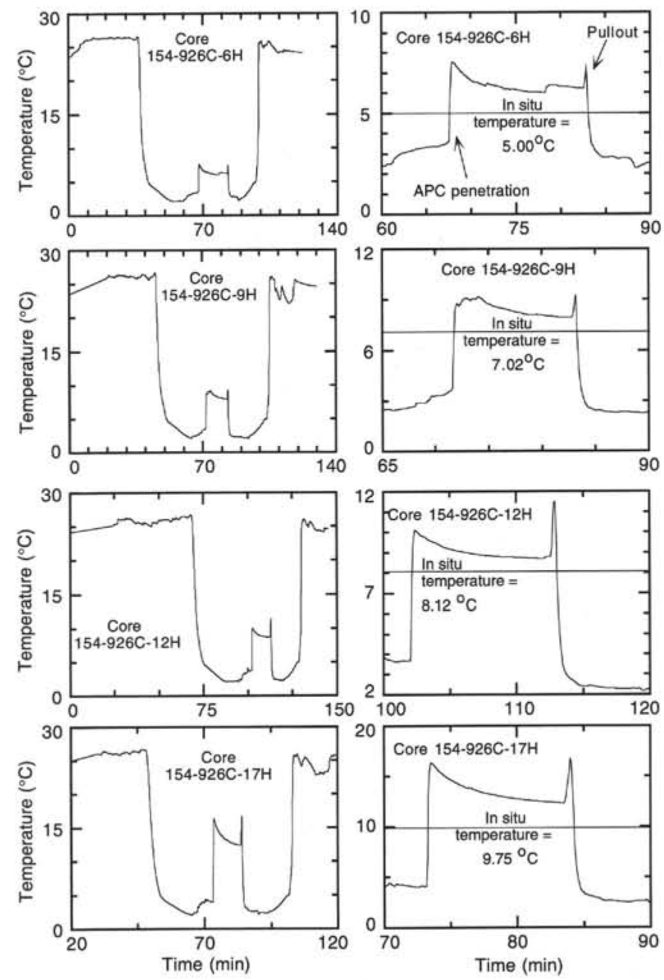

Figure 29. In situ temperature data from four deployments of the ADARA temperature shoe on Cores 154-926C-6H, -9H, -12H, and -17H.

The log density data at Hole 926B were adversely affected by borehole washout intervals between 380 and 360 mbsf, between 260 and 200 mbsf, and above 170 mbsf (see caliper column in Fig. 32).

Closer inspection of the natural gamma data indicates a marked change in the relative gamma-ray emissions from K and Th centered near 180 mbsf (Fig. 34). The log Th/K ratio was computed and there is a pronounced decrease in this ratio above 180 mbsf, corresponding to the lithologic Subunit IIA/IIB boundary near 7.5 Ma (see "Lithostratigraphy" and "Biostratigraphy" sections, this chapter). This change reflects a relative increase in K concentration above 180 mbsf. A similar decrease in the Th/K ratio occurs near 200 mbsf at Hole 925C (Fig. 34), again corresponding to the lithologic Subunit IIA/IIB boundary near 7.5 Ma (see "Lithostratigraphy" and "Biostratigraphy" sections, "Site 925" chapter, this volume).

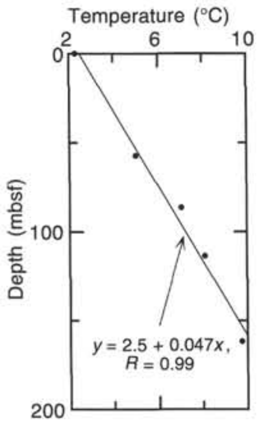

Figure 30. In situ temperature data, Hole 926C.

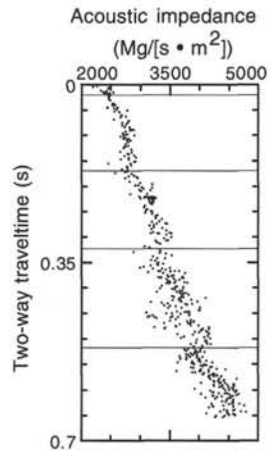

Figure 31. Acoustic impedance vs. two-way traveltime, Site 926.

Relative K and Th concentrations can be used to discriminate between different clay mineral assemblages (Fertl, 1979). Because illite and kaolinite are the dominant clay mineral phases in these sediments (see "Lithostratigraphy" section, "Site 925" chapter, this volume), the lower Th/K ratios above 180 mbsf in Hole 926B would suggest an increase in the abundance of illite (5%–6% K by weight; Fertl, 1979) relative to kaolinite (<<1% K by weight; Fertl, 1979).

This log-detected compositional shift can be compared to the core-based natural gamma measurements conducted on the MST. We took 10-s natural gamma measurements at 10-cm spacing on the Hole 926B cores (see "Physical Properties" section, this chapter). The Th and K data and computed Th/K ratio data for both core and log measurements are compared in Figure 35. Core K and Th were estimated using the window 3 and window 5 count rates from the MST data, respectively; the additional lower energy K and Th contributions were not computed. These data demonstrate that the core-based K and Th (and resulting Th/K ratio) data compared very favorably with the log measurements throughout the hole. Detailed core-log correlations (1–2 m) are possible in some intervals.

Data from the geochemical tool can also be used to assess downhole compositional changes. In particular, the Ca-yield log from this tool maintains a high correlation with the core-based $CaCO_3$ analyses (Fig. 36). The gradual Ca-yield increase downhole reflects increases in sediment density with burial and lithification. As the geochemical data will undergo extensive post-cruise processing, the data presented here must be considered only preliminary.

Orbital scale bedding cycles within the early Miocene and late Oligocene intervals could be resolved in several of the Site 926 logs. Sedimentation rates are relatively high for the early Miocene (near 2.2–2.8 cm/k.y. between 21 and 24 Ma; see "Sedimentation Rates" section, this chapter), expanding bedding cycles to between 1.0 and 1.3 m in length. Core reflectivity, magnetic susceptibility, and natural gamma are shown adjacent to the log natural gamma, susceptibility, resistivity, and Ca-yield data for the 400–460 mbsf interval at Hole 926B in Figure 37. This plot illustrates a strong correspondence between core and log measurements over this relatively high sedimentation rate interval; cycle periodicities are consistent with an as-yet unspecified climatic response at the tilt (41 k.y.) orbital band.

Comparison of Core and Log Physical Properties Measurements

Logging and laboratory compressional-wave velocities, bulk densities, and electrical resistivities obtained at Hole 926B are plotted vs. depth for comparison in Figure 38. The logging depths were adjusted to mbsf based on the correlation of the natural gamma profile measured downhole with the profile obtained on whole cores using the MST. Logging data have been edited before plotting. Clearly erroneous low compressional-wave velocities and bulk densities observed in intervals of poor borehole conditions have been removed, and the final compressional-wave velocity profile has been obtained by splicing together the two long-spacing acoustic velocity profiles. Laboratory compressional velocities and electrical resistivities were corrected to in situ temperatures calculated using the 0.05°C/m gradient measured at this site (see "Physical Properties" section, this chapter), but neither the bulk densities nor the *P*-wave velocities were corrected for porosity rebound.

Most of the steps and changes in gradients in the log profiles are echoed in the laboratory profiles, thus lending some support to both data sets. The two bulk-density profiles overlap almost perfectly over the entire interval studied. Only below about 300 mbsf do the profiles diverge slightly, the lab density being at most 0.05 g/cm^3 lower than the log values at the bottom of the studied interval (ca. 580 mbsf). This small divergence between the log and laboratory bulk-density profiles indicates a weak porosity rebound that does not exceed 2.5% (whereas, at about 550 mbsf, a porosity rebound of about 6% is expected in carbonate-rich pelagic sediments and a porosity rebound greater than 10% is expected in clay-rich pelagic sediments [Hamilton, 1976]).

Laboratory compressional velocities are lower than the log velocities, but the relative maxima and minima of the log velocity profile compare well with those in the laboratory profile. There are, however, two intervals over which log and laboratory data diverge: the interval from 225 to 260 mbsf, in which the log profile shows low velocities that probably result from poor borehole conditions at that depth; and the transition between lithologic Subunits IIIB and IIIC at about 460 mbsf, which shows up as a drop in the laboratory *P*-wave velocity profile that is not clearly echoed in the log profile. The lower velocities measured at laboratory conditions probably result from a decrease in sediment elastic rigidity during removal of overburden pressure (this hypothesis will be tested onshore through acoustic velocity measurements performed under various pressure conditions in consolidation cells).

Although the laboratory electrical resistivities are lower than the log resistivities, the trends and steps of the laboratory profile are clearly echoed in the log profile. At the present time, there is no clear explanation for the difference in the absolute resistivity values obtained during downhole measurements and in the laboratory.

Log Interpretation and Lithology

The natural gamma, density, sonic velocity, and resistivity logs provide confirmation of the major lithologic unit boundaries derived from the core descriptions (Fig. 32). The boundary separating lithologic Unit I, described as nannofossil clay alternating with clayey nannofossil ooze (see "Lithostratigraphy" section, this chapter), from

Table 13. Electrical resistivity measured at discrete intervals for all holes at Site 926.

Core, section, interval (cm)	Depth (mbsf)	Resistivity (Ωm)
154-926A-		
1H-1, 50	0.5	0.19
1H-2, 50	2	0.23
1H-3, 50	3.5	0.21
2H-1, 100	5	0.21
2H-3, 100	8	0.2
2H-4, 100	9.5	0.27
2H-5, 100	11	0.2
2H-6, 100	12.5	0.22
3H-2, 82	15.82	0.62
3H-3, 82	17.32	0.61
3H-5, 82	20.32	0.66
3H-6, 82	21.82	0.61
4H-5, 30	29.3	0.58
4H-6, 30	30.8	0.58
4H-3, 30	26.3	0.52
4H-7, 30	32.3	0.57
5H-2, 80	34.8	0.29
5H-3, 80	36.3	0.27
5H-4, 80	37.8	0.28
5H-5, 80	39.3	0.3
5H-6, 80	40.8	0.25
6H-5, 50	48.5	0.3
6H-2, 109	44.59	0.29
6H-3, 141	46.41	0.3
6H-4, 24	46.74	0.31
6H-7, 63	51.63	0.32
7H-1, 123	52.73	0.33
7H-2, 36	53.36	0.33
7H-3, 68	55.18	0.32
7H-4, 42	56.42	0.33
7H-5, 62	58.12	0.34
7H-7, 53	61.03	0.34
8H-1, 138	62.38	0.33
8H-2, 32	62.82	0.33
8H-3, 75	64.75	0.33
8H-4, 56	66.06	0.31
8H-5, 102	68.02	0.33
8H-6, 87	69.37	0.32
9H-1, 48	70.98	0.3
9H-2, 59	72.59	0.32
9H-3, 50	74	0.31
9H-4, 17	75.17	0.29
9H-5, 70	77.2	0.29
9H-6, 88	78.88	0.3
10H-1, 130	81.3	0.31
10H-2, 83	82.33	0.29
10H-3, 80	83.8	0.29
10H-4, 35	84.85	0.3
10H-5, 137	87.37	0.29
10H-6, 33	87.83	0.29
11H-1, 110	90.6	0.29
11H-2, 127	92.27	0.31
11H-3, 100	93.5	0.3
11H-4, 66	94.66	0.3
11H-5, 20	95.7	0.29
11H-6, 31	97.31	0.31
12H-1, 70	99.7	0.28
12H-2, 25	100.75	0.29
12H-3, 75	102.75	0.31
12H-4, 117	104.67	0.28
12H-5, 76	105.76	0.29
12H-6, 57	107.07	0.28
13H-1, 100	109.5	0.27
13H-2, 100	111	0.29
13H-3, 64	112.14	0.29
13H-4, 28	113.28	0.27
13H-5, 74	115.24	0.27
13H-6, 34	116.34	0.29
14H-1, 80	118.8	0.37
14H-2, 80	120.3	0.36
14H-3, 80	121.8	0.37
14H-4, 80	123.3	0.35
14H-5, 80	124.8	0.34
15H-1, 60	128.1	0.29
15H-2, 60	129.6	0.3
15H-3, 60	131.1	0.31
15H-4, 60	132.6	0.31
15H-5, 60	134.1	0.31
15H-6, 60	135.6	0.33
15H-7, 60	136.6	0.31
16H-2, 40	138.9	0.34
16H-1, 40	137.4	0.33
16H-3, 40	140.4	0.32
16H-4, 40	141.9	0.34
16H-5, 40	143.4	0.33
16H-6, 40	144.9	0.33
16H-7, 40	146.4	0.32
17H-1, 70	147.2	0.32
17H-2, 70	148.7	0.3
17H-3, 70	150.2	0.3
17H-4, 70	151.7	0.33
17H-5, 70	153.2	0.34
17H-6, 70	154.7	0.33
17H-7, 40	155.9	0.35
18H-1, 100	157	0.35
18H-2, 100	158.5	0.35
18H-3, 100	160	0.35
18H-4, 100	161.5	0.4
18H-5, 100	163	0.35
18H-6, 100	164.5	0.35
19H-1, 60	166.1	0.3
19H-1, 100	166.5	0.24
19H-1, 146	166.96	0.23
19H-2, 40	167.4	0.19
19H-3, 40	168.9	0.23
19H-3, 60	169.1	0.21
19H-5, 25	171.75	0.24
19H-5, 35	171.85	0.22
19H-5, 53	172.03	0.24
19H-5, 69	172.19	0.22
19H-5, 90	172.4	0.23
19H-5, 103	172.53	0.21
19H-5, 114	172.64	0.24
19H-5, 127	172.77	0.23
20H-2, 4	176.54	0.26
20H-2, 38	176.88	0.23
20H-2, 67	177.17	0.21
20H-2, 87	177.37	0.21
20H-2, 100	177.5	0.23
20H-2, 114	177.64	0.23
20H-2, 128	177.78	0.22
20H-2, 143	177.93	0.2
20H-3, 9	178.09	0.21
20H-3, 24	178.24	0.19
20H-3, 35	178.35	0.21
20H-3, 54	178.54	0.19
20H-3, 75	178.75	0.21
20H-3, 90	178.9	0.21
20H-3, 102	179.02	0.21
20H-3, 124	179.24	0.2
20H-3, 140	179.4	0.22
20H-5, 104	182.04	0.21
154-926B-		
1H-1, 37	0.37	0.24
1H-2, 37	1.87	0.23
1H-3, 37	3.37	0.24
1H-4, 37	4.87	0.27
2H-3, 34	10.34	0.28
2H-3, 79	10.79	0.28
2H-3, 102	11.02	0.28
2H-3, 134	11.34	0.27
2H-5, 20	13.2	0.27
2H-5, 40	13.4	0.27
2H-5, 78	13.78	0.28
2H-5, 119	14.19	0.27
3H-2, 54	18.54	0.3
3H-3, 50	20	0.32
3H-4, 50	21.5	0.36
3H-5, 50	23	0.31
3H-5, 50	23	0.34
4H-1, 140	27.4	0.37
4H-2, 110	28.6	0.4
4H-3, 110	30.1	0.51
4H-4, 110	31.6	0.38
4H-5, 110	33.1	0.35
4H-6, 110	34.6	0.35
5H-1, 124	36.74	0.3
5H-2, 30	37.3	0.31
5H-3, 37	38.87	0.29
5H-4, 47	40.47	0.31
5H-5, 63	42.13	0.29
5H-6, 59	43.59	0.28
6H-1, 129	46.29	0.28
6H-4, 16	49.66	0.28
6H-4, 36	49.86	0.28
6H-5, 57	51.57	0.28
6H-5, 121	52.21	0.29
7H-1, 62	55.12	0.28
7H-2, 68	56.68	0.28
7H-3, 29	57.79	0.28
7H-4, 83	59.83	0.28
7H-5, 55	61.05	0.28
7H-6, 54	62.54	0.28
8H-1, 105	65.05	0.29
8H-2, 16	65.66	0.28
8H-3, 50	67.5	0.3
8H-4, 70	69.2	0.29
8H-5, 104	71.04	0.29
8H-6, 27	71.77	0.29
9H-2, 112	76.12	0.29
9H-3, 39	76.89	0.29
9H-3, 128	77.78	0.28
9H-4, 38	78.38	0.29
9H-5, 97	80.47	0.28
9H-6, 40	81.4	0.28
11H-1, 60	93.1	0.31
11H-2, 60	94.6	0.27
11H-3, 60	96.1	0.29
11H-4, 60	97.6	0.28
11H-5, 60	99.1	0.29
11H-6, 60	100.6	0.29
11H-7, 60	101.93	0.28
12H-1, 100	103	0.27
12H-2, 100	104.5	0.26
12H-3, 100	106	0.26
12H-4, 100	107.5	0.27
12H-5, 100	109	0.29
12H-6, 100	110.5	0.27
12H-7, 20	111.2	0.29
13H-1, 80	112.3	0.31
13H-2, 80	113.8	0.27
13H-3, 80	115.3	0.26
13H-4, 80	116.8	0.29
13H-5, 80	118.3	0.28
13H-6, 80	119.8	0.29
13H-7, 80	121.3	0.28
14H-1, 70	121.7	0.33
14H-2, 70	123.2	0.29
14H-3, 70	124.7	0.25
14H-4, 70	126.2	0.25
14H-5, 70	127.7	0.26
14H-6, 70	129.2	0.26
15H-1, 100	131.5	0.25
15H-2, 100	133	0.24
15H-3, 100	134.5	0.24
15H-4, 100	136	0.24
15H-5, 100	137.5	0.25
15H-6, 100	139	0.25
15H-7, 100	140.5	0.25
17H-1, 60	150.1	0.26
17H-2, 60	151.6	0.26
17H-3, 60	153.1	0.29
17H-4, 60	154.6	0.29
17H-5, 60	156.1	0.26
17H-6, 60	157.6	0.26
17H-7, 60	159.1	0.31
18H-1, 90	159.9	0.3
18H-2, 90	161.4	0.32
18H-3, 90	162.9	0.29
18H-4, 90	164.4	0.29
18H-5, 90	165.9	0.29
18H-6, 90	167.4	0.26
19H-1, 60	169.1	0.3
19H-2, 60	170.6	0.27
19H-3, 60	172.1	0.34
19H-4, 60	173.6	0.41
19H-5, 60	175.1	0.3
19H-6, 60	176.6	0.29
19H-7, 10	177.6	0.41
20H-1, 60	178.6	0.34
20H-2, 60	180.1	0.33
20H-3, 10	181.1	0.38
20H-3, 60	181.6	0.33
20H-4, 60	183.1	0.33
20H-5, 60	184.6	0.31
20H-6, 60	186.1	0.31
21H-1, 90	188.4	0.3
21H-2, 90	189.9	0.29
21H-3, 90	191.4	0.27
21H-4, 90	192.9	0.27
21H-5, 90	194.4	0.27
21H-7, 20	195.2	0.27
21H-6, 90	195.9	0.27
22H-1, 80	197.8	0.43
22H-2, 80	199.3	0.32
22H-3, 80	200.8	0.3
22H-4, 80	202.3	0.26
22H-5, 80	203.8	0.27
22H-6, 80	205.3	0.27
23H-1, 100	207.5	0.3
23H-2, 95	208.95	0.31
23H-3, 96	210.46	0.28
23H-4, 100	212	0.28
23H-5, 100	213.5	0.3
23H-6, 105	215.05	0.25
23H-7, 60	216.1	0.27
24H-1, 55	216.55	0.3
24H-2, 55	218.05	0.27
24H-3, 55	219.55	0.3
24H-4, 55	221.05	0.26
24H-5, 55	222.55	0.27
24H-6, 55	224.05	0.27
24H-7, 52	225.52	0.26
25H-1, 100	226.5	0.28
25H-2, 101	228.01	0.31
25H-3, 58	229.08	0.29
25H-4, 100	231	0.31
25H-5, 128	232.78	0.35
25H-6, 100	234	0.31
25H-7, 30	234.8	0.27
26H-1, 90	235.9	0.3
26H-2, 90	237.4	0.29
26H-3, 90	238.9	0.34
26H-4, 90	240.4	0.27
26H-5, 139	242.39	0.36
26H-6, 50	243	0.37
27H-1, 71	245.21	0.3
27H-1, 107	245.57	0.28
27H-2, 70	246.7	0.32
27H-3, 64	248.14	0.36
27H-3, 130	248.8	0.33
27H-4, 70	249.7	0.34
27H-5, 93	251.43	0.29
27H-5, 110	251.6	0.31
27H-6, 70	252.7	0.33
28X-1, 30	254.3	0.25
28X-1, 60	254.6	0.3
28X-2, 30	255.8	0.31
28X-2, 111	256.61	0.29
28X-3, 55	257.55	0.36
28X-4, 80	259.3	0.31
29X-1, 69	259.69	0.3
28X-5, 10	260.1	0.32
29X-1, 136	260.36	0.31
29X-2, 68	261.18	0.32
29X-3, 68	262.68	0.41
29X-4, 41	263.91	0.36
29X-5, 130	266.3	0.41
29X-6, 28	266.78	0.32
30X-1, 141	270.01	0.27
30X-2, 70	270.8	0.29
30X-2, 140	271.5	0.28
30X-3, 57	272.17	0.37
30X-4, 60	273.7	0.36
30X-5, 83	275.43	0.42
30X-6, 34	276.44	0.38
35X-1, 36	317.26	1.06
35X-2, 40	318.8	1.29
35X-3, 40	320.3	0.95
35X-4, 40	321.8	0.81
35X-5, 40	323.3	0.77
35X-6, 40	324.8	0.76
35X-7, 40	326.3	0.68
36X-1, 50	327	0.83
36X-2, 50	328.5	0.89
36X-3, 50	330	0.73
36X-4, 50	331.5	0.78
37X-1, 100	337.2	0.78
37X-2, 100	338.7	0.68
37X-3, 100	340.2	0.7
37X-4, 100	341.7	0.58
37X-5, 100	343.2	0.65
38X-1, 50	346.3	0.76
38X-2, 50	347.8	0.72
38X-3, 50	349.3	0.67
38X-4, 50	350.8	0.74
38X-5, 50	352.3	0.69
38X-6, 50	353.8	0.69
38X-7, 10	354.9	0.7
39X-1, 80	356.3	0.81
39X-2, 80	357.8	0.72
39X-3, 80	359.3	0.72
39X-4, 80	360.8	0.82
39X-5, 80	362.3	0.91
39X-6, 80	363.8	0.98
40X-1, 50	365.6	0.9
40X-2, 50	367.1	0.91
40X-3, 50	368.6	0.74
40X-4, 50	370.1	0.94
40X-5, 50	371.6	0.86
40X-6, 50	373.1	0.8
41X-1, 40	374.8	0.88

Table 13 (continued).

Core, section, interval (cm)	Depth (mbsf)	Resistivity (Ωm)
41X-2, 40	375.76	0.64
41X-3, 40	377.26	0.73
41X-4, 38	378.74	0.78
42X-2, 53	386.13	0.79
42X-3, 79	387.89	0.8
42X-3, 97	388.07	0.79
42X-4, 117	389.77	0.86
42X-5, 4	390.14	0.75
42X-5, 128	391.38	0.8
42X-6, 22	391.82	0.92
43X-1, 101	394.71	0.72
43X-2, 98	396.18	0.67
43X-3, 44	397.14	0.7
43X-4, 78	398.98	0.72
43X-4, 143	399.63	0.73
43X-6, 79	401.99	0.69
44X-1, 34	403.74	0.81
44X-2, 43	405.33	0.81
44X-3, 44	406.84	0.71
44X-4, 82	408.72	0.83
44X-4, 111	409.01	0.76
44X-5, 22	409.62	0.73
44X-6, 85	411.75	0.75
44X-7, 4	412.44	0.83
45X-2, 50	415.1	0.79
45X-3, 78	416.88	0.79
45X-4, 38	417.98	0.82
45X-5, 72	419.82	0.86
45X-6, 12	420.72	0.85
45X-6, 72	421.32	0.86
46X-1, 26	423.06	0.95
46X-1, 90	423.7	1.06
46X-2, 63	424.93	0.95
46X-3, 67	426.47	0.96
46X-4, 40	427.7	1.02
46X-6, 76	431.06	1.02
47X-1, 39	432.79	1.11
47X-2, 76	434.66	1.02
47X-3, 139	436.79	0.97
47X-4, 70	437.6	0.87
47X-5, 138	439.78	1.02
47X-6, 95	440.85	0.94
48X-1, 113	443.23	0.89
48X-3, 90	446	0.89
48X-5, 20	448.3	0.89
49X-1, 38	452.08	0.87
49X-1, 87	452.57	0.97
49X-2, 113	454.33	0.85
49X-3, 115	455.85	0.83
49X-4, 70	456.9	0.71
49X-5, 120	458.9	0.74
50X-1, 49	461.89	0.74
50X-2, 50	463.4	0.77
50X-3, 50	464.9	0.8
50X-4, 50	466.4	0.68
50X-5, 50	467.9	0.66
50X-7, 20	469.1	0.76
50X-6, 60	469.5	0.81
50X-6, 65	469.55	0.81
51X-1, 20	471.2	0.85
51X-2, 20	472.7	0.85
51X-3, 20	474.2	1
51X-4, 20	475.7	1.03
51X-5, 20	477.2	0.85
51X-6, 20	478.7	1.02
52X-1, 30	480.8	1.2
52X-2, 30	482.3	1.1
52X-3, 30	483.8	1.09
52X-4, 30	485.3	0.92
52X-5, 30	486.8	0.93
52X-6, 30	488.3	0.87
53X-1, 20	490.4	1.1
53X-2, 20	491.9	1.01
53X-3, 20	493.4	1
53X-4, 20	494.9	0.97
53X-5, 20	496.4	0.96
53X-6, 20	497.9	1.01
54X-1, 50	500.4	1
54X-2, 50	501.9	0.9
54X-3, 50	503.4	0.87
54X-4, 50	504.9	0.77
54X-5, 50	506.4	0.7
54X-6, 50	507.9	0.73
55X-1, 30	509.8	1.16
55X-2, 30	511.3	1
55X-3, 30	512.8	0.92
55X-4, 30	514.3	0.94
55X-5, 30	515.8	1
55X-6, 30	517.3	1
56X-1, 40	519.6	1.02
56X-2, 40	521.1	0.98
56X-3, 40	522.6	0.91
56X-4, 45	524.15	1.02
56X-5, 40	525.6	1.09
56X-6, 40	527.1	1.01
57X-1, 50	529.4	0.88
57X-2, 50	530.9	0.74
57X-3, 50	532.4	0.82
57X-4, 50	533.9	1.13
57X-5, 50	535.4	0.92
57X-6, 50	536.9	1.1
57X-7, 50	537.9	1.34
58X-1, 100	539.5	1.16
58X-2, 69	540.69	1.28
58X-2, 109	541.09	1.1
58X-3, 135	542.85	1.3
58X-4, 76	543.76	1.15
58X-5, 11	544.61	1.18
58X-6, 25	546.25	1.48
58X-6, 70	546.7	1.08
58X-6, 90	546.9	1.39
58X-6, 103	547.03	1.28
59X-1, 45	548.65	1.01
59X-2, 12	549.82	1.02
59X-2, 29	549.99	1.05
59X-2, 37	550.07	1.29
59X-2, 41	550.11	1.14
59X-2, 46	550.16	1.25
59X-2, 48	550.18	1.09
59X-2, 143	551.13	1.3
59X-3, 98	552.18	1.11
59X-4, 30	553	1.31
60X-1, 59	558.49	1.2
60X-1, 113	559.03	1.1
61X-1, 18	567.78	1.33
61X-2, 63	569.73	1.32
61X-3, 23	570.83	1.19
61X-4, 147	573.57	1.21
61X-5, 30	573.9	1.35
62X-2, 7	575.06	1.15
62X-4, 10	575.09	1.23
62X-1, 24	575.23	1.29
63X-1, 61	575.6	0.99
63X-4, 70	575.69	1.07
63X-5, 70	575.69	1.05
62X-3, 73	575.72	1.22
63X-3, 86	575.85	1.02
63X-2, 111	576.1	0.98
62X-1, 115	576.14	1.45
154-926C-		
1H-1, 70	1.2	0.31
1H-2, 70	2.7	0.29
1H-3, 70	4.2	0.28
1H-4, 70	5.7	0.29
1H-5, 70	7.2	0.26
1H-6, 70	8.7	0.25
1H-7, 25	9.75	0.24
2H-1, 80	10.8	0.25
2H-2, 80	12.3	0.26
2H-3, 80	13.8	0.26
2H-4, 80	15.3	0.27
2H-5, 80	16.8	0.26
2H-6, 80	18.3	0.26
2H-7, 30	19.3	0.25
3H-1, 80	20.3	0.27
3H-2, 80	21.8	0.26
3H-3, 80	23.3	0.25
3H-4, 80	24.8	0.26
3H-5, 80	26.3	0.26
3H-6, 80	27.8	0.26
3H-7, 20	28.7	0.26
4H-2, 80	31.3	0.28
4H-3, 80	32.8	0.27
4H-4, 80	34.3	0.29
4H-5, 80	35.8	0.3
4H-6, 80	37.3	0.29
4H-7, 20	38.2	0.3
5H-1, 80	39.3	0.31
5H-2, 80	40.8	0.31
5H-3, 80	42.3	0.33
5H-4, 80	43.8	0.31
5H-5, 80	45.3	0.3
5H-6, 80	46.8	0.3
5H-7, 20	47.7	0.3
6H-1, 80	48.8	0.31
6H-2, 80	50.3	0.31
6H-3, 80	51.8	0.32
6H-4, 80	53.3	0.32
6H-5, 80	54.8	0.31
6H-6, 80	56.3	0.31
6H-7, 20	57.2	0.3
7H-1, 90	58.4	0.33
7H-2, 90	59.9	0.32
7H-3, 90	61.4	0.32
7H-4, 90	62.9	0.31
7H-5, 90	64.4	0.33
7H-6, 90	65.9	0.33
7H-7, 20	66.7	0.33
8H-1, 90	67.9	0.33
8H-2, 90	69.4	0.31
8H-3, 90	70.9	0.31
8H-4, 90	72.4	0.31
8H-5, 90	73.9	0.31
8H-6, 90	75.4	0.32
8H-7, 20	76.2	0.29
9H-1, 80	77.3	0.3
9H-2, 80	78.8	0.31
9H-3, 80	80.3	0.3
9H-4, 80	81.8	0.3
9H-5, 80	83.3	0.31
9H-6, 80	84.8	0.3
9H-7, 20	85.7	0.31
10H-1, 80	86.8	0.31
10H-2, 80	88.3	0.31
10H-3, 80	89.8	0.3
10H-4, 80	91.3	0.31
10H-5, 80	92.8	0.3
10H-6, 80	94.3	0.31
11H-1, 60	96.1	0.29
11H-2, 60	97.6	0.26
11H-3, 60	99.1	0.23
11H-4, 60	100.6	0.25
11H-5, 60	102.1	0.24
11H-6, 60	103.6	0.25
12H-1, 120	106.2	0.28
12H-2, 120	107.7	0.26
12H-3, 120	109.2	0.25
12H-4, 120	110.7	0.25
12H-5, 120	112.2	0.24
12H-6, 120	113.7	0.24
13H-1, 70	115.2	0.25
13H-2, 70	116.7	0.25
13H-3, 70	118.2	0.25
13H-4, 75	119.75	0.24
13H-5, 70	121.2	0.24
13H-6, 70	122.7	0.25
14H-1, 60	124.6	0.24
14H-2, 60	126.1	0.24
14H-3, 60	127.6	0.24
14H-4, 60	129.1	0.23
14H-5, 60	130.6	0.22
14H-6, 60	132.1	0.22
14H-7, 60	133.6	0.22
15H-1, 130	134.8	0.23
15H-2, 130	136.3	0.23
15H-3, 130	137.8	0.23
15H-4, 130	139.3	0.23
15H-5, 130	140.8	0.22
15H-6, 130	142.3	0.22
16H-1, 90	143.9	0.24
16H-2, 90	145.4	0.24
16H-3, 90	146.9	0.22
16H-4, 90	148.4	0.22
16H-5, 90	149.9	0.22
16H-6, 90	151.4	0.24
17H-1, 80	153.3	0.25
17H-2, 80	154.8	0.25
17H-3, 80	156.3	0.26
17H-4, 80	157.8	0.26
17H-5, 80	159.3	0.25
17H-6, 80	160.8	0.26
18H-1, 40	162.4	0.24
18H-2, 40	163.9	0.25
18H-3, 44	165.44	0.26
18H-4, 77	167.27	0.26
18H-5, 40	168.4	0.25
18H-6, 40	169.9	0.24
18H-7, 42	171.42	0.24
19H-1, 60	172.1	0.26
19H-2, 128	174.28	0.28
19H-3, 60	175.1	0.26
19H-4, 120	177.2	0.24
19H-5, 60	178.1	0.26
19H-6, 80	179.8	0.27
20H-1, 20	181.2	0.27
20H-2, 20	182.7	0.25
20H-3, 20	184.2	0.24
20H-4, 54	186.04	0.25
20H-5, 20	187.2	0.25
20H-6, 115	189.65	0.24
21H-1, 50	191	0.26
21H-2, 50	192.5	0.25
21H-3, 50	194	0.26
21H-4, 50	195.5	0.25
21H-5, 50	197	0.24
21H-6, 50	198.5	0.23
22H-1, 60	200.6	0.25
22H-2, 60	202.1	0.24
22H-3, 60	203.6	0.24
22H-4, 60	205.1	0.25
22H-5, 60	206.6	0.25
22H-6, 60	208.1	0.24
23H-1, 70	210.2	0.23
23H-2, 70	211.7	0.24
23H-3, 70	213.2	0.24
23H-4, 70	214.7	0.25
23H-5, 70	216.2	0.23
23H-6, 70	217.7	0.24
24H-1, 80	219.8	0.25
24H-2, 80	221.3	0.25
24H-3, 80	222.8	0.27
24H-4, 80	224.3	0.27
24H-5, 80	225.8	0.26
24H-6, 80	227.3	0.26
25H-1, 80	229.3	0.29
25H-2, 80	230.8	0.3
25H-3, 80	232.3	0.3
25H-4, 80	233.8	0.31
25H-5, 80	235.3	0.3
25H-6, 80	236.8	0.36
25H-7, 30	237.8	0.34
26H-1, 105	239.05	0.35
26H-2, 105	240.55	0.34
26H-3, 105	242.05	0.34
26H-4, 105	243.55	0.36
26H-5, 105	245.05	0.42
26H-6, 105	246.55	0.3
26H-7, 20	247.2	0.3
27H-1, 85	247.85	0.33
27H-2, 85	247.85	0.36
27H-3, 85	247.85	0.33
27H-4, 85	247.85	0.38
27H-5, 85	247.85	0.35
27H-6, 85	247.85	0.45
27H-6, 110	248.1	0.44
27H-7, 20	247.2	0.34
28X-1, 80	254.8	0.32
28X-2, 80	256.3	0.32
28X-3, 80	257.8	0.36
28X-4, 80	259.3	0.33
28X-5, 80	260.8	0.3
28X-6, 80	262.3	0.29
29X-1, 20	263.9	0.41
29X-2, 20	265.4	0.49
29X-3, 20	266.9	0.56
29X-4, 20	268.4	0.38
29X-5, 20	269.9	0.36
29X-6, 20	271.4	0.38
29X-7, 20	271.4	0.36
30X-1, 70	274	0.32
30X-2, 70	275.5	0.44
30X-3, 70	277	0.3
30X-4, 70	278.5	0.37
30X-5, 70	280	0.36
30X-6, 70	281.5	0.37
30X-7, 10	282.4	0.38
31X-1, 50	283.4	0.41
31X-2, 50	284.9	0.32
31X-3, 50	286.4	0.36
31X-4, 50	287.9	0.35
31X-5, 50	289.4	0.36
32X-1, 70	293.3	0.45
32X-2, 70	294.8	0.49
32X-3, 70	296.3	0.52
32X-4, 70	297.8	0.45
32X-5, 70	299.3	0.41
32X-6, 70	300.8	0.43
32X-7, 10	301.7	0.47
33X-1, 72	302.92	0.37
33X-2, 80	304.5	0.45
33X-3, 66	305.86	0.47
34X-1, 50	312.4	0.47
34X-2, 50	313.9	0.43
34X-3, 50	315.4	0.44
34X-4, 50	316.9	0.46
34X-5, 50	318.4	0.43
34X-6, 10	319.5	0.44
35X-1, 37	321.87	0.62
35X-2, 37	323.37	0.51
35X-3, 37	324.87	0.44
35X-4, 37	326.37	0.42
35X-5, 37	327.87	0.49
36X-1, 104	332.14	0.61

Table 13 (continued).

Core, section, interval (cm)	Depth (mbsf)	Resistivity (Ωm)
36X-2, 104	333.64	0.57
36X-3, 104	335.14	0.47
36X-4, 104	336.64	0.52
37X-1, 90	341.7	0.48
37X-2, 20	342.5	0.43
37X-3, 130	345.1	0.49
37X-4, 80	346.1	0.67
37X-5, 80	347.6	0.59
38X-1, 70	351.1	0.64
38X-2, 70	352.6	0.5
38X-3, 70	354.1	0.55
38X-4, 70	355.6	0.53
38X-5, 70	357.1	0.53
39X-1, 120	361.3	0.44
39X-2, 120	362.8	0.48
39X-3, 120	364.3	0.45
39X-4, 120	365.8	0.48
39X-5, 120	367.3	0.44
39X-6, 120	368.8	0.45
40X-1, 50	370.2	0.74
40X-2, 50	371.7	0.58
40X-3, 50	373.2	0.54
40X-4, 50	374.7	0.59
40X-5, 50	376.2	0.62
40X-6, 50	377.7	0.6
41X-1, 90	379.9	0.67
41X-2, 90	381.4	0.57
41X-3, 90	382.9	0.51
41X-4, 90	384.4	0.64
42X-1, 64	389.34	0.71
42X-2, 132	391.52	0.68
42X-3, 90	392.6	0.67
42X-4, 40	393.6	0.7
42X-5, 70	395.4	0.69
42X-7, 45	398.15	0.63

Unit II, a nannofossil ooze with varying clay content, is apparent on the natural gamma log, which illustrates the decreasing clay content toward the base of Unit I (130 mbsf). This log also reflects the decrease in clay content at the boundary between Subunits IIA and IIB (190 mbsf) before increasing sharply toward the base of Subunit IIB (240 mbsf). Increased lithification in Unit II is shown by the density and resistivity logs, but there is little change in sediment rigidity as reflected in steady velocities across this boundary.

The ooze-to-chalk transition associated with the Unit II/III boundary (240 mbsf) is not indicated by major physical properties changes at the boundary, but rather by prominent physical properties transitions within the upper part of Subunit IIIA. Gradual but steady increases in velocity coincide with relative decreases in clay content (lower gamma-ray values) within Subunit IIIA between 240 and 320 mbsf. The velocity increases in this interval of Subunit IIIA appear to be related to enhanced carbonate content and sediment rigidity. Resistivity increases markedly between 300 and 320 mbsf within Subunit IIIA, indicating enhanced tortuosity and grain interlocking. Both resistivity and velocity attain high and steady values toward the base of Subunit IIIA. A brief interval of lower velocities, resistivities, and bulk density coincide with a sharp increase in gamma-ray values (increased clay content) near the Subunit IIIA/IIIB boundary (370 mbsf; Fig. 32).

Bulk-density, velocity, and resistivity values increase markedly between 370 and 420 mbsf within Subunit IIIB. Increased clay contents near the Subunit IIIB/IIIC boundary (460 mbsf) stabilize the velocities near this interval. Declining clay concentrations below this interval contribute to increases in sediment lithification and rigidity as indicated by higher density, velocity, and resistivity values toward the base of Subunit IIIC.

Borehole Temperature

The temperature logging tool at the head of the Quad tool string indicated a maximum borehole fluid temperature of 17.9°C (Fig. 39). This temperature is significantly less than expected from the regional geothermal gradient (about 50°C/km) because the hole was circulated with seawater during drilling and before logging. The final Quad uplog data were collected approximately 10 hr after wiper-trip circulation. The second uplog profile is warmer by 3°C and reflects borehole warming (thermal rebound) over approximately 1 hr.

Shore-based Log Processing

Shore-based log processing figures for Site 926 are presented at the end of this chapter and processed geochemical logs appear in Figure 40. Shipboard calcium carbonate measurements are shown for comparison to the GST-derived oxides/carbonates. The normalization factor is displayed in Figure 40. A lower normalization factor represents better counting statistics and therefore higher quality data. The shore-based processed log data are on CD-ROM.

SUMMARY AND CONCLUSIONS

Situated at an intermediate depth (3598 m) on a plateau on the southern flank of the Ceara Rise, Site 926 will provide an excellent section for the study of the paleoceanography of the western equatorial Atlantic Ocean. The upper 350 m of section, cored in three parallel holes to ensure completeness, comprises a truly continuous sequence of pelagic foraminifer and nannofossil ooze grading to chalk at the base, covering the last 16 m.y. without any break. The preservation of calcareous microfossils is generally very good to excellent, and numerous high-resolution studies will be possible in these sediments. Below this, a 400-m-thick sequence of lower Miocene and Oligocene, greenish, rhythmically bedded chalk was recovered with the XCB. Again, the preservation of calcareous microfossils is very good, although the sediments become progressively more lithified with burial depth. In general, recovery was high in this sequence with downhole logs providing continuity over the intercore gaps.

Although calcium carbonate and terrigenous clay are the major constituents of the sediment recovered at Site 926, significant quantities of biogenic silica are present in the lower Miocene sediments (Fig. 3). The biogenic silica produces a large peak in the concentration of Si in the pore waters both at Site 926 and at Site 925 (where only trace quantities of biogenic silica remain in the sediment). A second significant feature of the pore-water profile at Sites 926 and 925 is the unusually high concentration of lithium.

The warm western areas of the tropical oceans are generally considered to represent the regions of most rapid evolution in the marine plankton, and this idea is supported by the calcareous microfossils (foraminifers and calcareous nannofossils) recovered at Site 926 (see "Biostratigraphy" section, this chapter). Preservation is generally excellent apart from the middle Miocene section, in which carbonate dissolution has affected the foraminifer assemblages. The material will prove ideal for detailed taxonomic and ecologic studies. An added attraction of the sequence is its proximity to many of the classic localities from which many of the species of Neogene tropical foraminifers were first described. Site 926 offers the continuity and temporal control that is invariably lacking in the classic land sections. The sediments adjacent to the Oligocene/Miocene boundary are thicker than at Site 925, suggesting that there may have been a brief, undetected hiatus at Site 925.

During the last 16 m.y. of global climatic deterioration, sedimentation rates have gradually increased from a low of about 12 m/m.y. in the middle Miocene to about 33 m/m.y. during the Pleistocene (Fig. 14). This increase is chiefly accounted for by an increasing flux of terrigenous material that presumably originates in the Amazon River; indeed, during the Pleistocene the biogenic carbonate flux actually decreased, as was observed at Site 925. However, the late Neogene increase in sedimentation rate is not solely the result of increased terrigenous supply. During the Miocene, episodes of severe dissolution caused the lysocline to shoal to depths shallower than 3600 m, reducing sedimentation rates at Site 926 by about 25%. During the lower Miocene, where siliceous microfossils are present in the sediments, sedimentation rates at Site 926 exceeded those at Site 925 by 8%.

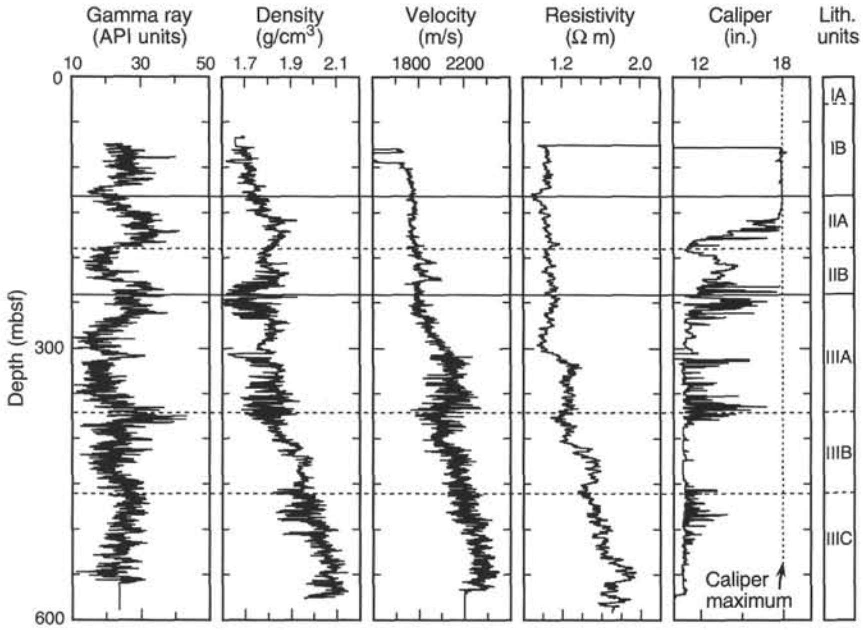

Figure 32. Summary of selected log data from Hole 926B. Lithologic units are shown at right (see "Lithostratigraphy" section, this chapter).

Table 14. Thermal conductivity measured on whole-round core sections for Site 926.

Core, section, interval (cm)	Depth (mbsf)	Thermal conductivity (W/[m · K])	Drift corrected thermal conductivity	Actual thermal conductivity (W/[m · K])
154-926A-				
1H-2, 78	2.78	1.12	1.04	0.98
1H-4, 78	5.78	0.88	0.93	0.89
1H-6, 78	8.78	1.11	1.05	0.99
2H-2, 75	12.25	1.01	1.02	0.97
2H-4, 75	15.25	1.19	1.11	1.04
3H-2, 75	21.75	1.19	1.1	1.03
3H-4, 75	24.75	1.22	1.2	1.11
3H-6, 75	27.75	1.04	0.97	0.93
4H-2, 75	31.25	1	1.02	0.97
4H-4, 75	34.25	1.19	1.11	1.04
4H-6, 75	37.25	1.25	1.11	1.04
5H-2, 75	40.75	1.25	1.15	1.07
5H-4, 75	43.75	1.36	1.25	1.16
5H-6, 75	46.75	1.32	1.16	1.08
6H-2, 75	50.25	1.34	1.22	1.13
6H-4, 75	53.25	1.02	1.04	0.98
6H-6, 75	56.25	1.43	1.24	1.15
7H-2, 75	59.75	1.51	1.37	1.25
7H-4, 75	62.75	1.13	1.12	1.05
7H-6, 75	65.75	1.47	1.35	1.23
8H-2, 75	69.25	1.37	1.25	1.15
8H-4, 75	72.25	1.48	1.4	1.28
8H-6, 120	75.7	1.29	1.2	1.11
9H-2, 75	78.75	1.17	1.08	1.02
9H-4, 75	81.75	1.29	1.25	1.15
9H-6, 75	84.75	1.22	1.14	1.06
10H-2, 75	88.25	1.23	1.13	1.06
10H-4, 75	91.25	1.07	1.07	1.01
10H-6, 75	94.25	1.36	1.25	1.16
11H-2, 75	97.75	1.35	1.23	1.14
11H-4, 75	100.75	1.1	1.1	1.03
11H-6, 75	103.75	1.43	1.31	1.21
12H-2, 75	107.25	1.26	1.16	1.08
12H-2, 75	107.25	1.34	1.22	1.13
12H-4, 75	110.25	1.19	1.17	1.09
12H-4, 75	110.25	1.88	1.72	1.54
12H-6, 75	113.25	1.24	1.15	1.08
12H-6, 75	113.25	1.29	1.2	1.11
14H-2, 75	126.25	2.27	2	1.77
14H-4, 75	129.25	1.17	1.16	1.08
14H-6, 75	132.25	1.24	1.15	1.08
15H-2, 75	135.75	1.31	1.2	1.11
15H-4, 75	138.75	1.22	1.19	1.11
15H-6, 75	141.75	1.4	1.29	1.19
16H-2, 75	145.25	1.32	1.21	1.12
16H-4, 75	148.25	1.19	1.17	1.09
16H-6, 75	151.25	1.34	1.24	1.15
17H-2, 75	154.75	1.42	1.29	1.19
17H-4, 75	157.75	1.52	1.43	1.3
17H-6, 75	160.75	1.49	1.36	1.25
18H-2, 75	164.25	0.9	0.94	0.9
18H-4, 75	167.25	1.58	1.44	1.31
18H-6, 75	170.25	1.55	1.33	1.22
19H-2, 75	173.75	1.53	1.39	1.27
19H-4, 75	176.75	1.52	1.39	1.27
19H-6, 75	179.75	1.55	1.34	1.23
20H-2, 75	183.25	1.45	1.32	1.21
20H-4, 75	186.25	1.24	1.21	1.12
20H-6, 75	189.25	1.63	1.39	1.27
21H-2, 75	192.75	1.42	1.29	1.19
21H-4, 75	195.75	1.62	1.51	1.37
21H-6, 75	198.75	1.5	1.37	1.26
22H-2, 75	202.25	0.78	0.84	0.82
22H-4, 75	205.25	1.62	1.47	1.34
22H-6, 75	208.25	1.71	1.45	1.32
23H-2, 75	211.75	1.39	1.26	1.17
23H-4, 75	214.75	1.53	1.39	1.27
23H-6, 75	217.75	1.69	1.44	1.31
24H-2, 75	221.25	1.68	1.51	1.37
24H-4, 75	224.25	1.28	1.24	1.15
24H-6, 75	227.25	1.56	1.34	1.23
25H-2, 75	230.75	1.44	1.31	1.2
25H-4, 75	233.75	1.5	1.42	1.29
25H-6, 75	236.75	1.47	1.35	1.24
26H-2, 75	240.25	1.47	1.33	1.22
26H-4, 75	243.25	1.23	1.2	1.12
26H-6, 75	246.25	1.5	1.3	1.2
27X-4, 150	253.5	1.76	1.57	1.42
28X-4, 150	260	1.68	1.51	1.37
29X-4, 150	269.7	1.51	1.37	1.25
30X-4, 150	279.3	1.64	1.47	1.34
31X-4, 150	288.9	1.74	1.56	1.41
32X-4, 150	298.6	1.08	1.08	1.02
33X-1, 63	302.83	1.39	1.28	1.18
33X-3, 85	306.05	1.39	1.22	1.13
34X-2, 75	314.15	1.37	1.25	1.15
34X-5, 80	318.7	1.53	1.32	1.21
35X-2, 75	323.75	1.4	1.28	1.18
35X-4, 80	326.8	1.34	1.28	1.18
36X-2, 75	333.35	1.43	1.31	1.21
36X-4, 75	336.35	0.79	0.85	0.83
37X-2, 75	343.05	1.21	1.11	1.04
37X-4, 30	345.6	1.5	1.42	1.29

Table 15. Summary of logging operations at Hole 926B.

24 February 1994	
Drillers' TD = 4215.29 mbrf, WD = 3609.5 mbrf, BOP = 3690.42 mbrf, (80.92 mbsf)	
0735 hr	Last core on deck (at 605.8 mbsf), Hole 926B. Begin wiper trip. Raise pipe to 3690.42 mbrf (80.92 mbsf).
1330 hr	Make up cable; rig up Quad without CNT-G.
1500 hr	RIH with Quad (NGT/DST/DIT/HLDT/LTT).
1700 hr	Quad at 4100 mbrf (490.5 mbsf); WHC not on. Begin Quad Pass 1 uplog (4100–3730 mbrf; 490.5–120.5 mbsf) at 900 ft/hr. WHC on at 3834 mbrf (224.5 mbsf).
1835 hr	End Quad Pass 1 uplog (repeat).
1855 hr	Begin Quad Pass 2 uplog (4193–3665 mbrf; 583.5–55.5 mbsf) at 900 ft/hr.
2100 hr	Pull up pipe to 3665 mbrf (55.5 mbsf); tool stuck at 3665 mbrf (55.5 mbsf) near lockable flapper valve.
2130 hr	Pump at 30 spm to open float valve; tool string in pipe
2200 hr	Quad POOH.
0000 hr	Quad rig down.
0030 hr	Lower pipe 3 stands; pump down another go devil.
0140 hr	Remove 3 stands pipe; rig up GHMT.
0215 hr	RIH with GHMT.
0440 hr	Begin GHMT Pass 1 uplog (4098–3895 mbrf; 488.5–285.5 mbsf) at 1800 ft/hr. Total field signal very low; NRMT not functioning.
0500 hr	End GHMT Pass 1; run down to TD.
0515 hr	Begin GHMT Pass 2 uplog (4054–3690 mbrf; 444.5–80.5 mbsf) at 1800 ft/hr.
0600 hr	End GHMT Pass 2; POOH.
0800 hr	Rig down GHMT.
0830 hr	Rig up GST/TLT tool string.
1125 hr	Begin GST Pass 1 uplog (4007–3935 mbrf; 397.5–325.5 mbsf) at 500 ft/hr.
1200 hr	End GST Pass 1; lower to TD.
1215 hr	Begin GST Pass 2 uplog (4069–3675 mbrf; 459.5–65.5 mbsf) at 500 ft/hr.
1500 hr	Tool hung up on bottom of pipe.
1550 hr	Tool free; POOH GST.
1700 hr	Rig down GST.
1800 hr	End logging operations.

Note: TD = total depth, WD = water depth, BOP = blowout preventer, CNT-G = compensated neutron porosity tool (Schlumberger version G), RIH = run in hole, NGT = natural-gamma spectrometry logging tool, DST = drill stem test, DIT = dual induction tool, HLDT = slim hole lithodensity logging tool, LTT = temperature logging tool, WHC = wireline heave compensator, spm = strokes per minute, POOH = pull out of hole, GHMT = geological high-sensitivity magnetic tool, and GST = gamma-ray spectrometry tool.

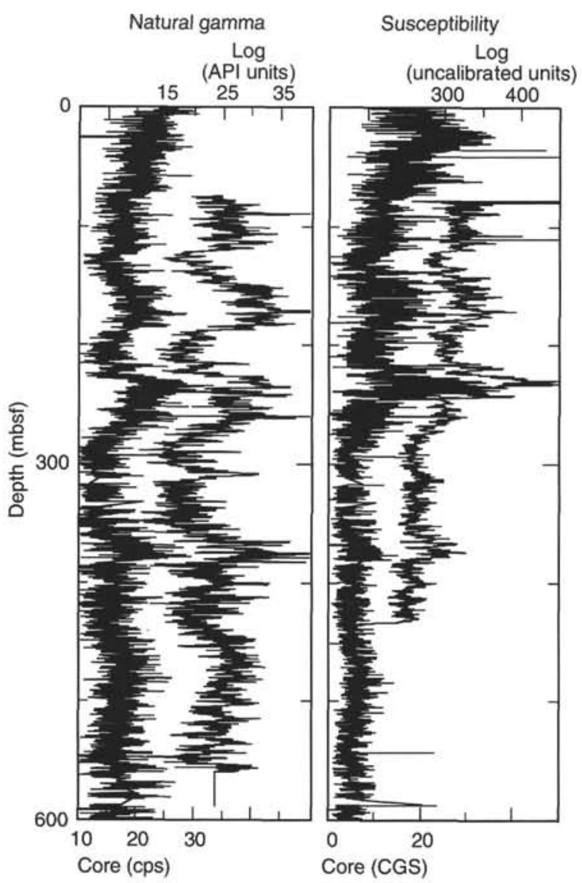

Figure 33. Comparison of core (left) and log (right) measurements of natural gamma activity and magnetic susceptibility from Hole 926B. Core data have not been corrected for background.

A composite section has been constructed on the basis of magnetic susceptibility and reflectance data that will enable high-resolution sampling to be conducted with maximum efficiency and minimum waste of samples. Figure 12 shows spliced magnetic susceptibility and reflectance records for the upper 288.45 mcd (the section down to 259.24 mbsf). The composite section will also enable us to generate accurate spliced records of natural gamma-ray emission, GRAPE density, and *P*-wave velocity. These records will be valuable as a means of correlating core and downhole logging data, and as proxies of sediment lithology.

The spliced records of magnetic susceptibility and of color reflectance can readily be correlated cycle by cycle with those generated for Site 925 over the whole of the Pleistocene and Pliocene and sections of the Miocene (Fig. 12). With further work, these detailed correlations will be possible over most, if not all, of the sections recovered. Thus, despite the lack of a paleomagnetic record at either Site 925 or Site 926, it is clear that we have the ability to make extremely detailed comparisons between erosional and biological fluxes to the seafloor at these sites on the Ceara Rise over the past 29 m.y.

In addition to the high-resolution records that have already been obtained by analyzing the sediment recovered at Site 926, the downhole logs at the site have provided invaluable information both at low and high resolution. For example, the downhole natural gamma log (also recorded in the MST track natural gamma measurements) shows a significant change in sediment composition at about 8 Ma (Fig. 35). At high resolution, both the natural gamma record and the resistivity record show distinct cyclicity with a 1.0- to 1.3-m wavelength through the late Oligocene and early Miocene part of the sediment column that unambiguously match the cyclicity observed in the cores recovered. This part of the section was recovered in a single hole (926B), and it is extremely valuable to have determined accurately the length relationship between the cycles observed in the recovered cores and the wavelength actually present in the sediment. In the siliceous sediments recovered in the eastern equatorial Pacific, cores recovered using the XCB were sometimes stretched by up to 50% (Hagelberg et al., 1992); it is evident, however, that in the chalks recovered at Site 926 the sediment was recovered at true scale.

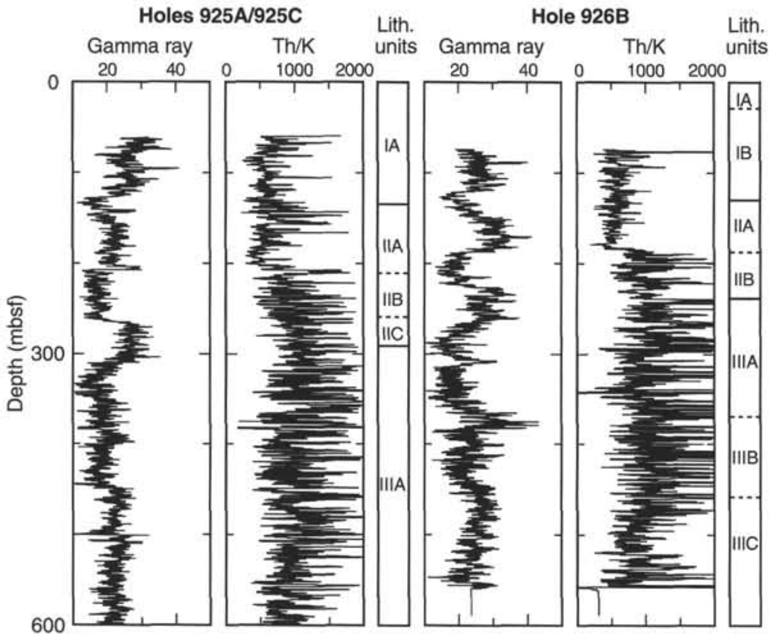

Figure 34. Th/K ratios for Holes 925A/925C (spliced) and 926B. Note the shift toward lower values (higher K concentrations) above the lithologic Subunit IIA/IIB boundary. This boundary corresponds to roughly 7.5 Ma and suggests increased illite concentrations (relative to kaolinite) after 7.5 Ma.

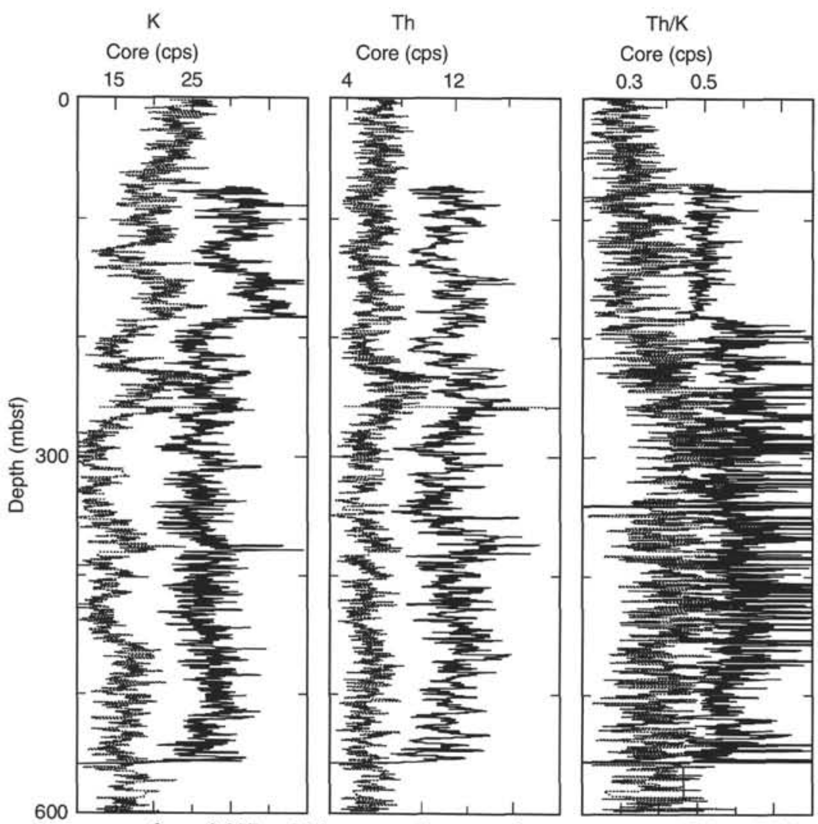

Figure 35. Comparison of core- and log-based K, Th, and Th/K ratio measurements at Hole 926B. Core data (dashed line) were derived from 10-s counts taken at 10-cm intervals (see "Physical Properties" section, this chapter). K and Th data were estimated from MST windows 5 and 3, respectively.

REFERENCES*

Archie, G.E., 1942. The electrical resistivity log as an aid in determining some reservoir characteristics. *Trans. Am. Inst. Min. Metall. Pet. Eng.*, 146:54–62.

Baldauf, J.G., 1987. Biostratigraphic and paleoceanographic interpretation of lower and middle Miocene sediments, Rockall Plateau Region, North Atlantic Ocean. *In* Ruddiman, W.F., Kidd, R.B., Thomas, E., et al., *Init. Repts. DSDP,* 94 (Pt. 2): Washington (U.S. Govt. Printing Office), 1033–1043.

Bassinot, F.C., in press. Sonostratigraphy of tropical Indian ocean giant piston cores: toward a rapid and high-resolution tool for tracking dissolution cycles in Pleistocene carbonate sediments. *Earth Planet. Sci. Lett.*

Benjamin, M., Johnson, N.M., and Naeser, C.W., 1987. Recent rapid uplift in the Bolivian Andes: evidence from fission-track dating. *Geology,* 15:680–683.

Berggren, W.A., Aubry, M.P., and Hamilton, N., 1983. Neogene magnetostratigraphy of Deep Sea Drilling Project Site 516 (Rio Grande Rise, South Atlantic). *In* Barker, P.F., Carlson, R.L., Johnson, D.A., et al., *Init. Repts. DSDP,* 72: Washington (U.S. Govt. Printing Office), 675–713.

Berggren, W.A., Kent, D.V., and Van Couvering, J.A., 1985. The Neogene: Part 2. Neogene geochronology and chronostratigraphy. *In* Snelling, N.J. (Ed.), *The Chronology of the Geological Record.* Geol. Soc. London Mem., 10:211–260.

Blow, W.H., 1969. Late middle Eocene to Recent planktonic foraminiferal biostratigraphy. *In* Brönnimann, R., and Renz, H.H. (Eds.), *Proc. First Int. Conf. Planktonic Microfossils, Geneva, 1967:* Leiden (E.J. Brill), 1:199–421.

Carlson, R.L., and Christensen, N.I., 1979. Velocity anisotropy in semi-indurated calcareous deep-sea sediments. *J. Geophys. Res.,* 84:205–211.

Chaisson, W.P., and Leckie, R.M., 1993. High-resolution Neogene planktonic foraminifer biostratigraphy of Site 806, Ontong Java Plateau (western equatorial Pacific). *In* Berger, W.H., Kroenke, L.W., Mayer, L.A., et al., *Proc. ODP, Sci. Results,* 130: College Station, TX (Ocean Drilling Program), 137–178.

Curry, W.B., and Lohmann, G.P., 1990. Reconstructing past particle fluxes in the tropical Atlantic Ocean. *Paleoceanography,* 5:487–505.

Fertl, W.H., 1979. Gamma ray spectral data assist in complex formation evaluation. *Log Anal.,* 20:421–423.

Fornaciari, E., Raffi, I., Rio, D., Villa, G., Backman, J., and Olafsson, G., 1990. Quantitative distribution patterns of Oligocene and Miocene calcareous nannofossils from the western equatorial Indian Ocean. *In* Duncan, R.A., Backman, J., Peterson, L.C., et al., *Proc. ODP, Sci. Results,* 115: College Station, TX (Ocean Drilling Program), 237–254.

Gieskes, J.M., 1981. Deep-sea drilling interstitial water studies: implications for chemical alteration of the oceanic crust, layers I and II. *In* Warme, J.E., Douglas, R.G., and Winterer, E.L. (Eds.), *The Deep Sea Drilling Project: A Decade of Progress.* Spec. Publ.—Soc. Econ. Paleontol. Mineral., 32:149–167.

Gieskes, J.M., Elderfield, H., Lawrence, J.R., Johnson, J., Meyers, B., and Campbell, A., 1982. Geochemistry of interstitial waters and sediments, Leg 64, Gulf of California. *In* Curray, J.R., Moore, D.G., et al., *Init. Repts. DSDP,* 64 (Pt. 2): Washington (U.S Govt. Printing Office), 675–694.

Hagelberg, T., Shackleton, N., Pisias, N., and Shipboard Scientific Party, 1992. Development of composite depth sections for Sites 844 through 854. *In* Mayer, L., Pisias, N., Janecek, T., et al., *Proc. ODP, Init. Repts.,* 138 (Pt. 1): College Station, TX (Ocean Drilling Program), 79–85.

Hamilton, E.L., 1970. Sound velocity and related properties of marine sediments, North Pacific. *J. Geophys. Res.,* 75:4423–4446.

————, 1976. Variations of density and porosity with depth in deep-sea sediments. *J. Sediment. Petrol.,* 46:280–300.

Hays, J.D., Saito, T., Opdyke, N.D., and Burckle, L.H., 1969. Pliocene-Pleistocene sediments of the equatorial Pacific: their paleomagnetic, biostratigraphic, and climatic record. *Geol. Soc. Am. Bull.,* 80:1481–1513.

Johnson, T.C., Hamilton, E.L., and Berger, W.H., 1977. Physical properties of calcareous ooze: control by dissolution at depth. *Mar. Geol.,* 24:259–277.

Kennett, J.P., and Srinivasan, M.S., 1983. *Neogene Planktonic Foraminifera: A Phylogenetic Atlas:* Stroudsburg, PA (Hutchinson Ross).

Kim, D.-C., Manghnani, M.H., and Schlanger, S.O., 1985. The role of diagenesis in the development of physical properties of deep-sea carbonate sediments. *Mar. Geol.,* 69:69–91.

Kroenke, L.W., Berger, W.H., Janecek, T.R., et al., 1991. *Proc. ODP, Init. Repts.,* 130: College Station, TX (Ocean Drilling Program).

Martin, J.B., Kastner, M., and Elderfield, H., 1991. Lithium: sources in pore fluids of Peru slope sediments and implications for oceanic fluxes. *In* Meyer, A.W., Davies, T.A., and Wise, S.W. (Eds.), *Evolution of Mesozoic and Cenozoic Continental Margins.* Mar. Geol., 102:281–292.

Mayer, L., Pisias, N., Janecek, T., et al., 1992. *Proc. ODP, Init. Repts.,* 138 (Pts. 1 and 2): College Station, TX (Ocean Drilling Program).

Mienert, J., Curry, W.B., and Sarnthein, M., 1988. Sonostratigraphic records from equatorial Atlantic deep-sea carbonates: paleoceanographic and climatic relationships. *Mar. Geol.,* 83:9–20.

Olafsson, G., and Villa, G., 1992. Reliability of sphenoliths as zonal markers in Oligocene sediments from the Atlantic and Indian oceans. *In* Proto Decima, F., Monechi, S., and Rio, D. (Eds.), *Proc. Int. Nannoplankton Assoc. Conf., Firenze 1989.* Mem. Sci. Geol., 43:261–275.

Parsons, B., and Sclater, J.G., 1977. An analysis of the variation of ocean floor bathymetry and heat flow with age. *J. Geophys. Res.,* 82:803–829.

Pearson, P.N., in press. Planktonic foraminifer biostratigraphy and the development of pelagic caps on guyots in the Marshall Islands Group. *In* Haggerty, J., Premoli Silva, I., Rack, F., and McNutt, M.K. (Eds.), *Proc. ODP, Sci. Results,* 144: College Station, TX (Ocean Drilling Program).

Raffi, I., Rio, D., d'Atri, A., Fornaciari, E., and Rocchetti, S., in press. Quantitative distribution patterns and biomagnetostratigraphy of middle and late Miocene calcareous nannofossils from equatorial Indian and Pacific oceans (Legs 115, 130, and 138). *In* Pisias, N.G., Mayer, L.A., Janecek, T.R., Palmer-Julson, A., and van Andel, T.H. (Eds.), *Proc. ODP, Sci. Results,* 138: College Station, TX (Ocean Drilling Program).

Rio, D., Fornaciari, E., and Raffi, I., 1990. Late Oligocene through early Pleistocene calcareous nannofossils from western equatorial Indian Ocean (Leg 115). *In* Duncan, R.A., Backman, J., Peterson, L.C., et al., *Proc. ODP, Sci. Results,* 115: College Station, TX (Ocean Drilling Program), 175–235.

Ruddiman, W., Sarnthein, M., Baldauf, J., et al., 1988. *Proc. ODP, Init. Repts.,* 108 (Sections 1 and 2): College Station, TX (Ocean Drilling Program).

Shipboard Scientific Party, 1989. Site 758. *In* Peirce, J., Weissel, J., et al., *Proc. ODP, Init. Repts.,* 121: College Station, TX (Ocean Drilling Program), 359–453.

Swart, P.K., and Burns, S.J., 1990. Pore-water chemistry and carbonate diagenesis in sediments from Leg 115: Indian Ocean. *In* Duncan, R.A., Backman, J., Peterson, L.C., et al., *Proc. ODP, Sci. Results,* 115: College Station, TX (Ocean Drilling Program), 629–645.

Takayama, T., 1993. Notes on Neogene calcareous nannofossil biostratigraphy of the Ontong Java Plateau and size variations of *Reticulofenestra* coccoliths. *In* Berger, W.H., Kroenke, L.W., Mayer, L.A., et al., *Proc. ODP, Sci. Results,* 130: College Station, TX (Ocean Drilling Program), 179–229.

Weaver, P.P.E., and Raymo, M.E., 1989. Late Miocene to Holocene planktonic foraminifers from the equatorial Atlantic, Leg 108. *In* Ruddiman, W., Sarnthein, M., et al., *Proc. ODP, Sci. Results,* 108: College Station, TX (Ocean Drilling Program), 71–91.

Woodruff, F., and Douglas, R.G., 1981. Response of deep-sea benthic foraminifera to Miocene paleoclimatic events, DSDP Site 289. *Mar. Micropaleontol.,* 6:617–632.

Wright, J.D., Miller, K.G., and Fairbanks, R.G., 1992. Early and middle Miocene stable isotopes: implications for deepwater circulation and climate. *Paleoceanography,* 7:357–389.

Young, J.R., 1990. Size variation of Neogene *Reticulofenestra* coccoliths from Indian Ocean DSDP cores. *J. Micropaleontol.,* 9:71–85.

---

*Abbreviations for names of organizations and publications in ODP reference lists follow the style given in *Chemical Abstracts Service Source Index* (published by American Chemical Society).

Ms 154IR-105

NOTE: For all sites drilled, core-description forms ("barrel sheets") can be found in Section 4 beginning on page 445. Forms containing smear-slide data can be found in Section 5, beginning on page 1087. High-resolution, conventional, temperature, and geochemical logs; sonic waveforms; and carbon, GRAPE, index properties, MAGSUS, natural gamma, *P*-wave, and reflectance data are presented on CD-ROM (back pocket) for Site 926.

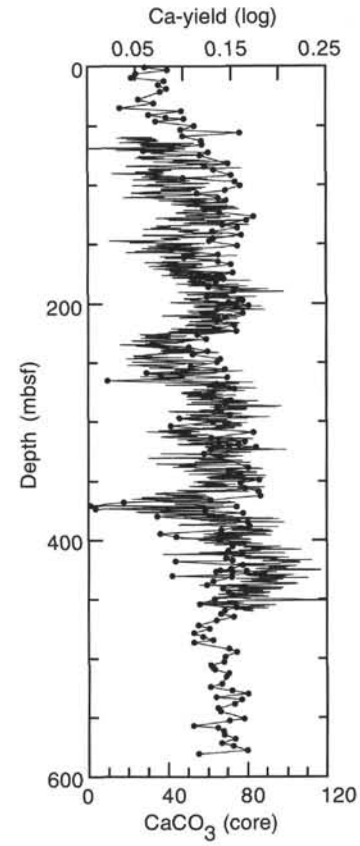

Figure 36. Ca-yield channel data from the geochemical logging tool compared to discrete core $CaCO_3$ % measurements (see "Geochemistry" section, this chapter).

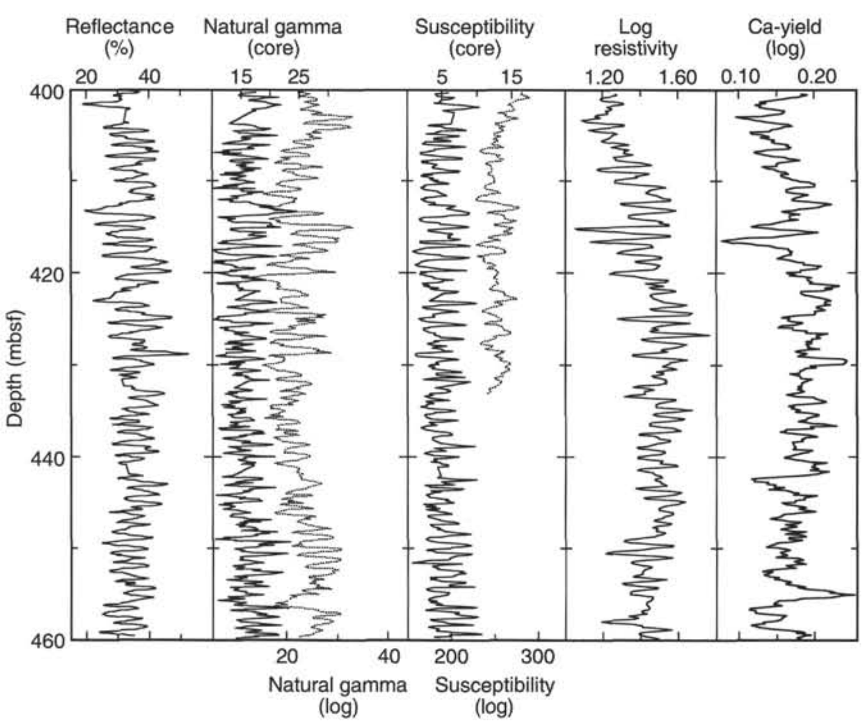

Figure 37. Comparison of core data (percentage of reflectance, natural gamma, and susceptibility) and log data (natural gamma, susceptibility, resistivity, and Ca-yield) for the interval from 400 to 460 mbsf in Hole 926B. Both core and log data sets resolve the 1- to 1.3-m bedding cycles apparent in the split cores. Sedimentation rates for this early Miocene interval (24–21 Ma) average 2.2–2.8 cm/k.y. (see "Biostratigraphy" section, this chapter).

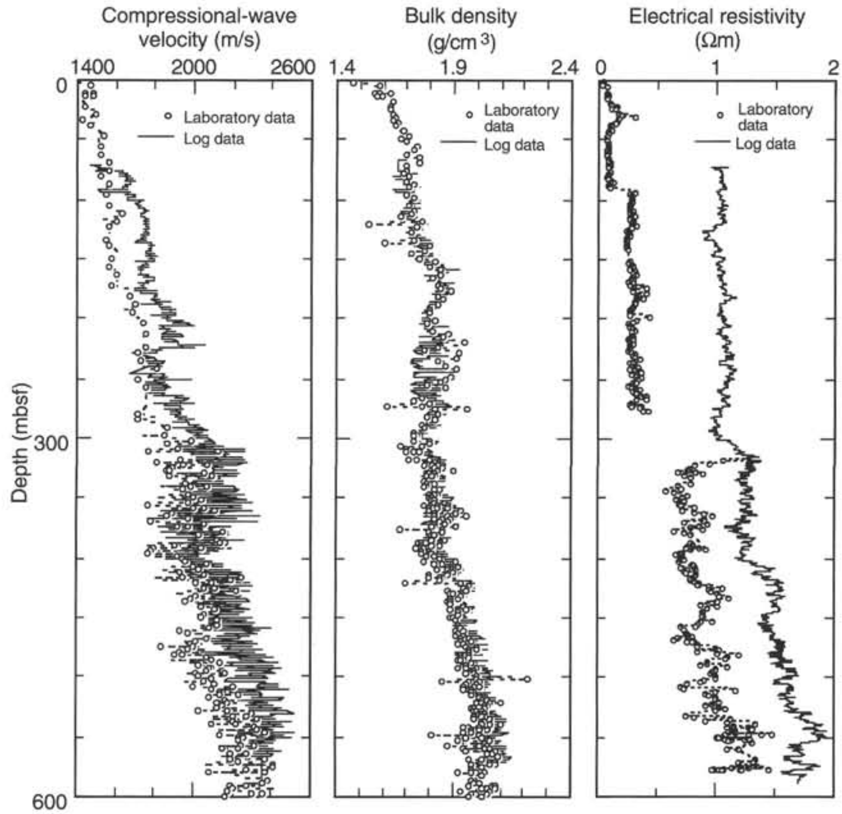

Figure 38. Comparison of core and log physical properties (compressional-wave velocity, bulk density, and electrical resistivity), Hole 926B.

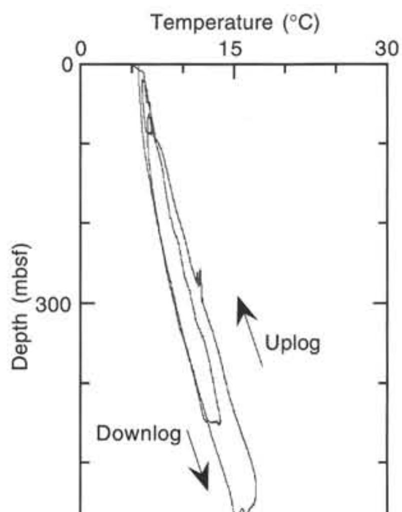

Figure 39. Borehole fluid temperature from the temperature logging tool, which was run during both passes of the Quad tool string. Temperature at total depth was 17.9°C approximately 10 hr after wiper-trip circulation.

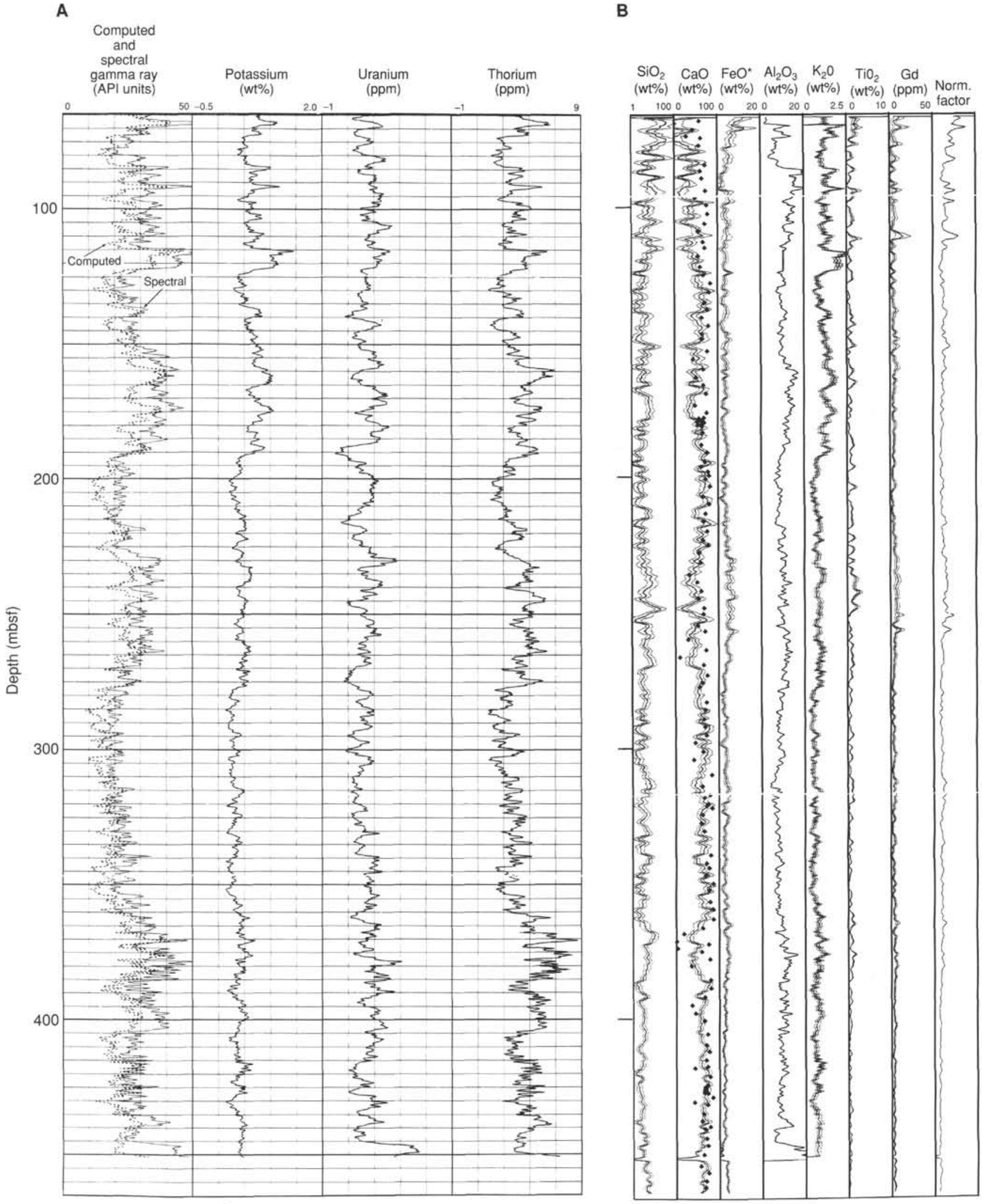

Figure 40. **A.** Processed natural gamma data from Hole 926B. **B.** Estimates of major oxide weight fractions from geochemical logs, Hole 926B. Solid diamonds represent shipboard carbonate measurements on core material. The oxide closure model normalization factor (F) is displayed to the right of the logs. A lower normalization factor represents better counting statistics and therefore higher quality data.

SHORE-BASED LOG PROCESSING

Hole 926B

Bottom felt: 3609.5 mbrf (used for depth shift to seafloor)
Total penetration: 605.8 mbsf
Total core recovered: 593.25 m (97.9%)

Logging Runs

Logging string 1: DIT/SDT/HLDT/NGT
Logging string 2: GHMT
Logging string 3: ACT/GST/NGT

The wireline heave compensator (WHC) was used to counter mild ship heave. The WHC was turned off at 105 mbsf during the DIT/SDT/HLDT/NGT run and at 97 mbsf during the ACT/GST/NGT run.

Drill Pipe

The following drill-pipe depths are as they appear on the logs after differential depth shift (see **Depth shift** section below) and depth shift to the seafloor. As such, there might be a discrepancy with the original depths given by the drillers on board. Possible reasons for depth discrepancies are ship heave, use of wireline heave compensator, and drill-string and/or wireline stretch.

DIT/HLDT/SDT/NGT: Bottom of drill pipe at ~77 mbsf for DIT tool, at 49 mbsf for NGT tool
ACT/GST/NGT: Bottom of drill pipe at ~64 mbsf

Processing

Depth shift: The reference run for depth shift was the DIT/SDT/HLDT/NGT main pass. For consistency with the core-log correlation performed by the logging scientists on board using multisensor track data, this run was first depth shifted +6.5 m. Then, all original logs were interactively depth shifted with reference to NGT from the DIT/SDT/HLDT/NGT run, and to the seafloor (–3609.5 m).

Gamma-ray processing: The NGT data have been processed to correct for borehole size and type of drilling fluid.

Acoustic data processing: The sonic logs have been processed to eliminate some of the noise and cycle skipping experienced during recording. The acoustic data were recorded in both "short-spacing" (DT, DTL, TT1, etc.) and "long-spacing" modes (DTLN, DTLF, LTT1, etc.). The data recorded in the short-spacing mode in the section of the hole below 400 mbsf are of very good quality, and no processing is necessary. In the upper part, however, processing was performed on long-spacing data, which appear to be of slightly better quality than the short-spacing data. The two portions of transit time have then been merged.

Geochemical processing: For a detailed explanation of geochemical processing, please refer to the "Explanatory Notes" chapter (this volume) or to the geochem.doc file on the CD-ROM in the back pocket. The elemental yields recorded by the GST tool represent the relative contribution of only some of the rock-forming elements (iron, calcium, chlorine, silica, sulfur, hydrogen, gadolinium, and titanium—the last two of which were computed during geochemical processing) to the total spectrum. Because other rock-forming elements are present in the formation (such as aluminum, potassium, etc.), caution is recommended in using the yields to infer lithologic changes. Instead, ratios (see acronyms.doc on the CD-ROM) are more appropriate to determine changes in the macroscopic properties of the formation. A list of oxide factors used in geochemical processing includes the following:

SiO_2 = 2.139
$CaCO_3$ = 2.497
FeO* = 1.358
TiO_2 = 1.668
K_2O = 1.205
Al_2O_3 = 1.889

FeO*=computed using an oxide factor which assumes a 50:50 combination of Fe_2O_3 and FeO factors.

Quality Control

Data recorded through pipe and/or bottom hole assembly should be used qualitatively only because of the attenuation on the incoming signal.

Hole diameter was recorded by the hydraulic caliper on the HLDT tool (CALI). The caliper closed at about 80 mbsf; therefore, no borehole size correction can be performed between this depth and the bottom of the pipe. For this reason, this portion of the data is not presented here.

The geochemical tool got stuck between 114 and 121 mbsf, resulting in anomalously high aluminum readings, which would have affected the estimate of all of the other elements. For this reason, the aluminum data has been interpolated (assuming a constant value). The results of the processing are presented along with the calcium carbonate measurements performed on board.

FACT = quality control curve in geochemical processing. The accuracy of the estimates is inversely proportional to the magnitude of the curve.

Details of standard shore-based processing procedures are found in the "Explanatory Notes" chapter, this volume. For further information about the logs, please contact:

Cristina Broglia
Phone: 914-365-8343
Fax: 914-365-3182
E-mail: chris@ldeo.columbia.edu

Elizabeth Pratson
Phone: 914-365-8313
Fax: 914-365-3182
E-mail: beth@ldeo.columbia.edu

Hole 926B: Resistivity-Velocity-Natural Gamma Ray Log Summary

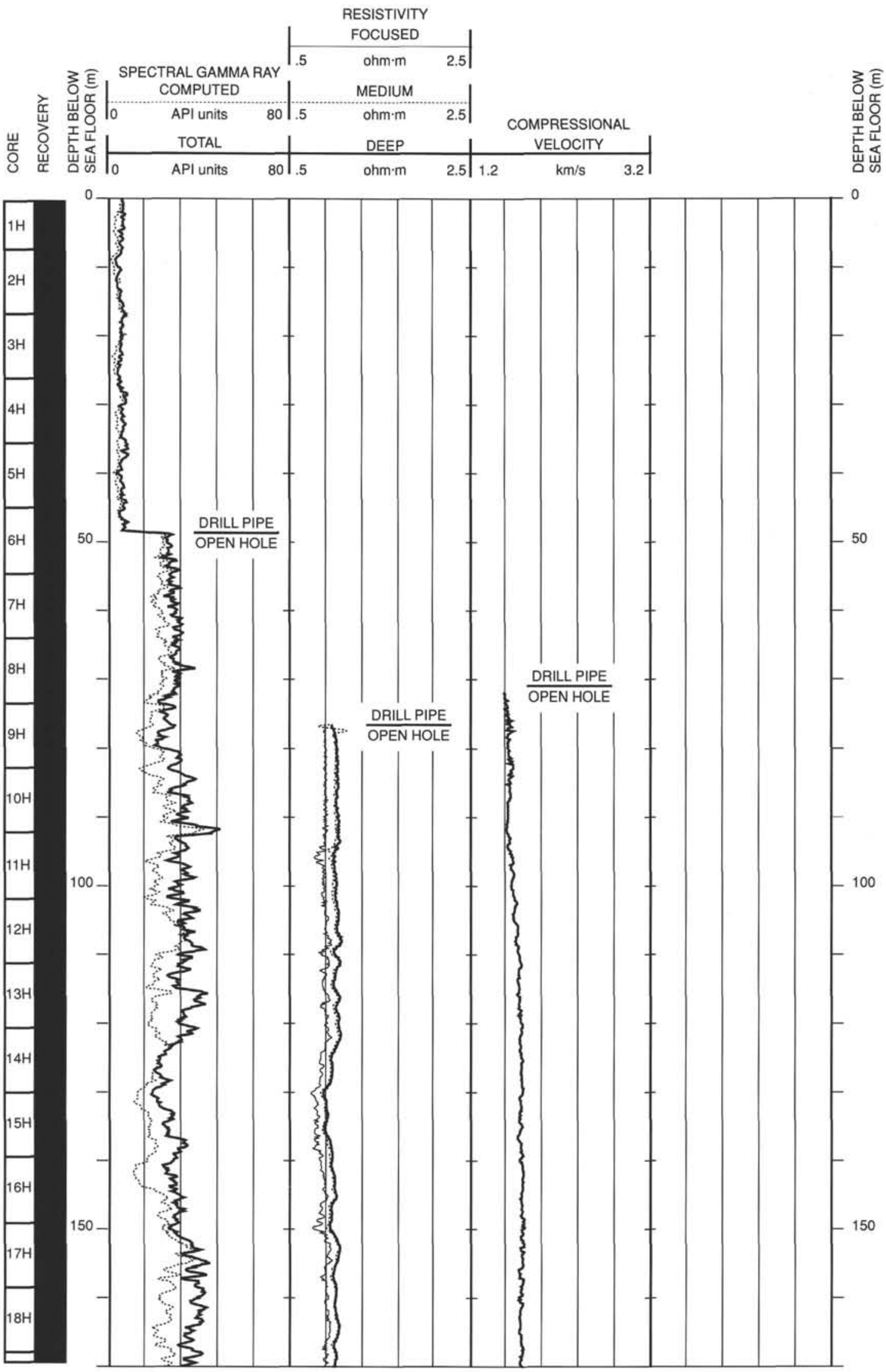

Hole 926B: Resistivity-Velocity-Natural Gamma Ray Log Summary (cont.)

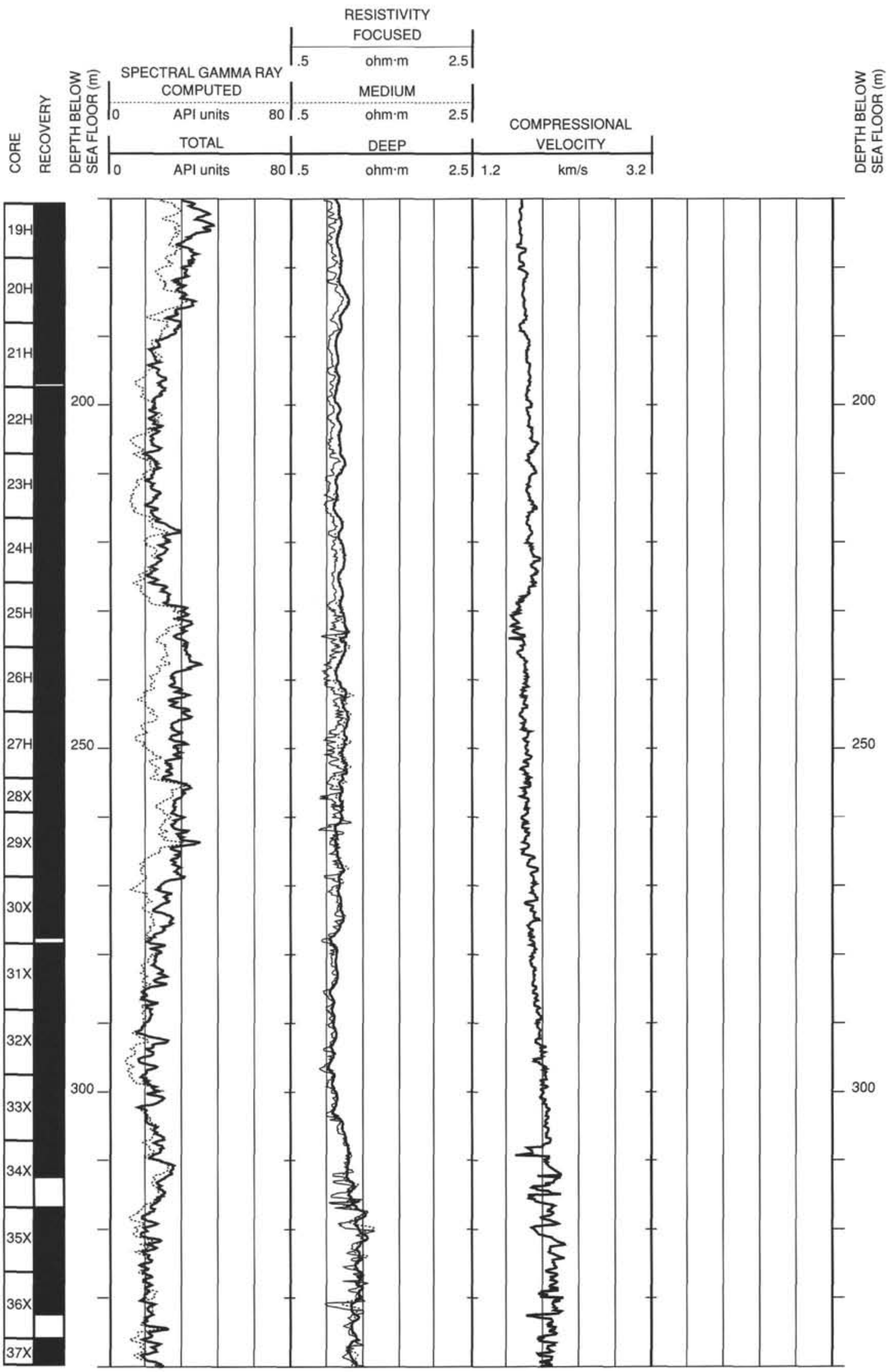

Hole 926B: Resistivity-Velocity-Natural Gamma Ray Log Summary (cont.)

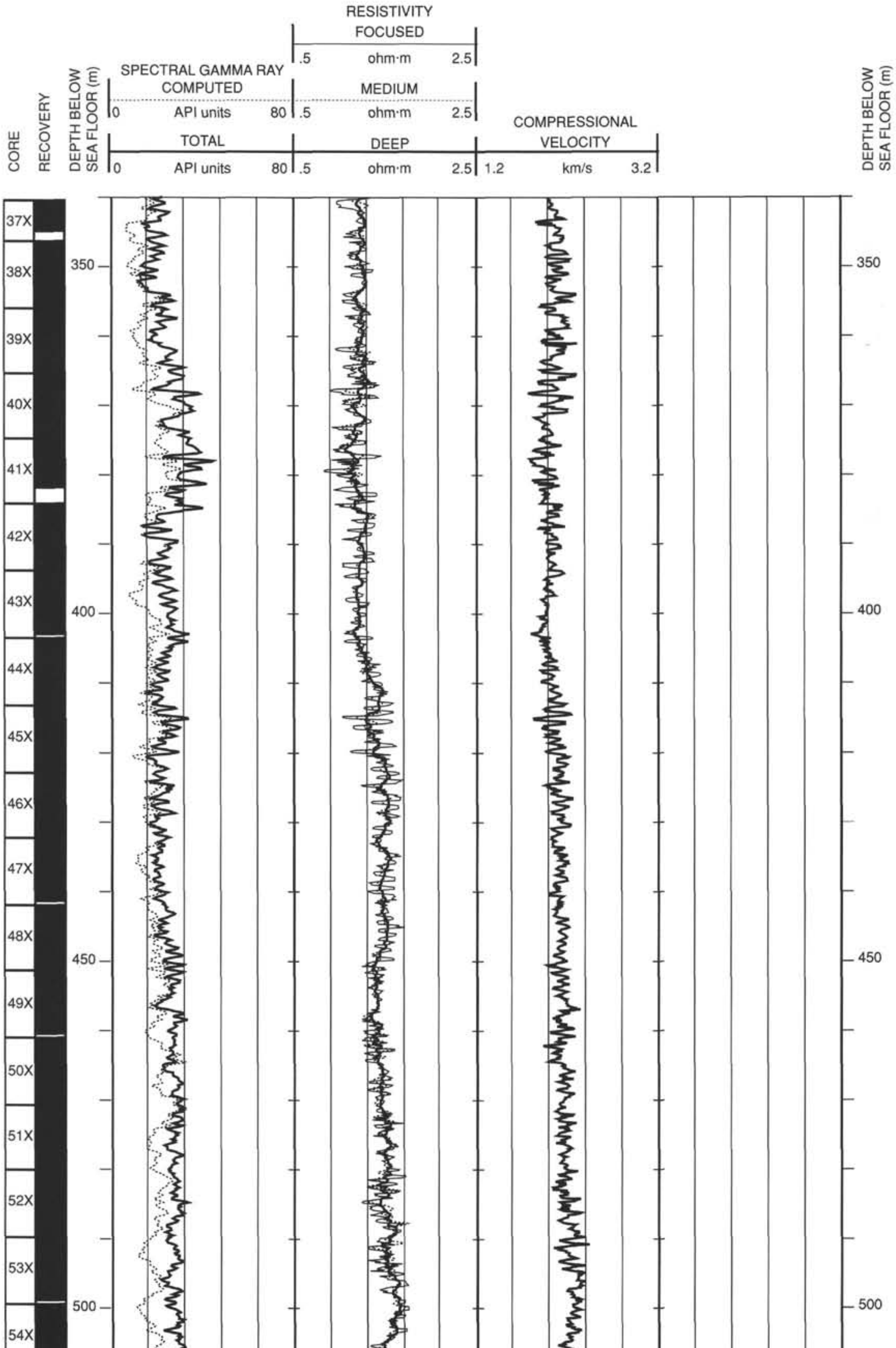

Hole 926B: Resistivity-Velocity-Natural Gamma Ray Log Summary (cont.)

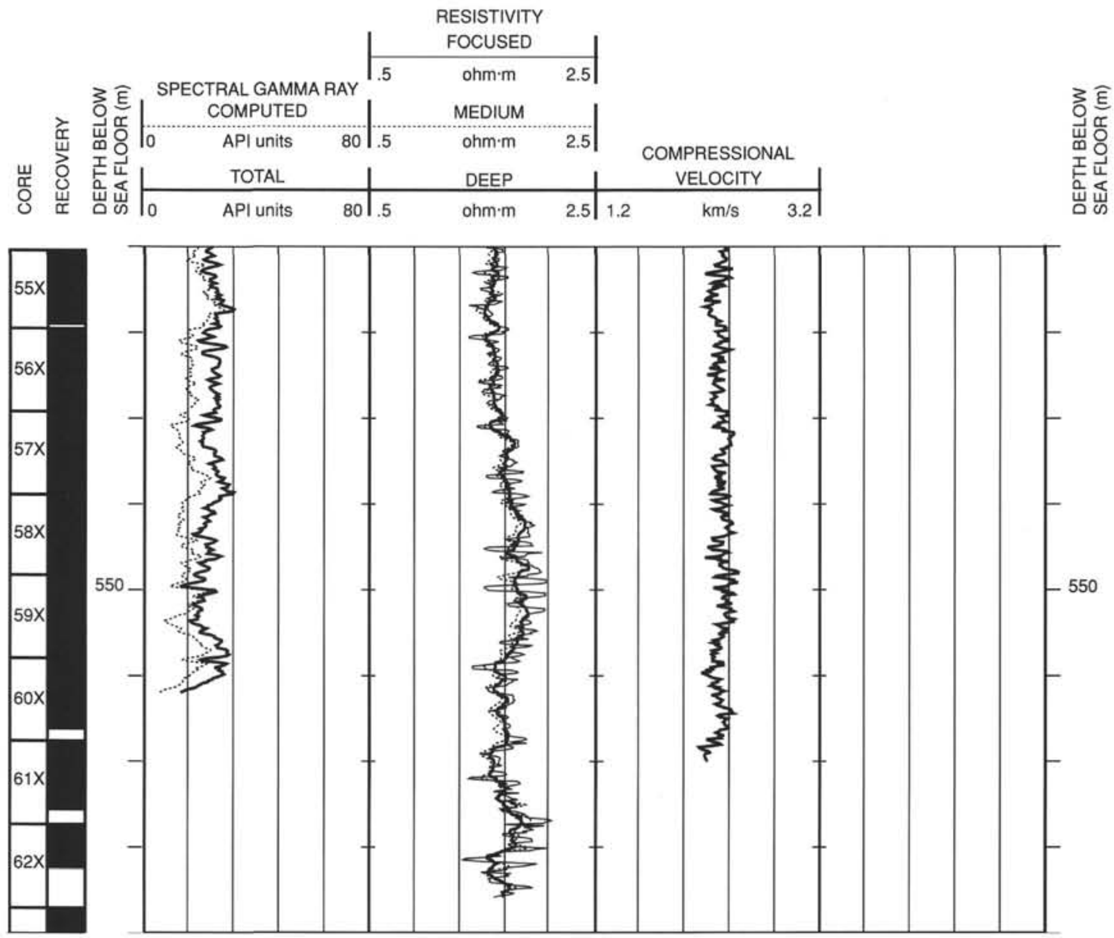

Hole 926B: Density-Natural Gamma Ray Log Summary

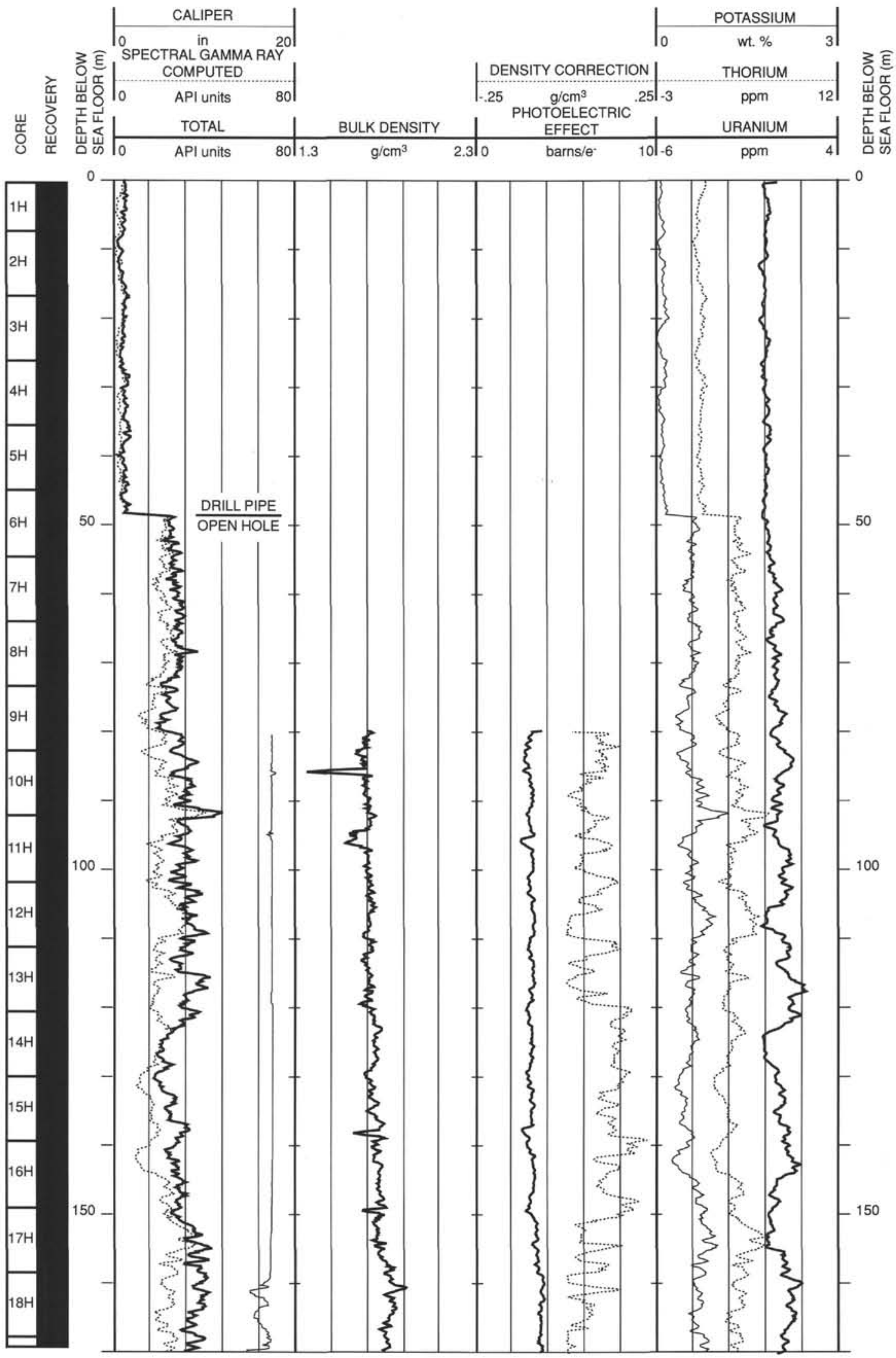

Hole 926B: Density-Natural Gamma Ray Log Summary (cont.)

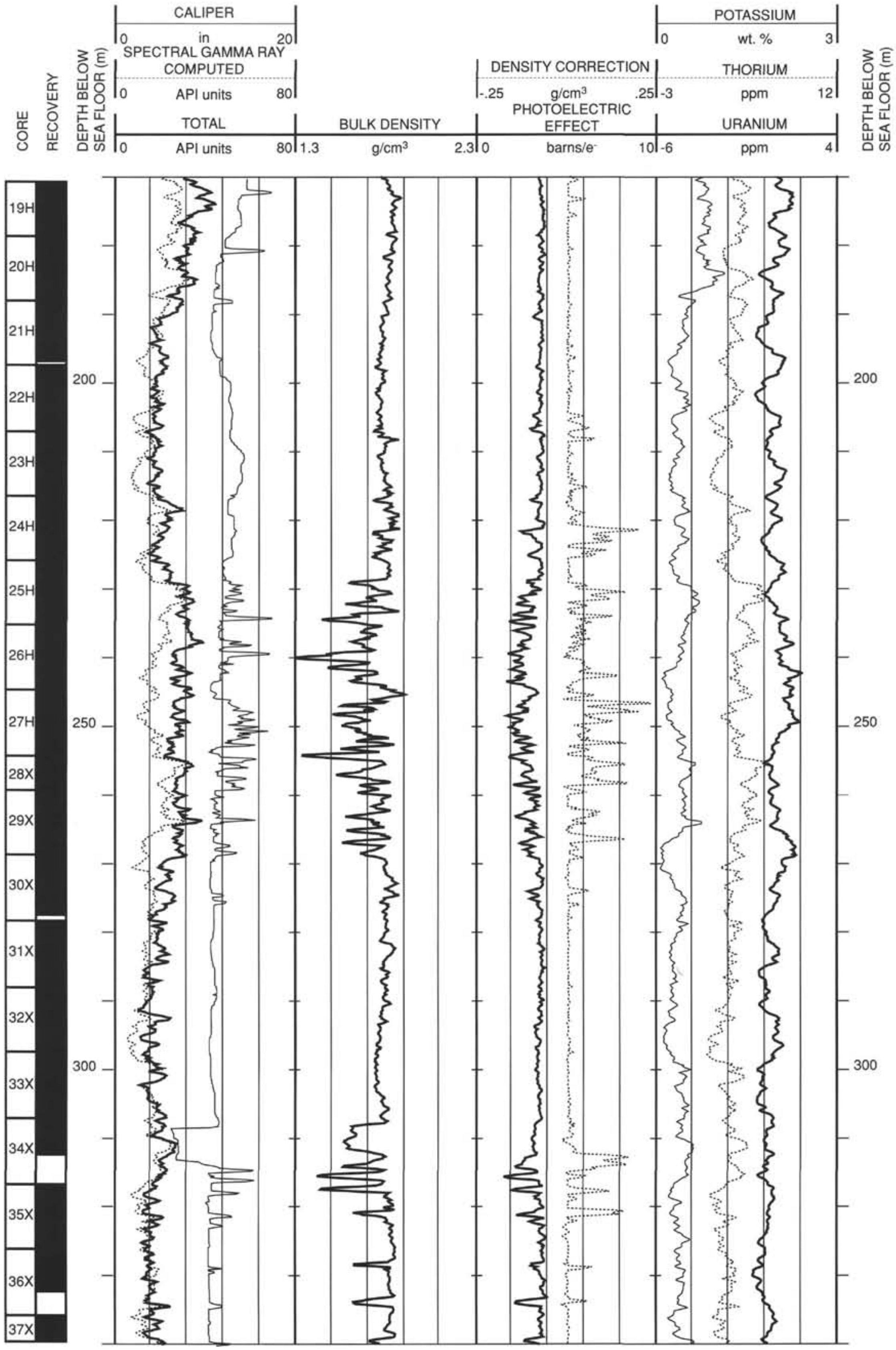

Hole 926B: Density-Natural Gamma Ray Log Summary (cont.)

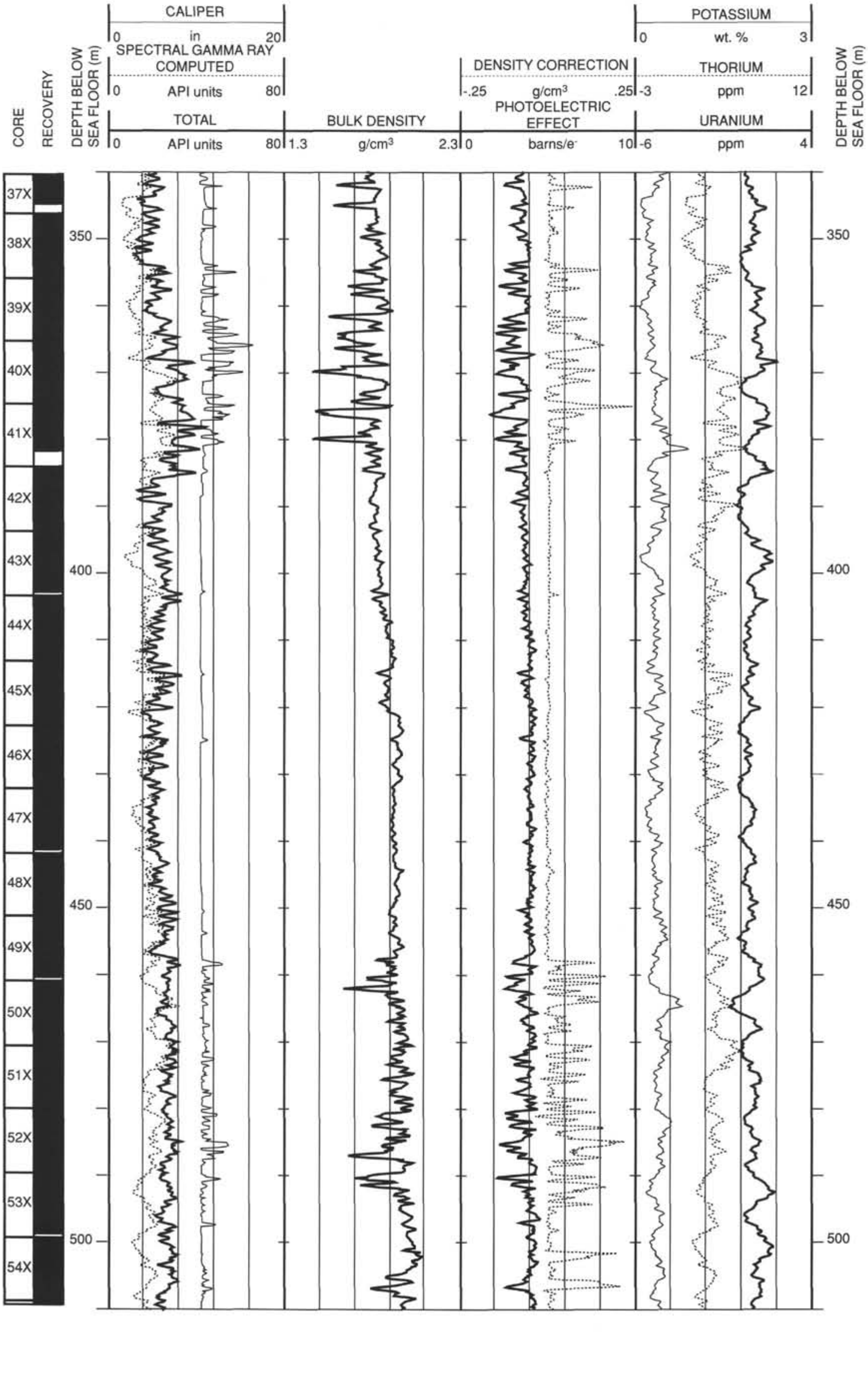

Hole 926B: Density-Natural Gamma Ray Log Summary (cont.)

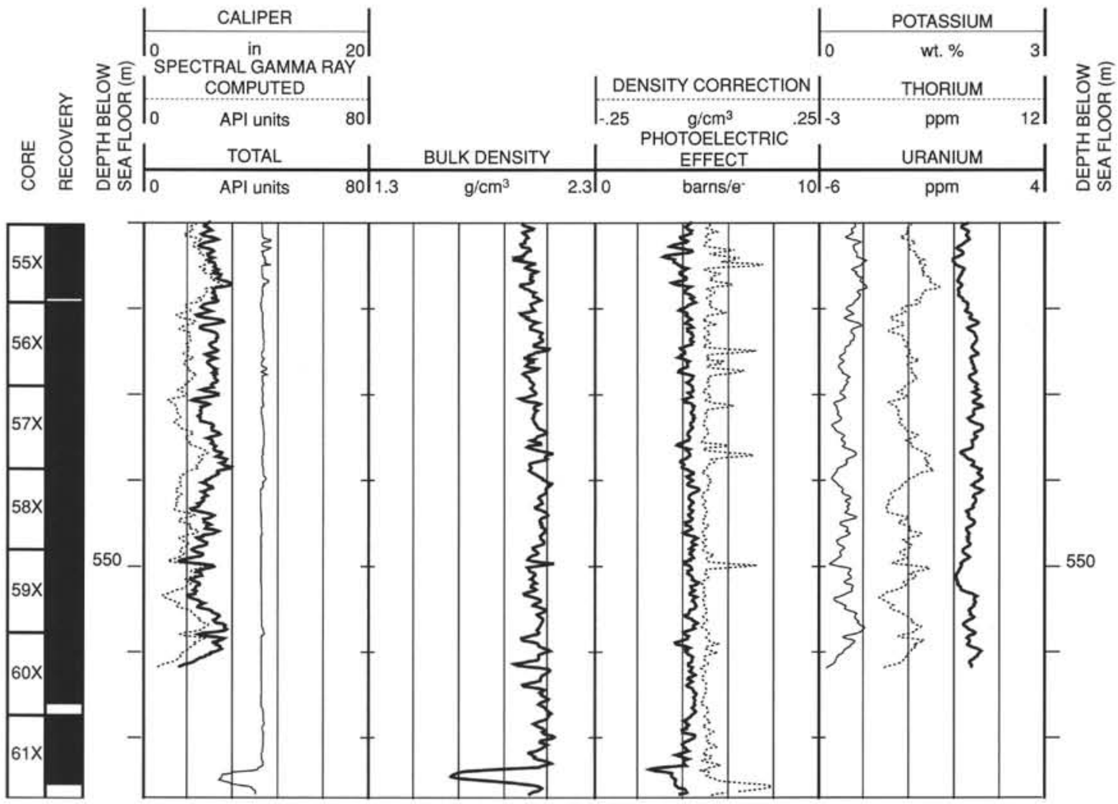

Hole 926B: Processed Natural Gamma Ray Log Summary

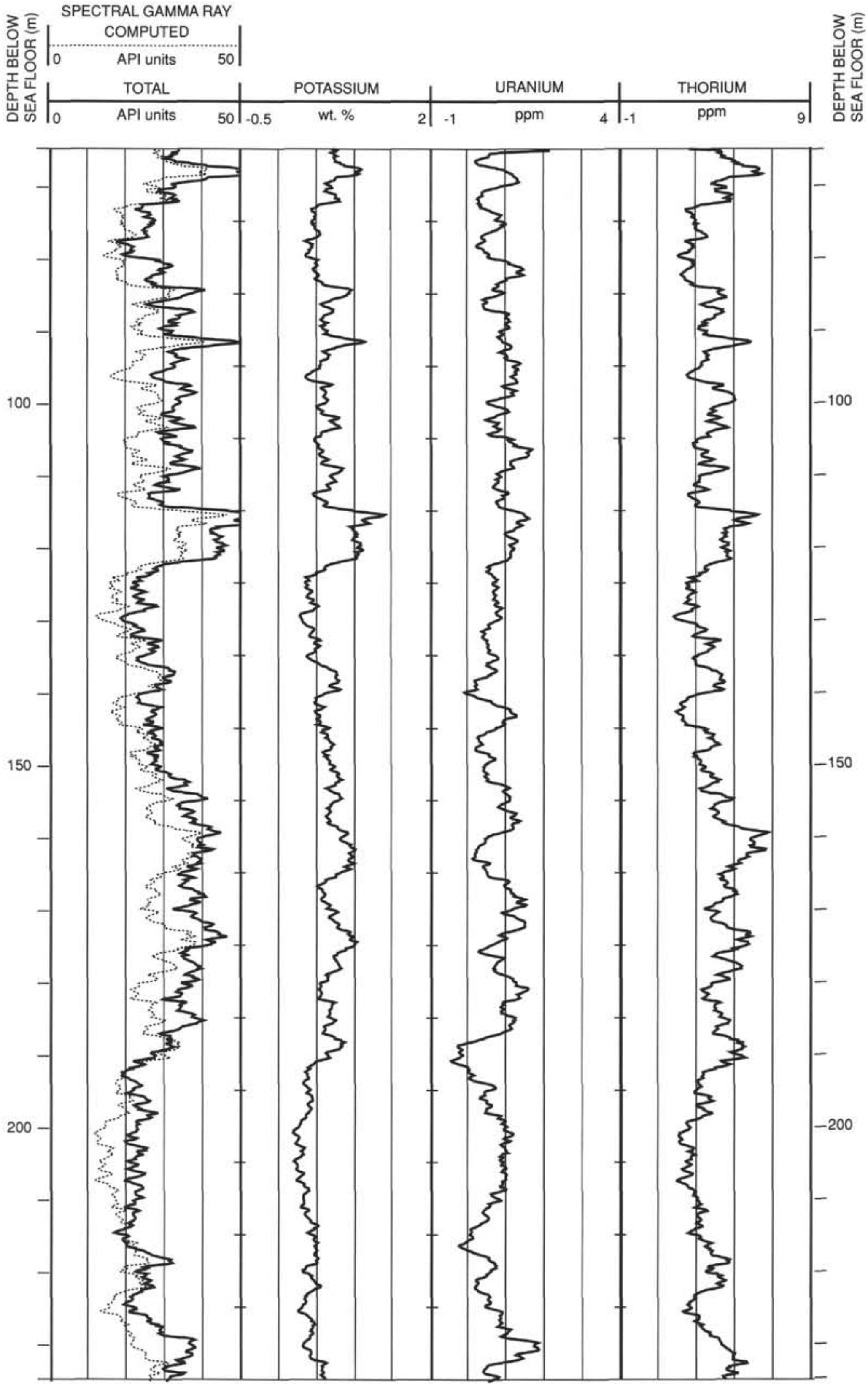

Hole 926B: Processed Natural Gamma Ray Log Summary

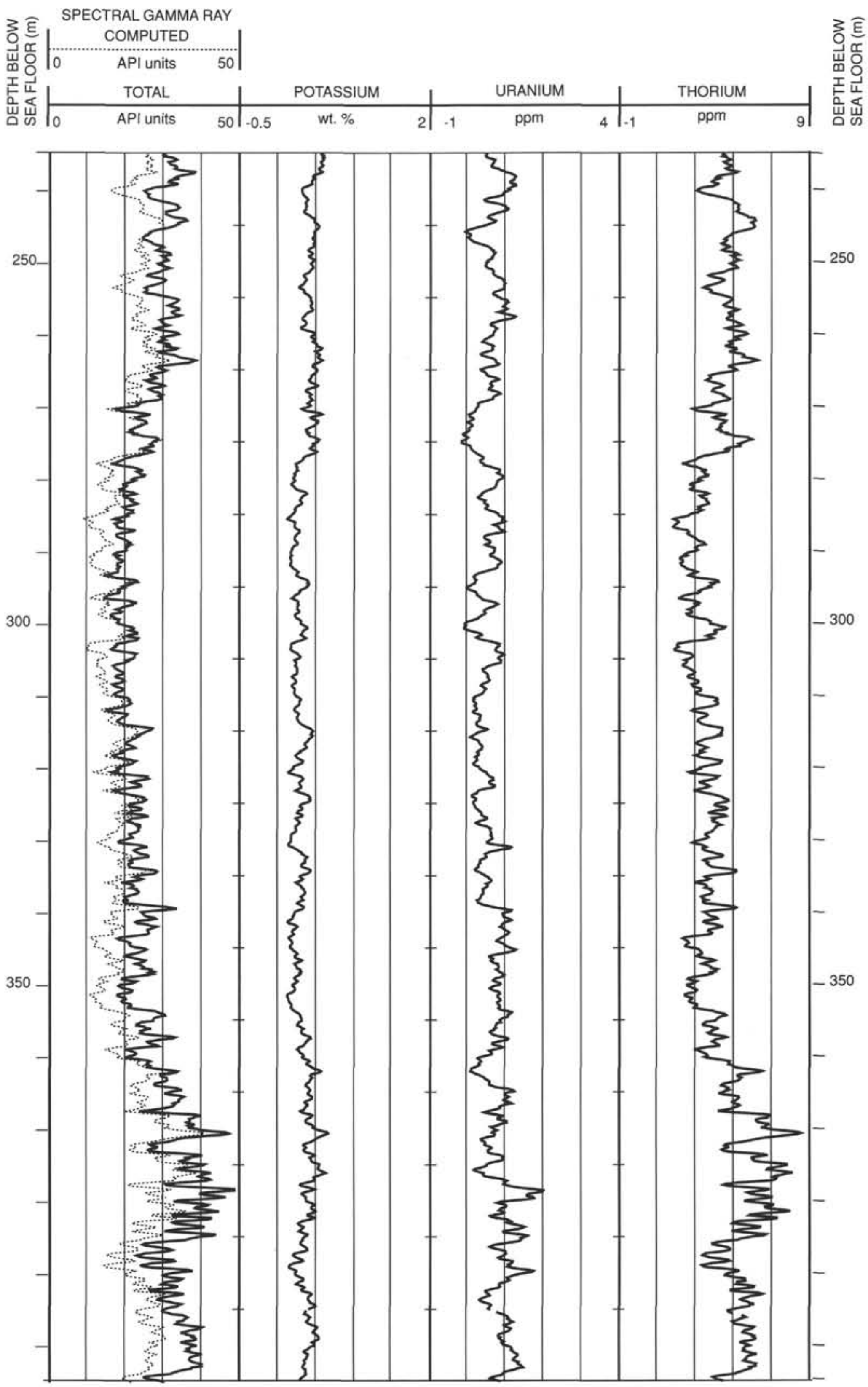

Hole 926B: Processed Natural Gamma Ray Log Summary

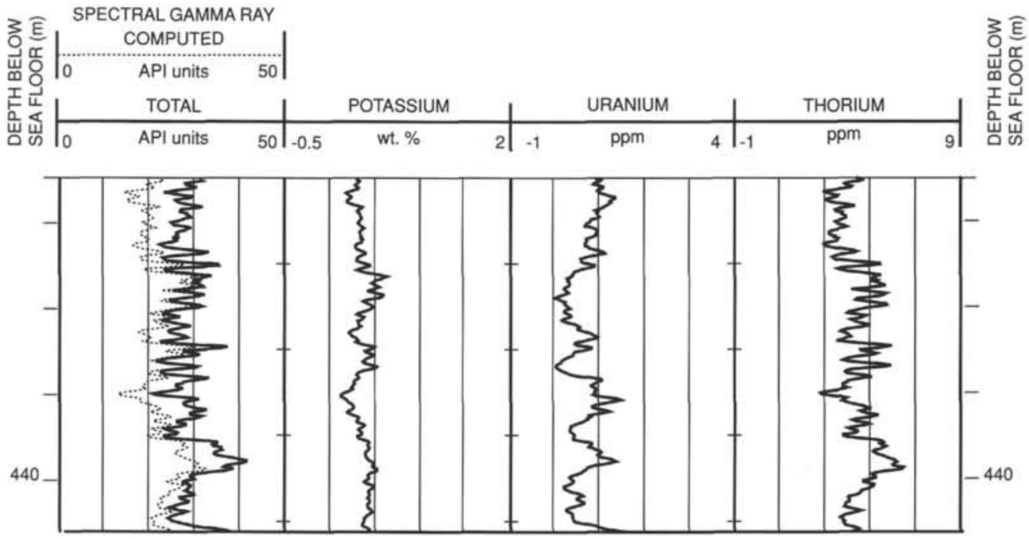

Hole 926B: Processed Geochemical Log Summary

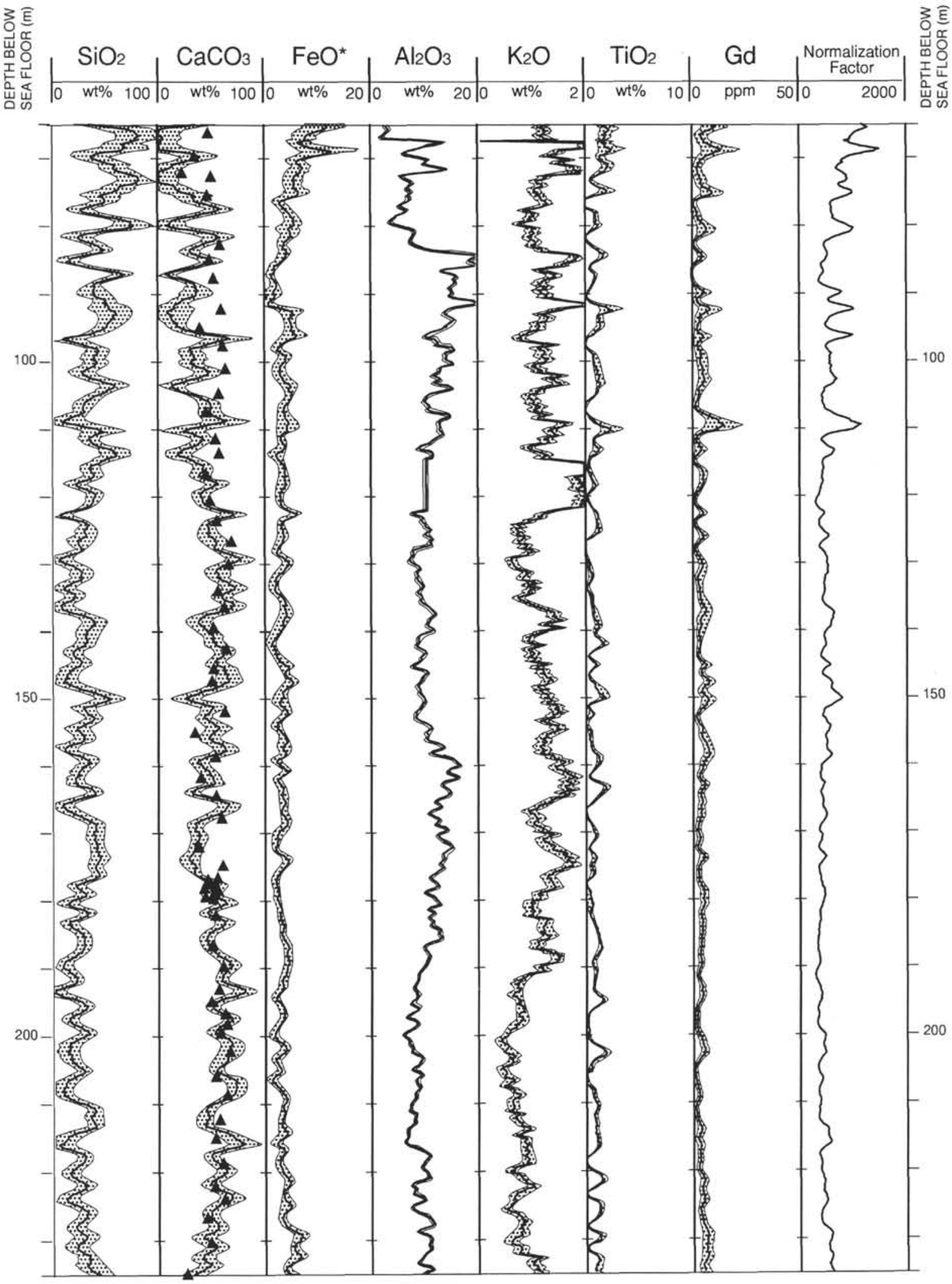

Hole 926B: Processed Geochemical Log Summary (cont.)

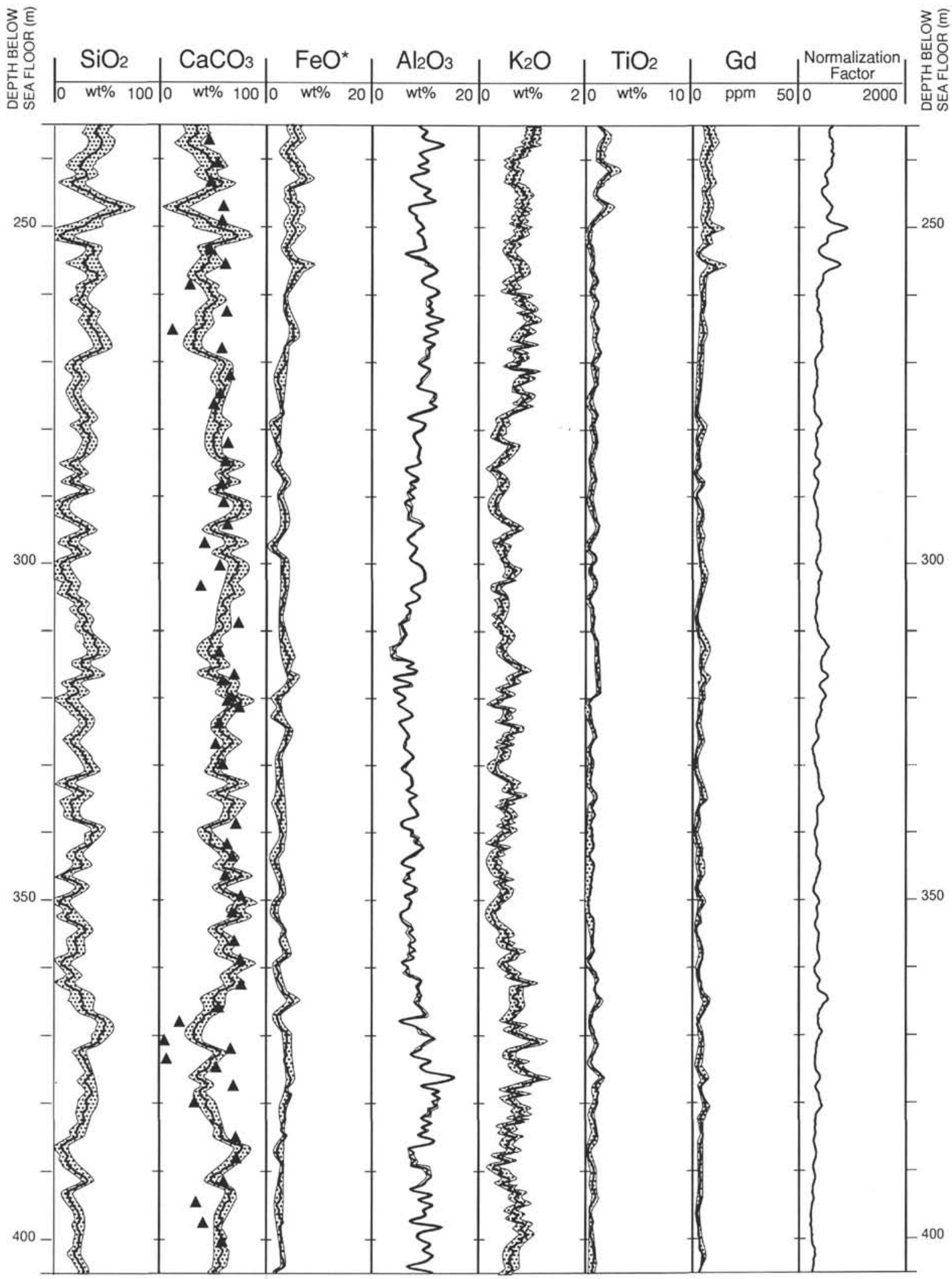

Hole 926B: Processed Geochemical Log Summary (cont.)